Durham University

Durham E-Theses

Crustal accretion during the earliest stages of intra-oceanic arc volcanism : examples from Fiji and Tonga, SW Pacific.

Mark R. Wharton

How to cite:

Wharton, Mark R. (1993) Crustal accretion during the earliest stages of intra-oceanic arc volcanism : examples from Fiji and Tonga, SW Pacific. Doctoral thesis, Durham University.

Use policy

The full-text may be used and/or reproduced, and given to third parties in any format or medium, without prior permission or charge, for personal research or study, educational, or not-for-profit purposes provided that:

- a full bibliographic reference is made to the original source
- a https://etheses.durham.ac.uk/id/eprint/1616/ is made to the metadata record in Durham E-Theses
- the full-text is not changed in any way

The full-text must not be sold in any format or medium without the formal permission of the copyright holders.

Please consult the full Durham E-Theses policy for further details.

Academic Support Office, The Palatine Centre, Durham University, Stockton Road, Durham, DH1 3LE
e-mail: e-theses.admin@durham.ac.uk Tel: +44 0191 334 6107
https://etheses.durham.ac.uk

Crustal accretion during the earliest stages of intra-oceanic arc volcanism: examples from Fiji and Tonga, SW Pacific.

by

Mark R. Wharton BSc. (Hons)
Royal School of Mines,
Imperial College, London.

The copyright of this thesis rests with the author.
No quotation from it should be published without
his prior written consent and information derived
from it should be acknowledged.

A thesis submitted in partial fulfilment of the requirements for the degree of Doctor of Philosophy

Department of Geological Sciences,
Durham University, UK.
August 1993

22 FEB 1994

To my parents

ABSTRACT

On the islands of Viti Levu, Fiji, and 'Eua, Tonga, in the south of the western Pacific island arc province, volcanic rocks which erupted during the earliest stages of intra-oceanic arc volcanism are preserved.

In southwestern Viti Levu, the oldest rocks are predominantly basic pillowed and massive lavas of the Yavuna Group. The lavas erupted into shallow water and are locally interbedded with shallow water limestones of Late Eocene to Early Oligocene age. Correction of the effects of later faulting and geochemical correlations provide the basis for a newly proposed volcanic stratigraphy. The lavas are classified on the basis of HFSE-contents and major element abundances. The oldest lavas in the sequence are boninites and depleted arc tholeiites which pass up-section into more fertile and ultimately, more enriched arc tholeiites. The oldest lavas can be directly compared with other sequences in the north of the arc province which were formed during subduction zone initiation. The climax of early arc activity was marked by the intrusion of a 40km^2 tonalite pluton, the Yavuna Stock.

Rocks of the lower Wainimala Group lie unconformably above the Yavuna Group and represent the earliest part of an Oligocene-Miocene island arc. Early volcanism took place within distinct volcanic edifice and inter-edifice terranes. Mainly andesitic, transitional calk-alkaline lavas erupted from major subaerial volcanic edifices. Elsewhere, tholeiitic magmas formed low-lying basaltic lava fields and small felsic volcanic centres on the seafloor. The intrusion of a dense bimodal dyke swarm into the underlying frontal-arc crust indicates that significant crustal extension accompanied the eruption of the inter-edifice lavas. Geochemical variations within the Wainimala volcanic suite are thought to have been generated through fractional crystallisation processes. While relatively slow ascent and mixing of magmas took place beneath the major edifices, efficient shallow-level fractionation and rapid ascent of magmas occurred in the areas between them, probably because of structural heterogeneities in the underlying crustal substrate.

Some lavas from 'Eua, Tonga, were derived from similar depleted sources to the lower Yavuna Group, athough mantle melting mechanisms may have differed. The nature of mantle source enrichments in the studied lava suites provides a good reflection of the variability that characterises the western Pacific arc province as a whole.

Declaration

I declare that this thesis, which I submit for the degree of Doctor of Philosophy at the University of Durham, is my own work and not substantially the same as any which has previously been submitted at this or another university.

Mark R. Wharton
University of Durham
August 1993

Copyright© Mark R. Wharton
The copyright of this thesis rests with the author. No quotation from it should be published without the written consent of Mark Wharton and information derived from it should be acknowledged.

ACKNOWLEDGEMENTS

Thanks are due to the following for help, advice and friendship during the past (nearly) four years. The NERC for studentship GT4/89/GS/026.

The supervisors, motivators and occasional drinking partners, Howard Colley and Julian Pearce. Thanks for the opportunities, the encouragement and signing the claim forms for the foreign conferences!

My 'third supervisor' and friend, Ben Hathway, for providing enthusiastic advice both in Fiji and in the UK during the course of the project.

Liam Hindle in Suva for collecting some of the samples and laying on hospitality at the weekends in Lucky Eddies. To Lucky Eddie himself for the dance routines!!

Ron 'K2 solo via Punjab airways' Hardy for his help and discussion in analytical work, and his fine sense of humour during the last weeks of the write-up.

John Mitchell at Newcastle University for the opportunity to carry out radiometric dating.

Tim Hopkins and Dave Plant for training and assistance with the probe set-up at Manchester. Likewise to Paul Suddaby and Dick Giddens at RSM, London.

Matthew Thirlwall and Elaine McPherson for the opportunity and assistance in carrying out radiogenic isotope analyses. Also Matty for sorting out the accommodation.

The other members of the geochem. travel club - Chezza (the founder member), Parky, Iannis, Mehmet, Vicky and Robin. Thanks too for keeping me supplied with stationary.

Aunty Sal, Dimitri, and Dave Peate for numerous pieces of information on geochemistry, Greek hair-cutting customs, and the family tree, amongst other things!

Parky, Bole, Kate, and Sarah, for useful discussions regarding mantle melting and beer, the Mull lavafield, the Troodos ophiolite and the southwest Pacific respectively.

Dave Tappin, Tony Crawford, Jim Gill, Jim Hawkins, Peter Rodda, Graeme Taylor and Jon Gascoyne for various discussions and contributions which have improved the arguments in this thesis.

Martin Whitworth for his help and encouragement over the past seven years during which time Sheff. Utd. have reached the Premier League and appeared at Wembley, while Preston North End have lurched back into the basement of English football.

Tony Gibbons for his superlative efforts in keeping '*The Minge*' on the road - she'll miss you!

John McDonald and his wife Evelyn of Waterloo, Broadford, for their fine hospitality and guidance around the Cuillins of Syke.

Dave Asbery for help with all things mechanical, electrical and financial.

The old-timers - Hunty, Gerald, Ruthy, Kealy and Billing. Thanks for the introductions to Rixy's, the Hill etc. Mossy you're in this section too because you wrote up too quickly!

The 'guilt-edged-scum' - Gary, Filthy, Mikey, Steeley, Nilpf, and Spod. Thanks for a memorable trip to the 'Dam - I'm sure it will be the first of many!

The 'new breed of postgrad' - Timmy A., Chris B., Zoe, Charlotte, Pete, John, Sue and Jipper.

Dave and Neville, Trish, Paul, Jane, Peter and Danny, for help and advice with many perplexing computer problems - almost always of my own making!

George Ruth for the new mouse, Gerry Dresser for the photos, Ron Lambert for the acid and George Randall for the thin-sections.

Alan Carr for photographic work *par excellence.*

The rowing boys Peter, Danny and Parky and the coxes, Wendy, Julie and Sarah for the great times and firm pressure at York, Berwick and on the Wear. Also to Tricky for shaping four lard-bellies into a respectable four.

Lynn, Carol, Karen, Julie, for generous assistance with departmental facilities and much amusing banter over the past four years.

Paul '*The magpie*' Laverick - thanks for getting the drinks in - even if it was with my own money !!

The Karakoram expedition team, Mikey, Caroline, Mike, Amanda and James, also Lu, Nick, Pierre and Rajab Ali for all the effort put into that memorable experience. And to all who helped us with the logistics - Roger, Andy Peckett, Donny, Tony Johnson, Carol, Lynn, Dave, Alan and Gary (that £500 was cool!).

Peter Ashford and Martin Eves for shining the red and yellow lights at the end of the tunnel. Sir Peter Holmes for the celebratory lunch.

Jane Hepworth for being outstandingly patient during the past few months (except for the meal in Bellos!). Thanks for still being my best friend.

Finally, to my parents, Malcolm and Linda, for all their help and support, both moral and financial, during my education.

CONTENTS

Appendices

CHAPTER 1

Introduction

1.1 Aim of the project

The western Pacific is now widely accepted as a type-locality for the study of convergent plate margin processes. Extensive programs of ocean drilling, dredging and surveying since the 1970's have greatly improved our knowledge of the tectonic and geochemical evolution of intra-oceanic arc-backarc systems. The oldest parts of intra-oceanic arcs, however, remain elusive to detailed study, because they are usually submerged or covered by the products of later arc volcanism (Stern & Bloomer 1989). This thesis describes the volcanology, structure and geochemistry of small areas of island arc basement that are exposed on the islands of Viti Levu, Fiji and 'Eua, Tonga (Fig. 1.1). Arc basement was uplifted and exposed in the southwest of Viti Levu during strike-slip faulting in the Late Miocene (Hathway 1993), while 'Eua forms a subaerial part of the Tonga Ridge in the forearc of the Tonga-Kermadec subduction zone.

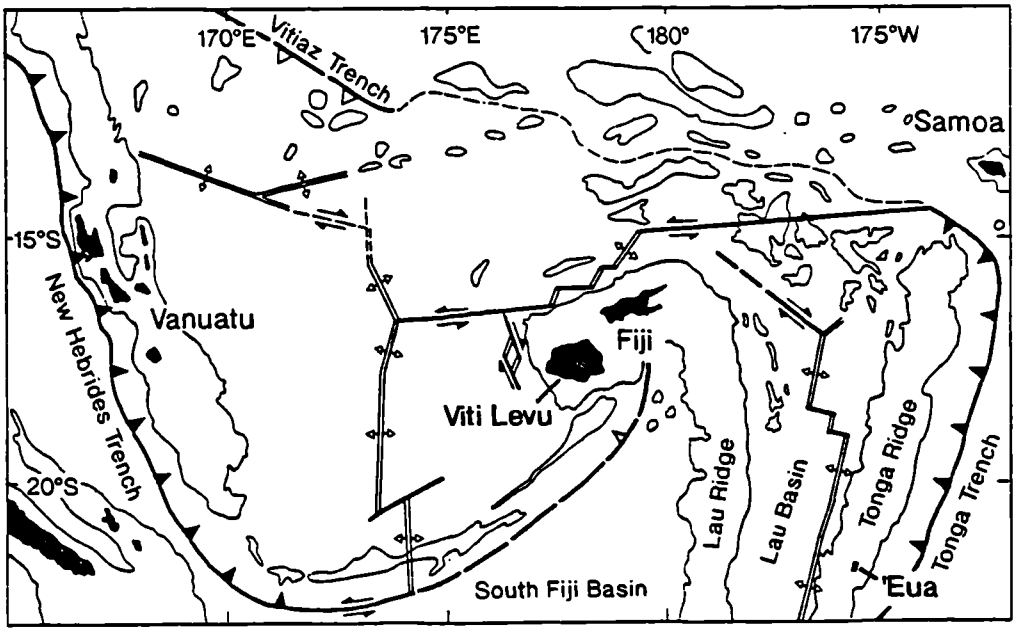

Fig. 1.1 The setting of Viti Levu, Fiji and 'Eua, Tonga, at the site of the complex arc-transform-arc subduction complex in the southwest Pacific. Black areas indicate subaerial exposure; submarine volcanic ridges are defined by the 2km bathymetric contour.

1.2 Background

Pioneering workers in the southwest Pacific recognised that large-scale, steep-flanked island arc ridges were separated by basins of intermediate to normal oceanic depth and that these features were developed within individual subduction zone systems (e.g. Karig 1971). The integration of these observations with plate tectonic theory led to several papers which attempted to reconstruct the tectonic history of the region through the closing of marginal basins and re-connecting of arc and remnant arc ridges (Karig 1974; Coleman 1976). The theme of cyclicity between volcanic events in arcs and adjacent marginal basins became established as a working hypothesis to which geochemical studies were applied, the focus of which was the most clearly defined arc-marginal basin pair in the region, the active Tonga arc and Lau basin (e.g. Hawkins 1976, Gill 1976, Ewart et al. 1977). In areas of greater tectonic complexity it was recognised that subduction zone reversals, transform faults and triple junctions could severely disrupt the simple arc-marginal basin geometric relationships. In these areas, valid tectonic reconstructions could only be made following the integration of a full spectrum of geological, geophysical and geochemical data (e.g. Colley & Hindle 1984).

Colley (1984) recognised the presence of pillow lavas, dykes and pelagic sediments in SW Viti Levu which he interpreted as part of an ophiolite complex. In this model, oceanic crust was obducted from the nearby South Fiji marginal basin along low angle thrust faults. This idea was modified following the discovery of new stratigraphic relationships by Ben Hathway of Oxford Polytechnic, who completed a doctoral thesis on the sediments of the area (Hathway 1988) and provided an important stratigraphic framework within which to study the complex igneous lithologies of SW Viti Levu (Hathway 1990). At this stage, the oldest igneous units in the study area were largely undifferentiated and were classified en-masse as part of an 'early arc stage' spanning a wide 45Ma to 10Ma age range (Whelan et al. 1985, Gill 1987). It was to follow on from the sedimentological work of Hathway with a detailed geological and geochemical study of the igneous rocks that this project was conceived by Dr. H. Colley and Dr. J.A. Pearce.

1.3 The Ocean Drilling Program initiative

In the northern part of the western Pacific arc province, better subaerial exposure and lesser tectonic complexity were major factors in the initiative of the Ocean Drilling Program (ODP) to drill holes into island arc basement with the aim of gaining a better understanding of crustal accretion processes in newly formed island arcs. ODP Legs 125 and 126 drilled holes in the Izu-Bonin and Marianas arc systems (Fig. 1.2) and the

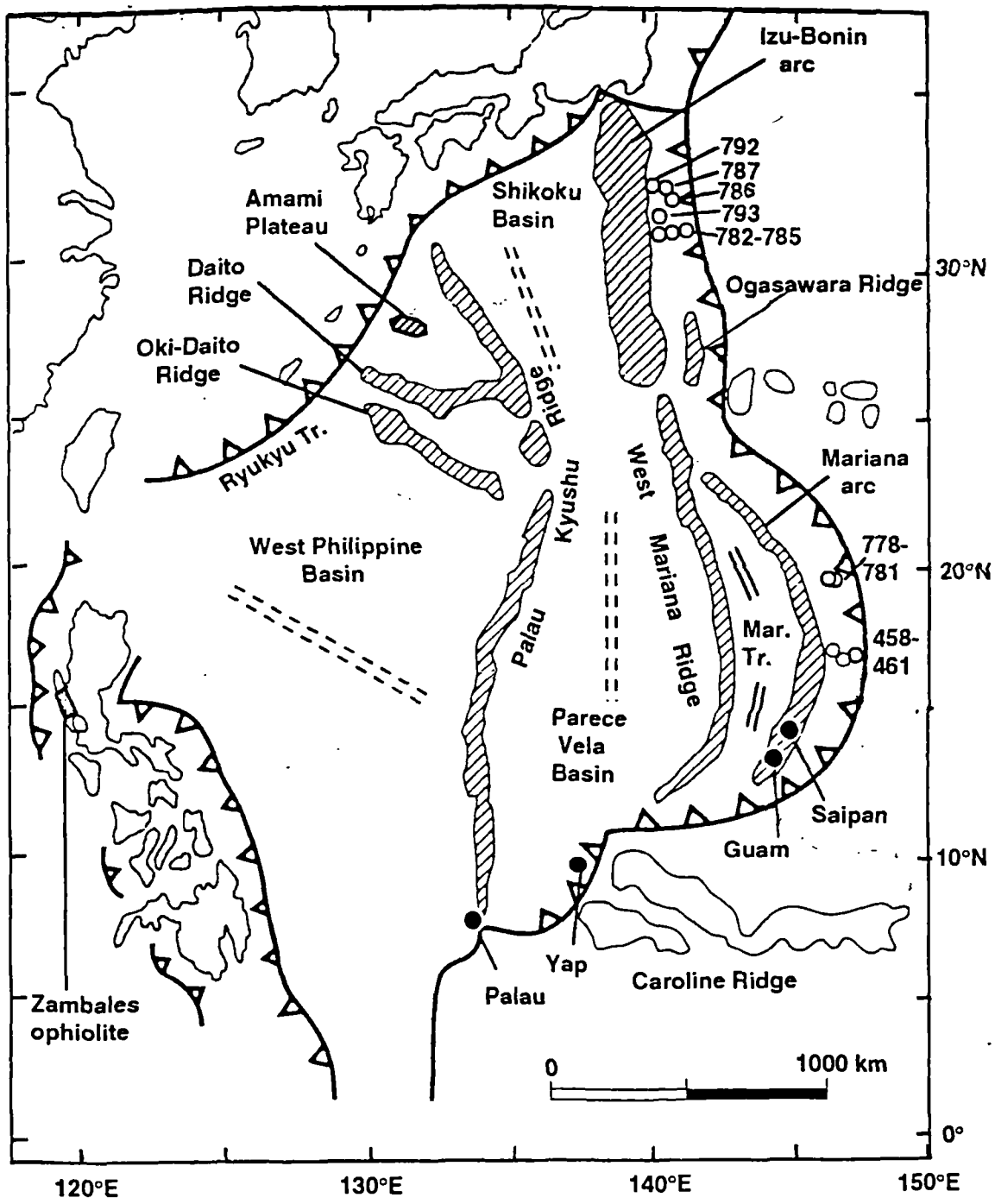

Fig. 1.2 Location of island arcs, remnant arcs, marginal basins and drill sites in the northern part of the western Pacific arc province (modified from Pearce et al. 1992b).

information gathered from these holes forms an important database with which to compare the rocks of similar age studied in this thesis. Important synthesis papers documented both the tectonic (Taylor 1992) and geochemical (Pearce et al. 1992b)

processes in the early arc terranes. The rôle of tectonic extension throughout the history of arc-basin system has now become recognised as fundamental in convergent plate margins that lack a well-developed accretionary wedge (Hawkins 1984). As a possible result of this subduction zone retreat or "rollback" and consequent plate decoupling, considerable overlap is now thought to exist between rifting and volcanic events in the arc and marginal basin (Taylor 1992). A broad evolutionary sequence for the initial 25Ma of the Western Pacific type of plate margin can be summarised as follows.

(i) Establishment of a protoarc (nascent arc) following the initiation of subduction at a transform fault (Casey & Dewey 1984). Characteristic eruption of depleted (tholeiitic) and ultra-depleted (boninitic) magmas.

(ii) Rifting of the protoarc edifice to form a trenchward frontal arc, a remnant arc, and an intervening backarc basin. The magmatic axis of the system becomes concentrated in the backarc basin where tholeiitic magmas are erupted during normal asthenospheric upwelling.

(iii) Establishment of a second phase of arc volcanism at the zone of crustal weakness between the rifted margin of the frontal-arc and the backarc. The volcanic rocks produced in the arc may be tholeiitic or calc-alkaline. The system eventually stabilises to become a mature arc, as accretion in the backarc wanes.

The older volcanic rocks of southwestern Viti Levu and 'Eua suites show contrasting volcanological and geochemical features which reflect the complexities of magma genesis in this transitional tectonic setting. Chapter 2 outlines the volcanic stratigraphy of the study areas to enable comparison with the chronology outlined above and provide a framework for the detailed fieldwork and sampling described in chapter 3. Chapter 4 documents the petrography and mineral chemistry of the igneous rocks collected and chapter 5 describes their major and trace element geochemistry, and discusses the implications for the volcanic stratigraphy. In chapter 6, various aspects of the geochemistry are modelled in order to gain an insight into petrogenetic processes operating in the early arc systems and in chapter 7 the major conclusions of the thesis are summarised and discussed. References cited in the text are contained in the thesis bibliography. The reference Hathway et al. (in prep.) refers to the forthcoming southwest Viti Levu geological bulletin to be published under the auspices of the Mineral Resources Department, Suva.

CHAPTER 2

Volcanic stratigraphy and dating

2.1 Introduction

This chapter summarises previous work on the igneous geology of southwest Viti Levu, Fiji and 'Eua, Tonga. The results of radiometric dating from this study are described, discussed and incorporated into a volcano-stratigraphic framework for the detailed geochemical sampling described in chapter 3. The volcano-tectonic evolution of the island arc sequences preserved on Viti Levu and 'Eua are then compared with the stratigraphy of the northwest Pacific arc province which is better studied in terms of its geology and geochemical evolution.

2.2 The volcanic stratigraphy of southwest Viti Levu

The area covered by this thesis is illustrated in Fig. 2.1. Revised stratigraphic units for the southwest Viti Levu area have been proposed by Hathway (1992). These refine the earlier definitions of Rodda & Band (1967) using new biostratigraphic and field evidence discovered during mapping work in the 1980's. A summary stratigraphic column is reproduced in Fig. 2.2. It incorporates the two major episodes of island arc accretion studied in this thesis, the Late Eocene to Early Oligocene **Yavuna Arc** and the upper Early Oligocene to Middle Miocene **Wainimala Arc.**

2.2.1 The Yavuna Group

The oldest rocks in the study area comprise the Yavuna Group of Hathway & Colley (in press) which crop out to the southeast of the town of Nadi (Fig. 2.1) and are interpreted by these authors to represent part of an Upper Eocene to Lower Oligocene volcanic arc, the Yavuna Arc. They are the only rocks of proven pre-Upper Oligocene age on Fiji and form the volcanic basement in southwest Viti Levu. The basement is clearly distinguished from the later, mainly sedimentary cover rocks by its significant positive gravity anomaly (Fig. 2.3). The Yavuna Group comprises pillowed and massive basic lavas overlain by volcaniclastic rudites and includes a number of

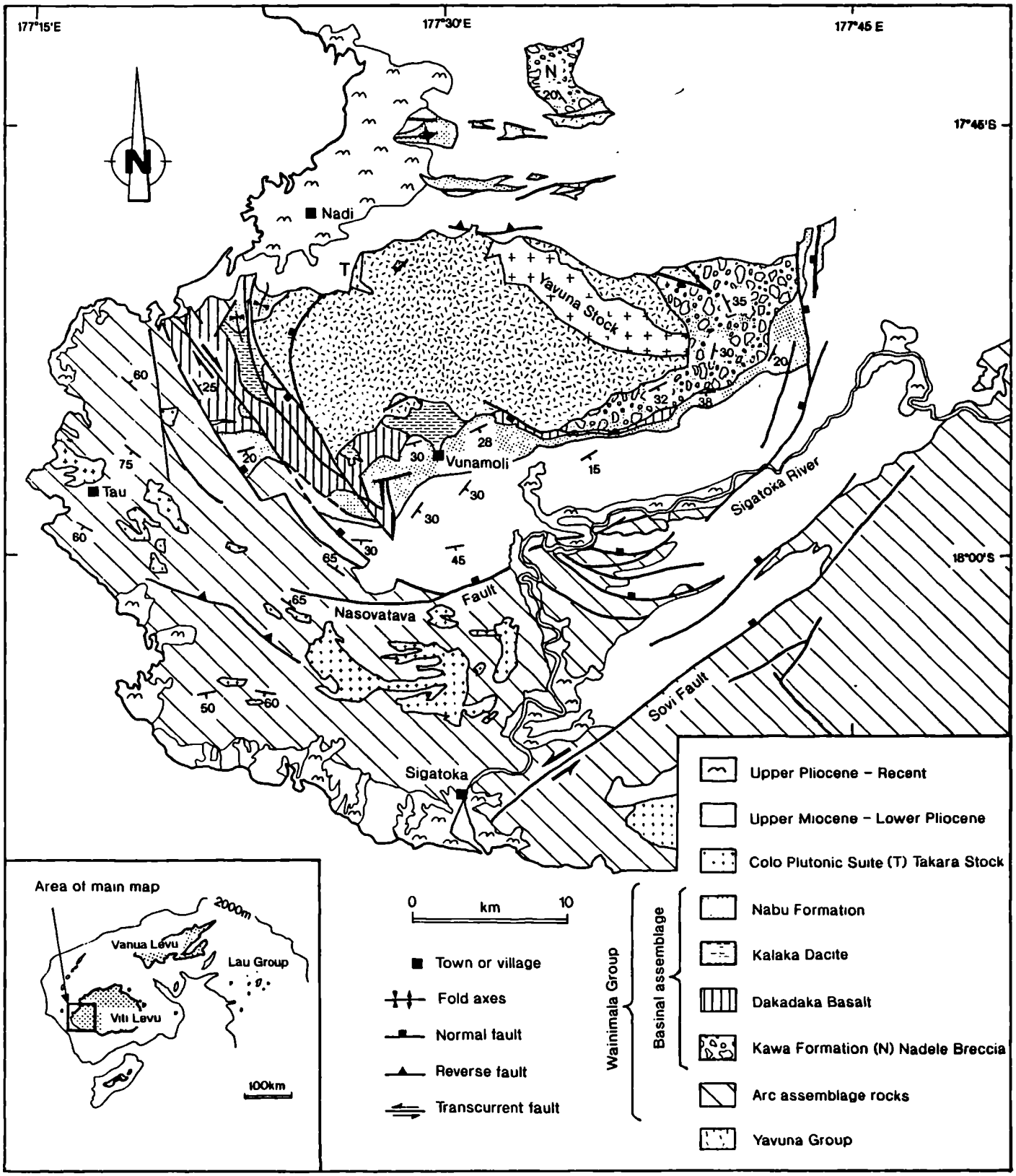

Fig. 2.1 Geological map of southwest Viti Levu to illustrate the area covered by this thesis.

interbedded limestone units. Most lithologies are affected by secondary alteration which shows a range from the zeolite to lower amphibolite metamorphic facies (Crook 1963). Colley et al. (1986) informally subdivided the lava field into the Namulomulo (Late Eocene) and the Nawaqadamu (Oligocene) units, based on the ages of the interbedded limestones, however, no specific within-group boundaries were delineated by these authors. Gill (1987), in a comprehensive description of the geochemistry of Fijian volcanic rocks, included rocks of the Yavuna Group in his *early arc stage* which incorporated volcanic episodes of ages 45 to 10Ma. The *early arc stage* volcanic rocks were further subdivided on the basis of HFSE element concentrations into low, medium and high-HFSE groups. Rocks from the southwest Viti Levu study area, including pillow lavas and dykes, were assigned to the high-HFSE group and to a separate, volumetrically minor, high magnesium basaltic andesite (HMA) group.

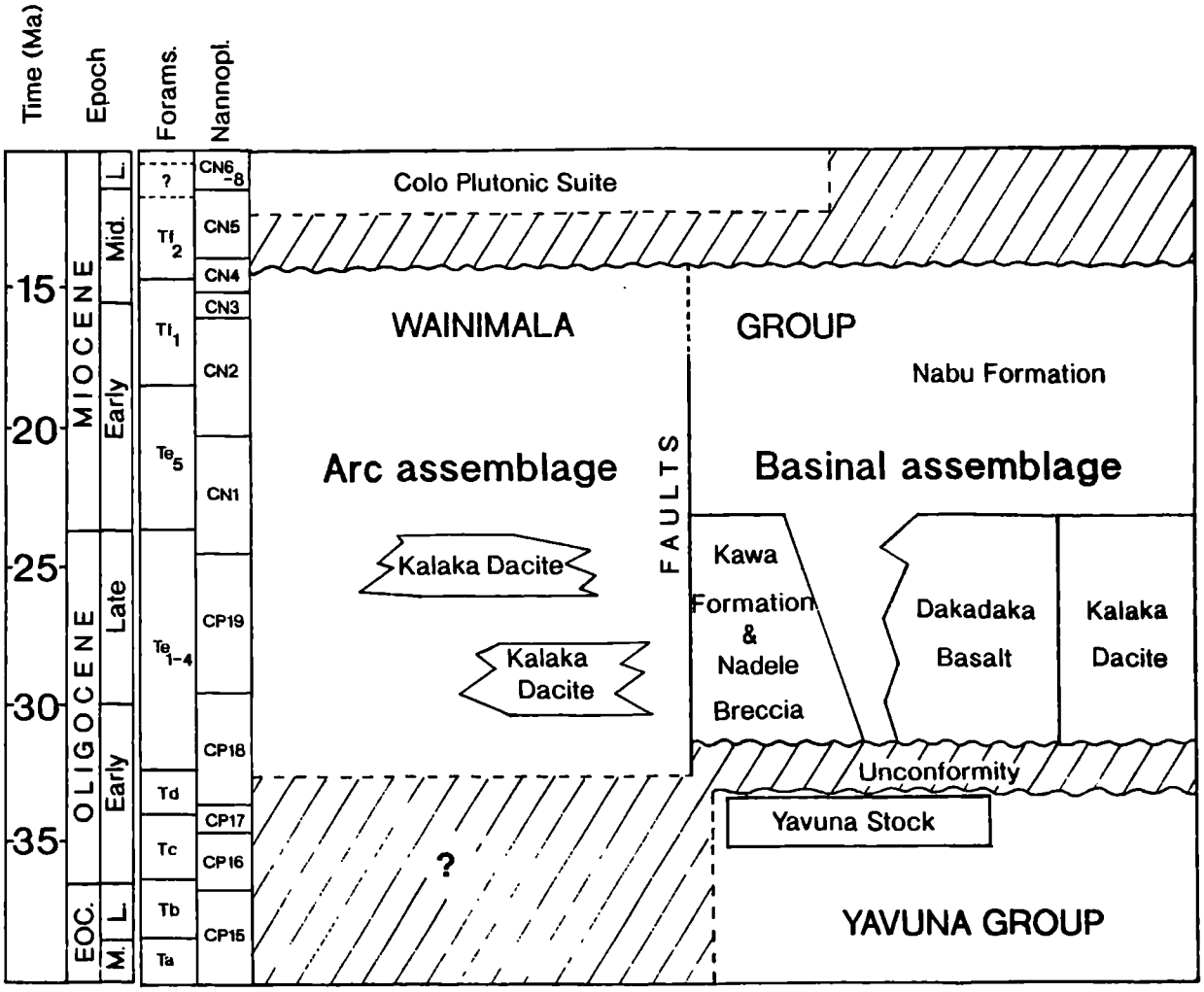

Fig. 2.2 Diagram to illustrate stratigraphic relationships in southwest Viti Levu.

The oldest parts of the lava pile crop out in the north of the Yavuna Group outcrop where they are interbedded with small limestone bodies containing an Upper Eocene (Tertiary letter stage b) foraminiferal assemblage (Cole, 1963). Although during previous accounts these relationships have been described as "usually obscure" e.g. Gill (1987), new unequivocal contacts between pillow lavas and interbedded limestones have been discovered in the area during this study (section 3.2.1.1). At structurally higher levels in the south of the Yavuna Group outcrop, volcaniclastic rudites overlie the lavas. The rudites are interbedded with limestones which yield a firm Lower Oligocene (Tertiary letter stage c) age. Dykes and gabbros belonging to the Yavuna Group are recognised by their intimate association with Yavuna Group pillow lava complexes, their similar alteration style and their commonly sinuous (i.e. non-chilled) contacts. The volcanic rocks are also intruded by the Yavuna Stock, an elongate NW-SE trending trondhjemite body which crops out in the eastern part of the Yavuna Group outcrop (Fig. 2.1).

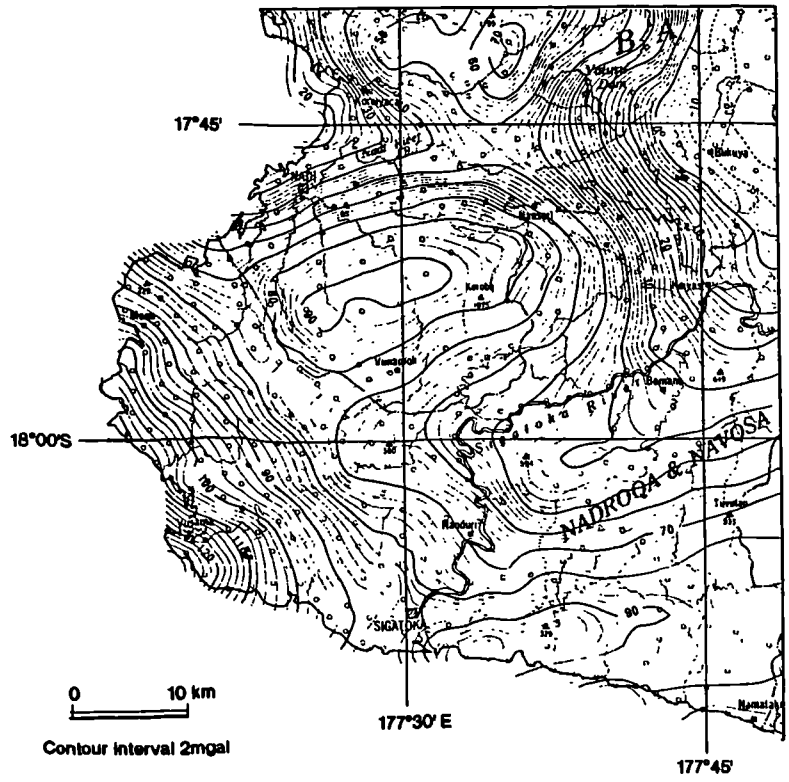

Fig. 2.3 Bouger anomaly map (ρ=2.67g/cm^3) demonstrating significant gravity anomaly around the Yavuna Group outcrop area (modified from Metal Mining Agency of Japan report, 1992).

Recent attempts to determine the palaeo-latitude of the Yavuna Block using palaeomagnetic techniques have unfortunately proved unsuccessful due to the nature of magnetic overprints associated with later volcanic episodes (G. Taylor, personal communication, 1992).

2.2.2 The Wainimala Group

The rocks of the Wainimala Group unconformably overlie the igneous basement of the Yavuna Group. In southwest Viti Levu, the group has been divided into two broad divisions, the *arc assemblage* and the *basinal assemblage* (Hathway in press b). The arc assemblage consists mainly of volcaniclastic rudites with subordinate lavas and limestones and is interpreted to represent the magmatic axis of the Wainimala arc. The base of the assemblage is not exposed but the assemblage is in total at least 4km thick. The oldest biostratigraphic dates recorded are Te_{1-4} to Tf_1 (broadly upper Early Oligocene-upper Early Miocene) on interbedded limestones (Fig. 2.2). The age of some of the interbedded basic lavas is thought to be Middle Miocene (Gill 1987). These include members of the low-HFSE group of the *early arc stage* of Gill (1987), akin to the classic 'island arc tholeiite' series of Jakes & Gill (1970). Lenses of massive dacite are also found interbedded with the volcaniclastic sediments and are assigned to the Kalaka Dacite Formation (Hathway in press b, Fig. 2.2). The arc axis is delineated and intruded by numerous tonalite and gabbro plutons of the Colo Plutonic Suite which extend across southern Viti Levu from WSW to ENE, and across southwestern Viti Levu from NW to SE (Fig. 2.1).

The majority of Wainimala Group samples studied in this thesis have been collected from the basinal assemblage which is largely separated from the arc assemblage to the south by major faults (Fig. 2.1). The basinal assemblage comprises the Kawa Formation and Nadele Breccia, which both consist mainly of volcaniclastic rudites; a bimodal suite of basic and felsic volcanic rocks assigned to the Dakadaka Basalt and Kalaka Dacite respectively; and the lowermost part of the Nabu Formation. This formation consists of volcaniclastic turbidite sandstones and mudstones, hemipelagic limestones, and acid tuffs, and also includes all of the wholly sedimentary upper part of the basinal assemblage. The underlying Yavuna Group rocks are cut by a pervasive bimodal dyke swarm which documents significant crustal extension during eruption of the basinal assemblage volcanic rocks.

2.2.2.1 The Nadele Breccia and the Kawa Formation

These formations are lithologically similar and are thought to be laterally equivalent (Wharton et al. in press). They consist mainly of redeposited rudites in which the dominant clast type is a characteristic grey, porphyritic andesite. Clasts of basalt and dacite also occur. The polymict nature of the rudites, the presence of rounded as well as angular clasts and the presence of sparse shallow-water limestone clasts indicates

that they were deposited on the dispersal aprons of major, in part subaerial, volcanic edifices (Hathway in press b). The Nadele Breccia (Rao in press), includes basalt pillow lavas and massive acid andesite lavas as well as volcaniclastic rudites, and is interpreted to represent part of an early Wainimala arc edifice constructed upon a substrate of Yavuna Group basement (Wharton et al. in press). The Kawa Formation probably represents the dispersal apron of a similar major edifice situated closer to the arc assemblage (Fig. 2.1). The Kawa Formation rests unconformably on the Yavuna Group, while the base of the Nadele Breccia is not exposed.

2.2.2.2 The Dakadaka Basalt

This formation crops out along the western and southern margins of the Yavuna Group outcrop (Fig. 2.1), and has a maximum exposed thickness of 300 to 400m. It consists mainly of massive and pillowed lavas with subordinate pillow breccias. The freshest lava surfaces are mid-grey to grey-green while weathered surfaces are a distinctive deep maroon colour. Pillow lavas contain up to 50% by volume of amygdales filled with zeolites or calcite and the lavas are commonly cut by networks of small mm-scale veins bearing the same secondary minerals. Massive basalts are generally more sparsely vesicular. Rare basalt dykes intruding the lavas are interpreted as feeders. Pink pelagic limestone is commonly present as an inter-pillow matrix or as fragments caught up in lava flows. No age data are available for the basalts themselves, but nannofossils in the Nabu Formation strata immediately overlying them indicate ages ranging from late Early Oligocene to earliest Miocene (Hathway in press b, Fig. 2.2).

2.2.2.3 The Kalaka Dacite

This formation consists of monomict dacite breccias, massive dacite flows and tuffs. Within the basinal assemblage, these rocks mainly occur along the southern margin of the Yavuna Group outcrop (Fig. 2.1), where they are interpreted as a series of small volcanic centres (Hathway, in press b). Up-section or lateral transitions from lava and breccia to thick-bedded dacite tuff are commonly seen around these centres.

2.2.2.4 The NW-SE dyke swarm intruding the Yavuna Group

This pervasive bimodal dyke swarm is widespread in extent across the Yavuna Group outcrop. Dark blue-grey basic dykes are common throughout the area, but pale-grey-fawn felsic dykes are more common in the western part of the swarm, where they are

seen to coalesce as feeders to at least one of the Kalaka Dacite centres (Hathway in press b). Although no direct field evidence is seen to link the basic dykes with the Dakadaka Basalt, the hypothesis that they form part of the feeder system to the basalts is investigated in a later part of the thesis. Measured sections through the Yavuna Group outcrop demonstrate that the dykes form up to 60% of the crustal section (Fig. 2.4), however, cross-cutting relationships are rare due to the consistent strike of the swarm across the area. Following extensive mapping work, Hathway (in press b) notes that at most of the locations where age relations are apparent, basic dykes cut or chill against felsic dykes; a felsic dyke was seen to cut and chill against a basic dyke at only one location. From these contact relationships, the author concluded that the two end-member compositional groups were of similar age, but that most of the felsic dykes were emplaced prior to the majority of the basic dykes, an assertion supported by the presence of NW-striking basic dykes in parts of the Kalaka Dacite.

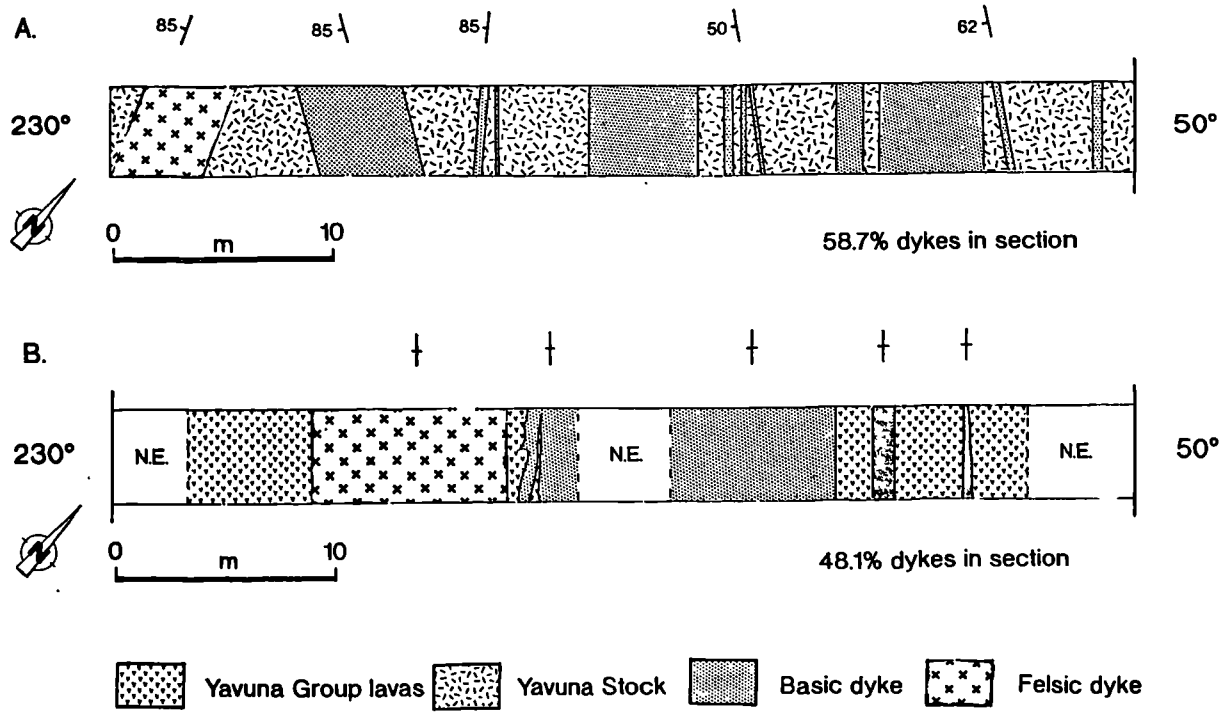

Fig. 2.4. Representative measured sections through the bimodal dyke swarm intruding the Yavuna Group. a - Namosi Creek (17°50.7'S, 177°33.7'E), b - Masi Creek (17°51.8'S, 177°26.2'E).

2.2.3 Later volcanic episodes

A major hiatus and disconformity separates the Nabu Formation from Late Miocene sediments of the Tuva Group (Fig. 2.5). During this hiatus, the Yavuna Group and Wainimala Group were intruded by the Colo Plutonic Suite, represented in the area by a small diorite intrusion, the Takara Stock (Fig. 2.1), and an associated NE-SW trending hornblende-andesite dyke swarm. These intrusives form part of the much larger and incompletely unroofed plutonic province which intrudes the axis of the Wainimala arc terrane across southern Viti Levu. To the north of the Yavuna Group outcrop sediments of the Nadi Group derived largely from reworking of Yavuna Group and Wainimala Group lithologies were deposited in the Nadi sedimentary basin during the Late Miocene (Fig 2.5). In the Late Miocene-Early Pliocene, the Nadi sedimentary Group was overlain with local unconformity by sediments of the Koroimavua Group (Fig. 2.5). These sediments were derived from shoshonitic volcanic centres in the Sabeto range several kilometres to the north of the study area and in addition, several shoshonite dykes related to the volcanic centres cut the Nadi Group sediments. Unconformably overlying the Koroimavua Group, further Late Pliocene shoshonite lavas and derived sediments of the Ba Volcanic Group crop out.

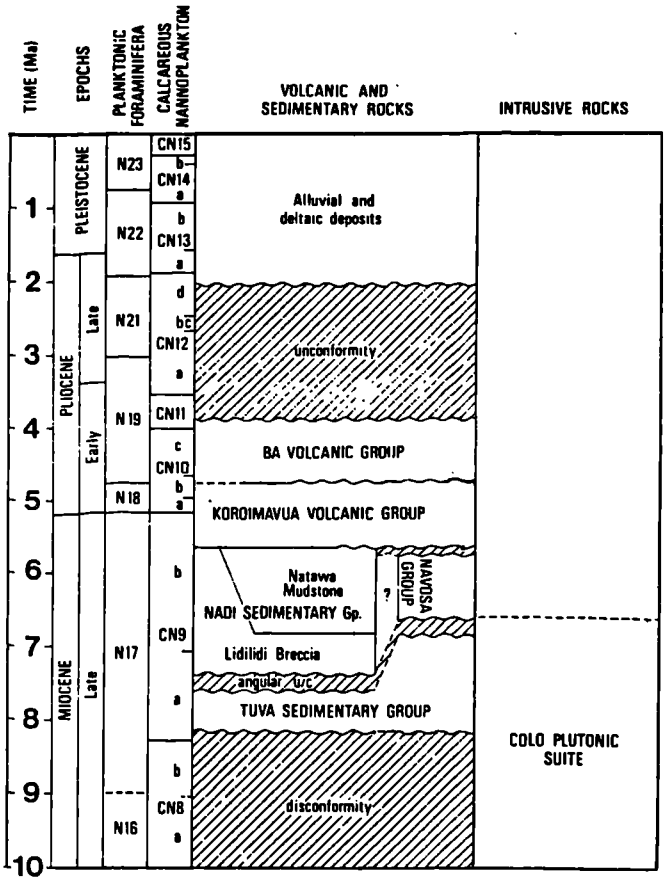

Fig. 2.5 Miocene-Recent stratigraphy of southwest Viti Levu, modified after Hathway (1993).

2.3 Radiometric dating on Viti Levu

2.3.1 Introduction

Radiometric dating using a conventional potassium-argon method was carried out in an attempt to provide greater resolution in parts of the volcanic stratigraphy. Experimental results were obtained in collaboration with Dr. J. G. Mitchell at the University of Newcastle and are presented table 2.1 together with the few samples from southwest Viti Levu dated previously. Full details of sample localities, petrography and analytical procedure are given in the relevant appendices. The choice of samples for radiometric dating was made primarily to ensure maximum coverage of each magmatic group by complementing those analyses already available in the literature. A corollary of this aim was that an assessment of the controls exerted by lithology and structure on the hydrothermal systems could also be made.

The samples exhibit varying degrees of secondary alteration with zeolites, smectite, chlorite, albite, calcite, epidote and hornblende as the dominant secondary phases. Within each volcanic group, however, alteration metamorphic assemblages are generally similar. Following Mitchell et al. (1992) samples were chosen on the basis of evidence for a single hydrothermal event only (e.g. one episode of secondary mineral veining or vesicle infilling), the assumption being that alteration would be associated with the same heat source as the magmatic event and thus be contemporaneous (Staudigel et al. 1981). The results are plotted in Fig. 2.6 to illustrate the comparison between the radiometric dates and the range of biostratigraphic dates obtained from sediments associated with the volcanic groups.

2.3.2 The Yavuna Group

2.3.2.1 Volcanic basement

K-Ar dates from the four basement samples from this study show a range in ages from 57.5±1.8Ma to 24.3±1.5Ma, with three of the four samples clustering between 24.3± 1.5Ma and 28.4±1.0Ma. The anomalously old sample of 57.5±1.8Ma is BH096, a dyke assigned to the volcanic basement on the basis of its alteration style and geochemistry. The dyke cuts another of the analysed basement samples, BH097 (28.4±1.0Ma). These samples were collected from Kawa Creek section which includes reworked boulders

Sample	Lithology	Notes	Method[1]	Age Ma±1σ	Reference
Yavuna Group					
WA48	Pillow lava	Primitive vesicular lava	Ar-Ar[2]	32.7±2.3	Whelan et al. 1985
WA45	Pillow lava	Evolved vesicular lava	Ar-Ar	29.5±1.4	Whelan et al. 1985
BH7	Gabbro	Upthrust basement	K-Ar	24.3 ±1.5	This study
BH097	Breccia clast	Primitive vesicular lava	K-Ar	28.4±1.0	This study
BH096	Dyke	Cuts BH097	K-Ar	57.5± 1.8	This study
VL031	Massive lava	Primitive massive lava	K-Ar	25.4± 0.7	This study
BH446	Dolerite	Stock contact aureole	K-Ar[3]	35.2 ±0.8	Webb 1990
GA456	Trondhjemite		K-Ar[3]	33.0± 1.0	McDougall 1963
DR1	Trondhjemite		Ar-Ar[3]	31.0±1.2	Whelan et al. 1985
Wainimala Group					
Arc assemblage					
WA4	Tholeiitic lava	From Colo pluton aureole	Ar-Ar	10.5±0.4	Whelan et al. 1985
WA2	Tholeiitic lava	From Colo pluton aureole	Ar-Ar	11.4±0.6	Whelan et al. 1985
Kawa Formation					
VL033	Andesite		K-Ar	28.1± 0.6	This study
BH197	Andesite		K-Ar	23.6± 0.5	This study
Dakadaka Basalt					
BH045	Pillow lava	Highly vesicular lava	K-Ar	8.26 ±0.3	This study
VL035	Pillow lava	Highly vesicular lava	K-Ar	5.98 ±0.31	This study
VL036	Pillow lava	Highly vesicular lava	K-Ar	13.6 ±0.4	This study
Dyke swarm cutting Yavuna Group					
BH119	Dyke	2% vesicles	K-Ar	22.9 ±0.4	This study
BH058	Dyke	15% vesicles	K-Ar	10.6 ±0.2	This study
Site 130	Dyke		K-Ar	20.2±2.4	Gascoyne (unpubl.)
Site 127	Dyke		K-Ar	30.5±22.1	Gascoyne (unpubl.)
Colo Plutonic Suite					
BH369	Dyke		K-Ar[3]	12.1± 0.5	Webb 1990
BH388	Dyke		K-Ar[3]	6.99± 0.2	Webb 1990
BH455	Dyke		K-Ar[3]	6.73± 0.15	Webb 1990
BH485	Dyke		K-Ar[3]	7.58± 0.08	Webb 1990
YX2002	Dyke		K-Ar[3]	12.0± 0.1	Fanning 1986

[1]Analysis of whole rock aliquot unless otherwise indicated.

[2]Heavy mineral concentrate.

[3]Hornblende separate.

Table 2.1 Summary of the radiometric dates from SW Viti Levu.

bearing a Late Eocene foraminiferal assemblage (Hathway et al. in prep.). The complete Kawa Creek section is thus conferred a Late Eocene maximum age, and in view of this, the radiometric date of the older sample BH096 is thought to be unreliable and without geological significance.

The remaining basement samples, together with the data reported by Whelan et al. (1985), form a grouping of ages from 29.5±1.4Ma to 24.3±1.5Ma (Fig. 2.6). These ages show marked disagreement with the range of older biostratigraphic dates, and may therefore record the date of resetting events associated with later episodes of magmatism. The samples show a wide range in potassium contents (O.189 wt.%-0.93 wt.%) for a similar calculated age which suggests that potassium exchange may have occurred at the time of alteration rather than subsequently (Mitchell et al. 1992). These authors made similar observations in samples from volcanic basement drilled during

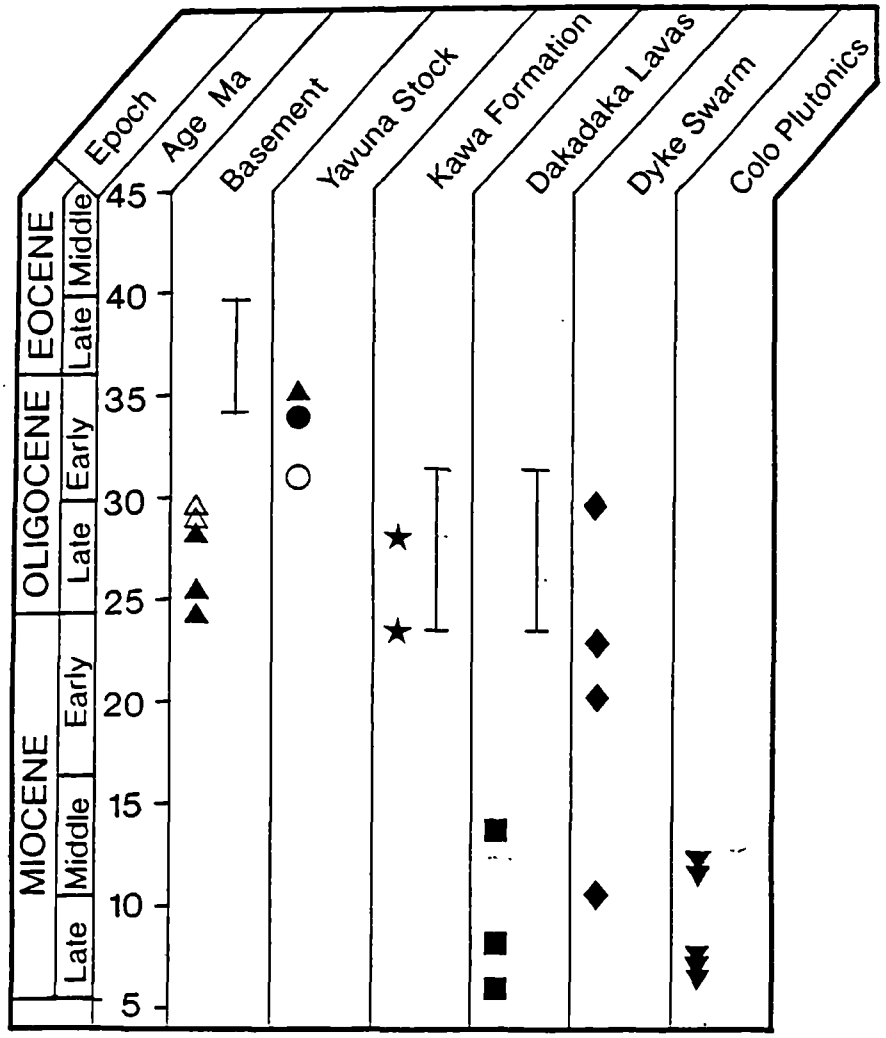

Fig. 2.6 Comparison between radiometric dates and range of biostratigraphic dates. Open symbols are Ar-Ar analyses, closed symbols are K-Ar analyses and bars give biostratigraphic range.

ODP Leg 125 and investigated this further by plotting the samples on a radiogenic ^{40}Ar vs. K_2O correlation diagram. The rationale behind the diagram is that if ^{40}Ar and K_2O are linearly correlated for a suite of samples as a consequence of a single episode of potassium and argon exchange, then any age calculated from the gradient of the line will have no immediate geological significance, except in the specific case where the intercept is zero, when the standard "isochron equation" will represent the age of closure of the system (Mitchell & Ineson 1988). The Yavuna Group volcanic basement data are plotted on such a diagram in Fig. 2.7a and conform at the 2σ confidence level to the "ideal" zero-intercept situation. The gradient of the fitted regression line can then be used to calculate an isochron age (t) using the equation:

$$t = 1804.08 \times \ln\left(\frac{^{40}Ar}{K_2O} \times 17.719 + 1\right)$$

Using this method the basement samples yield an isochron age of 25.1±1.1Ma which is interpreted to represent the age of the magmatic event responsible for the resetting of the basement radiometric dates. The radiometric dates of the basement samples are reasonably consistent when comparing the K-Ar analyses of this study and the Ar-Ar results of Whelan et al. (1985), and both show disagreement with the range of biostratigraphic ages from the basement (Fig. 2.6). At the time of publication, Whelan et al. (1985) proposed that the basement ages probably did record the basement magmatic event at 30-32Ma. In view of the more recent biostratigraphic evidence, however, which confers a Late Eocene age on the lowest parts of the basement, the dates of all basement lithologies so far analysed are considered to be reset.

One basement sample from the contact metamorphic aureole of the Yavuna Stock (BH446) has a somewhat older radiometric age of 35.2±0.8Ma (Fig. 2.6). This sample differs from the other basement samples in having metamorphic hornblende in its secondary mineral assemblage and was taken from the zone of contact metamorphism that extends up to several hundred metres away for the margin of the stock. Its systematics are discussed in full in the following section.

2.3.2.2 The Yavuna Stock

Analytical results for two Yavuna Stock samples from the literature, DR1 (Ar-Ar interpreted date on hornblende separate, 31.0±1.2Ma, Whelan et al. 1985) and GA456 (K-Ar date on hornblende separate, 33.0±1.0Ma, McDougall 1963) have been plotted

on Fig. 2.6. The samples give a reasonably consistent Early Oligocene age regardless of analytical technique and are interpreted as preserving the age of the intrusive event (Whelan et al. 1985). When compared with the basement sample from the contact aureole of the stock, BH446 (K-Ar date on hornblende separate, 35.2±0.8Ma), however, the two trondhjemite dates are slightly younger and are therefore interpreted as cooling ages for the intrusion. The paragenesis temperature of the amphibolite facies metabasic assemblages comprising hornblende and plagioclase (actinolite absent) is above 500°C (Winkler 1979). In contrast, paragenesis temperatures recorded by the greenschist facies metamorphic assemblages of basement samples from outside the contact zone lie within the range 300-500°C (Elthon 1981). The difference in susceptibility to resetting between rocks from inside and outside of the contact aureole therefore reflects the stability of hornblende-bearing amphibolite metamorphic assemblages as opposed to greenschist facies assemblages during subsequent hydrothermal episodes.

2.3.3 The Wainimala Group

2.3.3.1 The Kawa Formation

The Kawa Formation samples were selected for dating in order to provide an estimate of the age of onset of Wainimala arc volcanism in southwest Viti Levu. The samples show the greatest consistency with biostratigraphy of any of the volcanic groups studied (Fig. 2.6), with the dates obtained on VL033 (28.1±0.6Ma) and BH197 (23.6± 0.5Ma) both lying within the upper Early Oligocene-Early Miocene range for this formation. The samples are porphyritic andesite clasts and are considered to be among the earliest volcanic products of the Wainimala arc derived from principal volcanic edifices that were constructed upon the Yavuna Group substrate (Wharton et al. in press). It is notable that the two samples show an overlap in ages with the dates of the reset basement samples (Fig. 2.6) and, in order to investigate the significance of this overlap, the two samples are plotted on a radiogenic ^{40}Ar vs. K_2O correlation diagram (Fig. 2.7b) together with the basement isochron taken from Fig. 2.7a. The samples lie close to the basement isochron at the 95% confidence level suggesting a possible causal relationship between the magmatic age of the Kawa Formation samples (i.e. the earliest Wainimala arc activity) and the date of the basement resetting event.

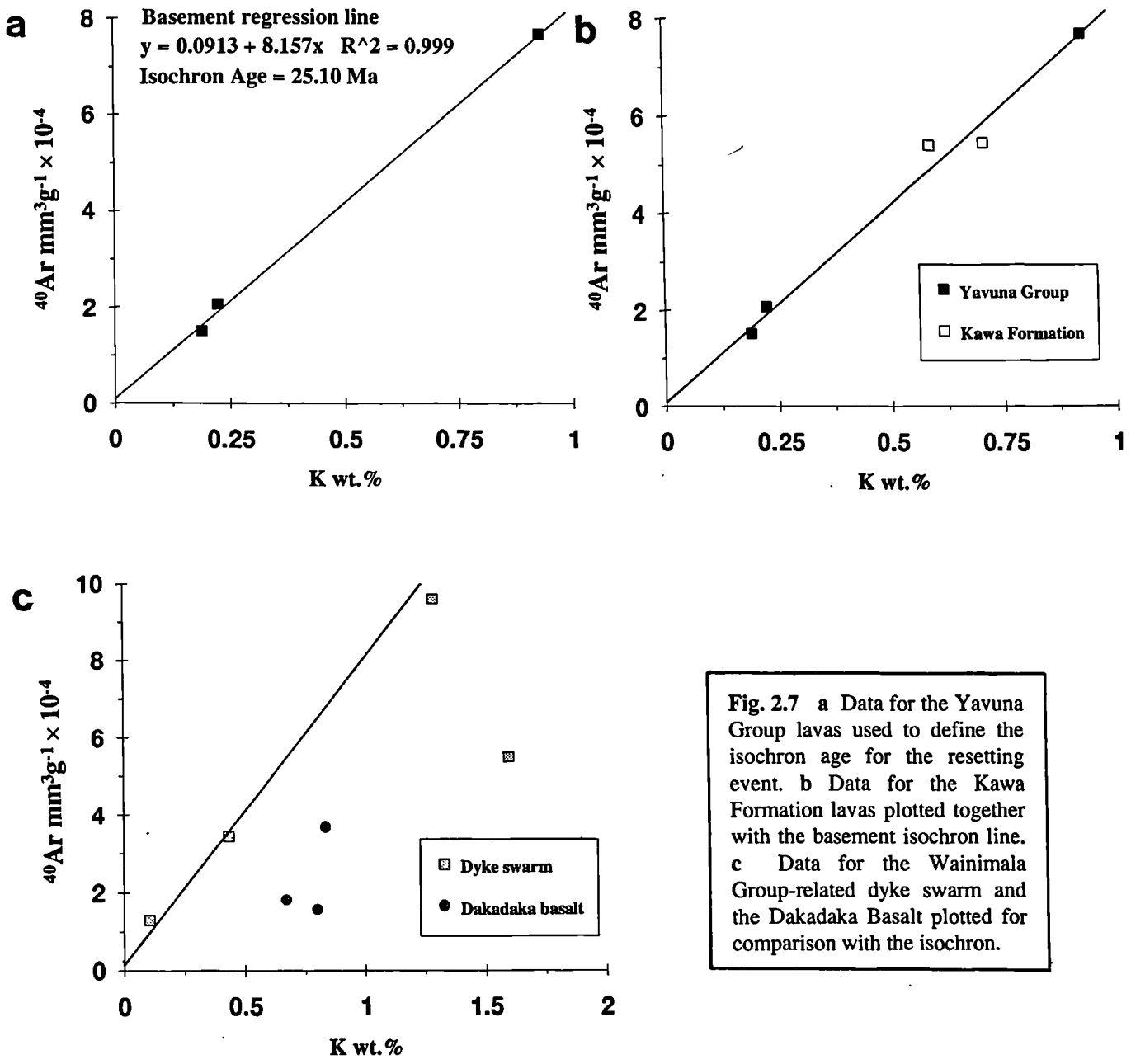

Fig. 2.7 **a** Data for the Yavuna Group lavas used to define the isochron age for the resetting event. **b** Data for the Kawa Formation lavas plotted together with the basement isochron line. **c** Data for the Wainimala Group-related dyke swarm and the Dakadaka Basalt plotted for comparison with the isochron.

2.3.3.2 The dyke swarm cutting the Yavuna Group

Radiometric dates for two members of the dyke swarm were obtained during this study. A further two samples taken at the time of the author's fieldwork have subsequently been dated by J. Gascoyne. The samples show the greatest range in ages of any group studied (30.5±22.1Ma to 10.6±0.2Ma for the four samples). Field relations link felsic members of the dyke swarm to the Kalaka Dacite, and as the bimodal sets of dykes showed at least some overlap in their intrusive history it follows from Fig. 2.2 that the basic dykes would be expected to show magmatic ages similar to or younger than those of the Kalaka Dacite. This broad upper Early Oligocene-earliest Miocene range is recorded by the two oldest samples, Site 127

(30.5±22.1Ma) and BH119 (22.9±0.4Ma) although the error estimate on the former is high. The other two samples, Site 130 and BH058 yield younger dates of 20.2±2.4Ma and 10.6Ma±0.2Ma respectively.

2.3.3.3 The Dakadaka Basalt

Three samples from the main lavafield of this Formation were analysed, together with a sample of lava occupying a similar stratigraphic in the Wainimala Group inlier in the Nadi Basin (Fig. 2.1). The samples yield radiometric ages which are clearly distinct from the biostratigraphic dates of this part of the Wainimala Group and range from 5.98±0.31Ma to 13.6±0.4Ma. The basalts are petrographically dissimilar from most other magmatic groups in their high amygdale contents (10-50%) and pervasive zeolite facies alteration assemblages. Most amygdale are filled with zeolites and brown smectite and veinlets on a mm to cm-scale pervade the majority of specimens, attesting to the passage of considerable volumes of fluids through the lavas.

Data for the dyke swarm and Dakadaka Basalt are plotted on a radiogenic ^{40}Ar versus K_2O correlation diagram in Fig. 2.7c together with the basement isochron of Fig. 2.7a. The three members of the dyke swarm with older radiometric dates plot on or slightly below the basement resetting isochron at the 95% confidence level and hence may record the age of the hydrothermal resetting event as defined by the basement isochron. The data for the Dakadaka Basalt and the younger dyke do not plot on any single regression line passing through the origin and thus cannot be interpreted to have any immediate geological significance. It appears that these samples have themselves undergone pervasive resetting during a later episode of hydrothermal activity. The preferential resetting of their radiometric dates may have been a direct consequence of their high (up to 50%) amygdale contents and porous nature (as evidenced by often dense networks of secondary veinlets pervading the lavas) which could facilitate the passage of later hydrothermal fluids. Such a resetting mechanism may also have affected the younger dyke sample, BH058, which has a high vesicle content (15%) and a reset radiometric date. Alternatively, the resetting of the Dakadaka Basalt dates could reflect the low paragenesis temperature of the zeolite facies assemblages which would be highly susceptible to K-exchange during any subsequent hydrothermal event.

2.3.4 The Colo Plutonic Suite

A major episode of intrusive igneous activity is recorded in the field area by the Colo Plutonic Suite (Fig. 2.1). Hornblende andesite dykes of this suite intrude the Yavuna

Group and the Wainimala Group and yield two sets of radiometric dates, 12.1±0.5-12.0±0.1Ma and 6.73±0.15-7.58±0.08Ma (Webb 1990, Fanning 1986). These dates compare closely with the previously reported range of ages for Colo plutons from southern Viti Levu 7.51±0.48Ma to 12.46±0.51Ma (table 3.2).

Pluton	Sample[1]	Age Ma ± 2σ
Wainamoli	AS2	9.44 ± 0.57
Korolevu	AS4	7.51 ± 0.48
Wainivalau	T25	12.46 ± 0.51
Wainiyavusewa	AS1	11.91 ± 0.26
Kabuna	NAT1	10.1 ± 1.6

[1]Analysis carried out by K-Ar on hornblende separates.

Table 2.2 Dates of Colo Plutons from southern Viti Levu (after Whelan et al. 1985)

The outcrop pattern of these plutons forms a major feature trending east-west across Viti Levu and airborne geophysical surveys over Viti Levu have indicated the presence of large areas of unroofed plutons with a similar structural trend (Hathway and Colley, in press). This large plutonic province has been interpreted as the result of an especially intense period of arc magmatism on Viti Levu (Gill 1987) and it is likely that the hydrothermal systems associated with the plutons were influential in resetting the radiometric dates of their country rocks during intrusion and cooling. In this respect it is interesting to note that analysis of tholeiitic lavas interbedded with arc assemblage sediments in southern central Viti Levu gave Ar-Ar radiometric dates of 11±1Ma (Whelan et al. 1985). The lavas, however, were sampled close to the contact of the Vanuabua Stock of the Colo Plutonic Suite, and although Whelan et al. (1985) argued that the dated lavas preserved low grade assemblages and therefore recorded actual magmatic ages, results from the Dakadaka Basalt in this study indicate that samples can retain a low grade metamorphic paragenesis yet still have their radiometric dates reset. Resetting of the low-grade sample dates by the Colo Plutonic Suite hydrothermal system provides an acceptable explanation for all of the anomalously 'young' dates which compromise the relationships indicated in Fig. 2.2.

2.3.5 Summary of controls on radiometric dating systematics

Two factors have emerged as providing the dominant controls on the resetting of radiometric dates.

(i). Later igneous episodes. The emplacement of dykes and plutons during arc volcanism is important in setting up widespread hydrothermal systems which are able to reset the radiometric dates of volcanic and plutonic country rocks. Petrological examination indicates that original low-temperature metamorphic assemblages may be fully preserved during this process.

(ii). Stability of primary metamorphic mineral paragenesis. Higher magmatic temperatures during intrusion and eruption lead to higher temperature mineral parageneses in the resulting igneous and metamorphic rocks. The occurrence of primary hornblende in the Yavuna Stock and secondary hornblende in the contact aureole was fundamental in preserving the dates of cooling and intrusion respectively during later hydrothermal events. In contrast, the zeolite facies Dakadaka Basalt was reset in preference to the greenschist and amphibolite facies rocks because later hydrothermal fluids were more easily able to disturb the K-Ar systematics of the lower temperature mineral paragenesis.

2.4 The Volcanic Stratigraphy of 'Eua, Tonga

2.4.1 Introduction

The stratigraphy of 'Eua was first described during the pioneering mapping and sampling work of Hoffmeister (1932). Subsequently, only minor modifications have been made to this overall scheme (Stearns 1971; Cunningham & Ascombe 1985; Tappin in press). The consensus map and sections of the island are illustrated in Fig. 2.8.

2.4.2 Volcanic Basement

The volcanic basement of 'Eua is exposed in parts along the eastern shoreline of the island (Fig. 2.8). Basement lithologies include coarse epiclastic rudites with angular igneous clasts and small pillow lava outcrops cut by a swarm of porphyritic andesite dykes. All of these lithologies are eroded and found as coarse debris strewn along the eastern shoreline of the island together with boulders of plutonic rocks which are not seen in situ. Scavenging amongst these boulders reveals fresher material more suited to geochemical analysis. The relationship between the igneous basement and the nearby Eocene limestone units has been described in most studies of 'Eua geology (Hoffmeister 1932; Stearns 1971; Cunningham & Ascombe 1985), however, a lack of exposure of contacts, complex faulting and reworking of sedimentary units, no

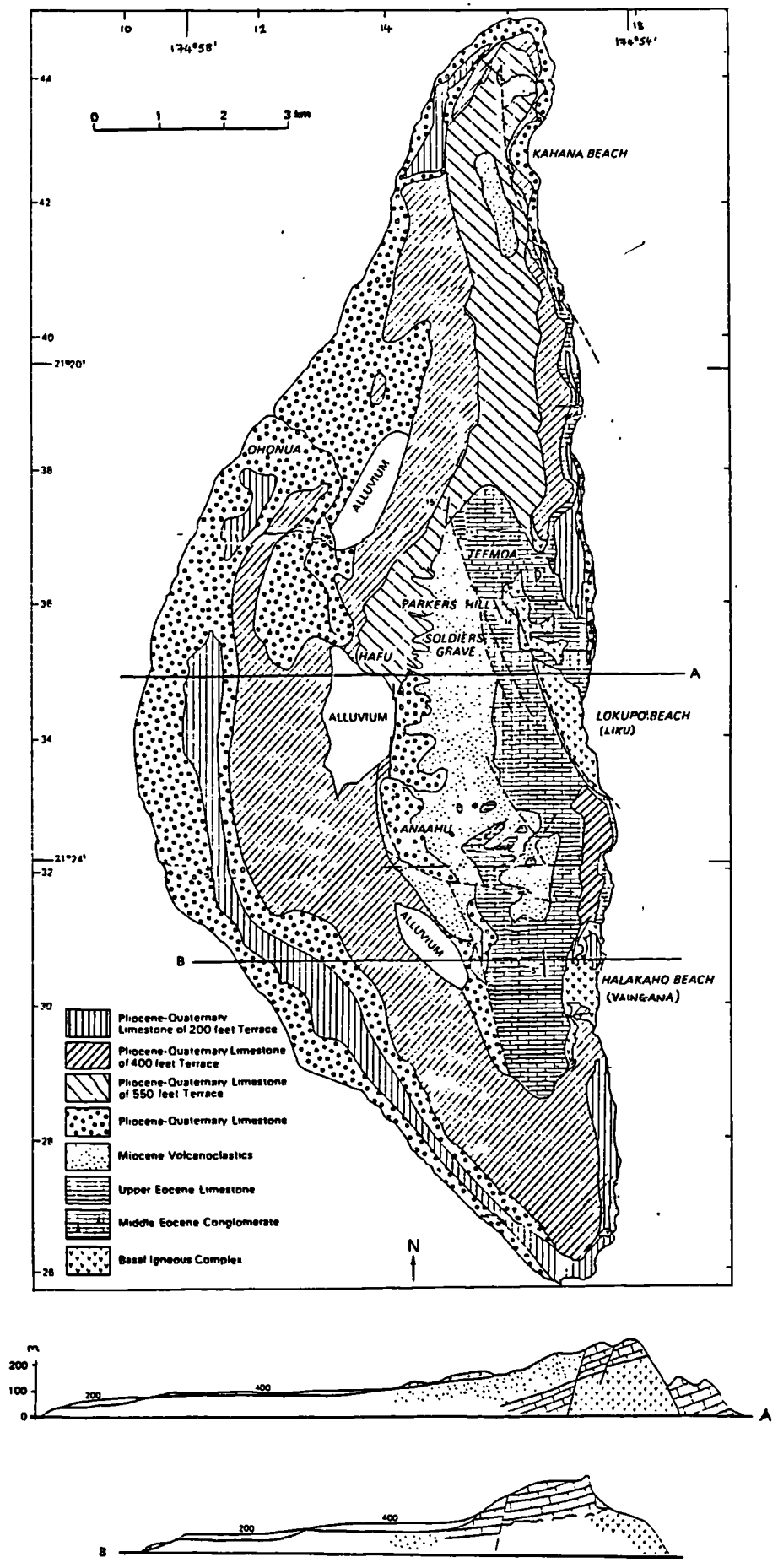

Fig. 2.8. Geological map and sections of 'Eua island. Tonga, modified from Tappin & Ballance (in press).

definitive age can be assigned to the basement through biostratigraphic methods. The size of the boulders on Liku beach (up to 35cm wide) indicates a proximal source for the igneous rocks which have probably been eroded from a nearby volcanic edifice. Similar basement lithologies have been inferred to form much of the basement of the Tonga Ridge (Duncan et al. 1985), an assertion that is supported by seismic reflection profile interpretations (Kroenke & Tongilava 1975; Herzer & Exon 1985).

2.4.3 Sedimentary geology of 'Eua

The oldest sedimentary unit on the island is a unit of Middle Eocene limestone containing reworked igneous clasts of aphyric basic lava types and coarser grained hypabyssal or plutonic material (Tappin & Ballance in press). These authors interpret the unit to represent a shallow water carbonate accumulation with input of igneous material from a nearby (?rising) hinterland. Limestones of Late Eocene age (Tertiary letter stage b) crop out to the north and south of the Tee Moa (Fig. 2.8) and differ notably from the Middle Eocene limestone by the absence of incorporated igneous clasts. No contact has been observed between the two limestone units or between the Late Eocene limestone and the basement. It is thought that contacts between the basement and limestones discovered in caves (Lowe & Gunn 1986) are probably the result of late stage cave sediment reworking (Tappin in press).

Younger volcaniclastic rocks crop out in the centre of the island (Fig. 2.8) dipping gently to the west at about 20° and showing unconformable or faulted contacts with the underlying Late Eocene limestones. The lithology comprises alternating mudstones and graded sandstones with a high carbonate component and some ash and pumice. The input of igneous material was probably derived from active volcanic centres on the Lau Ridge to the west of 'Eua at this time (Tappin in press; Whelan et al 1985). Limestones of Pliocene to Quaternary age are well exposed in the terraced cliffs and fringing reefs along the eastern seaboard of the island.

Many authors have noted that reworking of sedimentary units is a common feature of the succession on the Tonga Ridge, and as a result the stratigraphy of several units previously originally assigned on 'Eua have now been reassigned in the light of more detailed study. For example, the Upper Eocene tuffaceous marlstone of Stearns (1971), a type locality for many new species, is now considered to be a reworked submarine channel deposit of early Pliocene age (Cunningham & Ascombe 1985). The upper Middle Eocene limestone bearing igneous lithoclasts exposed on northern Liku beach has also recently been discovered to contain reworked faunas (B. Hathway,

personal communication 1991), and therefore cannot be used to provide an absolute minimum age for the igneous clasts. In view of these relationships, and also the extensive faulting along the eastern coastline, sedimentary units cannot be confidently used as dating horizons for the igneous rocks.

2.5 Radiometric dating on 'Eua

Radiometric dating on rocks from 'Eua has been carried out by two groups of scientists, whose results are summarised in table 2.3.

Sample	Lithology	Method	Age Ma±1σ	Comments
582-6-1C	Boulder, Liku beach	K-Ar[1]	19.2±0.7	Within 1σ when HF leached
582-6-1H	Boulder, Liku beach	K-Ar[1]	23.9±0.8	Within 1σ when HF leached
582-6-1L	Bas. and. boulder, Liku beach	Ar-Ar[1]	40-43	Poor Ar-Ar plateau, interpreted date
TA-6	Andesite lava flow, Vaingana	Ar-Ar[1]	32.9±1.8	Lies below Late Eocene limestone
TA-2A	Dyke, Liku beach	Ar-Ar[1]	18.3±0.8	No dykes intrude sediments on 'Eua
TA-2	Dyke, Liku beach	Ar-Ar[1]	16.6±2.0	No dykes intrude sediments on 'Eua
Eua 7	Tholeiitic basalt	Ar-Ar[2]	46.1	Analysis on plagioclase separate
Eua 18	Quartz gabbro	Ar-Ar[2]	46.6	Analysis on plagioclase separate

Sources of data: [1]Duncan et al. (1985), [2]Ewart et al. (1977).

Table 2.3 Summary of existing radiometric dates for 'Eua.

The 'Eua samples show a similar range of dates to samples of southwest Viti Levu, with the additional feature that on 'Eua, the older Eocene magmatic age is apparently preserved by some samples. Eocene radiometric dates were obtained by both groups of scientists on samples of gabbro and basic lava float, and on a porphyritic andesite boulder, presumably derived from the porphyritic andesite dyke swarm which crops out on southern Liku beach. In the absence of good stratigraphic control, the reliability of the other dates remains uncertain. Sample TA-6, an in-situ lava from the Vaingana basement outcrop has a radiometric age of 32.9±1.8Ma, although it lies in a position stratigraphically below the Upper Eocene limestone (Duncan et al. 1985). These authors suggest that the disparity may be explained by faulting of the succession, however, no such faults have been recognised in the area by this author. In the light of evidence from Viti Levu, resetting of the Vaingana data must be considered as an alternative explanation for the disparity. Magmatism at this time is recorded by a thick accumulation of Upper Eocene-Oligocene volcanogenic sediment in the well section

below Tongatapu (Cunningham & Ascombe 1985) as well as by magnetic anomalies associated with seafloor spreading in the South Fiji marginal basin. Sample TA-2A was obtained from an in-situ member of the andesite dyke swarm on southern Liku beach and yielded a date of 18.3±0.8Ma (Duncan et al. 1985). Although these authors interpret the date as recording that of the original magmatic event, no members of this dyke swarm have been recognised as cutting any of the Eocene or Miocene sedimentary units on 'Eua. The date also compromises that obtained on a lithologically and geochemically similar andesite boulder on Liku beach (40-43Ma, table 2.4). In view of the uncertainties described, the resetting of the dates obtained from in-situ dykes is considered a strong possibility.

Cunningham & Ascombe (1985) report similar equivocal radiometric K-Ar dates from the Kumimonu Nos. 1 and 2 exploration wells on Tongatapu. Here, gabbros drilled at the base of the exploration hole, below volcaniclastic rocks of Late Eocene age were dated at 13.9±1Ma and 21.3±0.4Ma. These dates were younger than those of the overlying sediments and thus the gabbros represent either Miocene sill-like intrusive rocks or basement rocks whose radiometric dates have been reset.

2.6 Regional correlations

As in other recent studies of island arc basement rocks, radiometric dating of the oldest lithologies on Viti Levu is only partially successful in revealing the magmatic ages of the volcanic edifices. The broad Late Eocene age revealed from biostratigraphic age cannot therefore be refined further using these methods. In contrast, some radiometric dates on 'Eua probably do record basement magmatic ages in broad agreement with the biostratigraphy. The results from Viti Levu and 'Eua can be compared to radiometric dates obtained on samples of ancient island arc basement in the Izu-Bonin forearc which was drilled by scientists during Leg 125 of the Ocean Drilling Program (Mitchell et al. 1992). These authors were successful in producing isochron dates for magmatic episodes at 41.3±0.5Ma (10 samples) and 34.6±0.7Ma (10 samples). The earlier isochron date adds to the general consensus of an episode of volcanism marking the initiation of Western Pacific subduction at 43.1±1.4Ma, as a result of the major change in absolute motion of the Pacific Plate (Clague & Dalrymple 1987). Whilst the Late Eocene minimum age for the Viti Levu basement supports this interpretation, the inferred Middle Eocene age of the 'Eua basement most likely pre-dates the 43Ma event, in common with a limited number of radiometric and biostratigraphic dates from the Northwest Pacific Arc Province e.g. Middle Eocene radiometric and biostratigraphic dates on boninite from Chichi-jima (Dobson 1986). The Early

Oligocene date of 34.6±0.7Ma from the ODP Leg 125 study was obtained both on dykes and sills which intrude the volcanic basement and on samples from the older basement whose radiometric dates had been reset. The authors link this event to extension recorded within the forearc region and to rifting of the protoarc edifice during earliest spreading in the Parece Vela marginal basin. On Viti Levu, a similar Early Oligocene date is recorded both in the primary igneous minerals and contact metamorphic minerals of the Yavuna Stock, while on 'Eua, the date is also recorded in lava flows from the Vaingana locality. As in the case of the northwestern Pacific arc province, rifting associated with marginal basin formation occurred in the southwest part of the province at this time and was recorded in the earliest magnetic anomalies of the South Fiji marginal basin (Weissel & Watts 1977; Davey 1982).

CHAPTER 3

Fieldwork

3.1 Introduction

This chapter describes fieldwork carried out in Viti Levu and 'Eua during two seven week field seasons in 1989 and 1990. In the case of 'Eua, rocks were sampled for geochemical analysis using the volcano-stratigraphic scheme established by previous workers and discussed in chapter 2. In Viti Levu, a fault-corrected reconstruction of the stratigraphy of the Yavuna Group is made in order to facilitate comparisons of creek sections up to 30km apart. The creek sections traversed are described and integrated into a model for crustal accretion in the protoarc.

The volcanological and structural geology of the Wainimala Group basinal assemblage is also described. The assemblage is further sub-divided into the principal volcanic edifice and inter-edifice terranes which show many of the geological features recognised in modern intra-oceanic arcs.

3.1.1 Access and exposure

The southwest Viti Levu field area is largely composed of rural farming land with a range in elevation from close to sea-level to over 1070m around Koromba summit. Previous studies of the oldest rocks have always been limited by problems of access in areas remote from the Nadi township, however, this situation has recently improved due to a network of new roads built by timber companies for the export of softwoods from the island's interior. The roads afford good access for a 4WD vehicle and most parts of the area can now be reached in a day by a drive and a walk. On 'Eua, access to the volcanic basement on Liku beach is easy, via a vehicle from the motel on the island's central road and a walk from the top of the 120m' limestone terrace down to sea-level.

3.1.2 Sampling strategy

As in many island arcs of the SW Pacific, tropical weathering has had an adverse effect on exposed rock; the intensity of the process on Viti Levu can be judged from the development of soil from fresh rock in roadcuts that are two years old. The problem is overcome, however, by better exposure in the freshwater creeks which drain the higher land in the south and east of the area and, although many of the creeks have sinuous courses and steep banks, it is usually possible to locate and fix a sampling position with the aid of a compass and aerial photographs. On 'Eua too, exposures are heavily weathered and here the freshest igneous material is often found among the basement derived boulders strewn across the beach. In addition to the problems of weathering, secondary hydrothermal alteration affects the volcanic rocks of both islands to the extent that fresh volcanic material is rarely found. Consequently, rock material taken for geochemical analysis was usually from the least altered parts of rims or cores of pillow lavas and dykes, whilst sampling of massive lavas concentrated on collection of the freshest material, usually as small rock chips. In the case of coarsely crystalline units such as gabbros and tonalites, larger samples were taken to reduce the possibility of crystal accumulation bias occurring during geochemical analysis.

The strategy adopted for sampling the large areas of Yavuna Group lava field was to traverse a number of creek sections through successively higher stratigraphic levels in the Yavuna Group, and supplement this information with samples from isolated outcrops between the creek sections. During this work, sampling of the Yavuna Stock was included in one traverse to supplement the gridwise sampling carried out in the 1970's by H. Colley. Wainimala Group lithologies and rocks of later volcanic episodes were sampled both during the creek traverses and during visits to specific localities in and around the margins of the Yavuna Group outcrop. In all cases the field terminology of previous authors is maintained, and modified terminology is only introduced during discussion of major and trace element geochemistry in chapter 5.

3.2 The Yavuna Group lava field

3.2.1 Structure

A volcanic stratigraphy for the Yavuna Group has been produced by projecting measured volcanic sections through the lava pile onto a single plane that enables correlations across the basement block to be made over a horizontal distance of some

30km. The vertical datum used for the projection plane was sea-level as taken from the Viti Levu 1:50000 series X754 map sheets. The horizontal base-line for the projection plane is drawn normal to the predominant topographic grain across the area i.e. normal to the drainage pattern across the area (Fig. 3.1). Correlation between traversed sections is then made in a primary sense by assuming that structural level within the lava field is related to topographic elevation (Fig. 3.2). The major columns drawn represent traversed creek sections, and samples collected from nearby ridges are included within the columns, their level depending upon the confidence with which a particular correlation can be made e.g. similarity of lava morphology or inter-lava matrix.

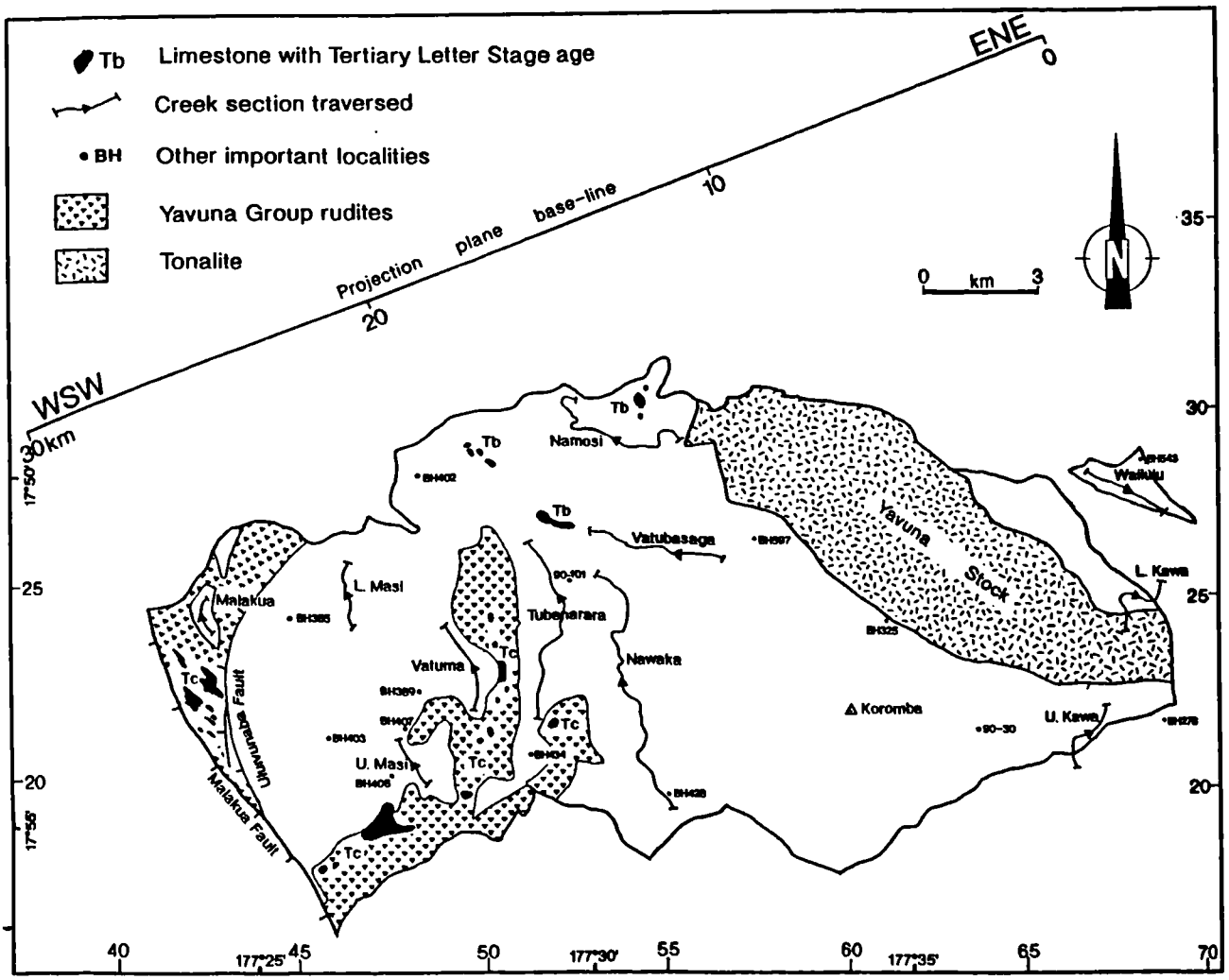

Fig. 3.1 Map to illustrate the location of the projection plane base-line normal to the pattern of drainage across the Yavuna Group outcrop. Creek sections and important individual localities are also annotated.

Having established a primary projection, corrections are then applied to the scheme using three secondary criteria:

(i) Restoring for the effects of known fault displacements.

(ii) Correlation of autochthonous sediments interbedded with the lavas.

(iii) Correlation of horizons of specific geochemical lava type within the stratigraphy.

Where faults cut through the basement lavas, they are usually recognised as zones of brittle fracture and are characterised by concentrations of angular volcanic protolith fragments. The fault zones are variable in width up to several metres across, however, because of the isolated nature of outcrops and the effects of later intrusions, they cannot be traced over great distances in any creek section. At the western margin of the block, major faults which cut and bound the basement block e.g. the Uluivunaba and Malakua faults, show evidence for significant normal movement (Hathway in press a). Correction for this normal offset is made by restoring the contact between basic lavas and the overlying breccia units in this area.

Within the central part of the Yavuna Group outcrop most of the mapped fault zones document small-scale transcurrent displacement of basement lithologies (Table 3.1).

Area	Type of deformation
Upper Nawaka Creek.	Fault sub-parallel to Wainimala Group dyke swarm.
Tubenarara Creek	Arcuate 100m wide N-S fault zone cuts Yavuna Group and Wainimala Group dyke swarm at a low angle. Dykes skewed around from N-NW trend to strike 100°-115° indicating sinistral shear.
Namulomulo Limestone	Series of silicified NNE striking shear zones subparallel to local strike of Wainimala Group dyke swarm.
East of Uluivunaba Fault	Zone of crushing and dislocation.
East of Takara Stock	Sinistral transcurrent faults affect Colo intrusives as well as basement lithologies indicating Late Miocene deformation.
Vatubasaga Creek	WNW-ESE striking fault probably an extension of the above fault zone.
Nawaqadamu Area.	NE striking rectilinear minor faults - affect both Wainimala Group and Yavuna Group country rocks. May be related to the parallel-oriented Colo dyke swarm to the north.
West of Koromba.	Closely spaced photo-lineaments with a similar trend to above.
South of Malakua Creek	Possible almost isoclinal folds (first recognised by Houtz 1959). Probably locally intense deformation associated with late rotation of the Yavuna Block.

Table 3.1 Mapped zones of deformation affecting Yavuna Group lavas (summarised in part from Hathway et al. in prep.).

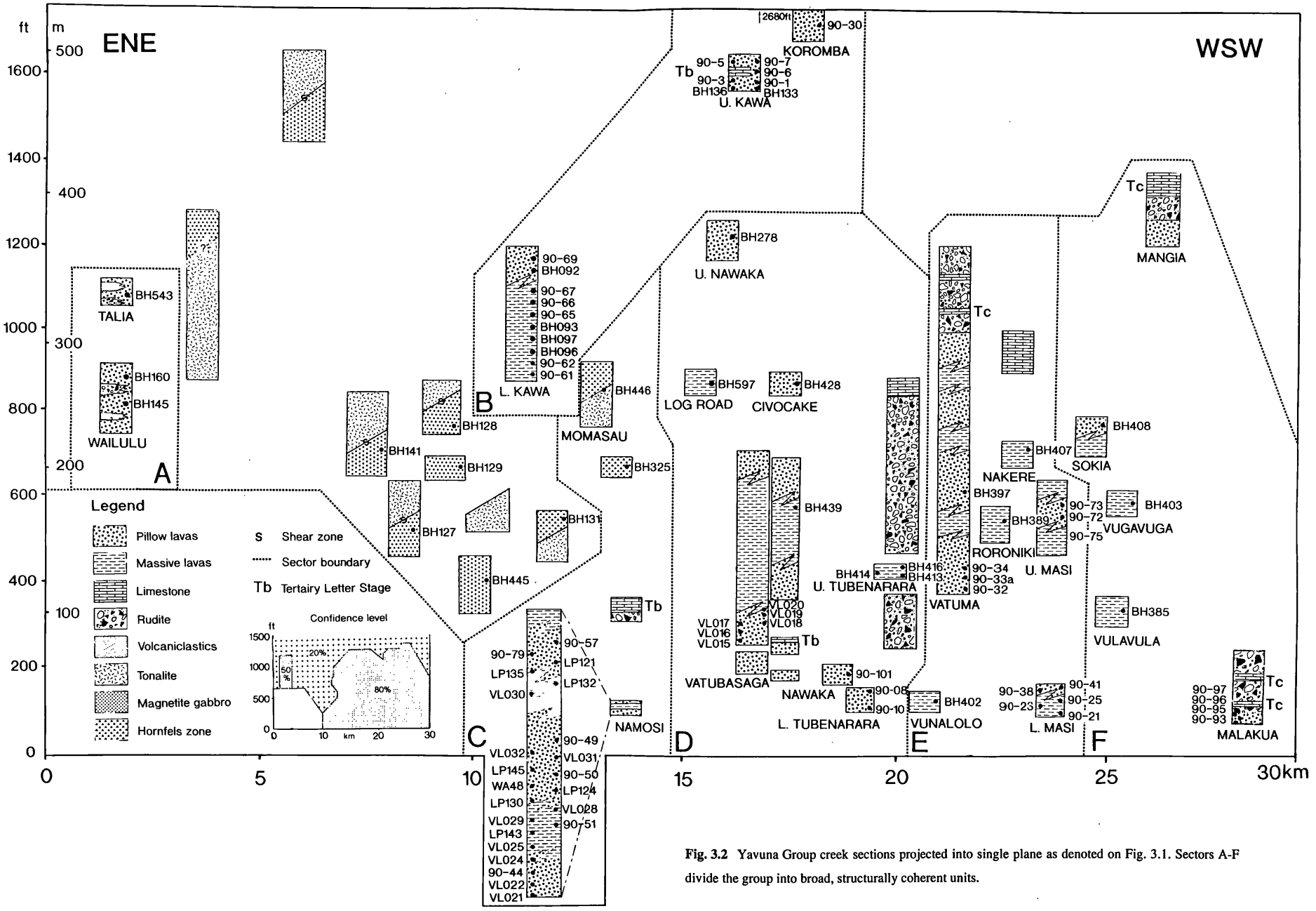

Fig. 3.2 Yavuna Group creek sections projected into single plane as denoted on Fig. 3.1. Sectors A-F divide the group into broad, structurally coherent units.

Inspection of regional fault patterns (Fig. 3.3) indicates that the Yavuna Group may have acted as a coherent fault-bounded block during the broadly E-W-directed sinistral strike-slip deformation which affected Viti Levu in the Late Miocene (Hathway 1993). The implications for such a model on the Yavuna Group are that the majority of deformation would occur at the margins of the rigid basement block where accommodation structures such as folds and faults would be expected to develop (Mandl 1987). Such zones of complexity are clearly recognised by other workers (e.g. Houtz 1959, Hathway in press a) and are reflected in the confidence levels given to the various creek traverses in the projection of Fig. 3.2. In the areas of greatest confidence, clear between-sector correlations are apparent both in the position of stratigraphic marker horizons such as the Late Eocene (Tertiary Letter Stage b) limestones and in the occurrence of geochemically similar lava types (discussed in full in chapter 5).

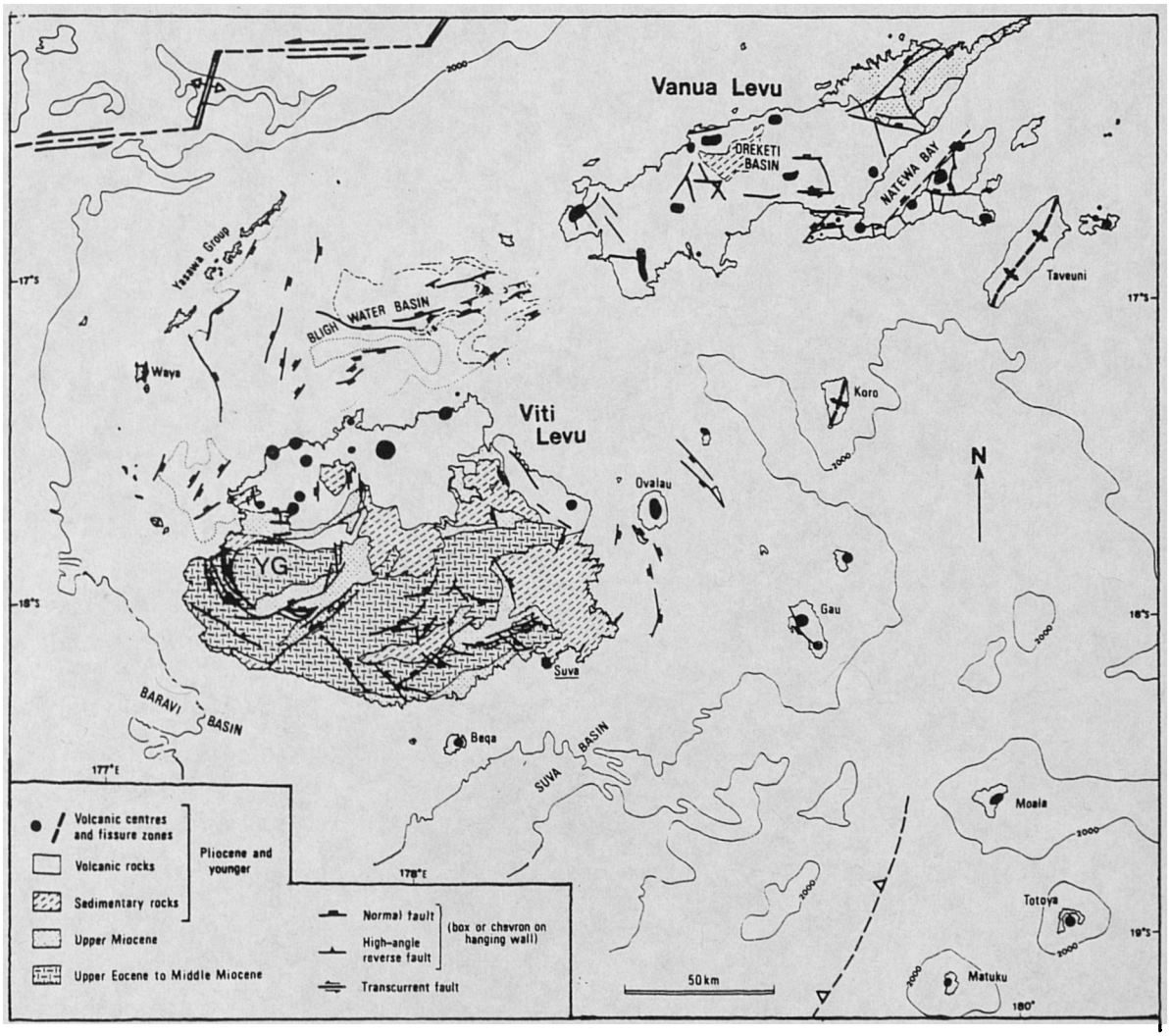

Fig. 3.3 Regional fault patterns indicating the position of the Yavuna Group as a faulted-bounded block within an E-W directed strike-slip deformation zone (modified from Hathway 1993).

In the central-eastern part of the Yavuna Group outcrop, particularly around the Yavuna Stock, structural relations are more complex and the resulting uncertainty is reflected in the low confidence level assigned to the position of these sections in the reconstruction (Fig. 3.2). Faulting is recognised in many parts of the Yavuna Stock and, along the northeastern margin of the main intrusion, pervasive shearing marks the boundary between the basic cumulates and the felsic portion of the pluton. Unfortunately, the faults cannot be traced over significant lateral distances because of the lack of suitable exposures and inaccessible terrain. Given the complexity of these relationships, secondary correlation criteria as listed above are used to correct this part of the stratigraphic scheme. The Kawa Creek section is correlated with the lower parts of sectors B and D on the basis of the interbedded Late Eocene stratigraphic markers in the upper part of the section where the fauna resembles directly that present in the Vatubasaga Limestone Member in the northern part of the Yavuna Group outcrop (Hathway et al. in prep.). This part of the reconstruction is further supported by distinctive geochemical signatures of the lavas in the section which show close correspondence to those of lower sector B (chapter 5). These correlations imply a total throw of ~400m over the 10km horizontal distance between the Upper Kawa Creek and Namosi Creek sections.

The fault bounded block around Talia Creek and Wailulu Creek forms the ENE-extreme of the stratigraphic reconstruction (Fig. 3.2). This area has been visited by B. Hathway who collected pillow lava samples from the area and reports a significant sedimentary component to the section including highly indurated sandstones, basaltic rudites and vitric tuffs interbedded with the lavas (Hathway et al. in prep.). The sandstones vary between fine lamellae interbedded with mudstones to one metre thick massive units. Tuff units are finely laminated, range from 10cm to 2m in thickness, and document a significant contribution of material derived from subaerially erupting volcanic edifices. In the absence of good structural control the sector is assumed to have retained its stratigraphic integrity and so provide evidence of increased protoarc maturity which shortly predates the edifice reworking documented by the upper Yavuna Group rudite units.

Fig. 3.4 shows the reconstructed volcanic stratigraphy of the Yavuna Group lava field based upon the preceding discussion. Several important points arise from the proposed reconstruction.

(i) The deepest and oldest areas of the lava field are exposed in the central-north and central-eastern parts of the Yavuna Group outcrop in the Namosi Creek and Kawa Creek sections.

(ii) There is a broad progression from interbedded pillowed and massive lavas to pillow lavas is recognised within the lava-field. Significant primary and reworked volcaniclastic material in the upper parts of the group document the emergence and erosion of protoarc edifices by the Early Oligocene.

(iii) An estimate of the total thickness of the lava pile can be made. From the base of the Namosi Creek section to the upper parts of the Votuma Creek section a minimum thickness of approximately 375m (1225ft) of lava is exposed.

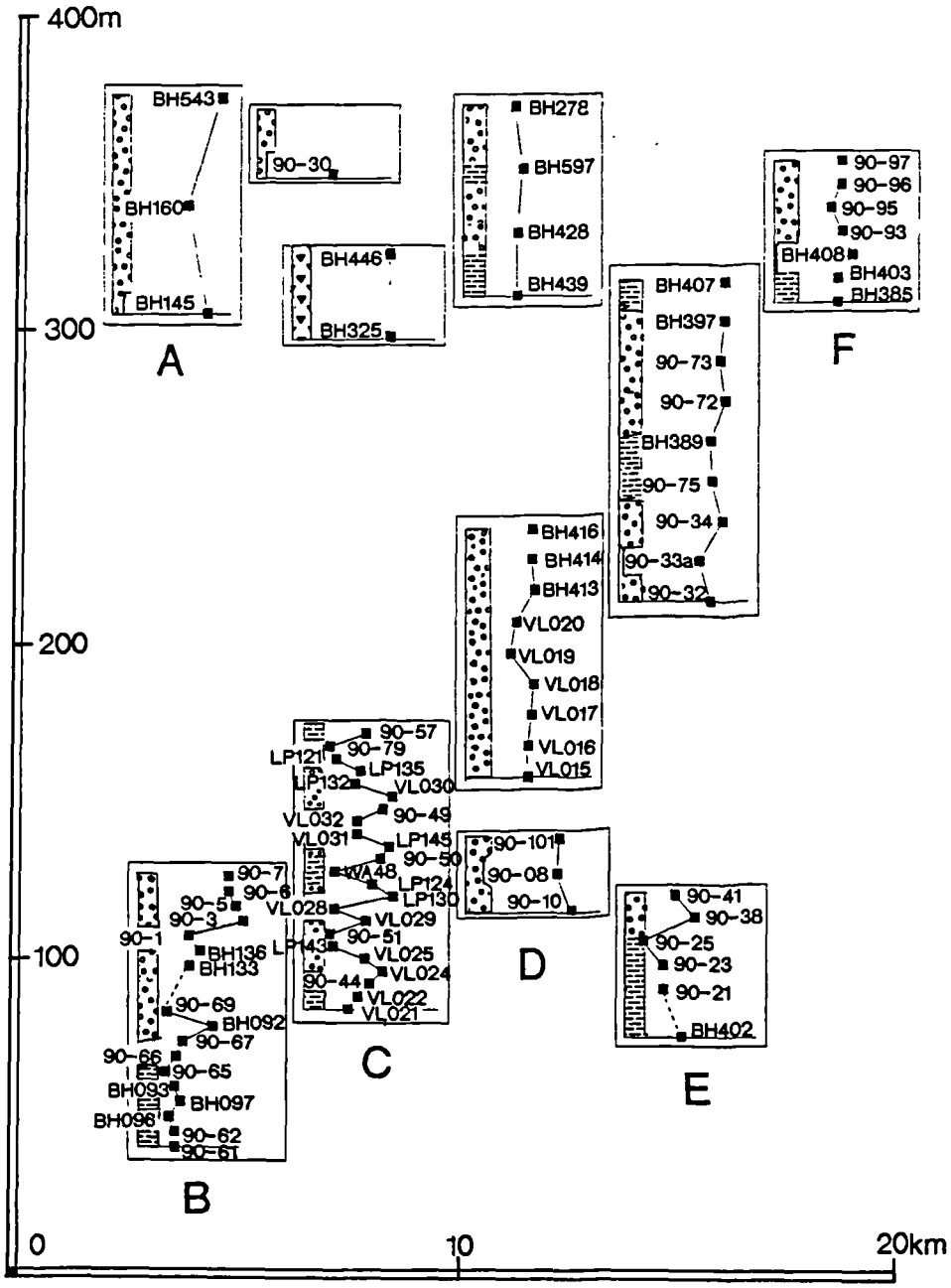

Fig. 3.4 Reconstruction of the Yavuna Group volcanic stratigraphy as described in text with effects of faulting and later intrusions removed.

3.2.1.1 Further stratigraphic divisions ?

In the northern part of the western Pacific arc province, other authors have used similar schemes as a basis for formal divisions of the volcanic stratigraphy into separate formations. For example, on Guam (Fig. 1.2), Reagan & Meijer (1984) divide major Eocene and Oligocene volcanic units into the *Facpi* and *Alutom Formations* respectively while on Saipan, Reagan et al. (1983) describe Eocene boninite dacites of the *Sankakuyama Formation* overlain by andesitic pyroclastic rocks and lavas of the Eocene-Oligocene *Hagman Formation*. In the Bonin islands, part of the Ogasawara Ridge (Fig. 1.2), Chichi-jima island, is divided into the *Marubewan Formation* comprising pillowed and massive lavas, breccia of boninite, bronzite andesite and dacitic composition; the *Asahiyama Formation* which comprises quartz dacite and rhyolite flows; and the *Mikazukiyama Formation* which comprises volcaniclastic sandstone and breccia (Pearce et al. 1992b, summarised from Umino 1985; Maruyama & Kuramoto 1981; and Dobson 1986). In all of the above cases, divisions are usually made on the basis of lithological boundaries mapped in the field. According to field-based criteria, a case could certainly be made for separating the sector A traverses of Fig. 3.2 from the remainder of the group on the grounds of its high sedimentary component. An alternative interpretation, however, would put the section as part of a gradational transition into the coarse reworked rudite units in the upper parts of sectors E and F. The merits of possible formal subdivisions are further discussed in chapter 7 in the light of geochemical evidence from the various sectors.

3.2.2 Creek traverses

The creek traverses are now described in detail. Fig. 3.1 shows the Yavuna Group outcrop and surrounding area and indicates the ten sections traversed as well as several important isolated outcrops. Grid references cited refer to the widely used Viti Levu 1:50000 series X754 map sheets.

3.2.2.1 Namosi Creek

The Namosi Creek section is the subject of particularly detailed study. As well as being easily accessible from several roads, it provides good exposure through the lowest parts of the lava pile from lavas interbedded with Late Eocene limestones in the north of the Yavuna Group outcrop, upstream to lavas intruded by the Yavuna Stock in the east (Fig. 3.1). Outcrops occur as isolated bodies along the creek course and rarely extend for more than a few metres.

The lower part of the section begins at the unconformity with the overlying Nadi Group rudites (WF522305). Typical outcrops of basement rock are 2-5m across and are mostly pillow lavas (Plate 3.1) which grade locally into massive lavas (Plate 3.2). The pillow lavas range between brown or grey-green in colour and are aphyric with purple or black glassy rinds sometimes developed. They range in size from 20cm to 80cm in width and are both rounded and elongate in form. The attitudes of the elongate pillows can be used to provide an estimate of structural attitude, however, in some cases the elongate forms are due to draping over constructional features prior to cooling. Pillow lava outcrops also pass laterally into pillow breccias which comprise particles of fragmented pillow lava with preserved glassy chilled margins set in a fused matrix of small glassy angular particles. These areas of hyaloclastite breccia are highly permeable and are often the site of intense secondary alteration marked by veins and clots of epidote and chlorite up to 30cm across. A 5m thick horizon of dacitic tuff and volcaniclastic debris dipping to the NE is interbedded with pillow lavas at the base of the section (Hathway et al. in prep.).

Higher in the section, well exposed lavas give way to a unit of massive microgabbro (WF533924). Within the microgabbro, metre-spaced zones of intense shearing are seen. Another smaller outcrop of a similar microgabbro lithology is gradational into the pillow lava, suggesting a common age for the lithologies, however, the zones of shearing are not seen in the adjacent pillow lavas. Pillow lavas exposed along the track directly above the microgabbro show a well defined sheet dip of 25° to the SE and probably represent a constructional pile draped over a central mound that is now occupied by the microgabbro. The edges of the pillow mound are gradational into massive lava and the whole section may represent part of a single volcanic eruptive centre.

Highly vesicular or amygdaloidal lava is occasionally encountered in the section. This lava type is cut through by networks of mm to cm-scale veins which contain secondary minerals, predominantly calcite and quartz. At one exposure, (WF523306), an inter-pillow matrix of red calcareous ooze is present indicating a period of eruptive quiescence, and probably relatively deep water conditions. Networks of small brittle faults cut both of the main lava types. The fault traces have no consistent orientation within the section but are locally highly disruptive and are best described as zones of crushing. They vary in width from a few cm to about 50cm in width, but due to the nature of the isolated exposures, the extent of individual faults is unknown. Kinematic indicators within the crush zones are not clearly displayed, and consequently, the extent of fault displacement cannot usually be measured. Other small faults appear directly

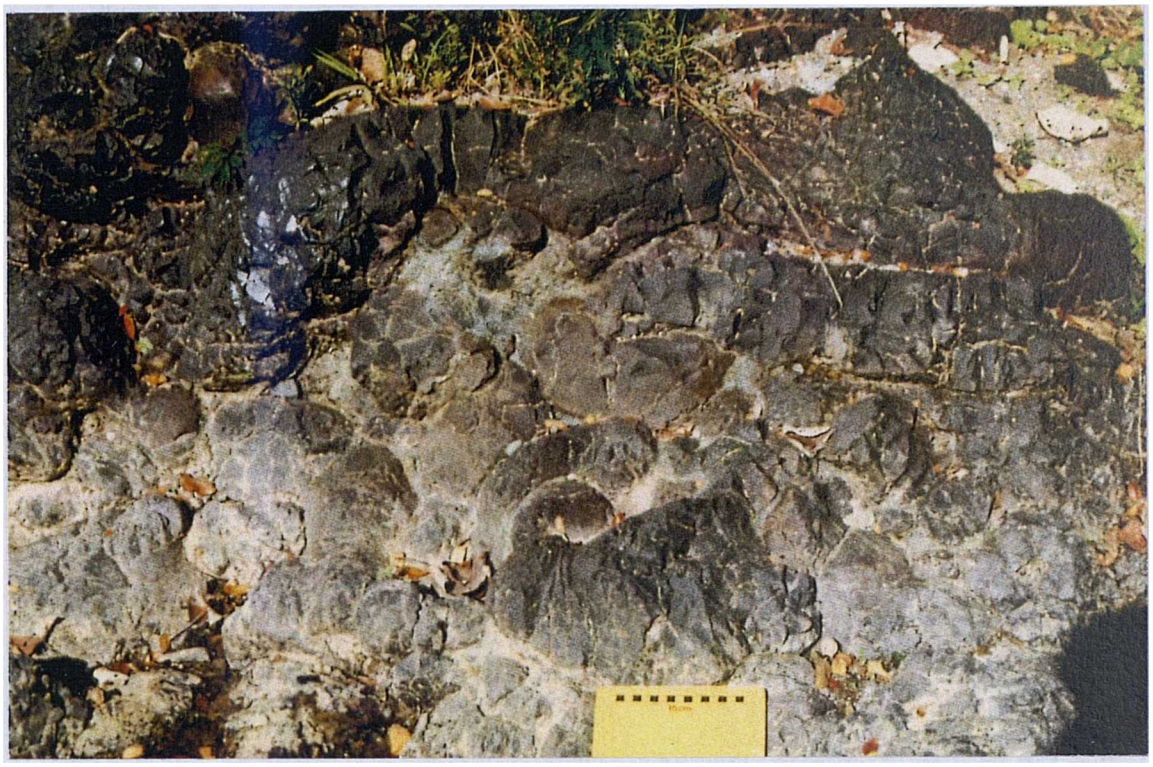

Plate 3.1 Dark brown weathered pillow lavas, Namosi Creek. Note elongate form of some pillows which may have acted as conduits to feed new pillow lavas at the edge of the constructional pile.

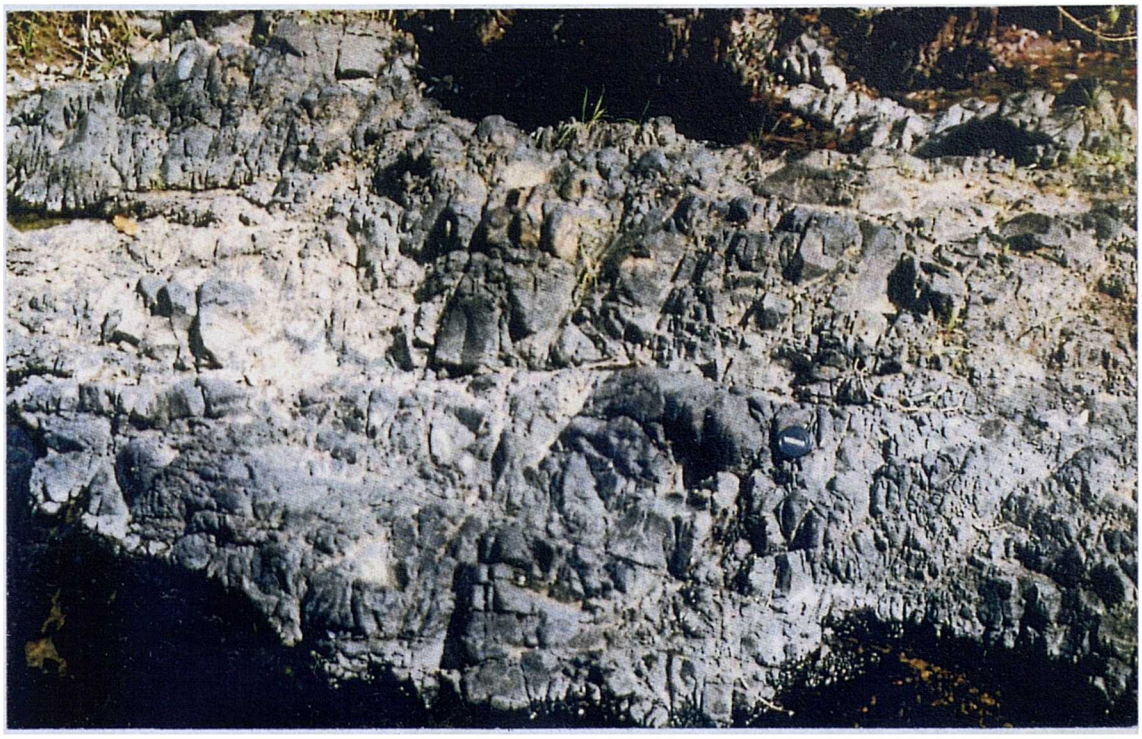

Plate 3.2 Pale-dark grey massive lavas, Namosi Creek. Outcrops grade locally into pillow lavas and are characterised by trellis-pattern fracture surfaces.

associated with horizons of talus between conformable pillow sequences; these areas probably represent small-scale scarp reworking from syn-volcanic faults.

Two basic dykes assigned to the Yavuna Group were seen in the Namosi Creek section. The dykes are clearly distinguished from the later, blue-grey, Wainimala Group-related dykes by their grey-green colour, sinuous margins, and their heavily altered and bleached form which resembles that of the lavas. These dykes have rare equivalents in other sections, notably Kawa Creek. The late blue-grey dykes in the section show generally NW-SE orientations and often weathered-out from the basement lavas by several tens of centimetres. No cross-cutting relationships are seen within the swarm and the dykes are estimated to comprise about 10-15% of the crustal section.

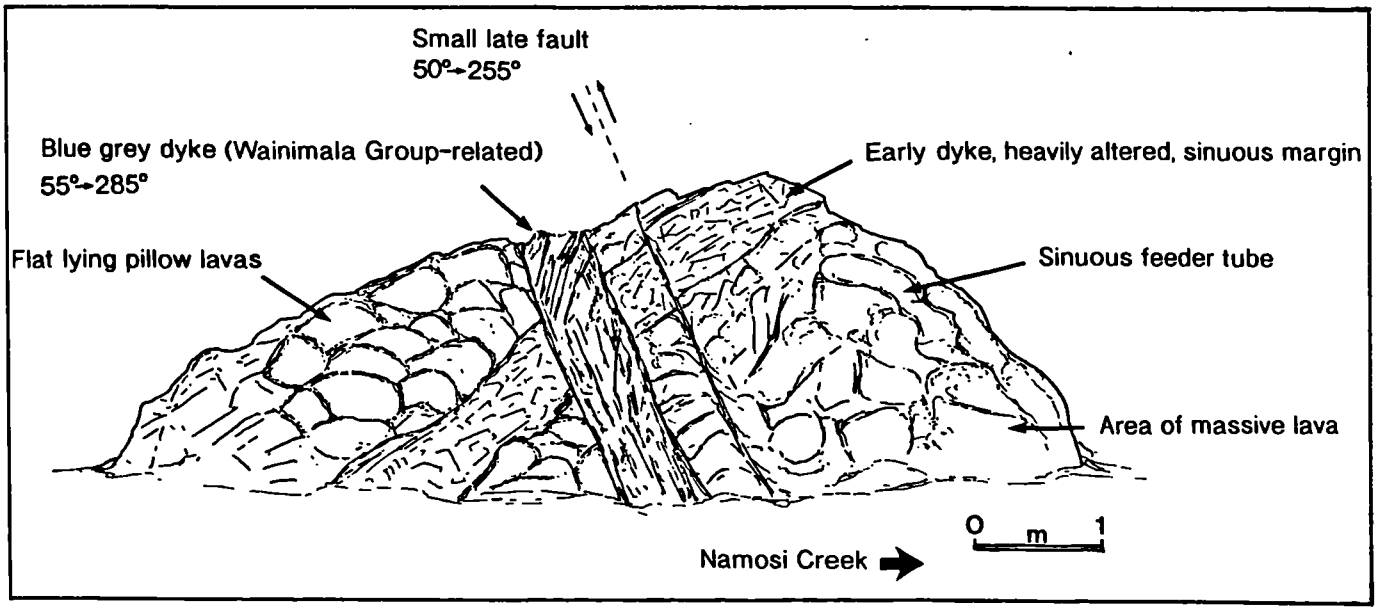

Fig. 3.5 Field sketch to illustrate relationships between dykes and lavas in Namosi Creek section.

The central part of the Namosi Creek section has fewer exposures. It includes the small hills to the north of the creek where Late Eocene limestones included in the Vatubasaga Limestone Member are interbedded with Yavuna Group pillow lavas (WF542300). The base of the hill comprises pillow lava breccia cut by numerous small faults. Subangular volcanic clasts up to 20cm wide were recovered from a matrix of fine-grained, deeply weathered, volcanic particles. The breccia grades laterally into volcanic sandstone composed of small angular basic fragments indicating that the unit is reworked rather than primary. The association with faulting suggests a talus deposit origin at the base of a small uplifted fault scarp.

Above the breccia an area of poor exposure gives way to pillow lavas which are deeply weathered to a soft matrix of brown clay minerals. Removal of several centimetres of

this covering reveals an interior of dark brown heavily weathered basic lava in which amygdales filled by calcite are preserved (Plate 3.3). Complete pillow lava outlines can be traced in the weathered outcrop and have widths of 30-40cm (Fig 3.6). The pillows are flat lying and intact at the contact with the limestone. There is no evidence for tectonism along the contact as suggested by previous workers (T. Vallier, personal communication, 1990). The limestone unit lies conformably on top of the pillow lavas and at its base, contains small particles of volcanic debris which define a crude, flat-lying bedding surface. The top of the limestone unit is not exposed but the lower contact is visible on other areas of high ground close to the hill, where it can be traced by the appearance of the distinctive yellow soil formed by decomposition of the limestone. Samples from this limestone are included in the detailed faunal descriptions which confer a Late Eocene (Tertiary Letter Stage b) age on the unit (Cole 1960; Hathway et al. in prep.). The limestones are largely detrital coralline pack stones, deposited on open marine shoals at depths of 20-100m (Hathway & Colley in press). One felsic dyke is seen cutting an outcrop of the breccia unit, but cannot be traced to other outcrops. The dyke is 80cm wide and steeply dipping with a NNE-SSW trend and contains small quartz phenocrysts set in a pale grey, glassy matrix. Other minor felsic dykes of this type occur within a minor swarm in this area (B. Hathway, personal communication 1990), and are assigned to the Yavuna Group by virtue of their close spatial association with the felsic tuffs and volcaniclastics in the section.

One sill-like exposure of Wainimala Group-related dacite occurs in the central part of the section. It crops out along a shear zone in a unit of massive basement lava and sends apophyses into the country rock in which small pods of pyrite-dominated mineralisation are concentrated. The dacite is cut by a later basic dyke which has glassy chilled margins and no apophyses.

The upper reaches of Namosi Creek were traversed from Yavuna village downstream through the tonalite contact which is crossed several times in the section due to both its faulted nature and the sinuous course of the creek. Small exposures of Yavuna Group country rock consist of a massive hornfels metabasite lithology with a mineral assemblage dominated by hornblende and plagioclase. These higher grade mineral assemblages result from contact heating during intrusion of the Yavuna Stock. Original igneous textures are destroyed within the hornfels zone which persists over distances of several hundred metres away from the contact. This part of the Namosi Creek section contains the greatest concentration of Wainimala Group-related dykes which comprise about 50-60% of the crustal section (Plate 3.4). The dykes are of the basic type and locally occur in composite form with internal margins that mark up to four bursts of

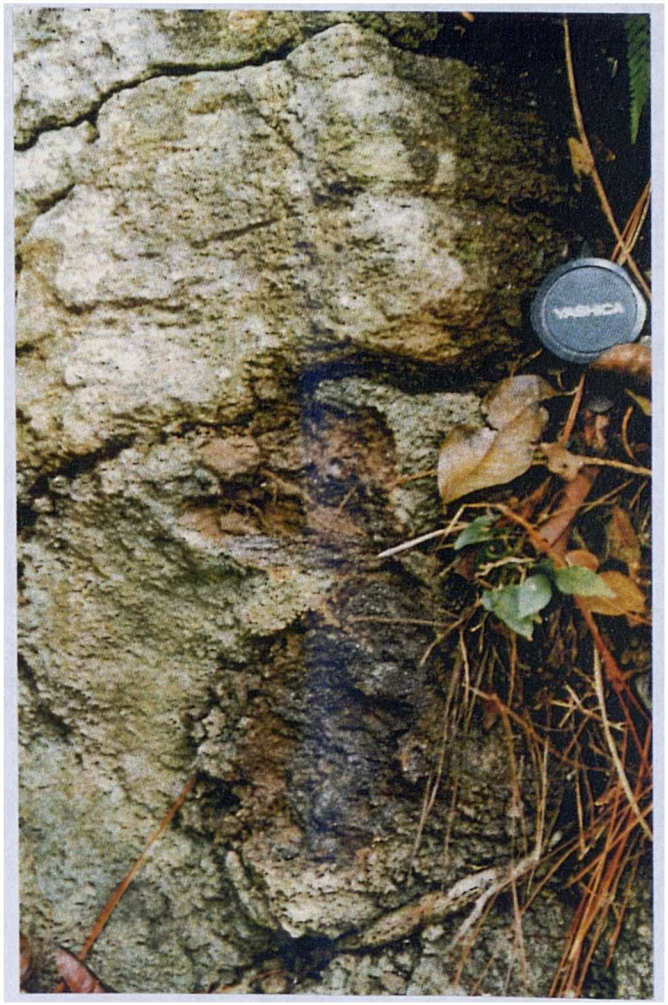

Plate 3.3 and Fig. 3.6 Photo and interpretation of interbedded pillow lavas and limestones of the Vatubasaga Limestone Member. The rocks are exposed on the banks of a dry stream-bed on the small hills north of central Namosi Creek section.

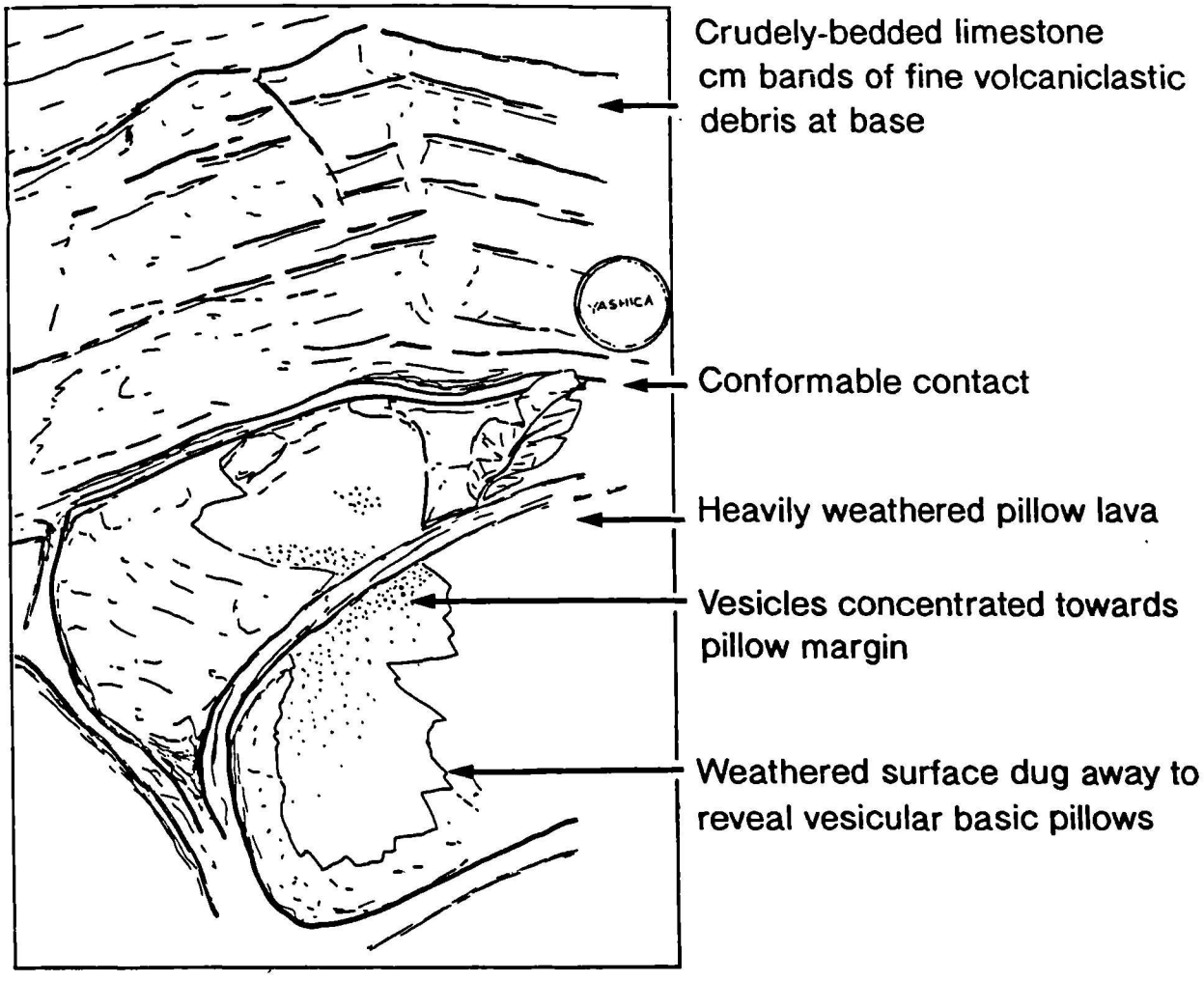

basic magma through a single fissure (Plate 3.5). In all cases, the internal margins of the multiple dykes are chilled and glassy and have a similar strike.

One Wainimala Group-related composite dyke was observed in this part of the section (Fig. 3.7). Although dykes of this type of dyke are rare, they provide important evidence for the synchronous generation of basic and felsic magmas in the basinal assemblage of the Wainimala Group. The initial intrusion was of the common basic dyke type and has a sharp 3-5cm wide chilled margin against the trondhjemite country rock. It was subsequently bisected by a felsic dyke with a 7-10cm wide diffuse and gradational contact, indicating that the earlier basic intrusion had not completely cooled. The felsic dyke is itself bisected by another basic dyke which forms the core of the composite intrusion. The margin of the central dyke is complex and lobate in form and is characterised by the development of mixed zones up to 1m across that contain basic blebs surrounded by intermediate composition dyke material. These blebs are interpreted as remnants of the core material that have remained isolated from any mixing and re-equilibration with the earlier felsic magma.

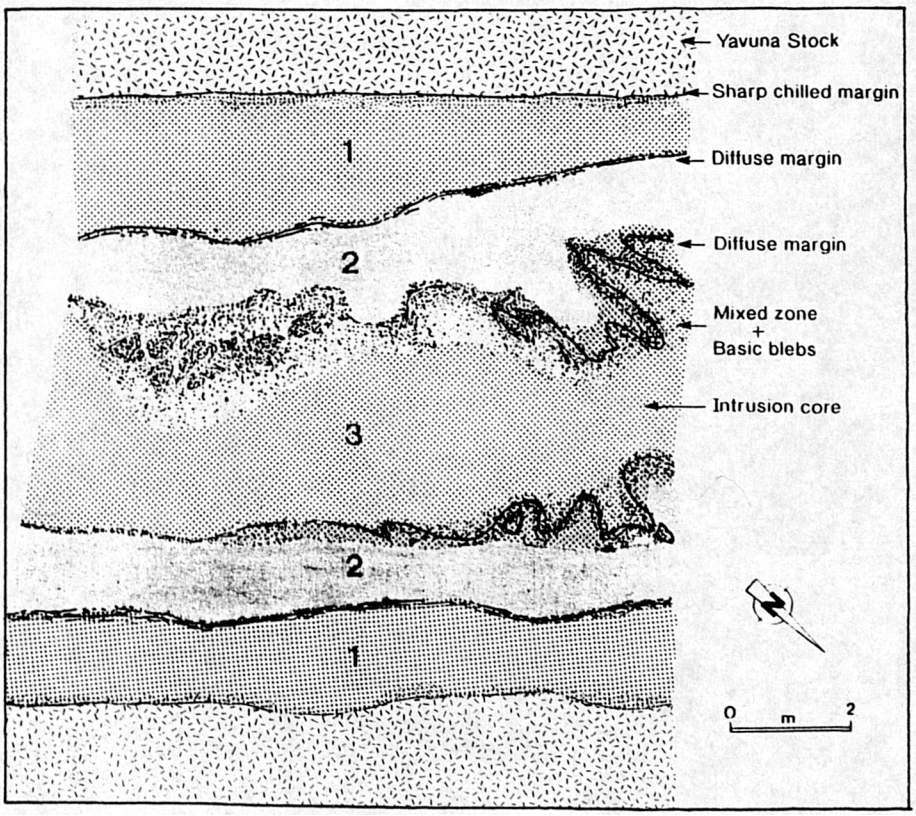

Fig. 3.7 Field sketch to illustrate field relations in composite dyke in upper Namosi Creek section. Numbers indicate order of basic and felsic intrusions.

Plate 3.4 Wainimala Group-related basic dykes intruding Yavuna Stock in upper Namosi Creek. Dykes are most commonly 2-5m wide and have glassy, cm-scale chilled margins against the tonalite.

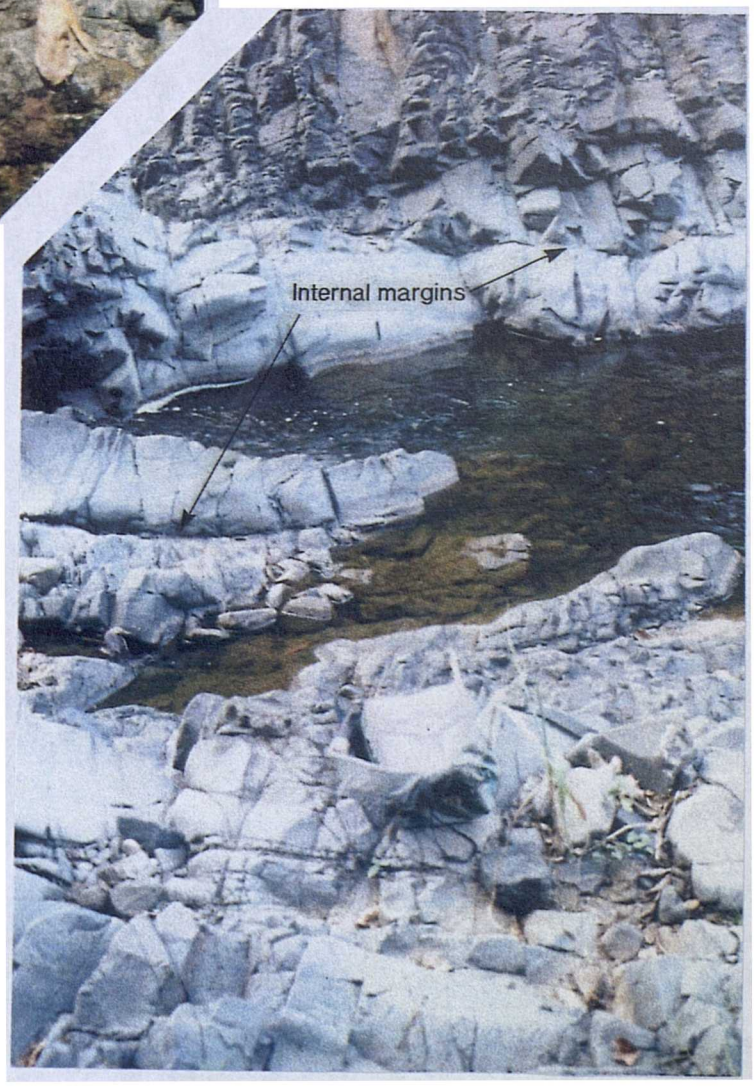

Plate 3.5 Composite dyke, upper Namosi Creek. Internal chilled margins are glassy and follow course of creek.

3.2.2.2 Vatubasaga Creek

Outcrops in Vatubasaga Creek are generally flat and slab-like, and are exposed in the bed and on the banks of the narrow creek. The section is dominated by pillow lavas and subordinate breccias with associated microgabbro pods and dykes. A type-outcrop at WF534268 is illustrated in Fig. 3.8. The outcrop demonstrates an intimate relationship between igneous lithologies which are compositionally gradational into one another. Pillow lavas range between 40-70cm in size and have aphyric glassy margins that are purple in colour and have a more commonly green-grey, partially crystalline interior in which altered plagioclase crystals are visible. Where vesicles are present, they are 1-2mm in diameter, spherical and concentrated at the margins of the pillow lavas. They are always filled with secondary minerals, dominantly calcite, chlorite, and zeolites. Secondary veins bearing pale-green epidote and quartz cut the pillow lavas and are especially common in areas of lava brecciation and jointing.

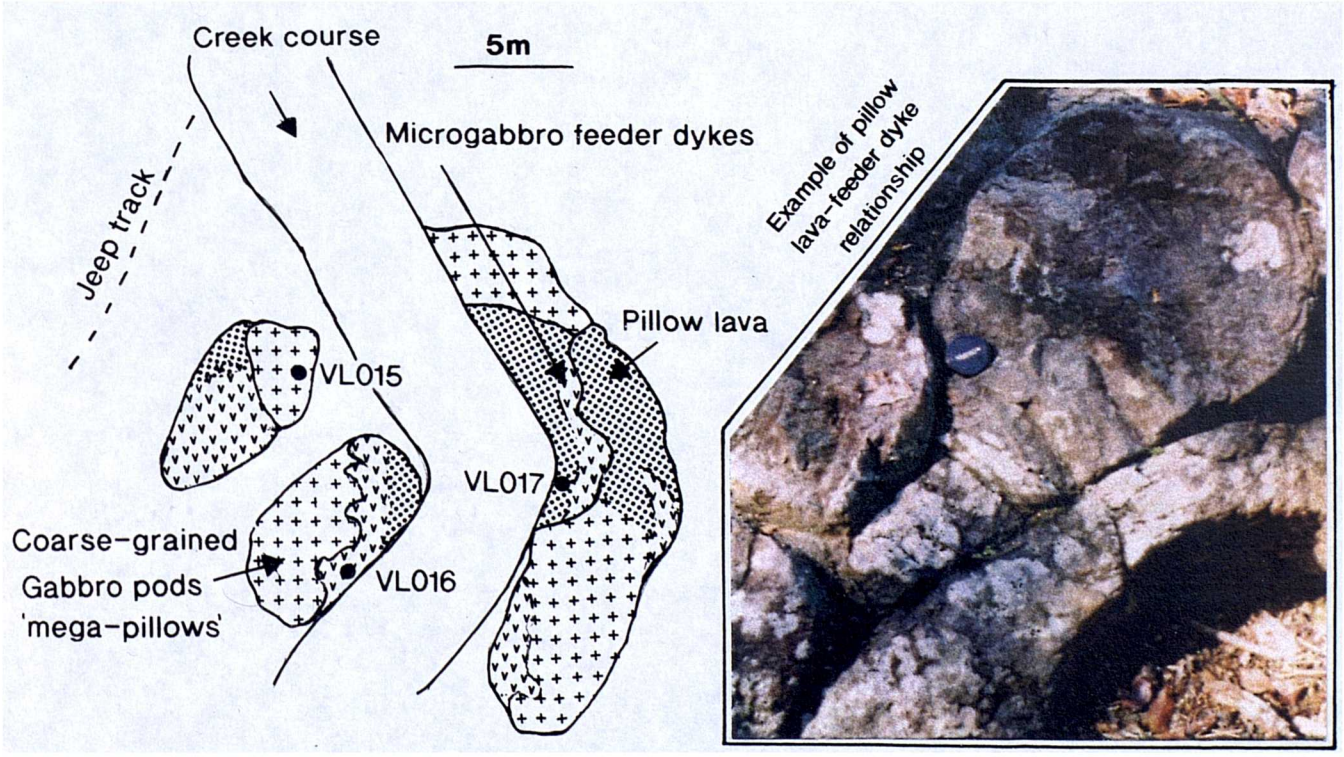

Fig. 3.8. Field sketch to illustrate relationships between lithologies in Vatubasaga Creek section.

The Yavuna Group dykes of this section show intimate relationships with the adjacent pillow lavas. They have widths ranging from 10-40cm and show textural gradations from microgabbro with a grain size of 0.5-1mm to aphyric pillow lava over a distance of a few tens of centimetres. As the exposures are slab-like, the dykes commonly pass in

and out of the plane of section, so that they cannot be traced through the outcrop for more than about one metre. In such cases, contacts with adjacent pillow lavas are seen, but chilled margins are not observed.

The gabbro pods are up to five metres in width, and have no preferred orientation. They have sub-ophitic textures involving plagioclase and late clinopyroxene that are visible in hand specimen. They show lobate, though not chilled, margins against the sinuous dykes which are in turn intimately associated and locally gradational into the pillow lavas. Several important features of these and similar outcrops in the section can be summarised as follows.

(i) No cross-cutting relationships are observed between the pillow lavas, dykes and gabbros.

(ii) No features diagnostic of injection of hot magma into cool wall-rock (e.g. dyke apophyses) are seen.

(iii) Continuous textural gradation is seen from gabbro pods through feeder tubes to pillow lavas.

All three lithologies are therefore interpreted to be cogenetic and part of the same magma plumbing system. The passage of magma can be traced from small reservoirs represented by the microgabbro pods, to feeder dykes and pillow lavas. The large microgabbro units are similar to 'mega-pillows' of the type well exposed in the Akaki Canyon section of the Troodos ophiolite, Cyprus (visited by the author in January 1992). The geology and magmatic plumbing systems of these composite pillow volcanoes in Cyprus are described in detail by Rautenschlein (1987) and provide a direct analogue to the Yavuna Group pillow complexes.

Limestones with a similar fauna to those in the Namosi Creek section are present in Vatubasaga Creek, and again appear to be interbedded with the pillow lavas (Plate 3.6). The limestone units are described in detail in Hathway et al. (in prep.) and contain internal bedding surfaces which dip steeply to the northeast as a result of later faulting.

Within the section, areas of intensely altered and bleached rock tens of centimetres wide are commonly observed. These zones of intense hydrothermal alteration in the greenschist facies are termed "epidosites" by Valsami & Cann (1992) and are characterised by often total replacement of the original igneous lithology by secondary minerals, largely quartz and epidote. The Vatubasaga Creek epidosites contain a distinct assemblage of green minerals chlorite and epidote as well as quartz,

Plate 3.6 Small limestone unit interbedded with pillow lavas, Vatubasaga Creek section.

calcite and sulphide minerals, and are commonly concentrated along joint and fault surfaces.

3.2.2.3 Kawa Creek

The Kawa Creek section is situated in the eastern part of the Yavuna Group outcrop area and is divided into upper and lower sections, to the south and north of the Yavuna Stock respectively. Both sections contain isolated exposures along the creek course through steep topography.

The upper section is easily reached from the nearby Koromba logging road and begins at the unconformable contact with the overlying Kawa Formation of the Wainimala Group. The basement lithology comprises pillow lavas ranging in size from 0.5m to 1m across. The pillows are brown to dark green in colour and are locally sheared and fractured along small faults where zones of hydrothermal alteration are concentrated. Small areas of brown, altered hyaloclastite breccia are interbedded with the pillow lavas. The basement is cut in two places by aphyric, Wainimala Group-related dykes. They have dark green, glassy surfaces and are the only dykes recorded in the section, confirming

that the dyke swarm dies out almost completely in the southeast of the Yavuna Group outcrop (Hathway et al. in prep). At one location 200m below the unconformity, a block of finely bedded calcareous siltstone and mudstone five metres in width is interbedded with the lavas. Its orientation at a high angle to the pillow lavas and its rounded edges suggest that it is a reworked exotic block, although no in-situ source for the reworked lithology was found. Foraminifera extracted from the sediment, which survived total recrystallisation, yield a Late Eocene age (Hathway et al. in prep.). Lower down the section towards the Yavuna Stock contact, pillow lavas continue to dominate. One small outcrop of felsic lava was observed in the section. It is interbedded with the pillow lavas as an ovate pod two metres wide. The contact between the Yavuna Stock and the lavas is displayed nearby in a highly weathered roadcut, where large angular xenoliths of basic lava stand out in the cliff against the pale brown weathered tonalite.

The lower Kawa Creek section is more difficult to reach and necessitates a steep and hazardous scramble down a forested slope from the logging track. The section begins at the angular unconformity where massive, basic Yavuna Group lavas are overlain by poorly sorted rudites of the Kawa Formation. The basement lava is massive with a dark grey to black appearance and is strongly jointed in a trellis pattern with fracture spacings of about 10cm. Black pyroxene and dark green chlorite are visible in the rock, but plagioclase is not seen. Several thin dykes cut the country rock along the section. The dykes are dark grey-green and highly altered and resemble those in Namosi Creek. They are assigned to the Yavuna Group on the basis of their alteration style which is characterised by clots of epidote and chlorite. They have a general NE-SE orientation and dip 45-70° to the northwest. Higher in the section, the basement lithology is a massive unit of occasionally porphyritic basic andesite lava. No contact is seen with the underlying dark grey unit, although one pale green dyke cuts the lava. Above this, the basement lavas are again massive and dark grey in appearance. More pervasive alteration is noted around the Yavuna Stock where many quartz, calcite and epidote bearing veins cut through the lava pile.

3.2.2.4 Votuma Creek

The dominant basement lithology in Votuma Creek is pillow lava and pillow breccia, overlain in upper parts of the section by epiclastic rudites (Fig. 3.2). Pillow lavas are purple to dark-grey while breccia units are more commonly dark-grey to black. Within the breccia units, pale green micrite limestone often forms an inter-fragment matrix (Plate 3.7). The lava fragments are angular, up to several cm in width and have chilled glassy rinds along their entire margins suggesting that eruption of the lava may have

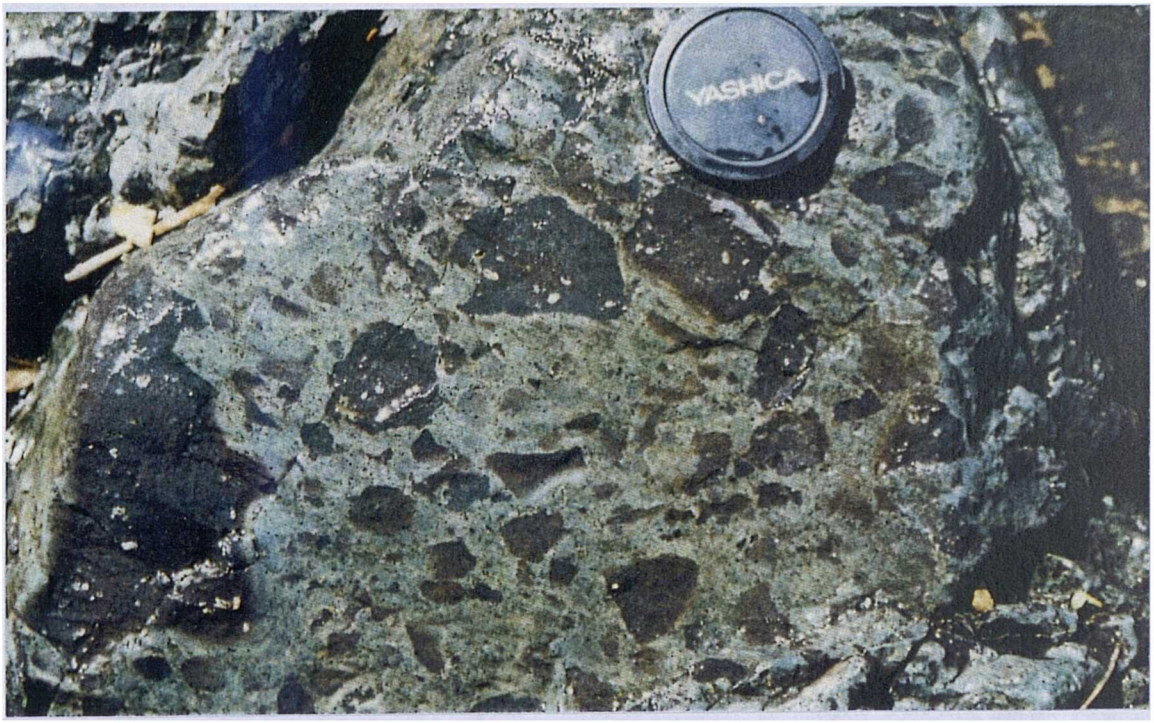

Plate 3.7 Angular pillow lava fragments set in a matrix of green micritic limestone, Votuma Creek.

Plate 3.8 Highly amygdaloidal massive lava cut by veins of calcite and epidote, Masi Creek.

taken place within water-saturated sediment. Interbedded within the usual pillow lavas and pillow breccias are small areas of highly amygdaloidal lava, similar to those seen locally in other creek sections (e.g. Namosi Creek, Masi Creek). Amygdales within the lava are filled with calcite and connected by networks of mm-scale veins (Plate 3.8). At one locality (WF497203), a waterfall cascades over a 15m high cliff of continuous pillow lava. The pillows have a general flat-lying appearance and show fracture controlled zones of alteration, bleaching and veining. The pillow lavas are overlain by a unit of reworked epiclastic rudite. The rudite has no apparent structure in the section, and contains angular to subangular clasts of basic lava in a matrix of poorly sorted volcanic fragments.

Throughout the section, Wainimala Group-related basic dykes are common and form both single and sheeted intrusions. The sheeted intrusions represent single fissures along which successive bursts of magma have bisected the earlier intrusions, resulting in composite dykes with internal chilled margins. The intrusions are usually composed of two or three separate dykes with concordant trends, steep internal contacts and localised flow textures defined by aligned plagioclase phenocrysts. In common with other sections both single and sheeted dykes show a lack of apophyses or xenoliths of country rock.

3.2.2.5 Masi Creek

The lower part of the Masi Creek section is dominated by massive lavas of the Yavuna Group (Fig. 3.2). The lavas are green to dark brown in colour and generally aphyric though occasionally finely plagioclase-phyric. Highly vesicular and brecciated lava locally comprises up to 5% of the outcrop. This lava type contains up to 40% by volume of amygdales filled with calcite and chlorite and linked by mm-scale calcite veins. These amygdales attest to high volatile contents in the parental magmas, a common feature of island arc magmas generally (Gill 1981). Pillow lavas are rarely encountered in the section. Where present, they are often strongly deformed and cut by secondary veins containing calcite and patches of epidote.

Dykes related to both the Wainimala Group and the Colo Plutonic Suite are common and locally comprise up to 70% of the section. The screens of Yavuna Group country rock between the dykes are often characterised by zones of intense crushing. Most of the tectonic deformation is related to the emplacement of the Middle-Late Miocene Colo dykes which trend NE-SW in the section, (perpendicular to the strike of the Wainimala Group dykes), have sheared margins, and commonly include xenoliths of basic Yavuna Group lava. The basic Wainimala dykes show sharp, glassy chilled margins, while felsic

dykes occasionally show apophyses into the country rock and may have sheared margins.

A separate traverse was conducted along the upper reaches of Masi Creek, close to the junction with Namaka Creek. Here the basement comprises massive lavas with extensive fracture systems related to the intrusion of the Wainimala Group Kalaka Dacite feeder dykes. Zones of secondary alteration are recognised as black patches of iron oxide after mafic minerals, and areas of bleached, pale-green lava are also common along fractures. Pillow lavas are locally interbedded with the massive lavas and dominate the section above the junction with Namaka Creek. They display sheared and elongate forms in areas of strongest deformation. In addition, small-scale late brittle zones of crushing cut both lava types. Where measured, the fault zones have transcurrent displacements of a few tens of centimetres.

Wainimala Group dykes comprise between 60% and 80% of the crustal section over distances of several tens of metres. Felsic dykes dominate the section and can be traced up-section into a NW-SE elongate ridge of Kalaka Dacite lavas and breccias (Hathway in press b). The dykes show strongly sheared margins and have well-developed columnar jointing. One felsic intrusion transgresses the basement lavas as a sill with a dip of 20° to the east, and joints perpendicular and parallel to the intrusion are present in the surrounding country rock.

3.2.2.6 Tubenarara Creek

The lower part of this section was traversed from the jeep track to the junction with Nawaka Creek. Three main outcrops of about 20m in width were found to contain undeformed purple pillow lavas with a maximum width of 50cm. Laterally impersistant horizons of purple-green hyaloclastite breccia form a matrix to some areas of pillow lava; however, no firm way-up indicator was discovered in any part of the section.

Wainimala Group dykes comprise at least 40% of the lower part of the section. Most are discrete intrusions, but one composite intrusion was observed. Fractured Yavuna Group pillow lavas are cut by a basic dyke with a broad N-S trend which shows a glassy, chilled eastern margin along which small angular xenoliths of basement lava occur. The basic dyke is compositionally uniform for a distance of 1.2m before showing a compositional change into a felsic dyke over a distance of 0 to 10cm.

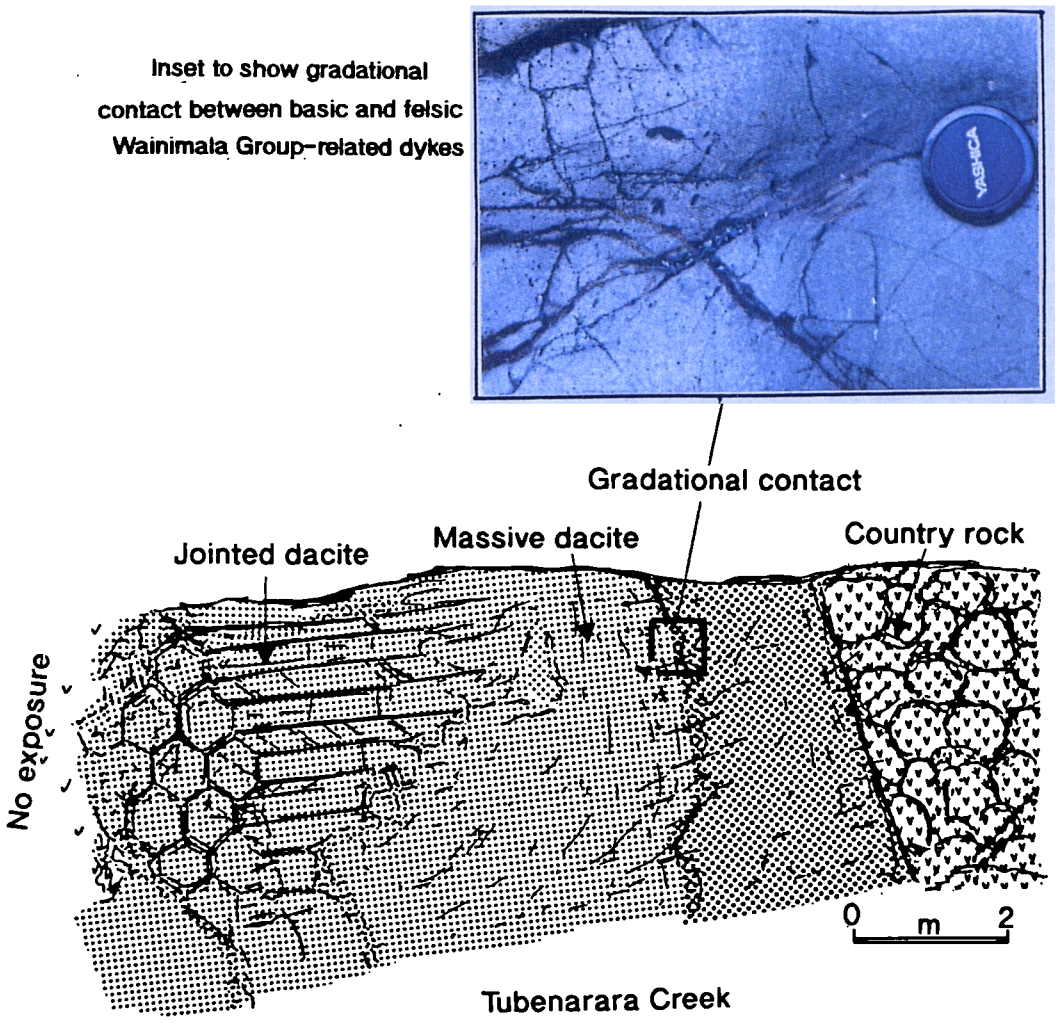

Fig. 3.9 Sketch to illustrate field relations in composite dyke in lower Tubenarara Creek

The felsic dyke has a structureless 1.5m wide outer zone, and a 2m wide core containing strongly developed columnar joints; its western margin is not exposed.

The central part of the section was visited during the traverse but not sampled. Pillow lavas again dominate, but basic Wainimala Group dykes are more common up-section where they comprise approximately 60% of the section. Multiple intrusions with internal chilled margins were seen at several locations. The upper Tubenarara Creek section (Fig. 3.2) is dominated by massive lavas and microgabbro which have been sampled by B. Hathway.

3.2.2.7 Nawaka Creek

Pillow lava and pillow breccia are the dominant basement lithology in the Nawaka Creek section (Fig. 3.2). Pillow lavas are flat-lying and gradational into massive lavas within the same outcrop. Small outcrops of highly amygdaloidal lava similar to that in Masi Creek are interbedded in the sequence. Occasional outcrops of brecciated lava set in a matrix of pale green micritic limestone also occur. The amygdaloidal lavas are cross-cut

by mm and cm-scale calcite-bearing veins which link up to large calcite-filled amygdales. Small clots of secondary epidote are developed in places along the veins.

Wainimala Group dykes comprise approximately 40% of the section, and basic and felsic members are present in broadly equal numbers. No cross-cutting relationships are observed. The dykes have NNW-SSE trends and are sub-vertical. Basic dykes are usually 2-4m in width whereas felsic dykes are mostly wider, with widths of 8-15m. The contacts of the basic dykes are sharp and chilled although occasionally lobate in form and flow-banded textures defined by aligned plagioclase laths are locally developed in the dyke cores. Dacite dykes invariably have shear fabrics developed along their margins in this section.

3.2.2.8 Malakua Creek

The Malakua Creek section is located to the east of the Uluivunaba Fault and includes Yavuna Group pillow lavas overlain by epiclastic rudites and Early Oligocene (Tertiary Letter Stage c) limestones. The section is dominated by green-purple pillow lavas often containing an inter-pillow matrix of pale green micritic limestone. The lavas are flat-lying and locally have rounded calcite-filled amygdales up to 5mm in width. A second type of matrix is unique to the section and comprises a secondary injection of basic lava which forms a chilled margin against the primary pillow lava (Plate 3.9). The lava infills are up to 10cm in width and may be inter-connected out of the plane of view. Small outcrops of dolerite and microgabbro grade texturally into units of pillow lava indicating a cogenetic relationship.

Up-section the pillow lavas units are overlain by rudites containing a variety of reworked basement clasts. These rudites map out on ridges and higher ground in the south and west of the Yavuna Group outcrop where they are capped by Early Oligocene limestones (Hathway in press a, Fig. 3.2). Mafic clasts within the rudites are similar in appearance to the underlying basement lavas and usually contain the characteristic veins filled with secondary minerals. Felsic clasts are also encountered; they contain plagioclase and hornblende as phenocryst phases, and are similar to clasts in the rudites of the Votuma Creek section. Both clast types are generally subangular indicating a local provenance, and are supported in a matrix of finer grained volcaniclastic material. Fining upward sequences are seen in places and crude bedding surfaces generally dip to the NW. Within the rudite units limestones occur as interbedded units. They are usually packstones or grainstones and are assigned to the Nawaqadamu Limestone Member of the Yavuna Group (Hathway et al. in prep.).

Plate 3.9 Secondary lava injection chilled against primary pillow lava, Malakua Creek.

Basic Wainimala Group dykes are common within the section, however, felsic dykes were not encountered. The basic dykes are 2-4m in width and have a consistent E-W trend suggesting that block rotation probably accompanied normal faulting along the Uluivunaba Fault (Fig. 3.1).

3.2.2.9 Lidilidi Creek

The Lidilidi Creek section occurs within the Late Miocene-Pliocene Nadi Sedimentary Group to the north of the Yavuna Block (Fig. 2.1). The section contains a high proportion of reworked Yavuna Group material which occurs as clasts and boulders and was shed off the northern part of the Yavuna Group outcrop area during uplift associated with strike-slip faulting. The section has not been added to the reconstruction of Fig. 3.2 because of its entirely reworked nature. Clasts in the section range in size from cm scale particles to boulders with widths in excess of 20m. The provenance of the clasts in the Nadi Group can be linked directly to the Yavuna Group, most clearly in the east of the area where the highest concentrations of tonalite clasts have been shed off the eroded Yavuna Stock (Hathway 1993). Within the large boulders, reasonably fresh igneous material can be obtained, and preserved lavas show the purple-brown colour common in the outcrops of the Yavuna Group to the south. Both massive and pillowed

lavas occur, and where pillows display well developed necks, consistent younging directions are seen throughout large boulders. Calcite-bearing veins cut both types of lava, and most outcrops are cut by small faults along which zones of crushing are concentrated. Smaller clast types cover the range observed in the Yavuna Block, and include basic lavas, microgabbros and cumulate gabbros. The clasts are dominantly angular and poorly sorted, and are set in a matrix of black calcareous mudstone.

Shoshonitic dykes are encountered within the creek section. These are associated with volcanic centres in the Sambeto mountain range several kilometres to the north of the section and commonly weather out from the friable rudites to form upstanding ridges and waterfalls. One sample from the shoshonite dyke swarm in nearby Nasasa Creek was taken for reference analysis.

3.2.3 Other localities

3.2.1.1 NW of Muasigasiga

Massive lavas similar to those in the Masi Creek section (3.2.2.5) also dominate the outcrops to the northwest of Muasigasiga in Rosoroso, Vulavula, Roroniki, and Vugavuga Creeks (Fig. 3.2). The massive lavas are generally dark grey and grey-green where heavily altered and occasionally grade into a coarser-grained microgabbro which is finely plagioclase-phyric.

3.2.3.2 Koromba

Around the Koromba summit area (WF637216), pillow lavas were sampled at an elevation of 820m (2680'). However, lack of continuous exposure or inter-pillow matrix makes their stratigraphic context relatively obscure (Fig. 3.2).

3.2.3.3 Talia and Lumulo Creeks

These creek sections contain some of the least altered Yavuna Group lavas with zeolite facies metamorphic assemblages predominant. The high sedimentary component of the sections has been described earlier (3.2.1) and pillow lavas have been collected by B. Hathway.

3.2.3.4 Other Nadi Basin inliers

A number of Yavuna Group inliers are recognised in the Nadi Basin on the basis of their lithology and alteration characteristics. The largest occurs in Lidilidi Creek as described above, whilst several others which are too small to be mapped are described briefly in Hathway et al. (in prep.) Three samples of Yavuna Group cumulate gabbro were collected by B. Hathway from exposures in the Nadi basin at Sulua Creek (WF660333)

and Natokuto Creek (WF565371), and from an upthrust fault-scarp exposure in the Nadi River (WF721367).

3.2.3.5 Yavuna stock contact aureole

Additional basement samples from within the contact aureole of the Yavuna Stock were collected by B. Hathway from Momasau Creek (WF610243), Nadi Creek (WF583265) and Quruvatu Creek (WF596298).

3.2.3.6 Sokia Creek

Hathway et al. (in prep.) record pillow lavas overlying massive lavas from 230m (750') elevation in Sokia Creek (Fig. 3.2). The pillows are generally very dark purple-grey in colour and aphyric.

3.2.3.7 Rudites in the southeast of the Yavuna Group outcrop

The epiclastic rudites form the stratigraphically highest part of the Yavuna Group and crop out around the Muasigasiga triangulation point and on the Namarasa/Masi and the Vatuma/Tubenarara watersheds (outcrop area illustrated in Fig. 3.1, after Hathway in press a). Limited parts of the sequence were traversed in the Malakua and Votuma Creek sections as described earlier and the sequence is also present on the slopes of Koromba mountain. The rudites contain predominantly angular clasts of grey-green and purple variably amygdaloidal, basic lava as described in the creek traverses above, together with less common plagioclase-hornblende phyric dacite clasts which seem confined to specific horizons such as part of Malakua Creek section (Hathway et al. in prep.).

3.3 The Yavuna Stock

3.3.1 Morphology

The Yavuna Stock is a large felsic pluton which intrudes the basement lava pile in the central-eastern part of the Yavuna Group outcrop (Fig. 3.10). The pluton has a marked NW-SE trend and is approximately 12km in length and 3.5km wide. The stock is divided into two main facies based upon outcrop mineralogy, a basic marginal zone of a few hundred metres width in the northeast of the intrusion, and a volumetrically dominant felsic zone which is largely separated from the basic marginal zone by a highly sheared contact.

The stock crops out through elevations of 120ft (37m) in the northwest (WF560288) to 1400ft (420m) in the southeast (WF690228) where the intrusion is unconformably overlain by epiclastic rudites of the Wainimala Group Kawa Formation. Below the

unconformity, up to 70% of the intrusion is occupied by basic country rock xenoliths

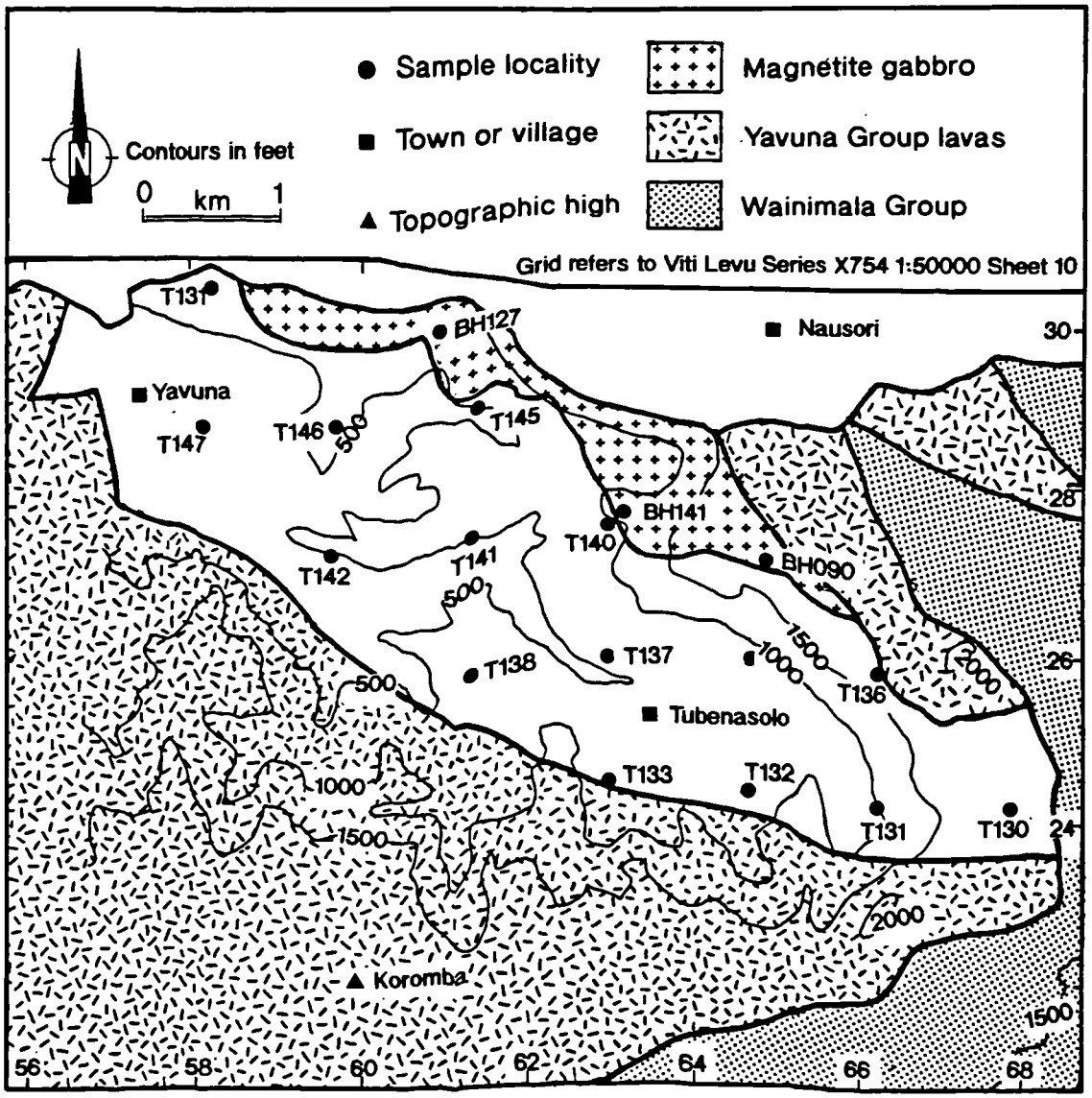

Fig. 3.10 Outcrop and sample localities of the Yavuna Stock. (Contact details from Hathway in press a)

(Plate 3.10) and, in accord with the elevated topography of the area, this part of the intrusion is interpreted as an upper wall or roof zone of the pluton. This assertion is further supported by the occurrence of roof-zone pendants of hornfels metabasite in parts of the Kawa Creek section (Hathway et al. in prep.). Within deeper levels of the stock, net-veining of the basement lava-pile is observed (e.g. WF565291). The mm-cm scale felsic veins isolate angular fragments of basic country rock and extend for several metres away from the margin of the intrusion. The SW margin of the stock is extensively faulted such that outcrops of trondhjemite occur up to 500m away from the margin illustrated in Fig. 2.1. An appreciation of the structural complexity and faulted nature of

the stock contacts can be gained from the projected outcrops in Fig. 3.2 The northeastern contact is poorly exposed but appears to be sheared in most locations. The transition from trondhjemite to the marginal gabbro zone is also characterised by shearing as described above, and xenoliths are notably absent in this portion of the trondhjemite intrusion. The country rock around the stock shows pervasive alteration and recrystallisation within a contact aureole up to several hundred metres wide. These textural and mineralogical transformations are described in chapter 4.

Plate 3.10 Xenolith-rich roof zone of the Yavuna Stock exposed along Koromba logging road.

3.3.2 NE marginal zone

The northeast marginal zone of the intrusion comprises a coarse-grained assemblage of basic cumulus crystals and is seen in places to be cut by small cm-scale aplite veins traceable to the main felsic pluton. The basic marginal zone is interpreted to represent a floor or sidewall to the intrusion and was sampled at three progressively higher levels within the intrusion (Fig. 3.10). The mineral assemblage is dominated by plagioclase, hornblende and magnetite which show a well defined crystallisation sequence. Both the plagioclase and hornblende can occur as large crystals up to 2mm in length. Magnetite is

usually the latest crystallising phase, occupying the interstices of the earlier cumulus minerals; it is occasionally accompanied by small traces of felsic melt distributed along the grain boundaries (Plate 3.11). The felsic melt comprises sub-mm crystals of quartz which lack internal sub-grain boundaries and appear to be primary igneous phases rather than secondary phases formed during secondary alteration processes

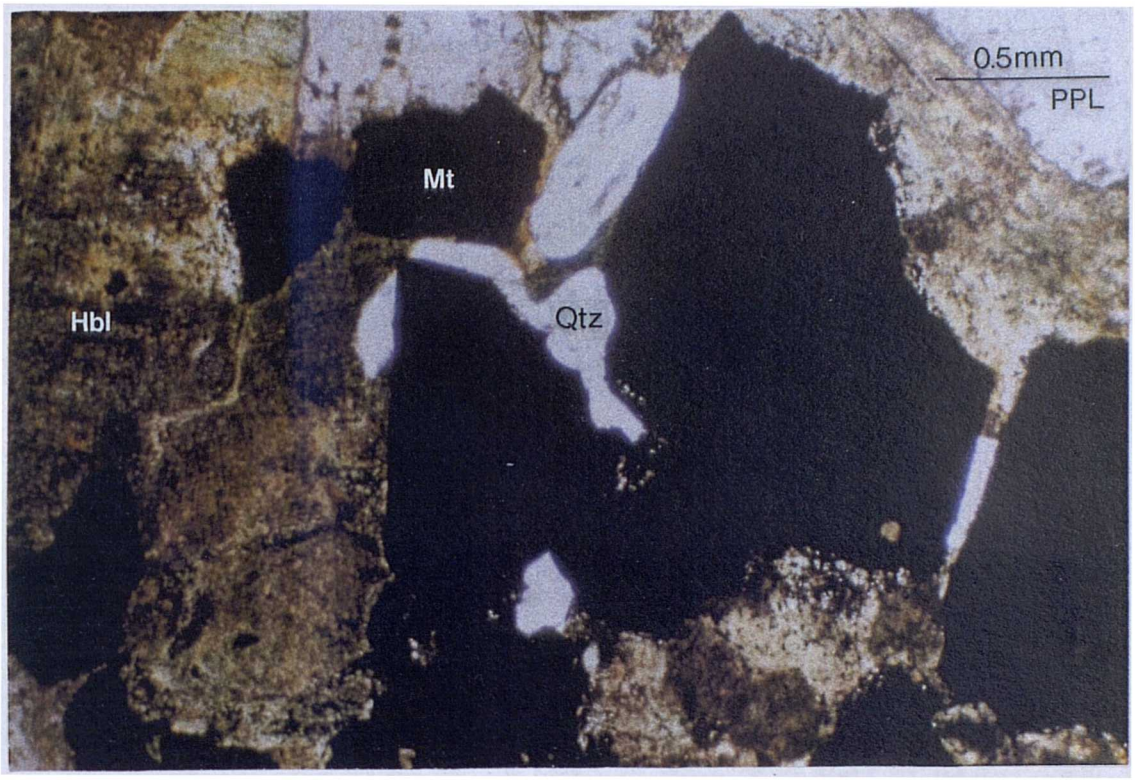

Plate 3.11 Tiny selvedges of silica-rich fluid trapped along the grain boundaries of the basic cumulate minerals of the marginal zone. Mt - magnetite, Qtz - quartz, Hbl - hornblende.

3.3.3 Main pluton

The main part of the Yavuna Stock shows marked uniformity in field appearance throughout; no further internal facies or contacts are observed. The main body of the pluton is coarse-grained and composed largely of an equigranular aggregate of plagioclase feldspar and quartz grains approaching 1cm in size with minor amounts of hornblende and chlorite. Samples collected from the tonalite show generally pervasive alteration of plagioclase to albite and sericite and hornblende breaking down to green biotite. The pluton was sampled on a gridwise basis during the 1970's by Dr. H. Colley who provided samples for this study (Fig. 3.10) in the form of rock powders crushed using a tungsten carbide tema mill.

3.4 The Wainimala Group

3.4.1 The Nadele Breccia

This formation consists mainly of redeposited rudites and includes clasts of basalt, andesite and dacite. The type section of the formation is exposed on the banks of Nasasa Creek (Rao in press) and includes some 200m of interbedded breccia, tuffaceous sediment and lavas. Clasts are mostly angular and range in size up to 3m across and are set in a dark green matrix of finer volcaniclastic material. Bedding surfaces are present in places within the section and range in dip from 13-45° generally towards the southwest. Samples of all clast types as well as in-situ pillow lavas were taken for geochemical analysis (Fig. 3.11). The polymict nature of the rudites, together with the presence of rounded as well as angular clasts, and the presence of sparse shallow-water limestones, led Hathway (in press b) to propose that the formation was deposited on the dispersal apron of a major, in part subaerial, volcanic edifice.

3.4.1 The Kawa Formation

Samples from the Kawa Formation were collected from within Wailulu Creek and from the ridge between Wailulu Creek and Loloti Creeks (Fig. 3.11). These samples are taken from close to the base of the formation and consequently contain geochemical signatures of the earliest part of the Wainimala arc. The rocks sampled were angular to sub-rounded, porphyrytic andesite clasts with visible phenocrysts of clinopyroxene, hornblende and plagioclase set in a blue-grey microcrystalline groundmass. The boulders are supported by a matrix of volcaniclastic sandstone and mudstone which contains a variety of other clast types including finely amygdaloidal basalt and blocks of limestone and coral up to 2m across (Hathway in press b). Parts of the unit are chaotic and structureless, while fining-up sequences and other sedimentary structures are observed in places. Type sections through the Formation in Wailulu and Kawa Creeks are described by Hathway (in press b), who interprets the formation as a sediment gravity flow deposit formed on the flank of a major volcanic edifice.

3.4.2. The Dakadaka Basalt

The Dakadaka Basalt Formation crops out around the southern and western margins of the Yavuna Group outcrop (Fig. 3.11). The formation is dominated by massive lavas but pillow lavas and breccias are also common. The lavas of the formation are distinctive in the field because of their highly vesicular nature (up to 50% by volume) and their

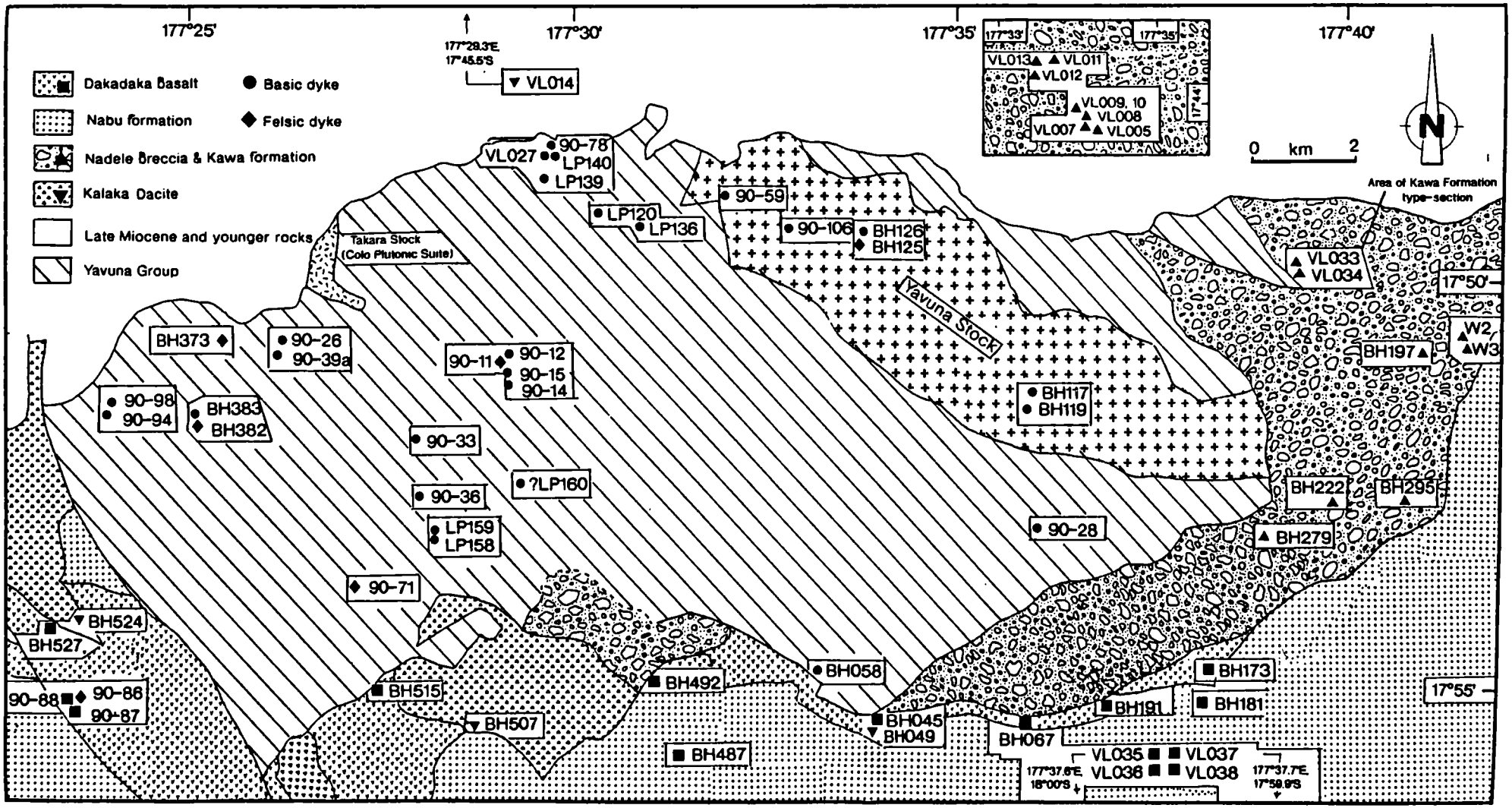

Fig. 3.11 Wainimala Group sample localities. Lithological details from Hathway (in press a).

characteristic deep red-purple colour on weathered surfaces. Vesicles are commonly filled with zeolites, calcite and clay minerals, and all lavas show some degree of alteration in the zeolite facies. Massive lavas show extensive evidence for lateral transport, including banding and contorted flow textures, and alignment and elongation of vesicles into layers. A pink calcareous mudstone is commonly observed as a matrix between pillow lavas and breccia frameworks, and the presence of originally aragonitic pteropod shells in the sediment are used by Hathway (in press b) to constrain the eruption of the basalts to water depths of several hundred metres. Basic dykes are seen to cut the lavas at several localities. The dykes are dark grey to black and are interpreted as feeder dykes.

An accurate volcano-stratigraphic reconstruction for the lava field cannot be made because of faulting and the disparate nature of the outcrop. However, based upon the structural attitudes of parts of the lava field, the total thickness of the succession is estimated to be at least 300-400m (Wharton et al. in press). The geochemical evidence for the basic dykes cutting the Yavuna Group being feeders to the lava field is discussed in chapter 7.

3.4.3 The Kalaka Dacite

The Kalaka Dacite Formation of the basinal assemblage crops out as massive units of monomict dacite breccia, dacite flows and tuffs. The dacites are concentrated into small volcanic centres which crop out to the south and west of the Yavuna Group in close association with the Dakadaka Basalt, and also occur in a small antiform in the Legalega inlier in the Nadi Basin (WF515366, Fig. 3.11). The dacites are pale grey and are usually plagioclase-phyric with rare quartz and mafic minerals also visible in hand specimen. Flow-banding textures defined by aligned plagioclase laths are common in the dacites and in their upper parts, many of the units pass gradationally through lapilli-stone tuffs and sandstones to the wholly sedimentary Nabu Formation (Hathway in press b).

3.4.4 The dyke swarm cutting the Yavuna Group

This pervasive bimodal dyke swarm is widespread in extent across the Yavuna Group outcrop (Fig. 3.12). Dark blue-grey basic dykes are common throughout the area, but pale-grey-fawn felsic dykes are more common in the west of the swarm where they coalesce as feeders to at least one Kalaka Dacite volcanic centre. Cross-cutting relationships within the swarm are rare due to the consistent strike of the swarm across the area (Fig. 3.12). Hathway (in press b) reports only seven cross-cutting relationships

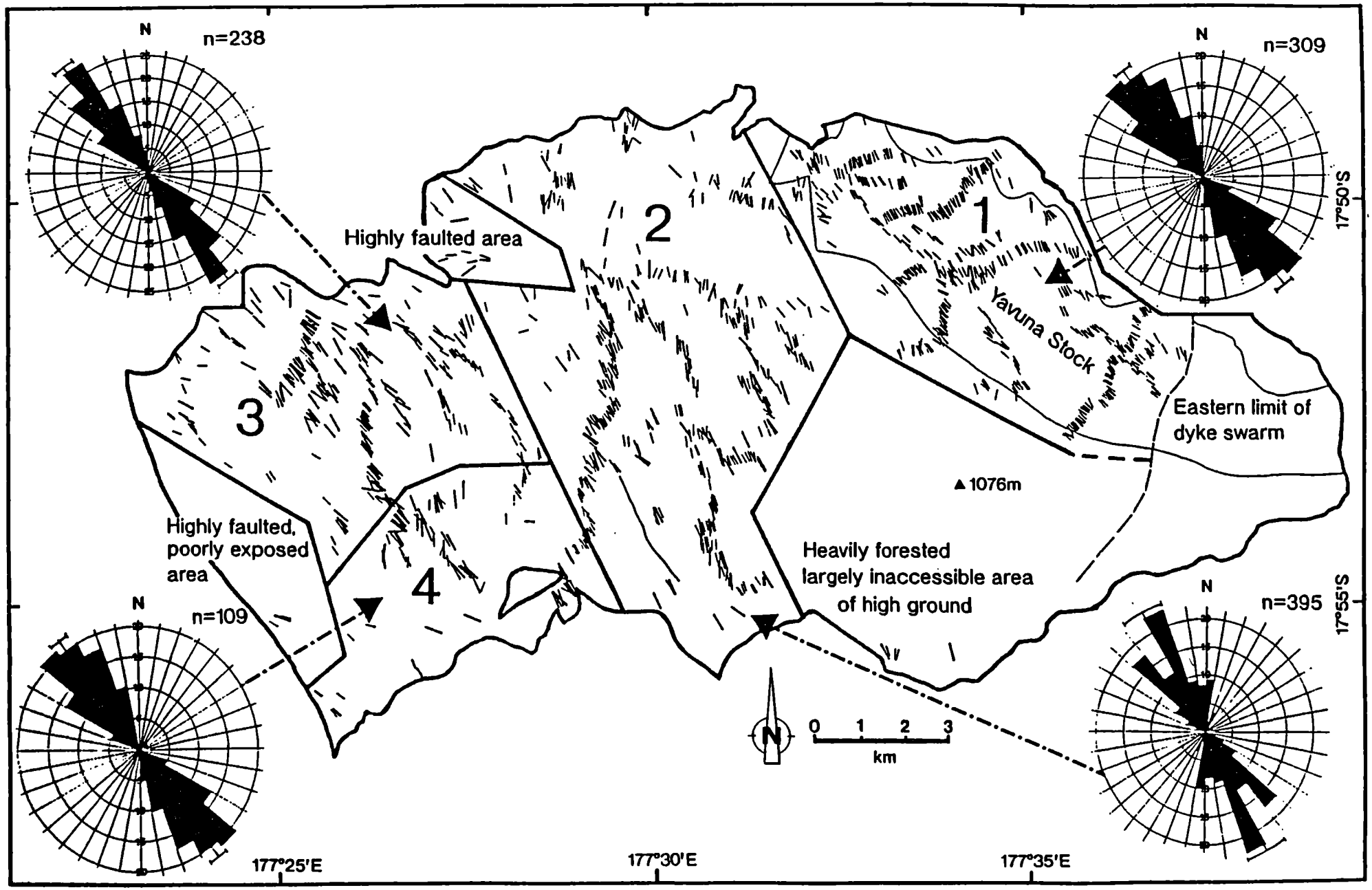

Fig. 3.12 Distribution of Wainimala Group-related dykes cutting the Yavuna Group. Measured dyke orientations for each subarea are displayed on rose diagrams. Figures give percentage, bar indicates statistical mean and standard deviation. Mean dip for dykes in each sub-area are: Area 1, 77° SW, area 2, 73° SW, area 3, 76°NE, area 4, 44° NE.

within the swarm and concludes that whereas the two end-member compositions are of similar age, with the majority of felsic members were emplaced prior to the majority of basic members. Basic dykes may be up to 11m wide but are more commonly between 0.5m and 5m wide, with cm-scale glassy chilled margins. The dykes are generally steeply dipping apart from in the south of the swarm (Fig. 3.12). Dyke margins are sharp and xenoliths of country rock are rare. Little disruption of the country rock appears to have taken place during dyke emplacement and, in areas of low concentration, the dykes often terminate in a series of small, cm-scale, finger-like projections. Most of the basic dykes are aphyric, although some are plagioclase-phyric. Alteration assemblages generally reflect lower greenschist facies metamorphic conditions.

Felsic dykes may be up to 30m across. However, they more commonly show similar widths to the basic dyke. In the west of the swarm, the dykes are compositionally homogeneous multiple intrusions. The dykes are invariably plagioclase-phyric but mafic phenocrysts are rare. In some cases, their intrusive style differs from that of the basic dykes. Although contacts are again sharp and well chilled, disruption of the surrounding country rock is more common, and the felsic dykes are seen locally to cut through the Yavuna Group as sill-like apophyses that connect adjacent sub-vertical dykes.

The swarm also contains composite dykes. Although rare, these dykes provide important evidence for the synchronous generation of basic and felsic magmas in the basinal assemblage. The example from Namosi Creek (Fig. 3.7) shows cyclic emplacement of basic and felsic magma with later bursts of magma bisecting the partially cooled outer parts of the intrusion. The example from Tubenarara Creek (Fig. 3.10) shows similar features, although it is less well exposed.

Small intrusive pods are occasionally encountered in areas of high dyke concentration. An ovate example from Masi Creek in the central-western part of the Yavuna Group outcrop is 2-3m across and was fed from beneath by a NW-SE basic dyke. The transition from basic dyke to pod is marked by a gradational change in texture from aphyric basalt to microgabbro.

3.5 Later volcanic episodes

3.5.1 The Colo Plutonic suite

The Colo Plutonic Suite comprises the small 1km^2 Takara diorite intrusion (WF475270), and a swarm of NE-SW trending, steeply dipping hornblende andesite dykes which crop

out to the south of the stock. Typical dykes of the swarm are described in the Masi Creek stream traverse where Colo dykes cut the earlier Wainimala Group-related dykes and commonly include angular xenoliths of basic Yavuna Group country rock along their margins. Considerable disturbance and fracturing of the country rock is observed in the vicinity of the Colo dykes, and similar fracturing also characterises the margins of the Takara Stock. The Colo dykes are characterised by a coarse-grained plagioclase-hornblende phenocryst assemblage with occasional fine grained cognate xenoliths set in a pale grey microcrystalline groundmass.

3.6 Environments of volcanism

3.6.1 The Yavuna protoarc

Crustal accretion within the Yavuna Group lava field is dominated by eruption of basic lavas, predominantly in shallow water. The lavas erupted as individual pillow lava complexes and as massive extrusive lava sheets. The constructional history of the pillow lava complexes can be inferred from field observations and comparison with ophiolite crustal sections (e.g. Troodos, Rautenschlein 1987) Magma erupts from fissures in the seafloor as small (<1m) pillow lavas. Inflation of some pillow lavas allows them to grow in size to 'mega-pillows' of several metres in width. The mega-pillows then become small magma reservoirs from which new pillow lavas grow as buds from the central core. As supply of magma continues, probably in episodic bursts, successive layers of pillow lava erupt, fed from the core to the surface through feeder tubes and a small 10-20m wide volcano is produced on the seafloor above the fissure. Continued eruption of pillow lava from the flanks of the volcano leads to local draping of the pillowed forms. Further inflation of the central mega-pillow transfers stress through the quenched and brittle upper parts of the pillow volcano. Reworked talus may be derived from the small scarps between successive eruptions, and eruption of further lava on top of talus surfaces allows the reworked units to be preserved and interbedded as breccia horizons on the flanks of the volcano. The mega-pillow core eventually cools at a relatively slow rate to produce a full range of microgabbro and gabbro in which ophitic and sub-ophitic textures can develop. The full range of lithologies produced is illustrated in three-dimensional form in Fig. 3.13.

Periodically, tectonism, uplift and erosion of fault scarps lead to downslope reworking and deposition of rudites on the flanks of the scarps (e.g. Namosi Creek central section).

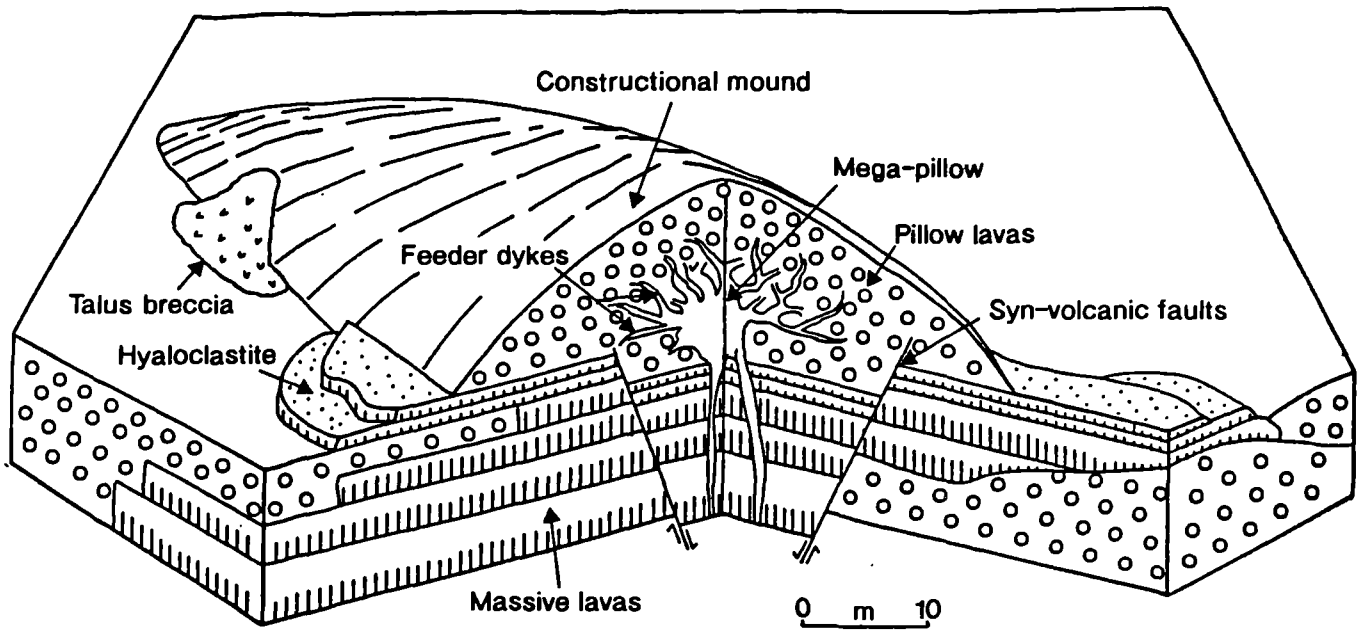

Fig. 3.13 Three-dimensional form of mega-pillow volcano complexes as inferred from field observations in the creek traverses (modified after Rautenschlein 1987). This example is based mainly upon lower Namosi and Vatubasaga Creek exposures with a mega-pillow core of 5-10m width and episodic inflation of the chamber through a fissure in the seafloor.

Limestone units were deposited in shallow water interbedded with pillow lavas on basement highs, and on shoals on the flanks of basement highs where they became interbedded with fine-grained reworked material. The area of shoaling across which the limestones were able to accumulate was several kilometres wide. Within sections with good stratigraphic control, e.g. Namosi Creek, both deeper water (micritic) and shallow water (packstone) limestones occur in close association suggesting rapidly changing environments of deposition. The pillow lava complexes are commonly overlain by massive lavas which may represent a period of renewed increased magma supply (Ballard et al. 1979). Vesicle contents in both pillowed and massive lava types range between 0-60% in interbedded lavas, suggesting that no simple correlation exists between volatile content and depth of eruption.

Felsic lavas are extremely rare in the lower parts of the Yavuna Group. They comprise less than 1% of total outcrop suggesting that crystal fractionation processes were not efficient during the protoarc volcanic stage. At higher levels in the Yavuna Group, basic and felsic lavas are present as clasts in the epiclastic rudites which overlie the lava pile in the SW of the area. The predominance of angular clasts indicates a proximal source for

the debris, and the presence of occasional rounded clasts indicates some degree of subaerial reworking (Hathway et al. in prep). The rudites most likely represent talus deposits derived from surrounding basement highs with interbedded shallow water limestones accumulating in shallow water on the flanks of the basement highs.

3.6.2 The Wainimala second arc

Wainimala Group basinal assemblage volcanism in the field area can sub-divided into two distinct terranes, the *edifice* and *inter-edifice* terranes. The edifice terrane is represented by the volcaniclastic debris aprons of the Nadele Breccia and the Kawa Formation which were deposited on the flanks of major, in part subaerial, volcanic edifices. Although the extent of the individual edifices cannot be mapped out, the Kawa Formation edifice was at least 20km closer to the eventual mature arc axis as defined by the belt of major Colo plutons on southern Viti Levu. The Kawa Formation unconformably overlies the Yavuna Group indicating that the principal edifices were, at least in part, developed on a crustal substrate provided by the Late Eocene-Early Oligocene basement.

Elsewhere in the basinal assemblage, between the principal edifices, basic and felsic magmas of the *inter-edifice* terrane were erupted onto the seafloor. Basalt erupted from aligned fissures, and in places was able to flow some distance along the seafloor with its eventual distribution probably being controlled by topography. Felsic lavas were also erupted from fissures in the underlying crustal substrate and formed small submarine volcanic centres on the seafloor. The pervasive bimodal dyke swarm cutting the Yavuna Group documents significant tectonic extension during basinal assemblage volcanism. Field evidence directly links the felsic members of the dyke swarm to the Kalaka Dacite and it follows that although direct field evidence is lacking, the basic members of the swarm may be genetically related to the Dakadaka Basalt. This possibility is further discussed in chapter 7 in the light of geochemical evidence.

The facies contrast between the lower part of the Wainimala Group basinal assemblage which includes volcanic rocks and volcaniclastic rudites and the upper part of the assemblage which is entirely sedimentary and dominated by fine-grained volcaniclastic turbidites and hemipelagic carbonates developed over a period of about 5ma (see Fig. 2.2). The facies contrast reflects the southerly migration of the axis of arc volcanism, from the area now exposed around the Yavuna Group outcrop, to that represented by the Wainimala arc assemblage to the south. Concurrent downthrow of the basinal

assemblage occurred across major faults and the axis of the mature arc became concentrated in southern Viti Levu where it is now delineated by the plutons of the Colo Plutonic Suite. The temporal structural and volcanological evolution of the basinal assemblage formations are illustrated schematically in Fig. 3.14.

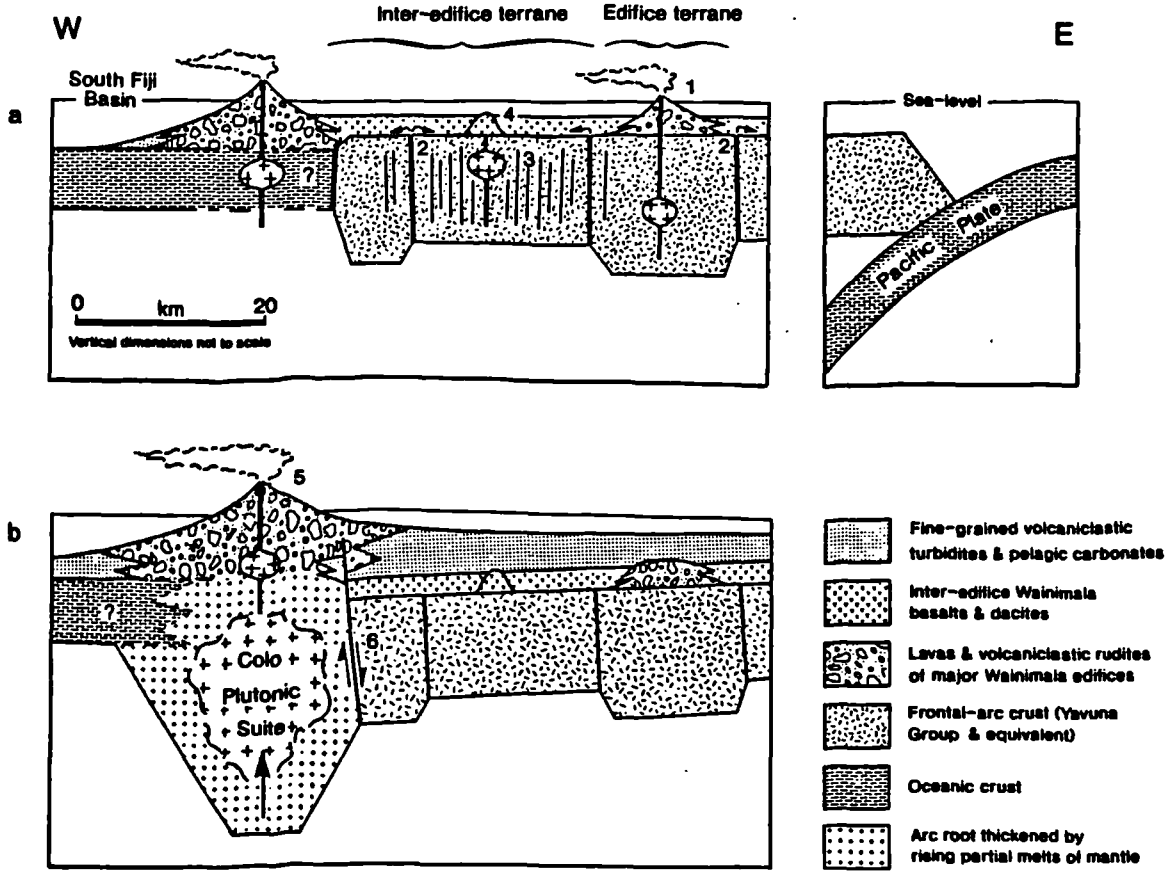

Fig. 3.14 Sections through Wainimala arc at early (Late Oligocene) and mature (early Middle Miocene) stages of arc evolution. **a 1.** Construction of subaerial volcanic edifices marking trenchward limit of volcanic front. Differentiation processes occur at depth and are complicated by magma-mixing. **2.** Eruption of primitive Dakadaka Basalt through the Yavuna Group substrate to form low-lying mafic lava fields on the seafloor. **3.** Shallow-level differentiation and pervasive emplacement of a bimodal dyke swarm in the inter-edifice terrane. **4.** Localised eruption of evolved magmas at submarine Kalaka Dacite centres. **b 5.** Retreat of volcanic front towards frontal-arc backarc transition. Concentration of arc axis in southern Viti Levu. **6.** Downthrow of basinal assemblage across major faults.

3.7 'Eua island, Tonga

Most samples taken were beach boulders from southern Liku beach (Fig. 2.8). In addition the dykes on South Liku beach were sampled. One day was spent at the Vaingana area (Fig. 2.8) where breccia clasts and lava flows were sampled.

CHAPTER 4

Petrography and mineral chemistry

4.1 Introduction

In this chapter, primary and secondary mineral assemblages and textures are described and illustrated and the implications of these variations for geochemical studies are discussed. Summary petrographic descriptions are listed in the appendix. Mineral chemistry data obtained with an electron microprobe are tested for their susceptibility to secondary alteration before being used in petrogenetic applications.

4.2 Primary igneous textures

When lava erupts under water, rapid cooling and quenching of the molten rock means that large crystals do not usually develop and, instead, extremely small crystals with dendritic or sperulitic morphologies are more common. This environment of crystallisation is termed the 'quench' environment by Cox et al. (1979) while that in which crystals have grown prior to eruption (in a magma chamber or conduit) is termed the 'intratelluric' environment. Evidence for crystallisation in both of these environments is found in the Yavuna Group and Wainimala Group sample suites.

The most commonly occurring texture is the *felsitic* texture defined by aggregates of radiating plagioclase fibres and acicular crystals set in a glassy or cryptocrystalline matrix. This texture characterises many of the samples taken from the margins of lava units. The degree of undercooling undergone by a portion of a pillowed or massive lava is critical to the texture developed. On moving from the rim towards the core of a pillow lava, for example, a lesser degree of undercooling occurs, crystallinity becomes higher and the minerals become coarser (Natland 1991). A full range of textures can thus occur within an individual pillow lava complex, and this transition from the quench to the intratelluric environment can be demonstrated on an outcrop scale in the mega-pillow units of Vatubasaga Creek. While the margins of the pillow volcanoes are felsitic, quench-environment lavas, the centres of the volcanoes are microgabbros and gabbros which contain the sub-ophitic textures more commonly associated with the

Plate 4.1 Sub-ophitic texture defined by elongate plagioclase laths that are partially enclosed by later-crystallising clinopyroxenes. From mega-pillow core, Vatubasaga Creek.

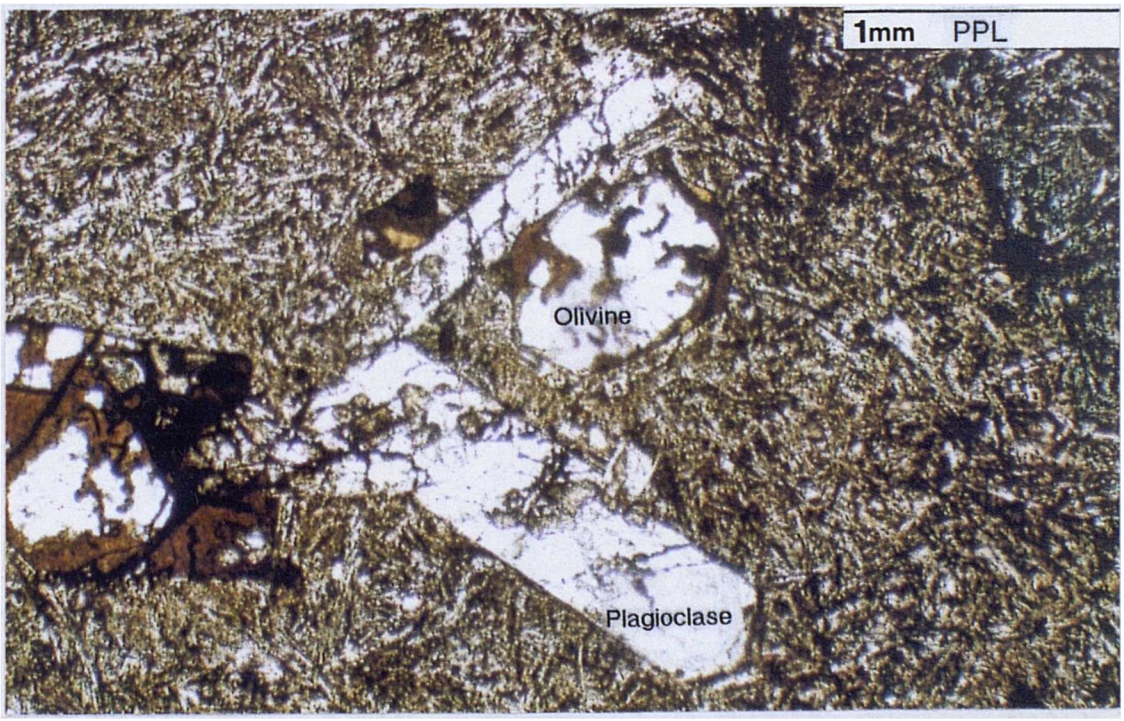

Plate 4.2 Porphyritic texture defined by pseudomorphed olivine and plagioclase phenocrysts set in a felsitic groundmass of tiny plagioclase laths. From pillow lava, Tubenarara Creek.

hypabyssal or plutonic environment (Plate 4.1). Lavas that are transitional between these two end-members may have *porphyritic* textures in which phases that crystallised in the intratelluric environment are carried into the quench environment and trapped within a fine-grained felsitic or glassy groundmass (Plate 4.2).

Vesicle or amygdale distributions within pillow lavas are also variable. In some cases, vesicles develop throughout a pillow lava while in other examples, vesicles occur only at the rim or are restricted to a concentric distribution within the pillow interior. Highly vesicular massive basalts, in which vesicles comprise up to 50% or more of the rock, occur at several horizons within the lava pile and in these cases, vesicle distribution is random and without preferred orientation or distribution (Plate 4.3).

4.3 Primary minerals

4.3.1 Spinel

Spinel is a ubiquitous accessory phase in the more primitive samples of the Yavuna Group and Wainimala Group. The spinel grains range in colour from very dark brown to pale straw yellow and usually occur in euhedral form (although the euhedra may be corroded) and often as inclusions within olivine phenocryts (Plate 4.4). The euhedral forms of the grains suggest an intratelluric origin for the mineral, which may have acted as nucleation sites for olivine prior to eruption. Sigurdsson & Schilling (1976) in their study of Mid-Atlantic ridge basalts found that spinels were restricted to less-evolved compositions (with FeO*/(FeO*+MgO)<0.75)[1], and a similar conclusion is reached for the Yavuna Group samples with spinels not occurring in more evolved rocks with Cr<120ppm. The spinels are classified for ease of description using the simple criteria of Table 4.1.

Hosted spinel	1
Not-hosted spinel	2
Pristine	a
Oxidised rims	b
Fully oxidised	c

Table 4.1 Spinel classification

Crystals that are overgrown and enclosed by another primary igneous phase (usually recognisable as an olivine pseudomorph) are referred to as 'hosted' or *type-1* spinels.

[1]FeO* is total iron

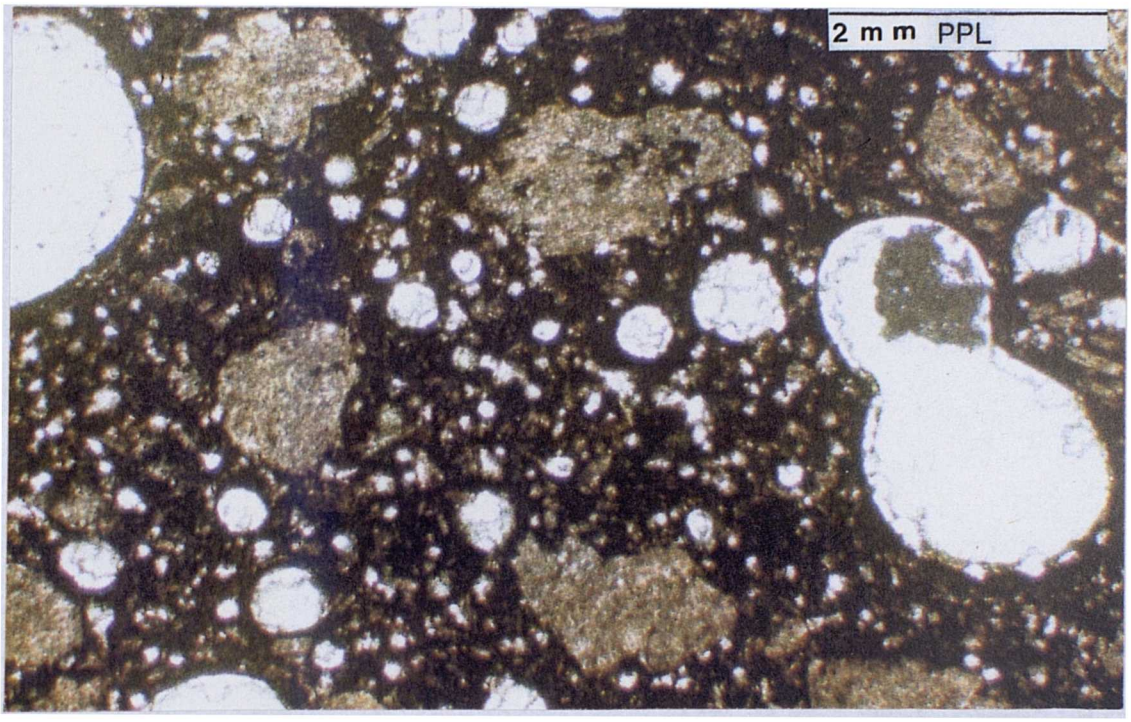

Plate 4.3 Highly vesicular lava from the lower Kawa Creek section. Plagioclase replaced by albite-sericite aggregate, groundmass dominated by dark brown, amorphous clay minerals.

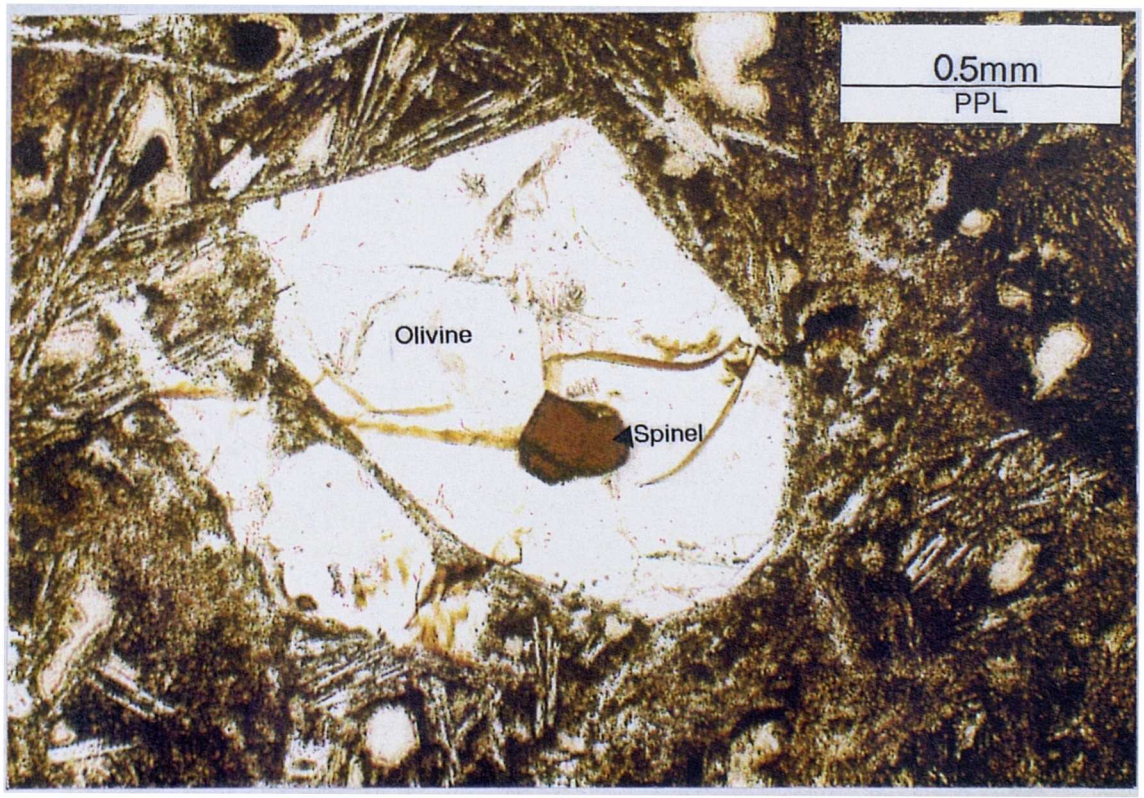

Plate 4.4 Type-1b spinel hosted within a pseudomorphed olivine phenocryst. From pillow lava, Namosi Creek

Non-enclosed individual grains are referred to as *type-2*. The second part of the classification refers to the state of alteration of the spinel grain when viewed in both transmitted and reflected light. Suffix *type-a* spinels are pristine with no *visible* sign of alteration using either microscopic technique. *Type-b* spinels have oxidised margins with development of an iron-oxide rim that encloses a pristine spinel core. *Type-c* spinels are fully altered, and the spinel is entirely oxidised and replaced by black iron-oxide. The classification was devised following reconnaissance work at Imperial College, London, in which the nature of spinel alteration was investigated using a combined electron microprobe and scanning-electron-microscope (SEM) facility. Spinel grains were analysed along core-rim traverses using a focused electron beam with a spot size of ~1μ m. The results of typical traverses are illustrated in Fig. 4.1 and indicate that significant chemical changes for petrogenetically useful element ratios can accompany the oxidation and breakdown of the pristine spinel phase. In the example of Fig 4.1a, the traverse across sample LP145 shows that the Mg/Mg+Fe ratio is the most severely affected ratio in the type-1b spinel grain with a decrease from Mg#=0.60 to 0.39 across the optically defined oxidised rim. In contrast, the Cr# is apparently unaffected by the alteration process, even within the magnetite rim, resulting in average Cr#=0.45 (n=10 spots, standard deviation = 0.021) for the traverse. The second example studied was a type-2b spinel in sample VL029 (Fig. 4.1b). This spinel showed a similar preservation of the Cr# across the altered rim (n=8 spots, average=0.40, standard deviation=0.012) while the Mg# again showed a marked decrease across the rim from Mg#=0.65 to 0.17.

These results indicate that the Cr# is little affected by the oxidative alteration processes so that pristine Cr# values are preserved even within the iron-oxide rims of the spinels. In contrast, the Mg# cannot be used as a reliable petrogenetic indicator in type-1c or 2c spinels or in the oxidised rims of type- 1b and 2b spinels. These results concur closely with those of Kimball (1990) who analysed a variety of pristine and altered spinels from a range of fracture-zone ultramafic rocks and ophiolites. This author concludes that alteration of the Cr# ratio is only likely to occur during the breakdown of spinel to form metamorphic hornblende, a reaction that has not been observed in this study. Alteration of the Mg# ratio, however, is widespread and may occur at lower temperatures due to the exchange of Mg^{2+} and Fe^{2+} that accompanies chlorite-forming reactions.

These results are further illustrated when the Yavuna Group data is plotted on a Mg#-Cr# diagram (Fig. 4.2a) using the well-known format of Dick & Bullen (1984). Displacement from an array of simple correlation between Cr# and Mg# occurs in a

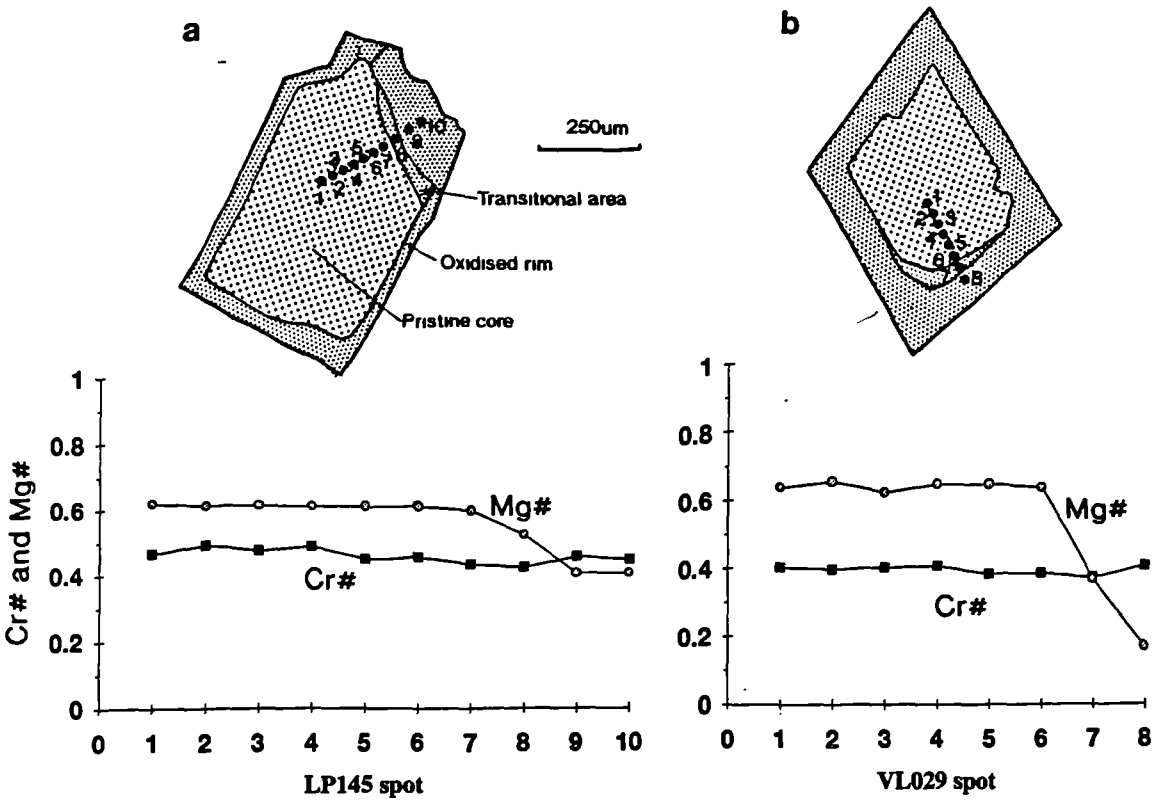

Fig. 4.1 Spinel core-rim compositional traverses. **a** shows a type-1b spinel (hosted, altered margins) in sample LP145 **b** shows a type-2b spinel (not hosted, altered margins) in sample VL029.

1c-type spinel (LP143) and also in a type-1b spinel (BH278). These shifts are unlikely to be a consequence of fractional crystallisation, because LP143, the sample with the lowest spinel Mg# (Mg#=9), has the highest whole-rock Mg# of the entire sample suite (Mg#=79.5). In the absence of any other obvious cause, the shift to low Mg# is considered to be entirely a result of alteration. If the two altered samples are corrected back to higher spinel Mg# then much of the Cr#-Mg# scatter of the Yavuna Group data would lie in a transitional position between the fields for oceanic basalts, backarc basalts and boninites as published by Dick & Bullen (1984), (Fig. 4.2b). Additional data from ODP Leg 125 and Troodos boninite spinels are also plotted in Fig. 4.2b for comparison with the Yavuna Group data. The recent ODP data illustrate that the Dick & Bullen (1984) boninite field is too narrow to encompass the entire Cr# range of boninites, probably because the it is biased towards refractory low-Ca boninites with high Cr# from Cape Vogel. The range of Mg# is also far greater than in the original boninite field, although, this may be an alteration-related effect. Dick & Bullen (1984) interpret the high Cr# of boninites and island arc basalts such as Troodos to represent derivation from a mantle source more depleted than that beneath mid-ocean ridges as a consequence of multi-stage melting histories and higher resultant degrees of partial melting. Their conclusions are supported by an extensive peridotite database which relates the difference in their *type-I* (Cr#<0.6) and *type-III* (Cr#>0.6) peridotites and associated volcanic rocks to the presence or absence of diopside in the mantle residue at the end of the melting event.

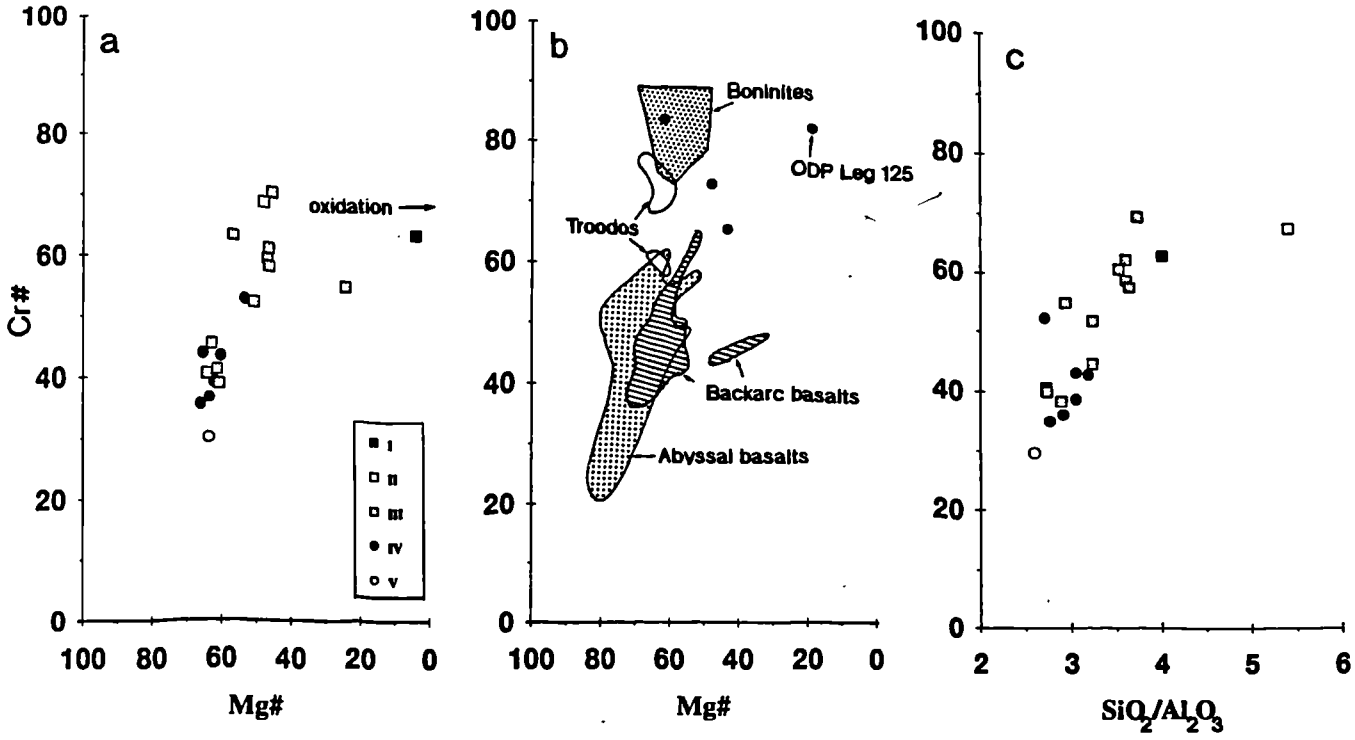

Fig. 4.2 **a** Cr#-Mg# diagram for Yavuna Group spinels using the format of Dick & Bullen (1984). **b** Cr#-Mg# diagram to illustrate compositional fields for abyssal basalts, boninites, Troodos ophiolite basalts, and backarc basalts (all from Dick & Bullen 1984) and ODP Leg 125 boninites (from Van der Laan et al. 1992). **c** Plot of Cr# versus SiO_2/Al_2O_3 for Yavuna Group data. Symbols correspond to magmatic groups as defined in chapter 5.

Irving (1976) presents convincing experimental evidence for additional complexity in spinel systematics of volcanic rocks. He investigates the influence of melt composition on the Cr# of co-existing spinel and his results suggest that the dependence of D_{Cr} on melt composition reflects the strong octahedral site preference of chromium. Thus, in a silica-rich, more polymerised melt, fewer of these sites would be available and Cr# in co-existing spinel would be higher. Fig. 4.2c provides strong support for the silica control hypothesis because the group II and III melts with relatively high SiO_2 contents (as defined in chapter 5) have Cr# at least as high as the group I (relatively low-SiO_2) boninite sample even though they are probably derived from less refractory sources and lower degrees of melting.

4.3.2 Olivine

Olivine is a common intratelluric phase in the least evolved Yavuna Group and Wainimala Group samples although the pervasive secondary alteration suffered by the lavas means that the phase is never seen in pristine condition. It can usually be

distinguished from clinopyroxene by the sharper angle of its terminal faces, its characteristic chlorite-calcite-smectite replacement assemblage, and the common presence of either pristine or altered Cr-spinel inclusions within or along the margins of the phenocryts. The olivine phenocrysts may exist as individual crystals up to 0.5mm across or in glomeroporphyritic clusters of smaller grains. Replacement products include smectite, calcite, chlorite and serpentine group minerals.

4.3.3 Clinopyroxene

Clinopyroxene occurs as small phenocrysts between 0.2 and 1mm in length and also as a groundmass quench phase. It is also the most common pristine phase in the lavas (e.g. Plate 4.5a). It is usually colourless when viewed in plane polarised light, although pale pink pleochroic varieties do occur. The phase breaks down during alteration to fibrous, pale green actinolite at its margins (Plate 4.5b) and, in the most altered samples, becomes fully pseudomorphed by actinolite, often with accompanying opaque phases (Plate 4.5c).

Compositional data for most analysed Yavuna Group clinopyroxenes fall along the diopside-augite boundary of the pyroxene quadrilateral as defined by Morimoto (1988), (Fig. 4.3a). Sample LP143, a high-Ca boninite sample, shows a more Mg-rich, Ca-poor augite composition. Primitive Wainimala Group samples also lie close to the augite-diopside boundary (Fig. 4.3a) with more evolved samples of the group trending toward increased Fe content along a similar trend to that of the Shiant Isles and Skaergaard tholeiitic intrusions (Fig. 4.3b). The main Yavuna Group data cluster has a generally higher Ca content than boninites from ODP Site 458, ODP Leg 125 high-Ca boninites and andesites from the Izu-Bonin arc, while LP143, the high-Ca boninite, plots within the ODP high Ca-boninite field. In terms of the trace elements, Ti and Na, only the four sets of data acquired through the accurate wavelength dispersive analysis technique can be plotted with confidence on a discriminatory diagram (Fig. 4.3c). The analysed samples show a range in composition between the boninite and MORB fields according to the criteria of Beccaluva et al. (1989) although assignment of the data into a unique boninite, arc tholeiite or basaltic andesite-andesite field cannot be made.

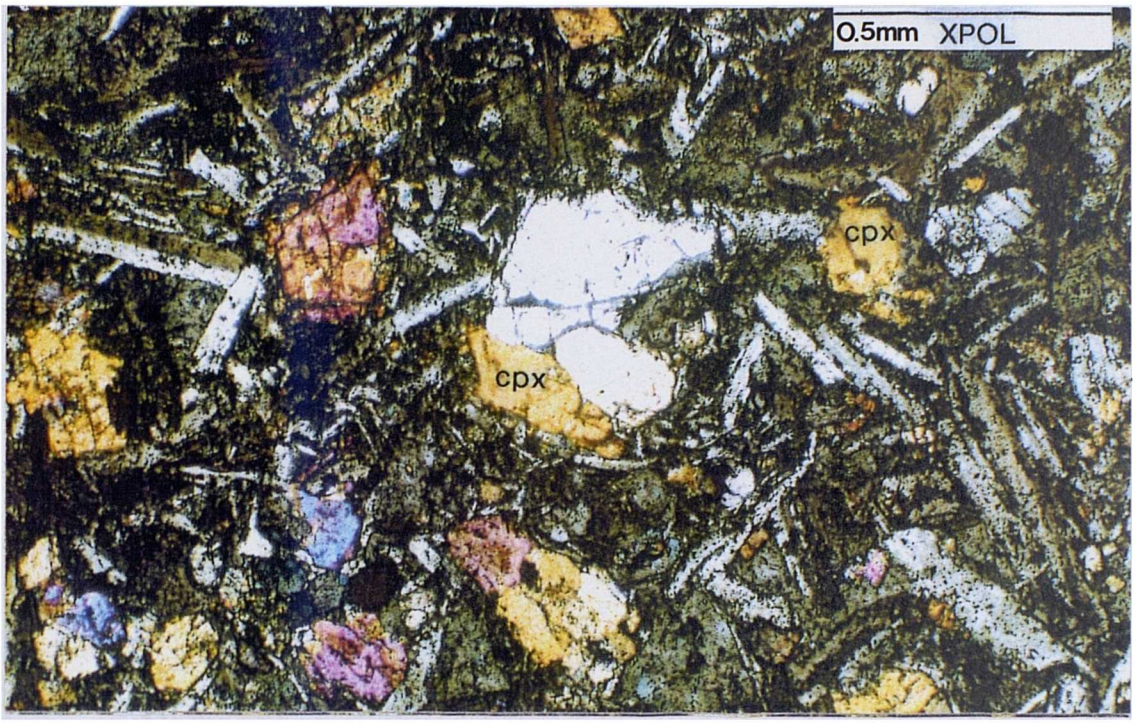

Plate 4.5a Pristine clinopyroxene microphenocrysts set in an albite-chlorite-quartz groundmass aggregate. Typical index-3 lower greenschist facies assemblage.

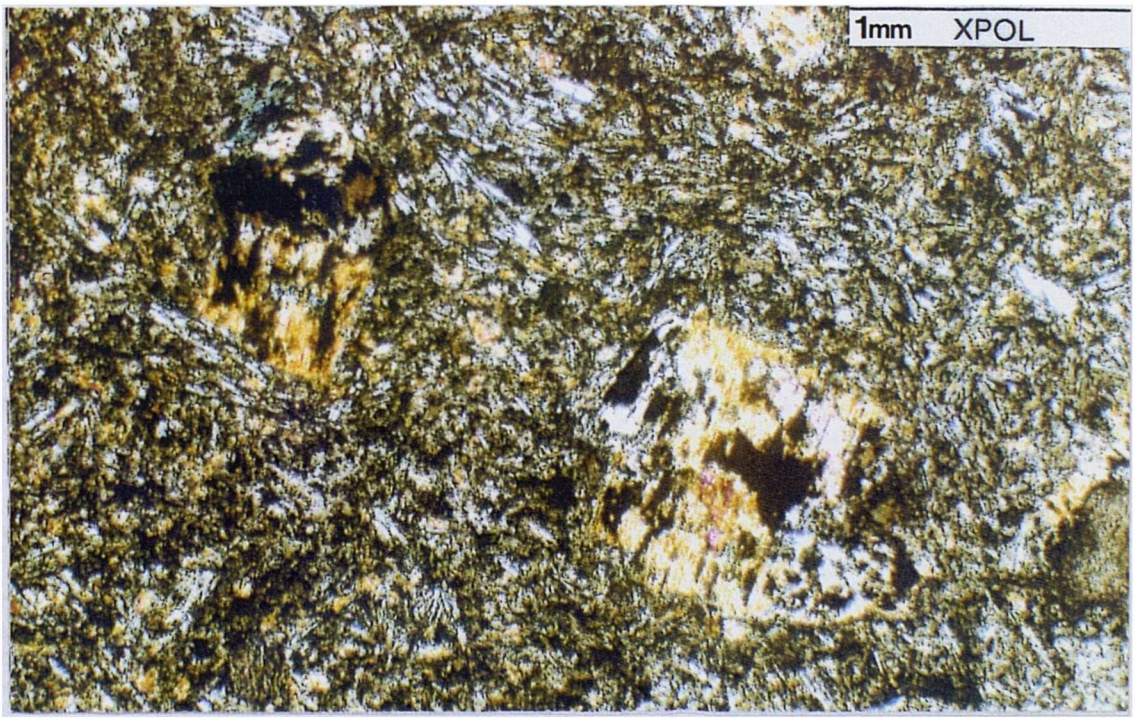

Plate 4.5b Clinopyroxene phenocrysts entirely replaced by aggregate of actinolite amphibole and iron oxide minerals. Typical index-5 metamorphic assemblage.

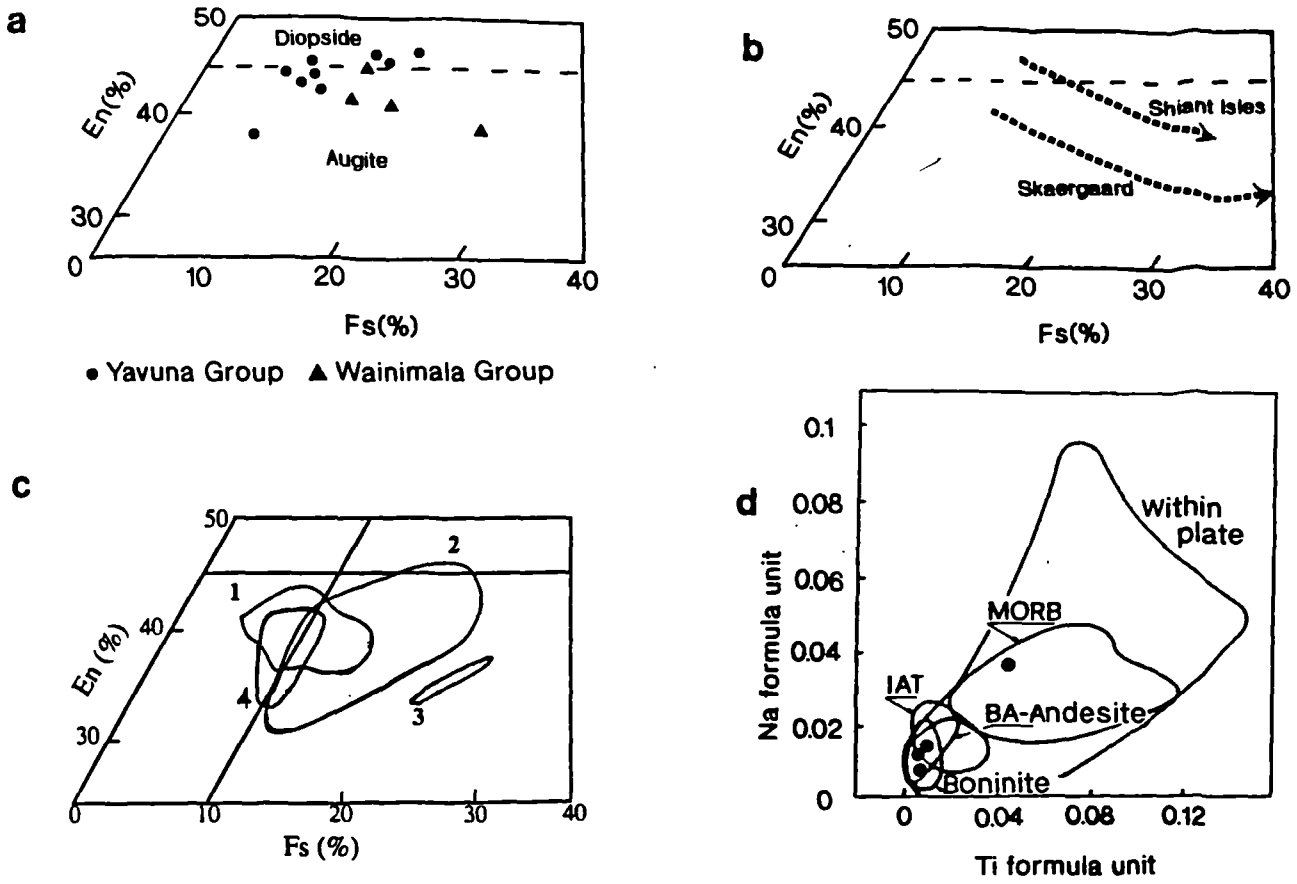

Fig. 4.3a Compositional data for Yavuna Group and Wainimala Group clinopyroxenes in the pyroxene quadrilateral defined by Morimoto (1988). **b** Comparative fractionation-related trends from an intrusive sill on the Shiant Isles, NW Scotland and from the Skaergaard intrusion (both from Deer et al. (1983). **c** Comparative clinopyroxene analyses from (1) Izu-Bonin andesites, (2) ODP Site 458 boninites, (3) Bonin Islands boninites, (4) ODP Leg 125 high-Ca boninites. Data from Lapierre et al. (1992) and Van der Laan et al (1992). **d** Yavuna Group WDS clinopyroxene data plotted on the discrimination diagram of Beccaluva et al. (1989)

4.3.4 Plagioclase feldspar

This low-relief phase exists as both an intratelluric and quench groundmass phase, although in most samples the primary mineral is invariably replaced by an albite-sericite assemblage. Phenocryts occur as either tabular crystals or more elongate laths up to 2mm in length. Relict zoning can be identified in some more evolved samples and is particularly characteristic of the porphyritic samples from the Kawa Formation and Nadele Breccia (Plate 4.6). These samples also show widespread corrosion and resorption of the plagioclase phenocryst cores. The core voids are filled by groundmass quench minerals indicating that the dissolution of the primary phase occurred in the

intratelluric environment rather than during post-eruptive alteration. The principal edifice lavas are consequently inferred to have undergone a complex history involving significant disequilibrium and magma mingling prior to eruption.

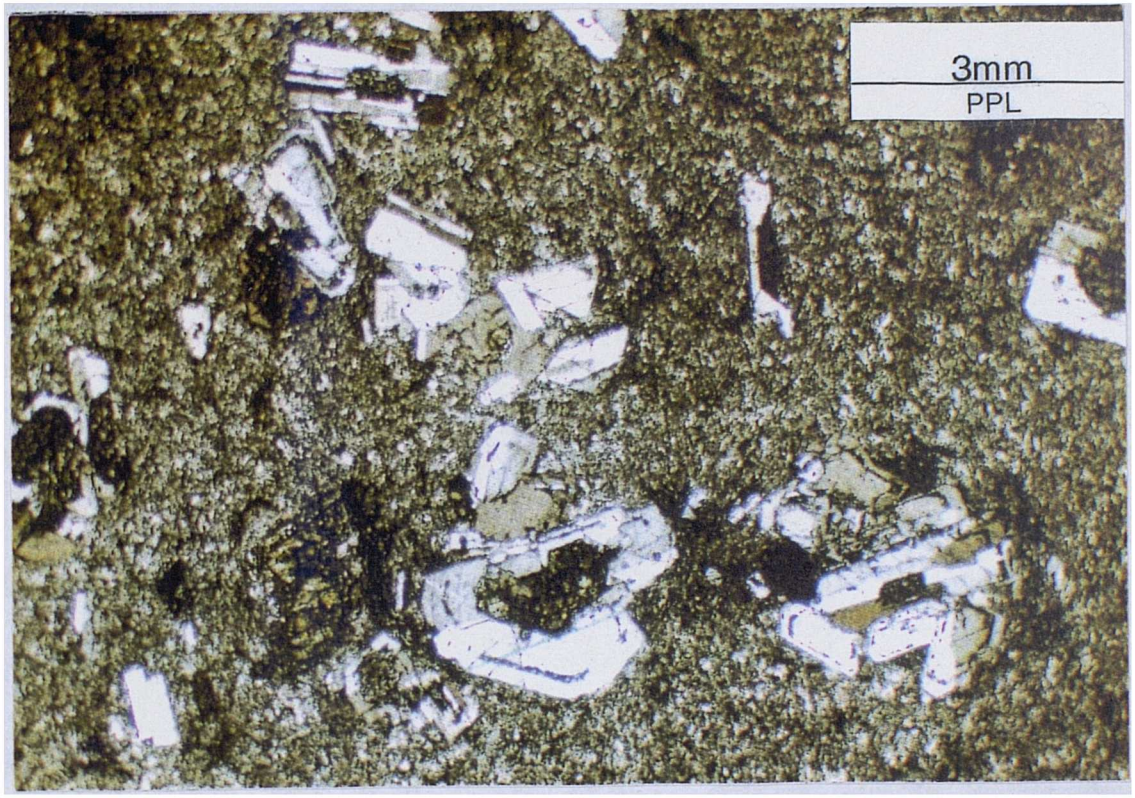

Plate 4.6 Photograph to illustrate compositional zoning in plagioclase phenocrysts of the principal edifice lavas. Phenocryst cores are resorped and the voids filled by quench groundmass minerals indicating that disequilibrium occurred in the intratelluric environment.

4.3.5 Iron oxide minerals

Opaque iron oxide minerals exist in a variety of forms throughout the sample suite. In the quench lavas of the Yavuna Group, finely disseminated specks of opaque iron oxide characterise the groundmass of some samples. In the slower-cooling mega-pillow units, oxide minerals form as a late-crystallising phase in the interstices of plagioclase and clinopyroxene. Euhedral phenocryts of magnetite are more common in evolved samples from each of the volcanic groups. In highly-altered samples, breakdown of the primary oxide to secondary sphene is noticed.

4.3.6 Amphibole

Hornblende is a commonly occurring intratelluric phase in the principal edifice lavas of the Nadele Breccia and Kawa Formation and is also present in trace quantities in some

highly evolved Kalaka Dacite samples. In heavily altered samples, the primary phenocrysts are replaced by chlorite and iron oxides. Hornblende also occurs as a primary metamorphic phase in the contact aureole of the Yavuna Stock. Secondary amphibole is present in many altered lavas in the form of pale green fibrous actinolite. The phase is formed during the breakdown of clinopyroxene and its presence can be used as a broad indicator of metamorphic grade within the greenschist facies.

4.3.7 Crystallisation orders

Where evidence for the order of intratelluric phase crystallisation was observed in a sample, the order is recorded in the appendix. As the primary classification of the sample suite is made using geochemical, rather than petrographic criteria, the full implications of the variations in crystallisation order are discussed in chapter 5.

4.4 Secondary minerals

The recognition of distinct secondary mineral parageneses provides the basis for a classification of alteration index. The alteration indices are taken directly from those proposed by Hathway et al. (in prep.) for the SW Viti Levu geological bulletin and are summarised below.

1. Zeolite-calcite-analcite-smectite. Augite may show patchy alteration to calcite but is otherwise unaltered. Plagioclase is generally replaced by secondary phases, but where not is clear and zoned. The zeolite facies.

2. Prehnite-calcite-chlorite. Augite is largely unaltered as above. Plagioclase albitized and flecked with sericite where not replaced by other secondary phases. The prehnite-pumpellyite facies.

3. Chlorite-epidote-calcite-(sphene-quartz). Plagioclase is albitized. Augite may be replaced by secondary phases, but is largely unaltered as above. No actinolitic amphibole. The albite-epidote-chlorite subfacies of the greenschist facies (Crook 1963).

4. Actinolitic amphibole-epidote-chlorite-(sphene-quartz). Some augite does remain, but the phase invariably is replaced by amphibole along its margins. Plagioclase is albitized and cloudy. The albite-epidote-actinolite subfacies of greenschist facies.

5. Actinolitic amphibole-epidote-(sphene-quartz). Augite is completely replaced by amphibole. Plagioclase is generally albitized, but may be clear and zoned. The greenschist facies.

6. Hornfels assemblage consisting of hornblende, plagioclase and iron oxides (also quartz in some cases).

The details of the metamorphic assemblages are based partly upon the regional study of secondary minerals by Crook (1963) which incorporated X-Ray diffraction (XRD) analysis. Secondary minerals are hosted in the groundmass of the samples as discrete veins or patches, as pseudomorphs after primary phases, or in amygdales. Primary mineral breakdown and reactions occurring during the formation of the secondary assemblages are summarised in Fig. 4.4. The diagram shows the range of secondary minerals encountered in each alteration assemblage. The range of temperatures spanned by each assemblage is indicated on the right of the diagram and is taken from the range of reactions and experimental work of Elthon (1981).

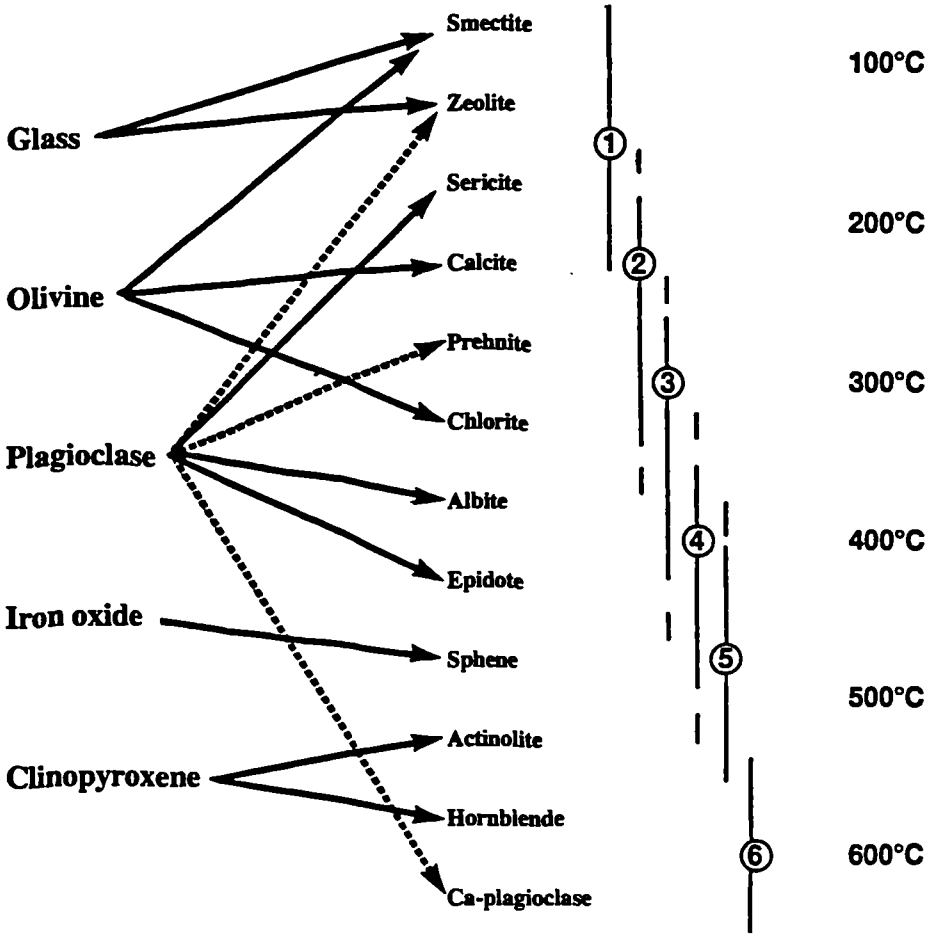

Fig. 4.4 Relationships between primary and secondary assemblages. Solid lines represent observed transformations/replacements, dotted lines are inferred or reported by Crook (1963). The range of alteration indices is given as a guide to the characteristic mineral parageneses and the temperature scale is taken from the experimental and petrographic study of Elthon (1981).

Each sample has been assigned an alteration index based upon the above classification. Almost all Yavuna Group samples show index-3 or higher greenschist assemblages. Index-5 and -6 assemblages characterise the contact aureole of the Yavuna Stock and also occur in the vicinity of the Colo Takara Stock and associated hornblende andesite dyke swarm (Hathway et al. in prep.). Within the Wainimala Group, a clear depth-dependant relationship is observed in the distribution of metamorphic facies. The lavas of the edifice and inter-edifice terranes are mainly index-1, zeolite facies lavas while the Wainimala Group-related dyke swarm that cuts the Yavuna Group is characterised by index-3, or higher, metamorphic assemblages.

Several index-1 Wainimala Group samples which showed extensive replacement of primary phases and volcanic glass by clay minerals were selected for XRD analysis to define precisely the clay mineralogy for comparison with ODP drill-core alteration assemblages (e.g. Taylor et al. 1992). An example of the XRD pattern for the typical dark-brown amorphous clay mineral alteration product is illustrated for one sample from the Dakadaka Basalt (BH045, Fig. 4.5). Clay minerals were separated from the bulk-rock sample using a conventional floatation technique and heated gently to dryness. The 5.9° 2θ angle corresponds to a 15Å spacing in the mineral which is characteristic of an illite/montmorillonite mixed layer smectite with 35-40% montmorillonite content (Bayliss et al. 1986).

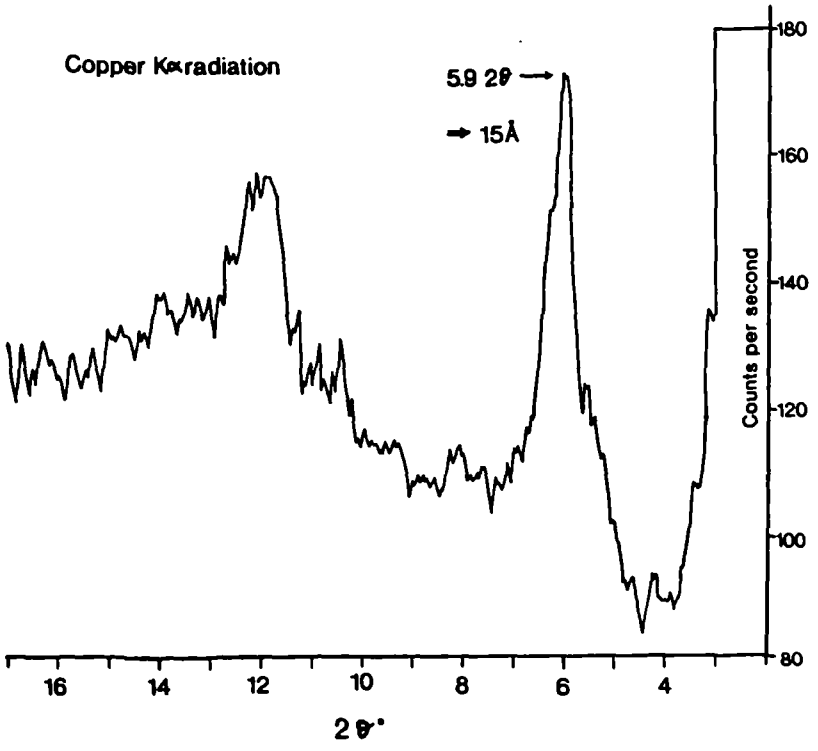

Fig. 4.5 XRD-pattern of dark-brown amorphous clay minerals in groundmass of Dakadaka Basalt sample BH045. See text for discussion.

4.5 Implications of secondary alteration for geochemical analysis

Post-eruptive alteration hampers almost all geochemical studies to some extent. In southwest Viti Levu, the extensive nature of the alteration process has been illustrated and must be accounted for when dealing with the geochemistry of the rocks. In some cases, geochemical changes accompanying visible signs of alteration can easily be predicted. For example, CaO and Sr systematics may be disturbed by the development of secondary calcite and epidote. However, the scale upon which this the mass-balance is disturbed is the critical matter for consideration in this study. In the case of a mineral vein, matter is undoubtedly transported in and out of a sample on a hand-specimen scale and disordered geochemical systematics will result. On the other hand, the breakdown of augite to actinolite or opaque Fe-Ti oxide to secondary sphene takes place on a sub mm-scale. This type of alteration will not, therefore, involve changes to the mass-balance of compatible and high-field-strength elements that are hosted within mafic and accessory phases. When preparing rocks for geochemical analysis, samples that were cut by secondary veins of 1-2mm width were hand picked to exclude obvious alteration products. In addition, large amygdale-filling minerals were also removed. Despite these precautions, however, some secondary material was unavoidably included in many samples and is reflected in considerable scatter in fractionation trends that involve potentially mobile elements (e.g. the CaO/Al_2O_3 ratio). The problems of element mobility is discussed in more detail in chapter 5.

CHAPTER 5

Major and trace element geochemistry

5.1 Introduction

This chapter utilises geochemical analyses of volcanic and plutonic rocks to provide a basic for assessing the nature of magmatic variability in the early arc sequences. Analytical data have been obtained using several methods during the course of the study (Table 5.1). Comparisons between data obtained using XRF and ICP-MS are described and discussed in the appendix together with details of analytical techniques, error estimates, and the full geochemical dataset.

Durham	X-Ray fluorescence spectrometry (XRF)	Major and trace elements 250 samples
Durham	Inductively-coupled-plasma-mass-spectrometry (ICP-MS)	Trace elements 30 samples
RHBNC London	Thermal ionisation mass spectrometry (TIMS)	Radiogenic isotopes 6 samples

Table 5.1 Details of analytical techniques

The chapter begins by describing the effects of post-eruptive alteration on whole-rock geochemistry. The rocks of the Yavuna Group and Wainimala Group are then classified using alteration-resistant geochemical criteria to provide a basis for a study of shallow-level and source-related magmatic processes in the protoarc and second arc.

5.2 Alteration effects

Several geochemical criteria that are commonly used for classification and discrimination in island volcanic series (e.g alkali contents, Rb/Zr and Ba/La ratios) must be applied with caution in the study of altered rocks because of the low ionic potential (charge/radius) of many key elements, and the consequent tendency for the elements to be preferentially mobilised during hydrothermal alteration processes. This presents a major problem in the study of altered arc rocks, because an input of large-ion-lithophile elements (LILE) carried by aqueous fluids from the subducting slab into

the source region of island arcs and the manifestation of this signature in the resulting melts has become a fundamental tenet of subduction zone geochemistry (McCulloch & Gamble 1991).

Two distinct styles of chemical alteration are recognised in this study. The most common type, which affects rocks from all of the volcanic groups studied, involves the redistribution of alkaline and alkaline-earth elements. In highly altered samples this results in variable amounts of leaching and enrichment of the elements K, Rb, Cs, U, Ba, Pb, Sr, as well as the major element oxides Na_2O, K_2O, and CaO, such that their concentrations in altered rocks may be unrepresentative of primary magmatic values. This effect (hereafter termed *type-1* alteration) can be demonstrated on an outcrop scale by plotting selected major and trace element concentrations of the altered and heavily veined sample VL017 normalised to a less-altered sample, VL016, taken from the same pillow lava complex (Fig. 5.1). Wide variations across the range of normalised LILE, as well as some major elements, are noted for the altered sample. In contrast, the rare-earth elements (REE), Th and other high field strength elements (HFSE) such as Zr, are essentially unaffected.

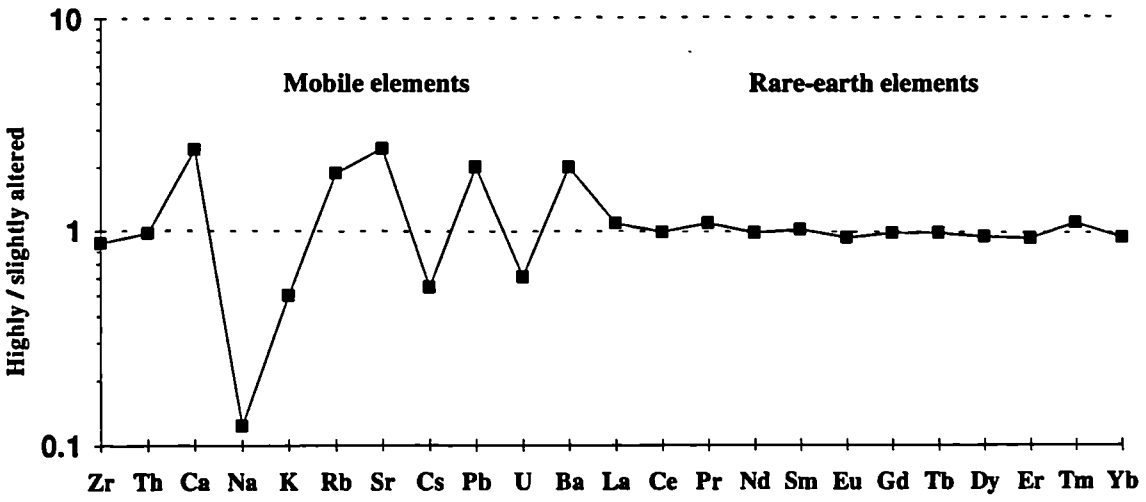

Fig. 5.1 Sample VL017 normalised to sample VL016 to illustrate type-1 alteration involving mobility of LILE and certain major elements. The REE, Th and the HFSE are comparatively unaffected.

The highly selective and unpredictable nature of type-1 alteration is further illustrated by plotting potentially mobile elements against alteration index using the criteria defined in chapter 4. Fig. 5.2 demonstrates that no simple correlation exists between element

mobility and metamorphic grade in the lava pile. There is, however, some sympathetic variation between the mobile major element oxides such as CaO and Na_2O and some trace elements. One clear example of this occurs in sample 90-25 in alteration group 5. This sample is highlighted in Fig. 5.2 and shows very high CaO (23 wt.%) yet low levels of Na_2O and K_2O that are close to background for the XRF technique. The increased CaO is accompanied by elevated Sr which leads to an anomalously high Sr/Zr ratio of 17; Rb, however, is apparently unaffected. Samples 90-6 and BH416 show contrasting anomalously high K_2O contents of 5.96-6.02 wt.%, but only background values for CaO, Na_2O, Sr and Rb. In another example, sample 90-55 shows an anomalously high Na_2O content of 8.55wt.%, yet background K_2O and apparently unaffected Sr and Rb contents. It is concluded that no uniform pattern of type-1 element exchange exists within the lava pile and that accordingly these elements cannot be used with confidence in geochemical interpretations.

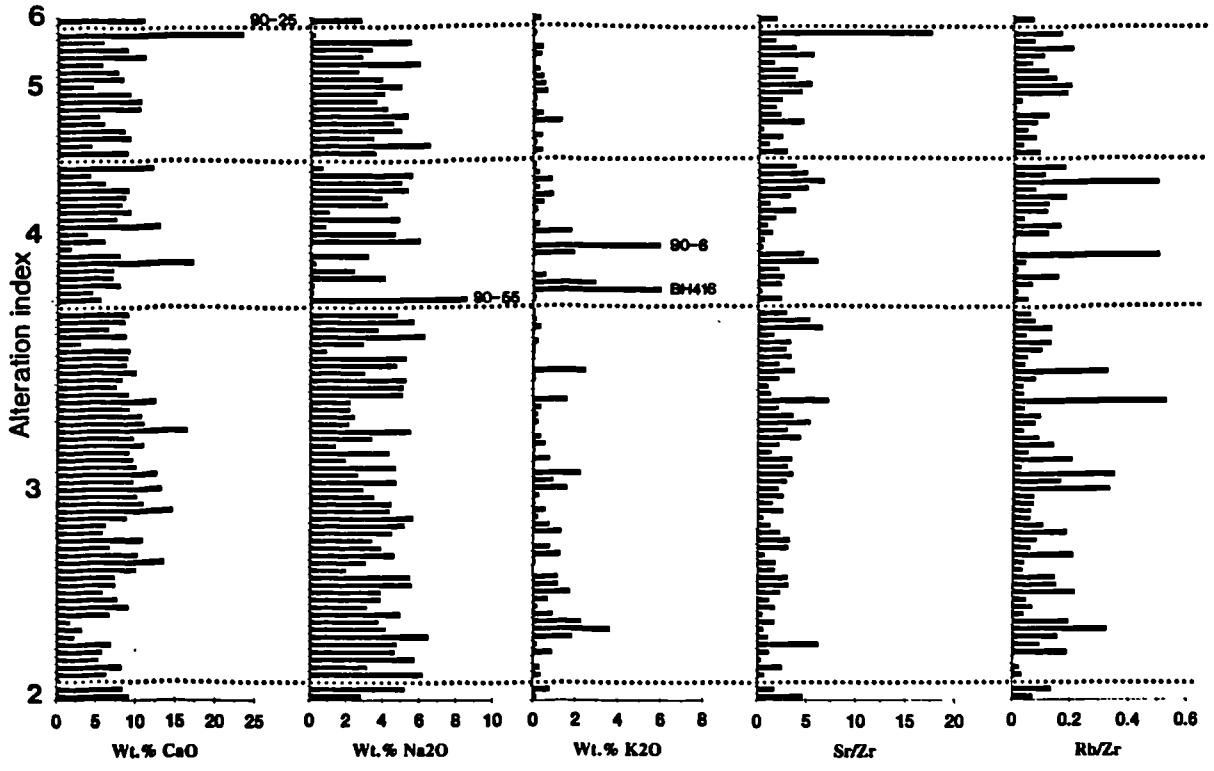

Fig. 5.2 Potentially mobile major element oxides and trace element ratios plotted against alteration index as defined in chapter 4.

While this behaviour is a predictable consequence for elements of the lowest ionic potential (Humphries & Thompson 1978), some authors have noted that Sr, although an element of low ionic potential, may show a lesser tendency to be remobilised in altered

rocks because the element is preferentially partitioned into the lattice of plagioclase phenocrysts rather than the glassy groundmass of volcanic rocks (e.g. Taylor et al. 1992). In a later part of this chapter, following the division of data into geochemical groups, the effects of alteration on Sr distribution is considered in more detail. The second style of alteration (hereafter termed *type-2*) is less common and affects mainly volcanic rocks from the Wainimala Group. It is characterised by redistribution of P, Y, and the rare-earth-elements and is highlighted in Fig 5.3 in which the multi-element profile for pervasively altered Dakadaka Basalt BH045 is shown normalised to the less-altered basalt BH173. This style of alteration is unusual in that the enriched elements in this case possess high charge/radius ratios, which means that theoretically at least, they should not easily be transported in aqueous fluids (Tatsumi et al. 1986). A similar alteration style is documented in arc basement rocks from ODP drill core (Taylor et al. 1992, Murton et al. 1992) and is attributed by these authors to the breakdown of volcanic glass to smectite-group clay minerals during hydrothermal alteration. The occurrence of this alteration-style in smectite-rich samples from the Wainimala Group (see XRD analysis of BH045, chapter 4) supports this assertion and allows affected samples easily to be screened out prior to geochemical interpretation.

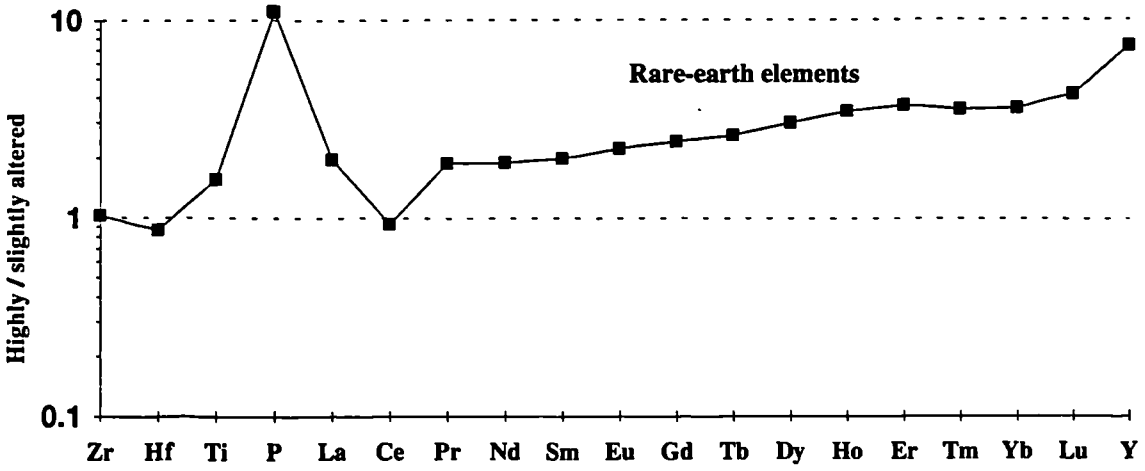

Fig. 5.3 Sample BH045 normalised to sample BH173 to illustrate type-2 alteration involving mobility of rare-earth elements, Y and P. High-field strength elements are comparatively unaffected.

A third type of alteration is peculiar to the Dakadaka Basalt Formation and involves enrichment of MnO in the altered sample up to levels of 0.44 wt.%. This *type-3* alteration is consistent with an origin through precipitation of an Mn-oxide on the surface of the rock. Although samples with visible Mn crusts were sawn and cleaned thoroughly before crushing, impregnation of some samples has clearly occurred,

probably through precipitation in micro-fractures in the rock. The secondary Mn-oxide deposits are an obvious consequence of the 'black-smoker' type Fe-Mn mineralisation which characterise parts of the Wainimala Group (Colley & Walsh 1987).

5.3 The Yavuna Group

5.3.1 Classification

Traditionally, most classifications of island arc volcanic rocks are based upon the division into *tholeiitic*, *calc-alkaline* and *alkaline* series following the FeO*[1]/MgO and alkali content criteria of Miyashiro (1974). These divisions were refined by Gill (1981) to include reference to the rate of change of FeO*/MgO with SiO_2 and, while this classification is still widely used in the literature, it is somewhat biased towards intermediate andesitic compositions and does not provide sufficient resolution for the study of the primitive arc volcanic rocks which comprise much of this thesis. Over the past decade, new classification schemes have been developed to cover the wide range of depleted and ultra-depleted compositions sampled from the Eocene and Oligocene arc terranes of the western Pacific. Most schemes use variations in the contents of high-field-strength elements, for example, Ti, Y, and Zr, to distinguish arc tholeiites, depleted arc tholeiites and boninites, with further refinements being made using major elements such as SiO_2 and CaO, e.g. Crawford (1989), Arculus et al. (1992). Many authors emphasise that divisions of this sort are arbitrary and that in most cases group boundaries of this type should be considered transitional in nature.

HFSE contents are used as the major discriminant in assigning lavas of the Yavuna Group (YG) to separate geochemical groups. While Ti, Y, and Zr have individually been used to classify subduction-related lavas by previous authors, a multi-element classification scheme is used in this study. Y concentrations are used as a primary discriminant because of the evidence for Zr enrichment in some boninite suites (Hickey & Frey 1982; Pearce et al. 1992b) and the possible anomalous effects of second stage mantle partial melting on Ti and Zr abundances (Parkinson 1993). The primary Y discrimination was made by arbitrarily separating the Yavuna Group data into six groups of increasing HFSE content (Fig. 5.4a). The samples were assigned to groups on the basis of their Cr-Y abundances. Covariation in the compatible (Cr) and incompatible (Y) elements allow the effects of fractional crystallisation to be evaluated and separated

[1]FeO* = Total iron

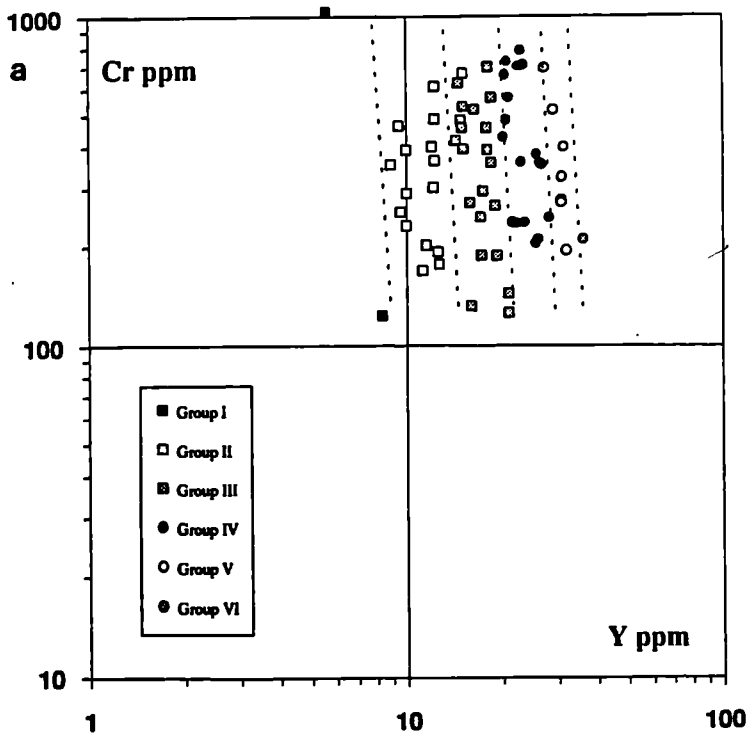

Fig. 5.4a Classification of least-evolved Yavuna Group lavas into six sub-groups of successively higher HFSE-content. The primary HFSE-assignment is made using Y content.

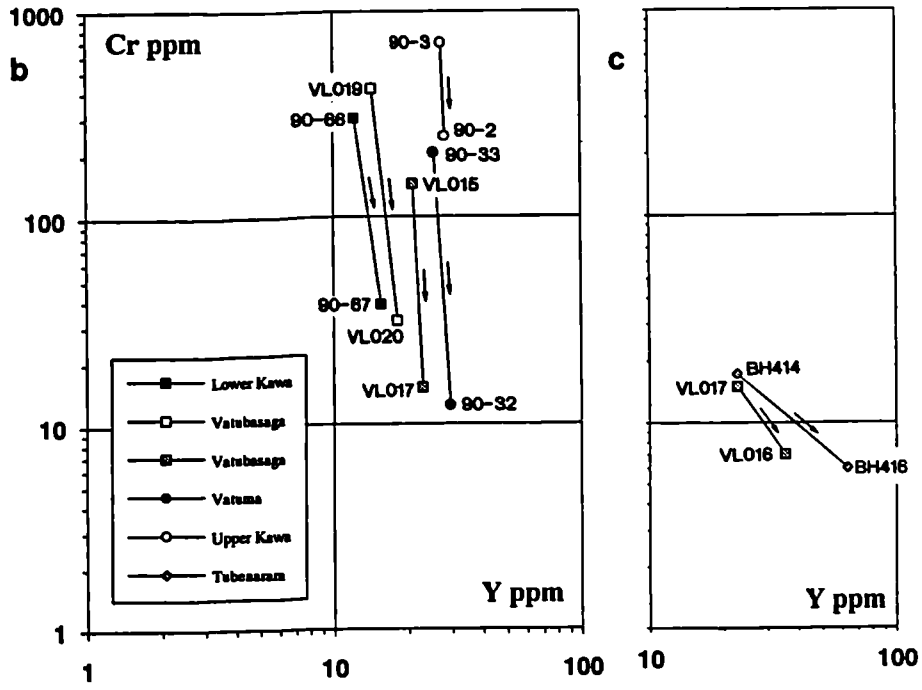

Fig. 5.4b Fractionation trends derived from individual outcrops in the Yavuna Group. Subvertical trends above 20ppm indicate that the compositions of the parental lavas of the sub-groups are not related through simple fractionation processes and reflect variations in the mantle source. c Shallowing of fractionation trends at Cr< 20ppm

from the trace element signatures of the mantle source that are preserved in the parental melts of each group (Pearce 1982). The gradients of the lines defining the group boundaries were derived by regression of data from cogenetic lavas sampled within individual outcrops (Fig. 5.4b). It is important to note that the subvertical trends on this diagram strongly imply that the parental magmas to each separate group are unrelated through simple fractionation processes at Cr>120ppm. The second step of the procedure involved checking the primary classification against similar plots for the elements Ti and Zr. In cases where both Ti and Zr abundances give a different classification for a sample, then that sample was re-assigned. These samples are rare and may have been affected by type-2 alteration which can cause Y-mobility. In cases where only one of the Ti or Zr abundances gives a different classification, then the Y classification was retained. The final group classifications for Ti and Zr are shown in Fig. 5.5a and 5.5b respectively.

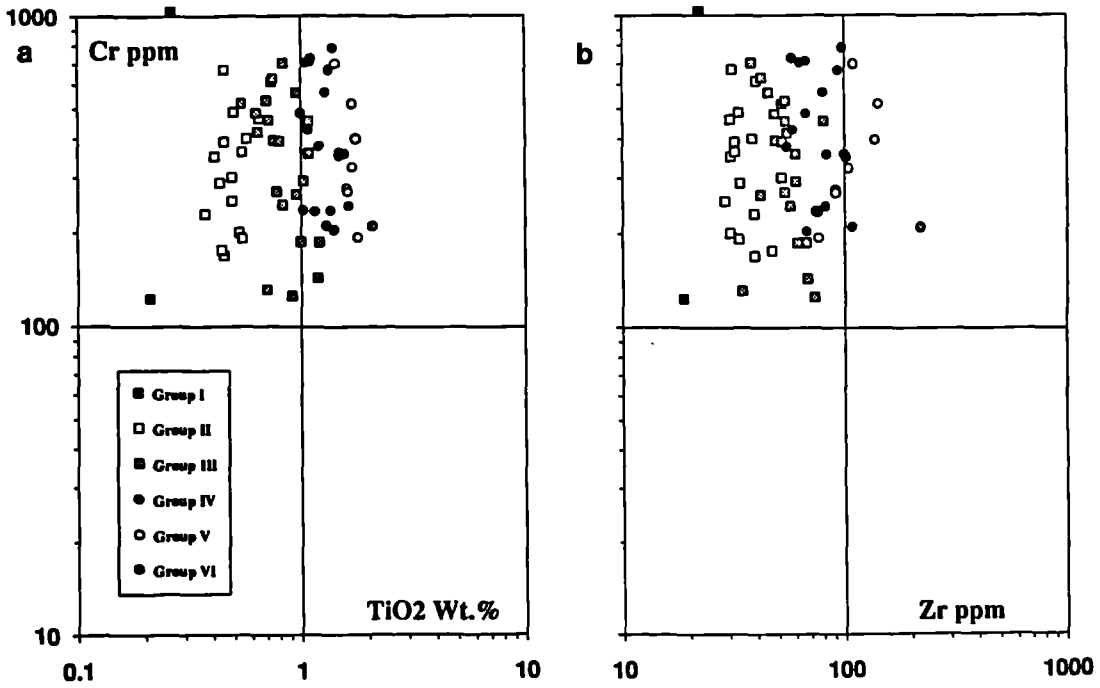

Fig. 5.5a and b Comparative TiO_2 and Zr concentrations for least-evolved Yavuna Group samples assigned to sub-groups primarily on the basis of Y contents.

Generally good separation is seen for the six groups on these plots although there are several samples which plot in anomalous positions in one or more of the diagrams. Possible causes of these variable HFSE ratios are investigated in chapter 6. Given the number of samples analysed, it is impractical to make a more rigid HFSE-based classification. Division of the data into 10 groups, for example, would involve unnecessary complexity and would not alter the petrogenetic arguments presented later

in the thesis. Samples from 'Eua cannot be given a rigid classification according to the scheme because none of the analysed samples have Cr>120ppm. However, the fractionation trends suggest that the parental 'Eua magmas had very low HFSE abundances, similar to those of the YG I or YG II melts.

The classification scheme was applied to more evolved Yavuna Group samples (i.e. Cr<120ppm) by extrapolation of fractionation trends to this compositional range. Although only two such trends are recorded (Fig. 5.4c), the vectors are sub-parallel to those of other arc volcanic suites (Pearce 1982). The shallowing of the trends was attributed by this author to the incoming of plagioclase in the fractionating assemblage. The classification is applied to an individual sample by giving the primary HFSE group number of the parental magma followed by the letter E (for evolved). For example, sample VL016 (Cr=15ppm, Y=23ppm) is assigned to Group IVE.

Within such an HFSE-based classification scheme, only the YG I melts can, by virtue of their very low HFSE abundances, be considered as boninites (following the criteria of Hickey & Frey 1982, 0.1wt.%<TiO_2<0.5wt.%). YG II melts are transitional to boninites in this sense but should, more precisely, be classified as tholeiites. Plotting the Yavuna Group data on a standard Miyashiro-type discrimination diagram illustrates the difficulty of making an entirely rigid classification (Fig. 5.6).

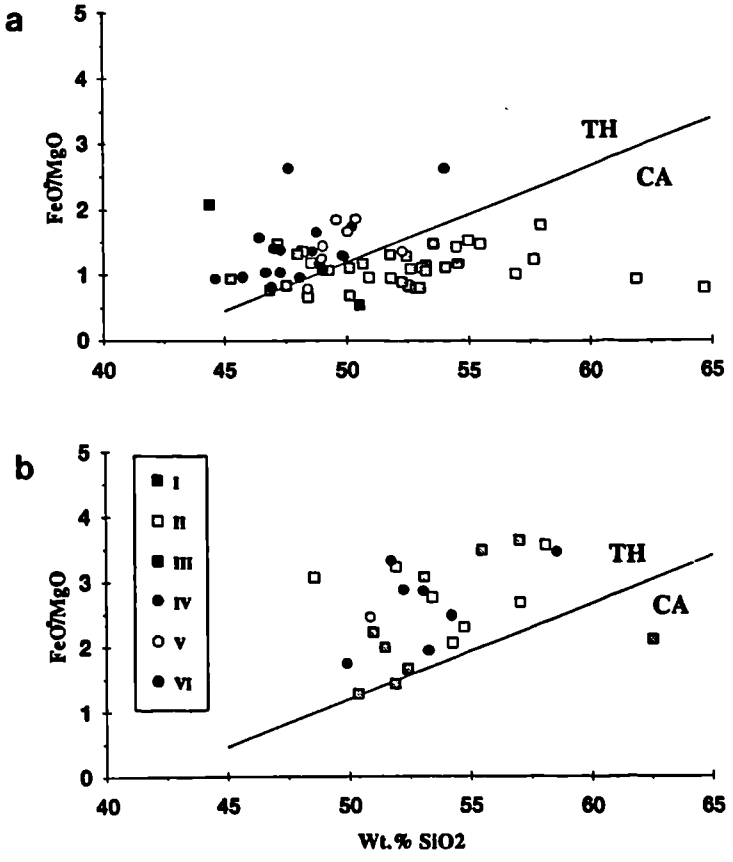

Fig. 5.6a SiO_2-FeO*/MgO plot of least-evolved (Cr>120ppm) Yavuna Group lavas. **b** Similar plot for Yavuna Group lavas with Cr<120ppm. Diagrams from Miyashiro (1974).

Primitive samples (Cr>120ppm) show no clear trend to higher FeO*/MgO yet show a wide range in SiO_2. High SiO_2 contents are particularly apparent for the Yavuna Group II (YG II) melts and become a less pronounced feature in YG III and IV. SiO_2 contents of boninites and depleted arc tholeiites generally show a similarly wide range (from 52-66 wt.% for the Cape Vogel, Troodos, New Caledonia, Bonin Islands and Marianas Trench suites, Crawford et al. 1989). Differentiated samples (Cr<120ppm) illustrate a well-defined tholeiitic fractionation trend with lower FeO*/MgO ratios only occurring with the onset of iron-oxide fractionation at high SiO_2 (Fig. 5.6b). The least differentiated Yavuna Group samples are compared with the full boninite dataset from ODP Leg 125 in Fig. 5.7. The ODP boninites all have SiO_2>50 wt.% and are grouped on the basis of CaO contents into low, intermediate and high-Ca types (Arculus et al. 1992). Again, on this basis, the only lavas that can be classified as boninites are those from YG I which are low-SiO_2, high-Ca type boninites. The other groups form a transitional spectrum from the high SiO_2 and low HFSE contents of YG II towards higher HFSE and lower SiO_2 in YG III and IV. In terms of SiO_2 and CaO, YG I melts cannot be considered transitional to YG II-VI. The latter groups are therefore formally classified separately.

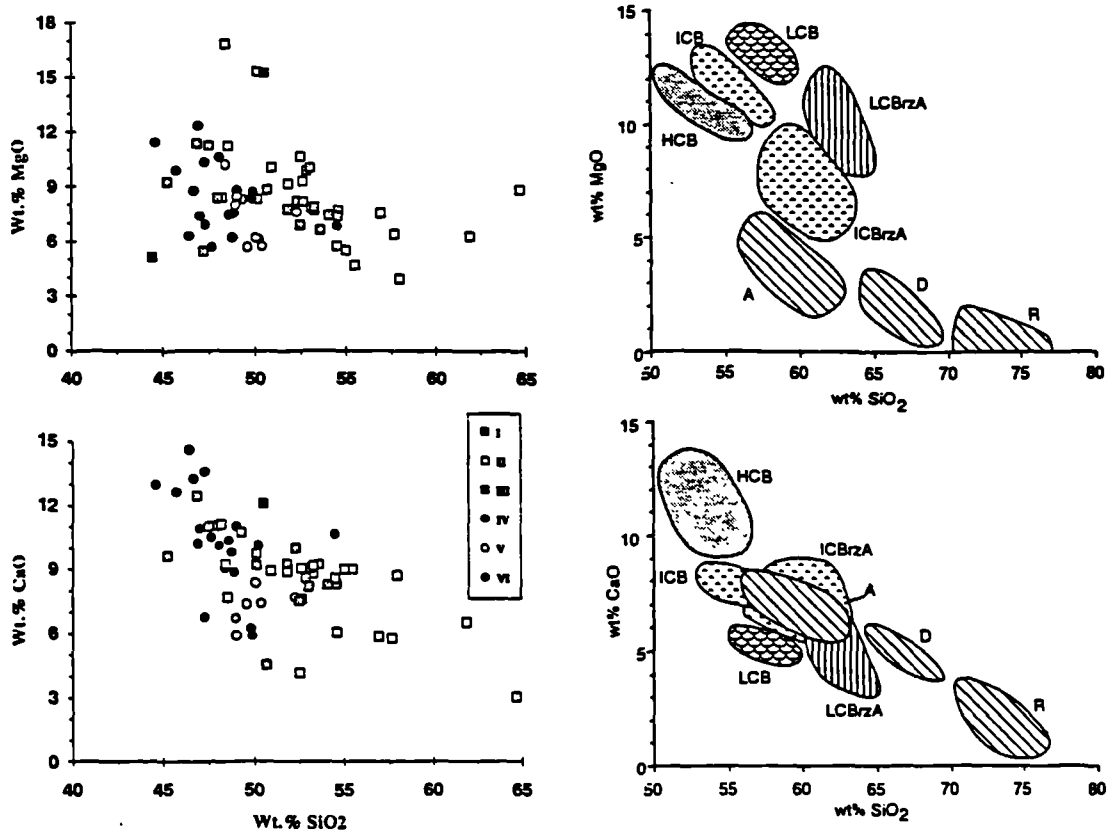

Fig. 5.7 Plots of SiO_2-MgO and SiO_2-CaO for Yavuna Group and ODP Leg 125 data. LCB=low-Ca boninite, LCBrzA=low-Ca bronzite andesite, ICB=intermediate-Ca boninite, ICBrzA=intermediate-Ca bronzite andesite, A=andesite, D=dacite, R=rhyolite, HCB=high-Ca boninite.

The terms 'depleted' and 'enriched' are used to refer to HFSE abundances from Fig. 5.4a, and the prefix -Si is used to refer to displacement on Fig. 5.6a. All of these groups are classed as tholeiites on the basis of the fractionation trajectories of evolved samples (Fig. 5.6b) and the term 'arc' is included in each group to emphasise the tectonic setting. Table 5.2 summarises the full classification. It is important to note that the term 'island arc tholeiite' as defined by Gill (1981) would correspond to the term 'depleted arc tholeiite' in this study. This is seen as an unavoidable consequence of making a precise classification of the unusually wide range of compositions present within the Yavuna Group.

Group	Classification of parental melts
YG I	High-Ca boninite
YG II	High-Si depleted arc tholeiite
YG III	Transitional high-Si arc tholeiite
YG IV	Arc tholeiite
YG V	Enriched arc tholeiite
YG VI	Highly-enriched arc tholeiite

Table 5.2 Summary classification of the Yavuna Group lavas

5.3.2 Geochemical variation within the Yavuna Group stratigraphy

5.3.2.1 HFSE group variations

The volcanic stratigraphy outlined in chapter 3 is used as the basis for assessing compositional variation in the Yavuna Group. Fractionation-corrected Y contents are shown within the structurally-corrected volcanic stratigraphy taken from chapter 3 (Fig. 5.8). Analysed basement samples whose position in unknown within the scheme (e.g. clasts in Nadi breccia etc., 9 samples in total) are omitted from the diagram. The fractionation correction is made using the IS (incompatible standardised) method of Taylor (1990) in which the value of the incompatible element in the lava is normalised to a primitive (700 ppm Cr) composition using the equation:

$$\text{IS value} = g\,(C\text{-}CS) + I$$

where: g = Gradient of liquid line of descent (average of regression lines from Fig. 5.4)

C = Compatible element concentration in lava

CS = Compatible element standardising value (700 ppm Cr)

I= Incompatible element concentration in lava

The resulting IS values enable more valid comparisons to be made between sectors of the reconstruction, and result in several important observations.

(i) The most depleted YG I and YG II melts are found in the lowest parts of the Yavuna Group. They do not occur in the upper parts of the group.

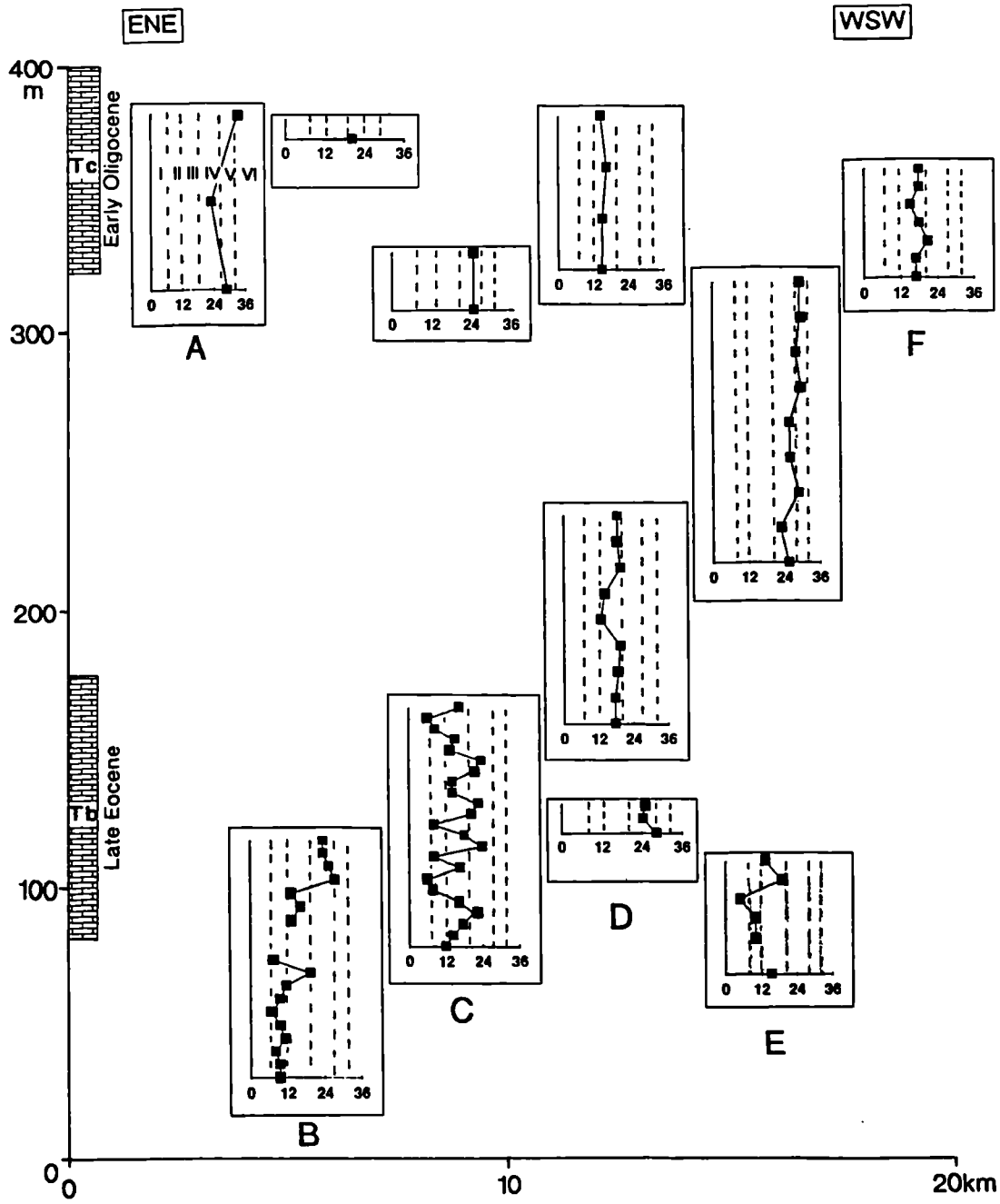

Fig. 5.8 Geochemical variation within the Yavuna Group volcanic stratigraphy of Fig. 3.4. based upon HFSE-classification. Horizontal scale for each sector is fractionation-corrected Y content in ppm. Sub-vertical lines on each plot show HFSE-group divisions as defined on Fig. 5.4a.

(ii) Fine-scale cyclicity between melt types is seen in the lower sections, for example in Namosi Creek, sector C, where successive eruptions of depleted and more fertile compositions (YG I-IV) occur within a few metres of each other within the volcanic succession. No great thickness of any one geochemical group persists in this sector.

(iii) In contrast, higher stratigraphic levels comprise more consistent exposures of individual melt types on this scale. The sectors show changes in composition over several hundred metres of vertical exposure, for example, in upper subarea E.

(iv) Relatively enriched YG V and YG VI melts occur only in the upper part of the Yavuna Group in the eastern sector A.

(v) The broad time scale denoted by the Late Eocene and Early Oligocene marker horizons enables an estimate of the duration of eruptive cycles to be made. Initial eruptions in the protoarc were dominated by YG II lavas, interbedded with types YG I-IV lavas. Consecutive YG III melts then dominated the eruptive cycles, passing up into persistent YG IV and finally interbedded types YG IV-VI lavas. The entire transition took place within 5-6Ma.

Variations of the type involving interbedded depleted and ultra-depleted lavas are common in the north of the western Pacific arc province (e.g. Arculus et al. 1992; Reagan & Meijer 1984; Hawkins et al. 1984; Umino 1986) and also in some ophiolite complexes (e.g. Troodos; Flower & Levine 1987; Cameron 1985). Furthermore, the refractory nature of such melts have been used to infer the unique tectonic and thermal conditions pertaining to protoarc magmatism (e.g. Van der Laan et al. 1989; Stern & Bloomer 1992; Pearce et al. 1992b). The broad transition from depleted and ultra-depleted melts to enriched melts as documented in the Yavuna Group, however, has not previously been documented in the north of the province.

5.3.2.2 Variations in fractionation history within the Yavuna Group

This group of observations is made in order to assess the role of magma chamber processes during accretion in the protoarc. The assessment is made using absolute Cr contents to define the measure of differentiation from primary liquids that were originally in equilibrium with mantle peridotite (Fig. 5.9). The definition of primary liquid follows the criteria of Perfit et al. (1980) that Cr content should exceed 500pm and Ni content should exceed 250ppm. The diagram illustrates that the greatest proportion of possible primary melt compositions occurs at the base of the Yavuna

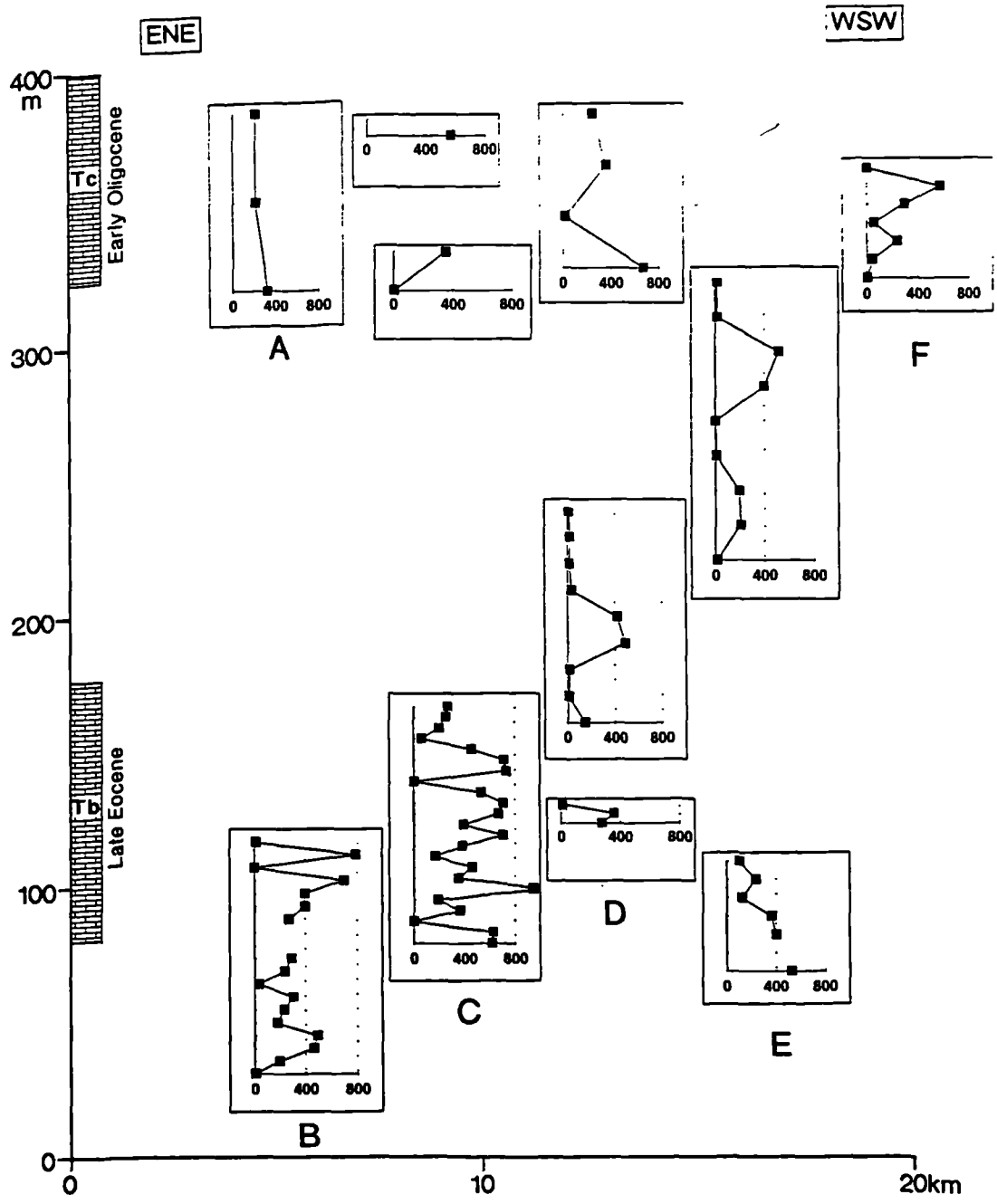

Fig. 5.9 Variations in fractionation history within the Yavuna Group volcanic stratigraphy of Fig. 3.4 based upon Cr content. Horizontal scale for each sector is Cr content in ppm.

Group in sector B, and the lower parts of sectors C and E. More evolved compositions do exist in these sections but they are usually represented as single flows interbedded between more primitive melts. At higher stratigraphic levels, evolved lavas are more common as multiple units, for example in mid-sector D, which are then further overlain

by primitive melts. No uniform upward decrease in Cr content exists as might be expected if fractionation was occurring solely as a response to increased crustal thickness in the protoarc. Rather, eruptions appear episodic throughout the sequence, with small-scale fractionation episodes and renewed primitive magmatism characterising the lowest part of the group, and more persistent cycles of alternate evolved and primitive magmatism dominating up-sequence.

5.3.3 Compositional controls on fractionation history

Fractionation histories for the six magmatic groups distinguished in the Yavuna Group are now assessed. The ratios Sc/Y, Ti/Zr (or V/Ti) are useful in identifying effects of clinopyroxene and magnetite fractionation respectively (Woodhead et al. 1993) while CaO/Al_2O_3 allows plagioclase control to be monitored (Perfit et al. 1980). Sc/Y variations are illustrated in Fig. 5.10 in which the ratios are plotted against wt.% MgO as an index of differentiation. The least evolved samples of each group define a trend of decreasing Sc/Y across YG I-VI. As demonstrated in the Cr-Y plot (Fig. 5.4b) the primitive samples of each group cannot be related by simple fractionation vectors and so the Sc/Y range is interpreted to be a source-related feature.

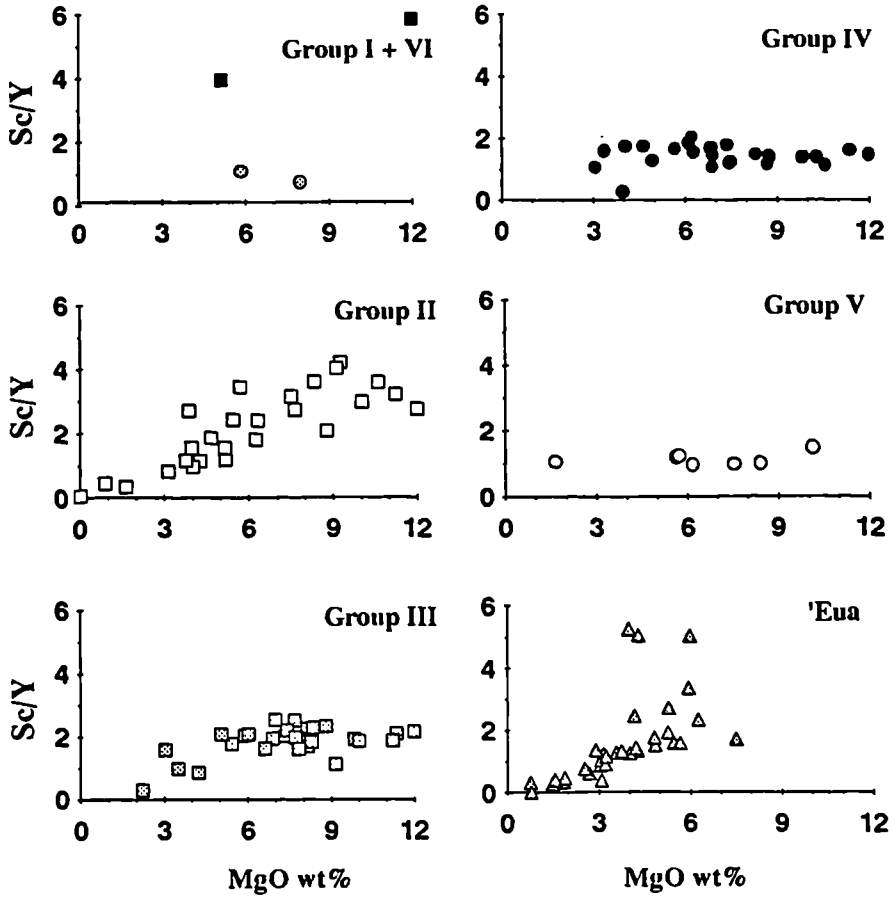

Fig. 5.10 Sc/Y ratio plotted against wt.% MgO for Yavuna sub-group and 'Eua lavas.

As fractionation proceeds and MgO decreases, the inflection in the trend and decrease of the Sc/Y ratio is taken to reflect the incoming of clinopyroxene as a liquidus phase (Woodhead et al. 1993). The inflection clearly occurs at high MgO (~9 wt.%) in YG II and but at lower MgO (4-5%) in YG III. In YG IV, V and VI, no clear trend of decreasing Sc/Y is defined by the data. 'Eua samples define a range of Sc/Y at 6% MgO which is also interpreted to be a source-related feature. This is because the high Sc/Y 'Eua samples are glassy and do not contain accumulated clinopyroxene phenocrysts which could possibly lead to high Sc/Y. The low Sc/Y group defines a strong clinopyroxene control line from 6% MgO.

Ti/Zr and V/Ti ratios are considered together in Fig. 5.11. It is apparent that for the Yavuna Group data, more scatter is present at any given MgO in the Ti/Zr ratio than the V/Ti ratio. This is unlikely to be an analytical artefact as all of these elements are analysed with good accuracy and precision using the XRF technique. It is also difficult to explain purely by variations in the proportion of accumulated magnetite crystals because the wide Ti/Zr scatter is particularly noticeable at the primitive end of the compositional range where glassy, non-porphyritic samples dominate the sample suite (compare, for example, YG II data for Ti/Zr and V/Ti). In the absence of any other obvious cause, this feature is also interpreted to represent a source-related feature and is more fully investigated in chapter 6. According to the V/Ti plots, magnetite fractionation commences at 6% MgO in YG II, after which the V/Ti ratio drops sharply. In YG III, IV and V, inflections on these two plots are progressively less well defined. 'Eua samples again display a range in both ratios which is interpreted to be a source-related feature for the same reasons outlined above. The 'Eua low Sc/Y data group follows the YG II trend on both plots.

CaO/Al_2O_3 variations are illustrated in Fig. 5.12. This ratio is obviously the most susceptible to alteration as evidenced by the widespread development of calcite and epidote throughout the suite and consequently the ratio is interpreted with caution. It is noticeable that the primitive YG I boninite melt has a CaO/Al_2O_3 ratio close to 1 in close agreement with values from other high Ca-boninite suites e.g Troodos upper pillow lava suite, Crawford et al. (1989). The other groups have primitive CaO/Al_2O_3 ratios of 0.5-0.7. The least differentiated 'Eua samples show clustering around CaO/Al_2O_3=0.5-0.6. Most of the Yavuna sub-groups show a decrease in the CaO/Al_2O_3 ratio with fractionation, although points of inflection cannot be defined with certainty. The 'Eua dataset shows a clear decrease in the ratio from ~6% MgO.

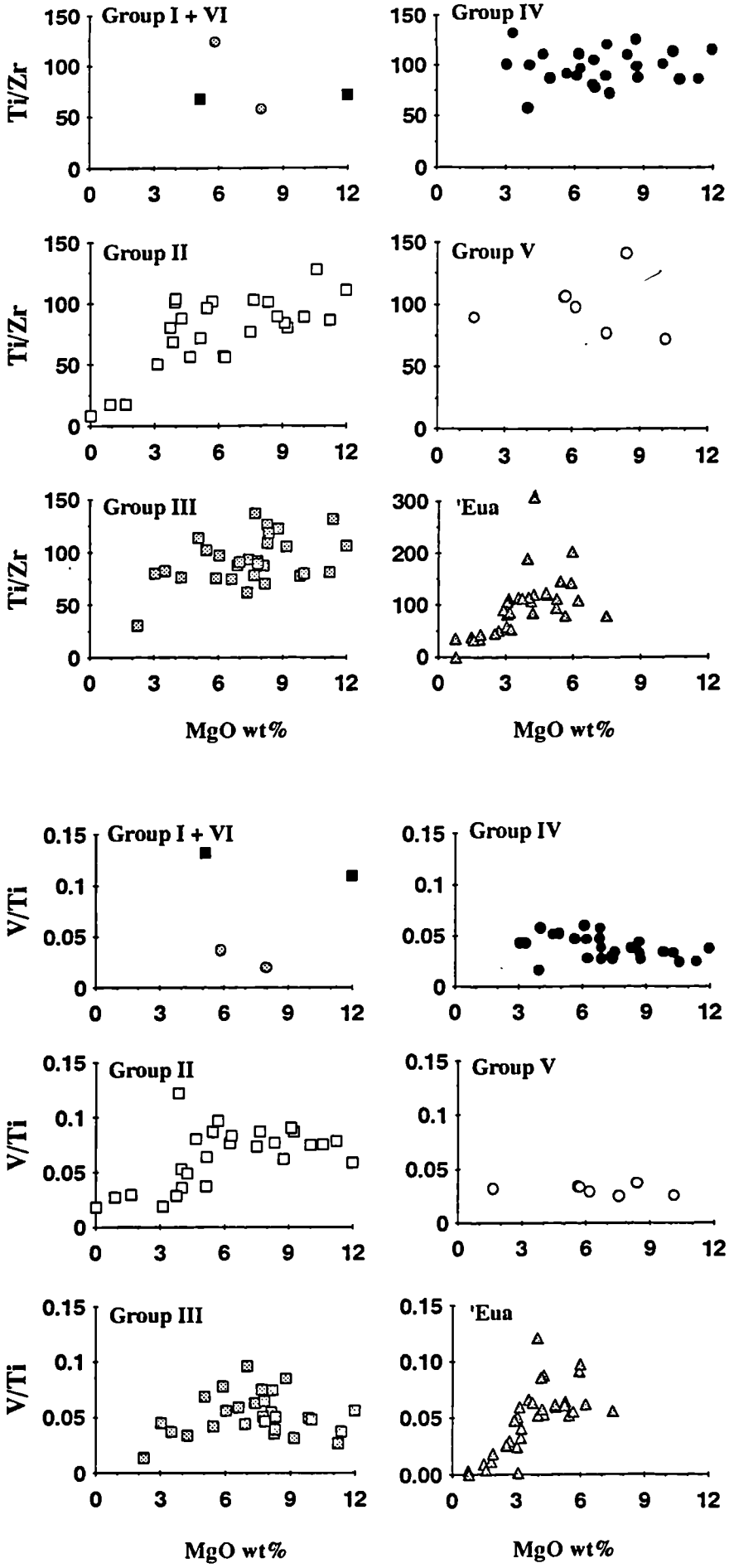

Fig. 5.11 Ti/Zr and Ti/V ratios plotted against wt.% MgO for Yavuna sub-group and 'Eua lavas.

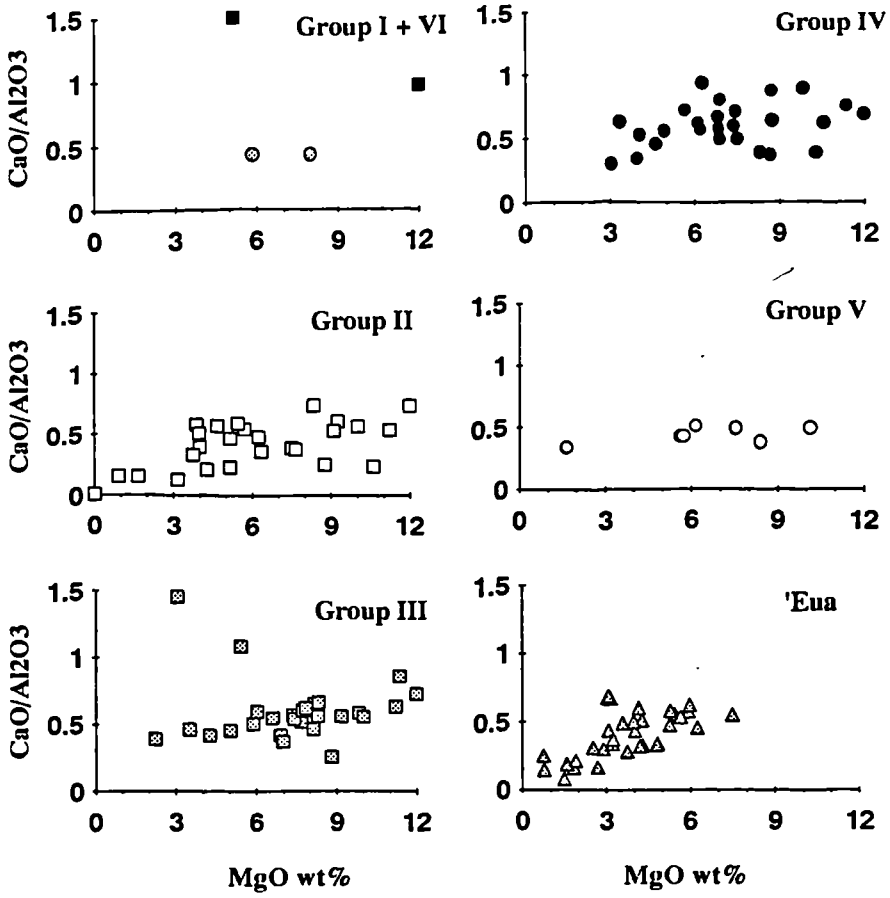

Fig. 5.12 CaO/Al_2O_3 ratio plotted against wt.% MgO for Yavuna sub-group and 'Eua lavas.

The geochemical variations described above for each magmatic group document possible changes in liquidus phase relations across the YG I-VI compositional spectrum. Table 5.3 shows how these fractionation trends compare with the crystallisation orders observed in thin-section.

The petrographic data further supports the hypothesis that fractionation history can be linked to parental magma composition as defined by HFSE content. The most clearly defined variation is the diminishing role exerted by clinopyroxene from YG II through YG V. The role of plagioclase is more difficult to assess because of alteration but fractionation of this phase probably begins earlier in YG III than YG II. Magnetite fractionation trends are best developed in YG II and decrease in importance through YG III, IV and V.

Similar contrasts in fractionation history are well documented features in lavas from different tectonic settings such as mid-ocean ridge basalts (MORB), backarc basin basalts (BABB), island arc tholeiites (IAT) and boninite series volcanics (BSV), (e.g. Natland (1991); Fryer et al. (1990); Sinton & Fryer (1987); Ewart et al. (1977); Reagan & Meijer (1984); Van der Laan et al. (1989)). Similar differences are also recorded

Group	Sample	Ol	Cpx	Pl	Mt	Sp	Order	Geochem. inferred order
II	90-79	5	3	1			Ol-Cpx-Pl	Cpx control from 9-10% MgO
II	90-65	5	10				Ol-Cpx	Pl control unclear
II	LP121	3	5	25			Ol-Cpx Pl	Mt control at 6% MgO
II	90-66		5	15			Cpx-Pl	
III	BH278	1	2	5		1B	Pl-Cpx	Pl control from 11-12% MgO
III	90-63		20	60	5		Pl-Cpx-Mt	Cpx control from 6% MgO
III	90-57		?10	?2			Pl-Cpx	Mt control from 5% MgO
III	90-80	3	2	1		1C	Cpx-Pl	
III	VL029		30	40	5		Pl-Cpx-Mt	
III	VL015		25	50	5		Pl-Cpx-Mt	
IIIE	BH403		1	1			Pl-Cpx	
IV	90-38	1		4			Pl-Cpx	Pl control unclear
IV	VL024	3		8			Ol-Pl	Cpx control from 4% MgO
IV	90-10	1		1		1B	Ol-Pl	Mt control from 4% MgO
IV	90-2		1	4			Pl-Cpx	
IVE	BH566		20	40	5		Pl-Cpx-Qtz	
V	90-08	1		1			Ol-Pl	No clear fractionation
V	90-08R	1		1			Ol-Pl	trends observed across
V	90-34	1		8			Ol-Pl	range
V	BH145	1	1	1		1A	Ol-Pl	
V	90-73	?5		1		1C	Ol-Pl	

Table 5.3 Comparison of crystallisation orders observed in thin-section with crystallisation orders inferred from geochemistry.

within individual ophiolite complexes (e.g. Troodos, Thy & Xenophontos 1991) and have been used in conjunction with geochemical variations to develop models for transitional tectonic settings (e.g. Oman, Alabaster et al. 1982). The common predominance of clinopyroxene over plagioclase in arc-related environments is widely recognised (Perfit et al. 1980) and generally attributed to higher oxygen fugacity (fO_2) and volatile contents in the arc magma source which leads to a shift in cotectic relationships when mineral phases precipitate (Kushiro 1969; Kudo & Weill 1970; Merzbacher & Eggler 1984). The assertion that volatiles are important in genesis of arc rocks is supported by the vesicle-rich nature of many arc lavas (Gill 1981) and by recent data which documents the presence of magmatic water contents in fresh volcanic glasses of arc and backarc volcanic rocks that are significantly higher than those of MORB or ocean island basalts (OIB), (e.g. Cameron (1985); Newman & Van der Laan (1992); Hochstaeder et al. (1990)). In this study, vesicle contents across the Yavuna Group compositional range are illustrated in Fig 5.13. While no vesicles were observed in the YG I boninite lavas, YG II lavas contain up to 30% by volume of vesicles filled by a variety of secondary minerals. The other groups contain fewer vesicle-rich samples and

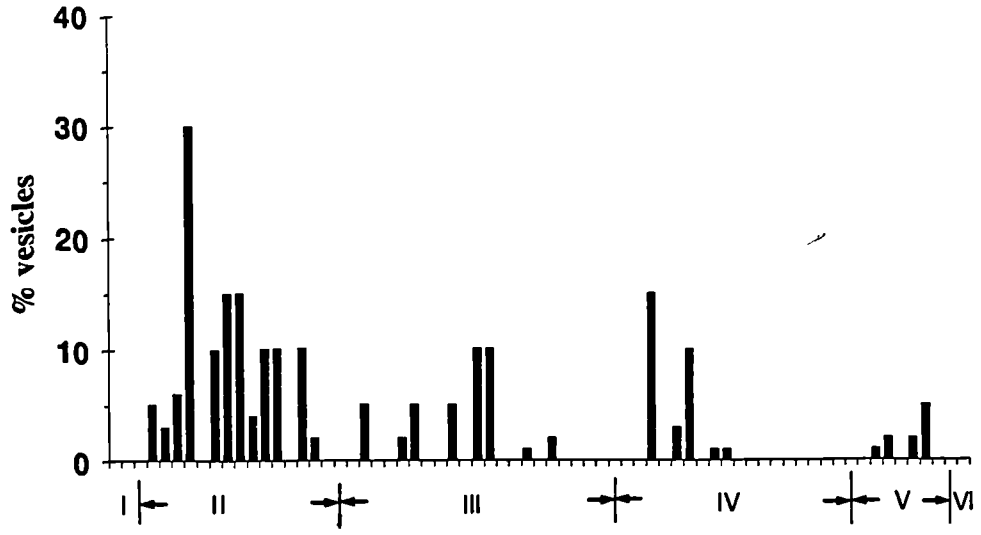

Fig. 5.13 Vesicle contents observed in thin-section for Yavuna sub-group lavas.

none have the high levels of YG II. However, the extent to which sampling bias affects this statistic is not known.

5.3.4 Implications for petrogenetic modelling

Evaluation of the fractionation trends is an important step to make before using the HFSE and other element groups in petrogenetic modelling. When plotting the fractionation trends in this chapter, each ordinate ratio has involved a less incompatible element divided by a more incompatible element so that as fractionation involving the phase of interest begins, the ordinate trace element ratio decreases. This enables the data to be screened for fractionation effects for use in the modelling of chapter 6, where it is imperative that trace element ratios are as close to those of primary liquids as possible.

5.3.4.1 Use of Sr, Th and REE in petrogenetic modelling

As demonstrated in Fig. 5.1, the contents of Th remain close to primary magmatic values even during extensive greenschist facies alteration. Some mobility of the REE has been documented (alteration type-2) but the affected samples can be screened out easily because of the distinctive alteration signature which also involves P and Y. For Sr, alteration patterns were observed to be less predictable, although some anomalously high and low Sr values accompanied leaching or enrichment of major element oxides, in particular, CaO. If these anomalous samples are omitted from the dataset, some of the scatter, especially to high and low Sr, is removed (Fig. 5.14). The resulting Sr dataset shows broad correlation with the Th and Ce data with the highest element/Zr ratios

occuring in YG II followed by broadly decreasing values of the ratios across the range of YG III, IV and V. It is significant that these variations in potentially mobile incompatible element ratios are matched by the Nb/Zr data which involves two of the least mobile high-field-strength elements. It is concluded that, within the *screened* primitive lava dataset, Th, Ce and Sr abundances can be used with a fair degree of confidence to represent primary magmatic abundances.

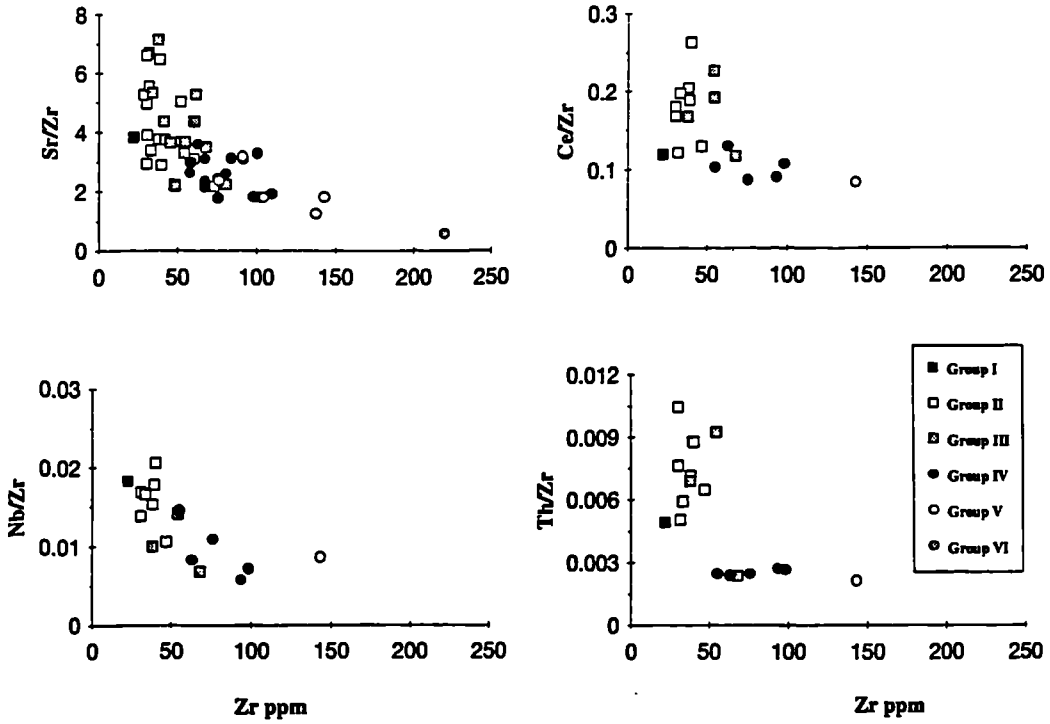

Fig. 5.14 Plots of Sr/Zr, Ce/Zr, Nb/Zr and Th/Zr against Zr for least-evolved Yavuna Group lavas. Sr/Zr-Zr plot includes only screened samples following the removal of samples with anomalous Na_2O, K_2O and CaO contents from the dataset. Other plots include all data obtained by ICP-MS.

5.4 The Wainimala Group

5.4.1 Introduction

The disposition of Wainimala Group (WG) samples around the often faulted margins of the Yavuna Group together with a lack of structural information on these outcrops makes it impractical to attempt a detailed volcano-stratigraphic reconstruction such as that proposed for the Yavuna Group. There is, however, significant volcanological and petrographic diversity within the Wainimala Group which merits geochemical investigation. The most important aspect of this diversity is the contrast between the *principal edifice* terrane represented by the Nadele Breccia and Kawa Formation lavas

and the *inter-edifice* terrane represented by the Dakadaka Basalt, dyke swarm cutting the Yavuna Group and Kalaka Dacite.

5.4.1 Classification

It is clear from the field descriptions of chapter 3 that the Wainimala Group (WG) as a whole contains a greater proportion of differentiated samples than the Yavuna Group (YG). This point is emphasised by Fig. 5.15 which shows that 75% of WG samples have MgO<6%, the level at which significant fractionation effects were documented in YG samples (Table 5.3).

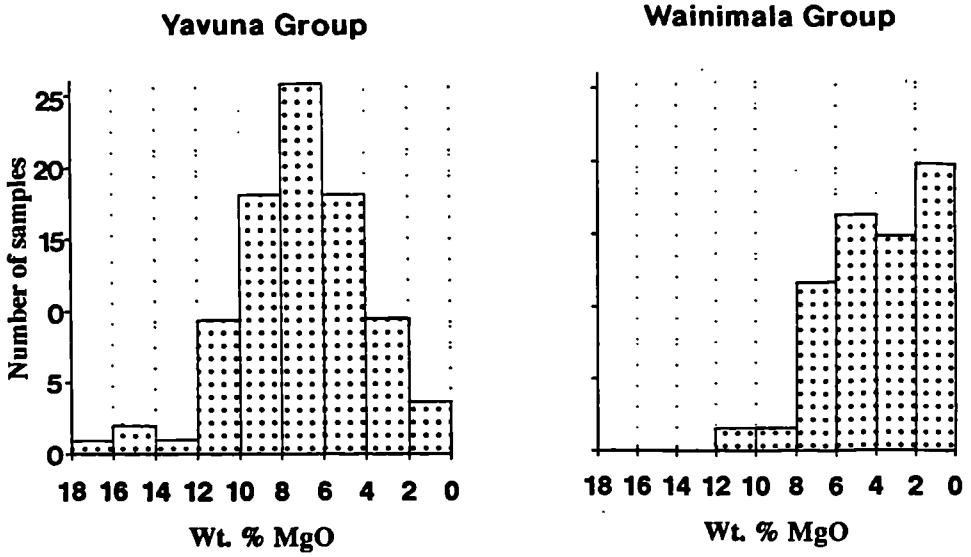

Fig. 5.15 Comparative wt.% MgO contents for Yavuna Group and Wainimala Group.

According to the Y-based classification proposed for the Yavuna Group lavas, the most primitive WG samples are equivalent in composition to the YG III melts (Fig. 5.16). One sample, BH119, lies on the border towards YG II but it does not share the high-SiO_2 characteristics of YG II (BH119 has 47.73 wt.% SiO_2). When plotted on a Miyashiro-type discrimination diagram (Fig 5.17), the Wainimala Group samples collectively define a tholeiitic fractionation series with increasing FeO*/MgO over the range 45-65% SiO_2. Although some samples show petrographic evidence for breakdown of mafic minerals during alteration, with replacement of olivine and augite by secondary chlorite and amphibole, these processes have not led to significant scatter in bulk-rock FeO*/MgO ratios. Differentiated samples with high SiO_2 contents are unsuited to this diagram because of the lowering of FeO*/MgO ratios which accompanies fractionation of Fe-Ti oxides.

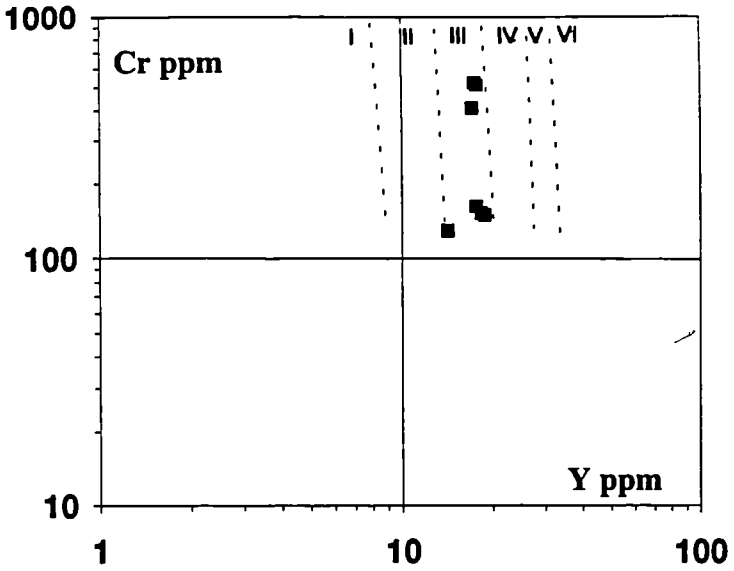

Fig. 5.16 Least-evolved Wainimala Group samples plotted on HFSE classification diagram of Fig. 5.4a

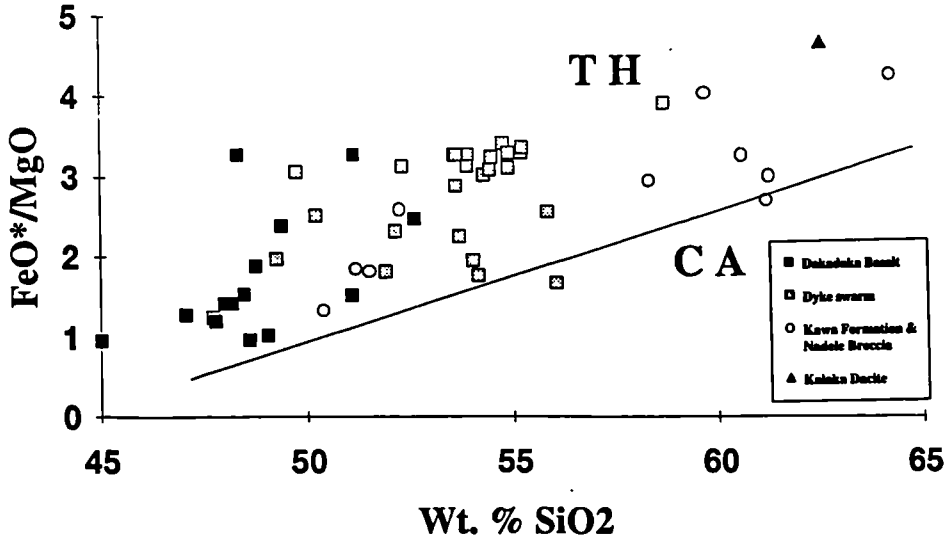

Fig. 5.17 Wainimala Group samples plotted on a standard FeO^*/SiO_2 discrimination diagram (after Miyashiro (1974)).

The full range of samples can, however, be displayed on a Ni versus MgO classification diagram (Fig 5.18) as devised by Gill (1981) to discriminate between tholeiitic and calc-alkaline orogenic volcanics. Most of the inter-edifice lavas (the Dakadaka Basalt, Kalaka Dacite and dyke swarm) plot within the mainly tholeiitic low Ni/MgO field A as defined by Gill (1981) rather than the field defined by most orogenic basalts and andesites. The Dakadaka Basalt is the least evolved group geochemically, although no samples have Ni contents high enough to represent liquids in equilibrium with mantle peridotite. In contrast, samples from the principal volcanic edifices (the Kawa Formation and Nadele Breccia) evolve into the mainly calc-alkaline high Ni/MgO field B which is defined by lavas erupted through areas of thick transitional-continental crust, for example in Peru, Turkey and Mexico (Gill 1981). The reasons for these Ni/MgO variations are poorly

understood, but one possible explanation may lie in the sensitivity of D_{Ni} to pressure during partitioning into olivine (Parkinson 1993).

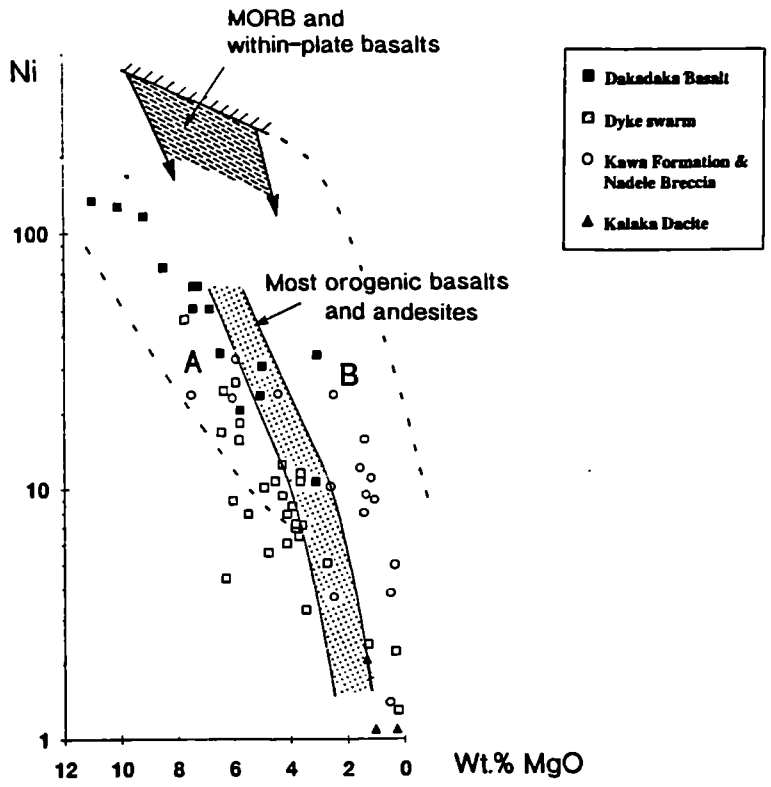

Fig. 5.18 Wainimala Group samples plotted on the Ni-MgO diagram of Gill (1981).

A plot of SiO_2 vesus K_2O (Fig. 5.19) further illustrates the wide compositional range shown by the data. However, although samples plot within each of the low, medium and high-K fields, much of the scatter to high and low-K values occurs within the most altered greenschist-facies samples from the dyke swarm. The samples from the other groups cluster mainly along the low-K and medium-K field boundary on this diagram. Broad divisions based upon SiO_2 are made after Gill (1981) for use when discussing the volcanic groups i.e. basalt < 53% < andesite < 64% < dacite < 70% < rhyolite. SiO_2 values for the Kalaka Dacite show a wide compositional range that may be enhanced by silica mobility, a feature which was recognised in these samples in thin-section. The samples are thus termed high-Si dacites (following Gill & Stork 1979) rather than rhyolites in order to retain their field nomenclature.

In summary, the inter-edifice lavas of the Wainimala Group are classified as low or medium-K arc tholeiite series. Although the principal edifice lavas cannot be distinguished from the inter-edifice lavas using the classic Miyashiro criteria, the edifice lavas show high Ni/MgO ratios which are characteristic of calc-alkaline volcanic series erupted through transitional-continental crust.

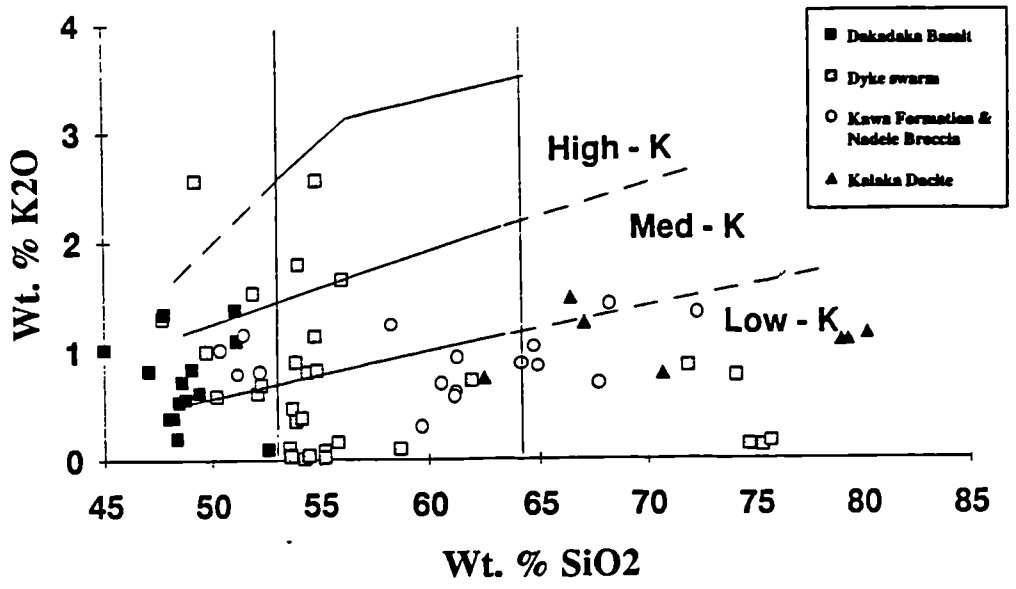

Fig. 5.19 Wainimala Group samples plotted on a wt.% K_2O-SiO_2 diagram with fields modified after Cole et al. (1985).

5.4.2 Relationships between volcanic groups

In order to investigate relationships between the volcanic groups in more detail, the trace element ratios Sc/Y, Ti/Zr and V/Ti and the major element ratio CaO/Al_2O_3 have been plotted against wt.% MgO as an index of differentiation (Fig. 5.20). Samples containing accumulated crystals lead to scatter in all three ratios.

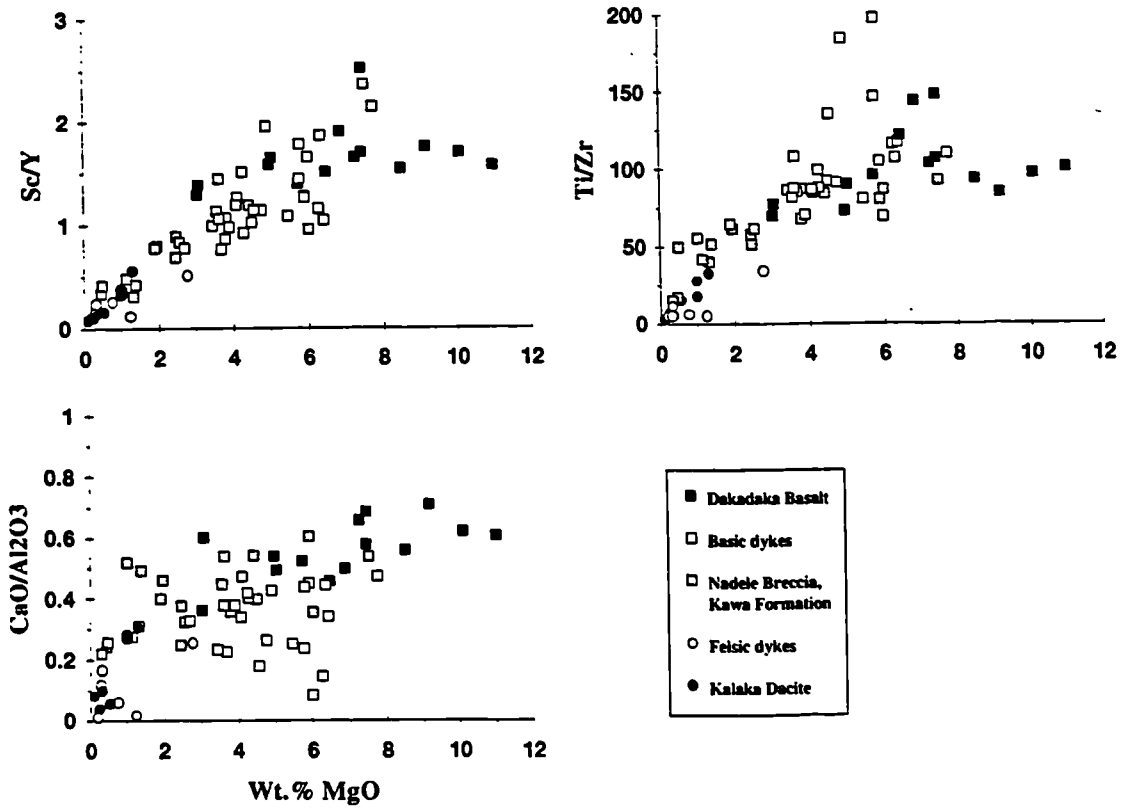

Fig. 5.20 Sc/Y, Ti/Zr and CaO/Al_2O_3 ratios plotted against wt.% MgO for Wainimala Group samples.

This feature is particularly noticeable for the Ti/Zr ratio in some basic dyke samples which reflects their high modal magnetite content. Additional scatter is caused by alteration. In particular, in the CaO/Al_2O_3 plot, leaching of CaO during greenschist facies alteration is clearly indicated for many of the dyke swarm samples. Apart from these discrepancies, the fractionation trends again most closely resemble those of the YG III lavas across the range of MgO. Sc/Y ratios begin to decrease slightly later than the CaO/Al_2O_3 ratio suggesting that clinopyroxene followed plagioclase as a liquidus phase. The Ti/Zr trend shows a marked inflection at 4-5% MgO. It is notable that the spread of Ti/Zr ratios for the inter-edifice terrane represented by the Dakadaka Basalt, dyke swarm and Kalaka Dacite includes a compositional gap in the range (Ti/Zr=34-64). This gap is further investigated in Fig 5.21 where the samples are shown on a SiO_2-Ti/Zr plot for comparison with fractionated-generated compositional gaps in arc volcanic suites compiled by Brophy (1991). Although the SiO_2 gap shown by the inter-edifice lavas is not as strongly defined as many of the compiled arc suites, the Ti/Zr gap corresponds directly to the range of values of all of the intermediate principal edifice samples (10 samples, Ti/Zr=40.0-64.5) and suggests a fundamental difference between the two terranes with respect to Fe-Ti oxide stability.

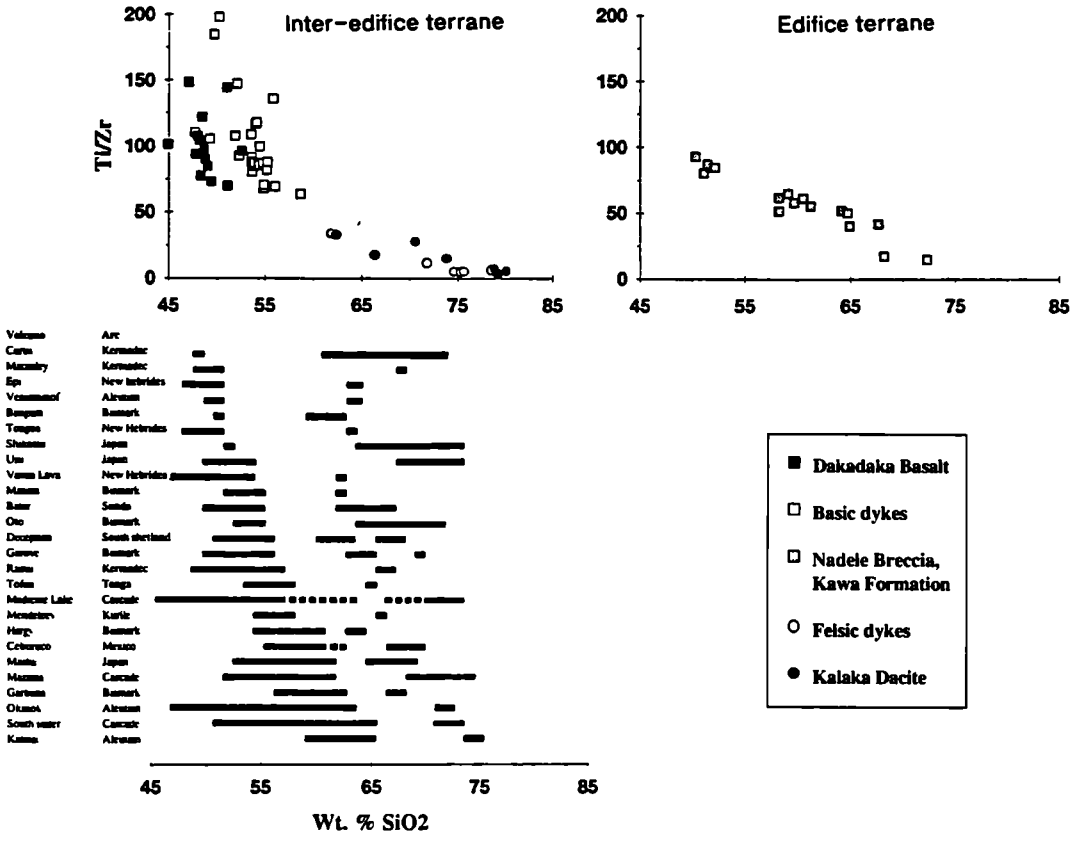

Fig. 5.21 Plots of Ti/Zr-SiO_2 for edifice and inter-edifice lavas. Comparative fractionation-generated SiO_2 gaps for other arc volcanoes are summarised after Brophy (1991).

This is further underlined by the similarity in overall geochemical signatures for the two suites for all alteration-resistant elements except Ti (Fig. 5.22).

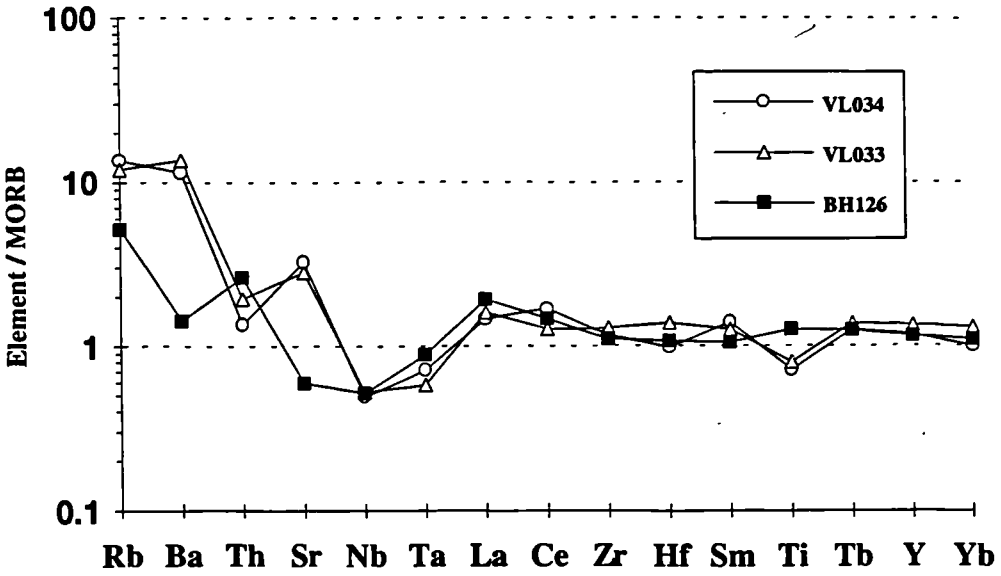

Fig. 5.22 Multi-element profiles for two principal edifice lavas (VL033, VL034) and one inter-edifice lava (BH126). Similarity of data for all alteration-resistant elements suggests that similar sources were tapped by each terrane.

5.4.3 Contrasting processes in the edifice and inter-edifice terranes

The geochemical contrasts noted above suggest that different physical or chemical controls may have operated in the respective plumbing systems of the edifice and inter-edifice terranes rather than in their mantle source. Similar geochemical variations between tholeiitic and calc-alkaline volcanic suites were noted within the Aleutian arc by Kay & Kay (1982). These authors related tholeiitic volcanoes to the edges of major arc crustal segments where magmas could easily rise to the surface and undergo shallow, closed system fractionation, while calc-alkaline volcanoes were related to the central parts of crustal segments where transit through the crust was impeded and differentiation was forced to occur at deeper levels. Although this field and geochemical study of the Wainimala Group is on a smaller scale than the Aleutian arc-wide example, similar inferences regarding the role of the crustal substrate can be made. The possibility of a greater filtering effect for the frontal arc substrate beneath the principal volcanic edifices is supported by the petrographic evidence for magma mixing and disequilibrium in the edifice lava pile. The presence of hydrous phases in the lavas may also reflect differentiation under deeper, more oxidising conditions (Arculus & Wills 1980). The high Ni/MgO ratios in the edifice lavas, which are similar to those from arcs formed on

thick transitional-continental crust, also provide support for this hypothesis. In the inter-edifice regime, less efficient crustal filtering would lead to more rapid ascent of magma through the crustal substrate, shallower levels of crystallisation, and a lesser probability of magma mixing.

5.5 Summary

Aspects of major and trace element geochemistry have been studied within the framework provided by field and stratigraphic relations. Three types of secondary alteration are documented, the least constrained and most problematic of which is the mobility of the LIL-group elements. REE and Th are less affected by alteration processes and together with a subset of Sr data, and the HFSE, they can be more confidently applied to petrogenetic arguments in chapter 6.

The protoarc and second arc lavas show geochemical signatures which reflect their respective tectonic settings. The lower Yavuna Group is dominated by primitive melts with a greater proportion of evolved lavas up-section probably reflecting an increasing role for fractionation processes during growth of the protoarc edifice. The fractionation history followed by various magmatic groups can be linked to primary melt composition which in turn can be linked to the presence of volatiles in the mantle source.

During crustal accretion in the second arc, the role of fractionation processes was more pronounced, reflecting eruption of these magmas through the pre-existing protoarc substrate provided by the Yavuna Group. Heterogeneities within the crustal substrate were probably fundamental in forcing magmas to fractionate at different levels in the crust, leading to controls on the eruptive style (principal edifice or inter-edifice terrane) and geochemistry (transitional calc-alkaline or tholeiitic) of magmas erupting in the arc.

CHAPTER 6

Petrogenesis

6.1 Introduction

In this chapter geochemical variations within and between the volcanic units defined in earlier chapters are modelled to constrain magmatic processes during early arc volcanism.

Data from the lower Yavuna Group documents magmatism during the earliest stages of subduction while data from the lower Wainimala Group documents magmatism occurring at the onset of the second arc volcanic event. It is demonstrated that key trace element ratios can be fractionated in these settings through several independent processes. These include depletion of the mantle source by previous melting events, variations in the degree and type of mantle melting, variations in the residual source mineralogy, and enrichment of the source by a variety of siliceous melt and aqueous fluid metasomatic agents.

6.2 The earliest stages of subduction

6.2.1 Melting theory

In chapter 5, volcanic groups within the basement were defined on the basis of high-field-strength element (HFSE) abundances. The same group of elements provide the basis for modelling mantle melting processes following the screening of fractionated samples. Melting models have been constructed using the equations for equilibrium melting (also known as batch melting), fractional melting and accumulated fractional melting published in Shaw (1970) and Shaw (1977). The relevant equations are summarised below:

Equilibrium (batch) melting:

$$\frac{C_l}{C_o} = \frac{1}{D_o + F(1-P)} \qquad (6.1)$$

Accumulated fractional melting:

$$\frac{C_l}{C_o} = \frac{1}{F}\left[1-(1-PF/D_o)\right]^{1/P} \quad (6.2)$$

Fractional melting:

$$\frac{C_l}{C_o} = \frac{1}{D_o}(1-PF/D_o)^{((1/P)-1)} \quad (6.3)$$

where: C_l = concentration of element in melt

C_o = concentration of element in source

D_o = bulk partition coefficient for element with respect to source

P = bulk partition coefficient for phase proportions entering melt

F = degree of partial melting

These equations describe non-modal melting processes and hence can account for the exhaustion of phases during the melting process. The variations in element concentrations in melts and residual sources produced by the different melting schemes are illustrated for the moderately-incompatible element Zr in Fig 6.1. The diagram shows that Zr concentration in the melt is similar for the three melting regimes at low degrees of melting but that at degrees of melting >1%, Zr concentrations in the resulting melts differ significantly. The concentrations in the batch and accumulated fractional melts are broadly similar across the melting range. Using a starting composition of 9.37ppm Zr, melts formed by 0.1% partial melting contain approximately 180ppm Zr. This decreases to ~35ppm Zr in the melts formed by 30% melting. In contrast, Zr concentrations in fractional melts decrease more sharply between 2% (131ppm Zr) and 30% melting (0.2ppm Zr) so that at high degrees of melting, very low concentrations of incompatible elements are reached. The removal of melt from the system during fractional melting is reflected in the rapidly decreasing Zr content of the fractional melting residue during melting. This model predicts that during fractional melting incompatible elements can be effectively stripped from the mantle source to leave concentrations of incompatible elements in the most refractory peridotites that are below detection limits for conventional geochemical analytical techniques. The degree of melting at which this is achieved depends upon the incompatibility of the element. For example, highly-incompatible elements such as Nb are reduced to background levels in the source at correspondingly lower degrees of partial melting.

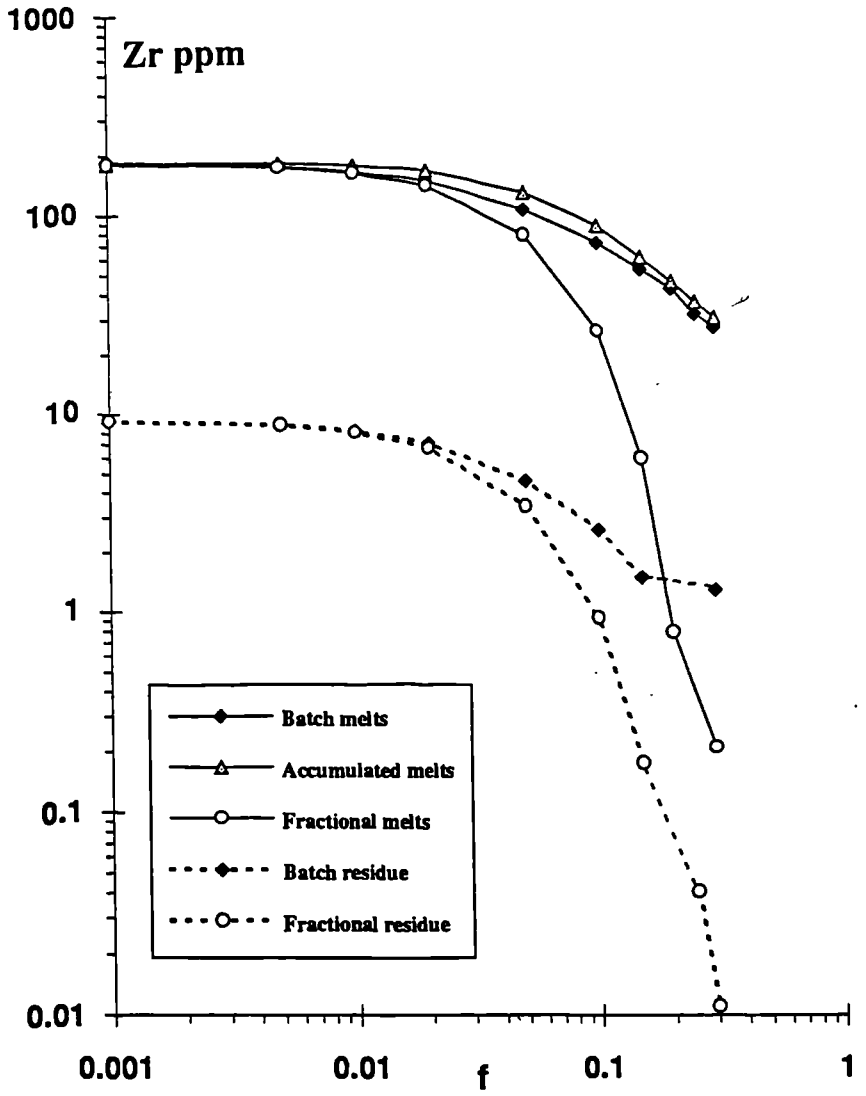

Fig. 6.1 Comparison between concentration of Zr in melts produced by equilibrium (batch), fractional and accumulated fractional (pooled) melting. Initial concentration of Zr in source = 9.37ppm. f on abscissa indicates extent of melting.

6.2.2 High-field-strength element systematics

Selected trace element ratios are plotted against Zr for the least evolved lavas from the Yavuna Group (YG) and 'Eua in Fig. 6.2. These ratios are generally unaffected by alteration but are sensitive to variations in residual source composition and the nature of the melting process. Along the abscissa of the plots, group differences for the YG samples defined in chapter 5 are broadly maintained with the use of absolute Zr concentration. This element is used in modelling in preference to Y and Ti because its partition coefficients with respect to mantle minerals are well documented, and because plots presented in this form can be used to enable direct comparison with the comprehensive data-set for arc and back-arc systems presented by Woodhead et al. (1993). In all cases, the ordinate ratio involves an incompatible element / more incompatible element.

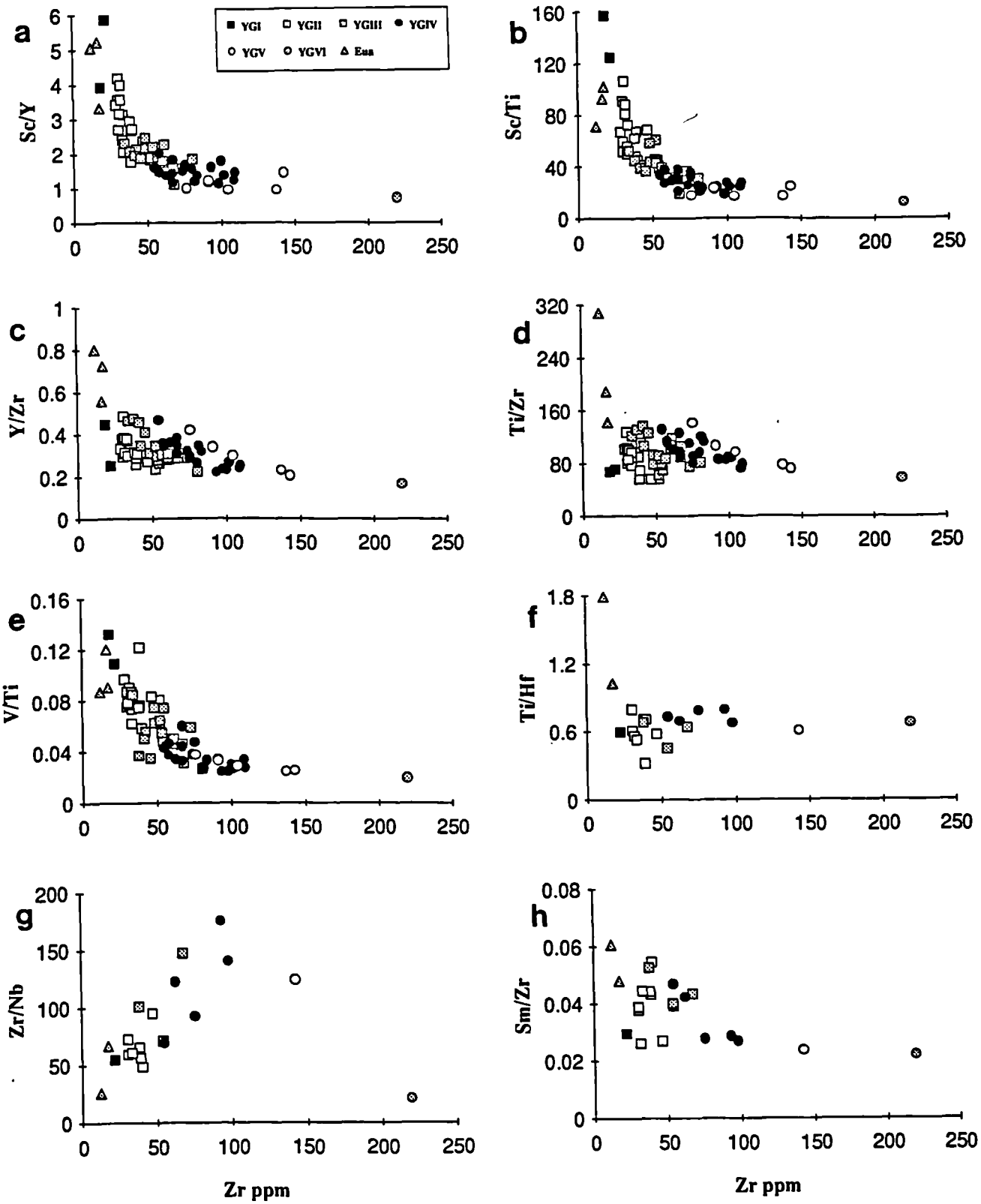

Fig. 6.2 Trace element ratios plotted against Zr for least evolved Yavuna Group and 'Eua lavas. For each plot, ordinate ratio involves an incompatible element/more incompatible element.

Fig. 6.2 illustrates that the least evolved representative samples from 'Eua have low Zr contents (12-18ppm), lower than the YG I boninites (19-22ppm). Eua samples also have higher Ti/Zr (143-308), Y/Zr (0.56-0.80) and Ti/Hf (1.1-1.8) than the YG I samples. Ratios involving Sc (e.g. Sc/Y, Sc/Ti) are similar to, or slightly lower, than the YG I ratios.

The Yavuna Group dataset follows relatively smooth trends between YG I-VI in the ratios Sc/Y, Sc/Ti and V/Ti. For Ti/Zr and Y/Zr, however, an increasing range in the ratios is noted towards the low-Zr end of the compositional spectrum. A similar feature exists in the Ti/Hf and Sm/Zr ratios although the trend is less well defined in the latter due to the smaller quantity of data. In the Zr/Nb plot, the ordinate ratio involves the element with the greatest incompatibility in the melting assemblage (Nb). Both the 'Eua data and the YG I-IV data define a trend of decreasing Nb/Zr with decreasing Zr which deviates markedly from the trend of the more enriched YG V and VI data.

In accord with the melting theory defined by equations 6.1-6.3, it is impossible to produce the trends of opposite curvature (i.e. convex and concave trends in Fig. 6.2) in ratios of an incompatible element / more incompatible element through melting of a unique, homogenous mantle source. It follows that either non-unique, heterogeneous mantle sources or differences in the melting process, or both, must be invoked to explain the geochemical differences in the lavas.

Fractionation of Ti/Zr ratios is well documented among the boninitic series volcanic rocks of the Western Pacific e.g. Hickey & Frey (1982); Taylor et al. (1992); Murton et al (1992) and has usually been attributed to metasomatic addition of Zr to the mantle source. Low Ti/Zr ratios are also reported in some arc tholeiite suites, e.g. Vanuatu, Woodhead et al. (1993). In contrast, these authors attributed fractionation of Ti from Zr to the presence of residual amphibole in the mantle source during melting. As the range of lavas studied in this thesis spans much of the boninite-arc tholeiite compositional spectrum, their detailed trace element systematics provide a useful test of these contrasting hypotheses.

6.2.3 Modelling of HFSE variations

Two HFSE ratios showing contrasting variations between magmatic groups, Sc/Y and Ti/Zr, are modelled to study the effects of melting mechanism and source composition on the geochemistry of the resulting melts. Source compositions have been calculated following the method of Woodhead et al. (1993) in which the widely-used N-MORB

trace element concentrations of Sun & McDonough (1989) are back-calculated to a depleted MORB mantle (DMM) source assuming that the N-MORB concentrations result from 10% batch melting of the source. Resulting DMM source compositions are listed in Table 6.1.

(all ppm)	Zr	Ti	Y	Sc	V
N-MORB (DMM)	9.37	1260.5	4.4	19.81	87.23
Batch residues	**Zr**	**Ti**	**Y**	**Sc**	**V**
DMM-5%	4.54	828.79	2.82	19.23	74.31
DMM-10%	2.64	565.11	1.78	18.36	60.81
DMM-15%	1.59	362.37	1.02	17.07	46.56
Fractional residues	**Zr**	**Ti**	**Y**	**Sc**	**V**
DMM-5%	3.38	768.71	2.62	19.28	74.12
DMM-10%	0.96	413.58	1.31	18.58	60.09
DMM-15%	0.19	181.42	0.47	17.62	45.11

Table 6.1 Summary of source compositions used in the melting model of chapter 6.

Melt compositions for these sources are then calculated using the batch and accumulated fractional melting equations. Additional melt compositions are calculated for sources more depleted than DMM. These depleted sources are calculated as both batch and fractional melting residues following the extraction of 5%, 10% and 15% partial melts from the DMM source (Table 6.1). Realistic source mineralogy and melting coefficients for the melting models are taken from Kostopoulos & James (1992) and Woodhead et al. (1993).

The results of the model for Sc/Y ratios are illustrated in Fig. 6.3 in which the modelled melt compositions are shown for direct comparison with the actual data. It was noted in chapter 5 that fractionation of mafic phases produces trends on these diagrams that plot sub-parallel to the melting trends. However, this complication has been minimised by selecting only the most primitive samples from the Yavuna Group suite (n=65 samples, average Ni=150ppm, Cr=388ppm, Mg#=60). For the Sc/Y versus Zr plot, the modelled melting trends define smooth curves to increased Sc/Y with increased degree of melting. Differences between the two melting regimes are most apparent during melting of strongly depleted sources i.e. those which have lost between 10% and 15% melt. Melts with Sc/Y ratios >2.5 must be derived from sources more depleted than DMM.

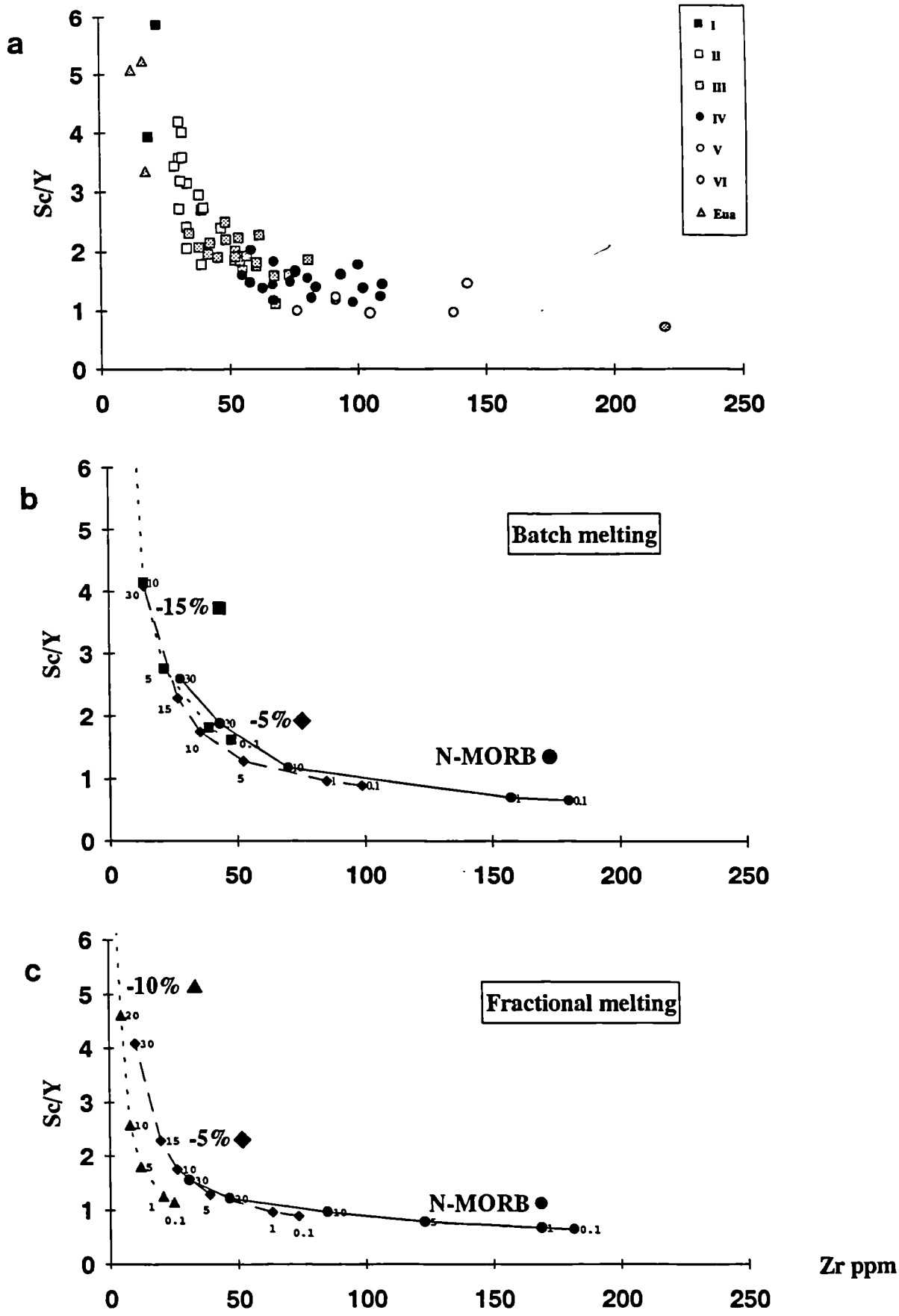

Fig. 6.3 Results of melting models for Sc/Y ratio using N-MORB and three more depleted sources (-5%, -10% and -15% melt) as summarised in Table 6.1. **b** and **c** illustrate the models for batch and fractional melting respectively. Small figures indicate degree of partial melting and large figures indicate the degree of source depletion.

For 'Eua and YG I data, batch melting, even of strongly depleted sources, can only produce high Sc/Y at the highest degrees of melting (Fig. 6.3b). The high Sc/Y ratio can, however, be produced at lower degrees of melting of more depleted sources if fractional melting residues are invoked (Fig. 6.3c). This mechanism of increasing the Sc/Y ratio reflects the preferential loss of Y relative to Sc during previous melt extraction events which also results in a successive shift to lower absolute Zr concentration for each of the depleted melting trends. YG IV and III data can be explained as a range of melts produced through either successively higher degrees of melting (6-30%) of a uniform DMM-type source, or slightly decreasing degrees of melting of successively more depleted sources (for example, up to 20% melting of DMM for YG IV and up to 15% melting of DMM-5% for YG III). The latter explanation has the advantage of allowing the YG II and YG I melts to be viewed as more extreme melts that are transitional in the sequence and formed by slightly lower degrees of melting of progressively more depleted sources. This option is further supported by major element criteria, for example, the Al_2O_3/TiO_2 ratio which was used by Ewart & Hawkesworth (1987) to assess source depletion in the Tonga arc system. High Al_2O_3/TiO_2 ratios are commonly regarded as reflecting magma production from a source more depleted in these elements than MORB (Sun & Nesbitt 1978). Fig. 6.4 shows that the statistically determined correlation coefficient (r=0.94) between the trace-element (Sc/Y) and major element (Al_2O_3/TiO_2) depletion indices is highly significant for the representative data-set at the 99% confidence level.

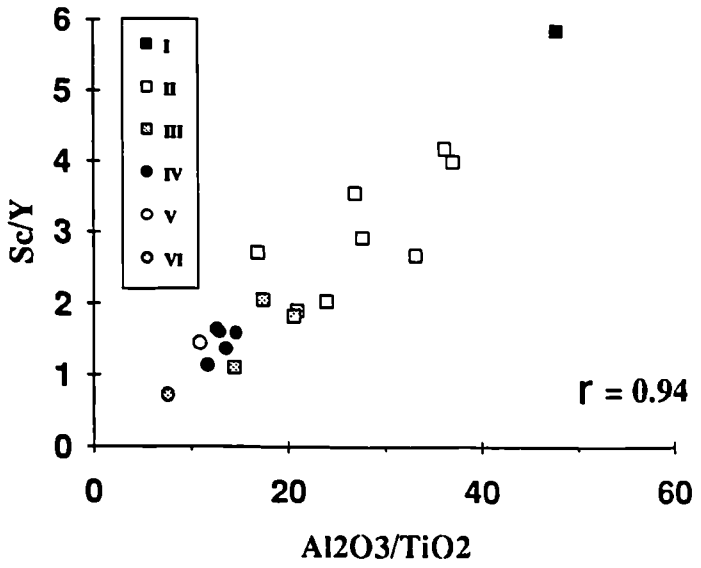

Fig. 6.4 Al_2O_3/TiO_2 - Sc/Y plot for representative Yavuna Group lavas.

The volumetrically minor YG V and VI melts have compositions that require very small degrees of melting of the DMM source or, in the case of YG VI melts in particular, higher degrees of melting of sources more enriched than DMM. As these samples are found only in the uppermost part of the Yavuna Group, their geochemistry reflects mantle melting processes in a mature arc setting. Their geochemistry provides support for the assertion of Gill (1987) that enriched sources may play an increased role in magma genesis as the arc matures and, accordingly, their petrogenesis is dealt with in a later section.

Ti/Zr variations in the modelled melt compositions follow similar trends to Sc/Y with increasing degree of melting and source depletion (Fig. 6.5). The 'Eua samples have Ti/Zr ratios ranging up to 310, amongst the highest published values for any arc basalts and matched only by samples from the Tonga arc (e.g. Ewart et al. 1977). Such extreme ratios cannot be produced by even the highest degrees of batch melting (Fig. 6.5b), and hence require that incompatible elements were stripped from the mantle source during previous fractional melting events (Fig. 6.5c). The data for YG I-IV shows a contrasting trend with displacement to low Ti/Zr ratios that cannot be accounted for either by high degrees of melting of the DMM source, or by melting of any of the more depleted sources. The low Ti/Zr ratios therefore require an alternative explanation which might be found either in a change in the melting parameters such that D_{Ti} becomes greater than D_{Zr}, or in an enrichment of the mantle source in Zr relative to Ti, prior to melting.

6.2.3.1 Melting in the presence of amphibole

The first hypothesis can be tested by invoking a phase with a high partition coefficient for Ti relative to Zr as being present in the mantle source. Suitable phases include amphibole, rutile and other accessory phases. However, experimental evidence argues strongly against the presence of the latter in the mantle wedge during melting (Ryerson & Watson 1987). A modified version of the HFSE model has therefore been constructed using a simplified hornblende-lherzolite starting composition in which hornblende replaces clinopyroxene in the source assemblage. Partition coefficients for amphibole are taken from Pearce & Parkinson (in press). The most important feature of the model is the high partition coefficient for Ti ($K_D\ Ti^l_{hbl}$ = 1.2-2.0 c.f. $K_D\ Ti^l_{cpx}$ = 0.4) which results in a higher bulk distribution coefficient for this element in the amphibole-bearing source. The resulting melt trends in Fig. 6.6b illustrate that while low Ti/Zr melts can be produced from the modified DMM and depleted sources, only very small degrees of melting, for example 1-5% melting of the DMM+amphibole source, can be considered

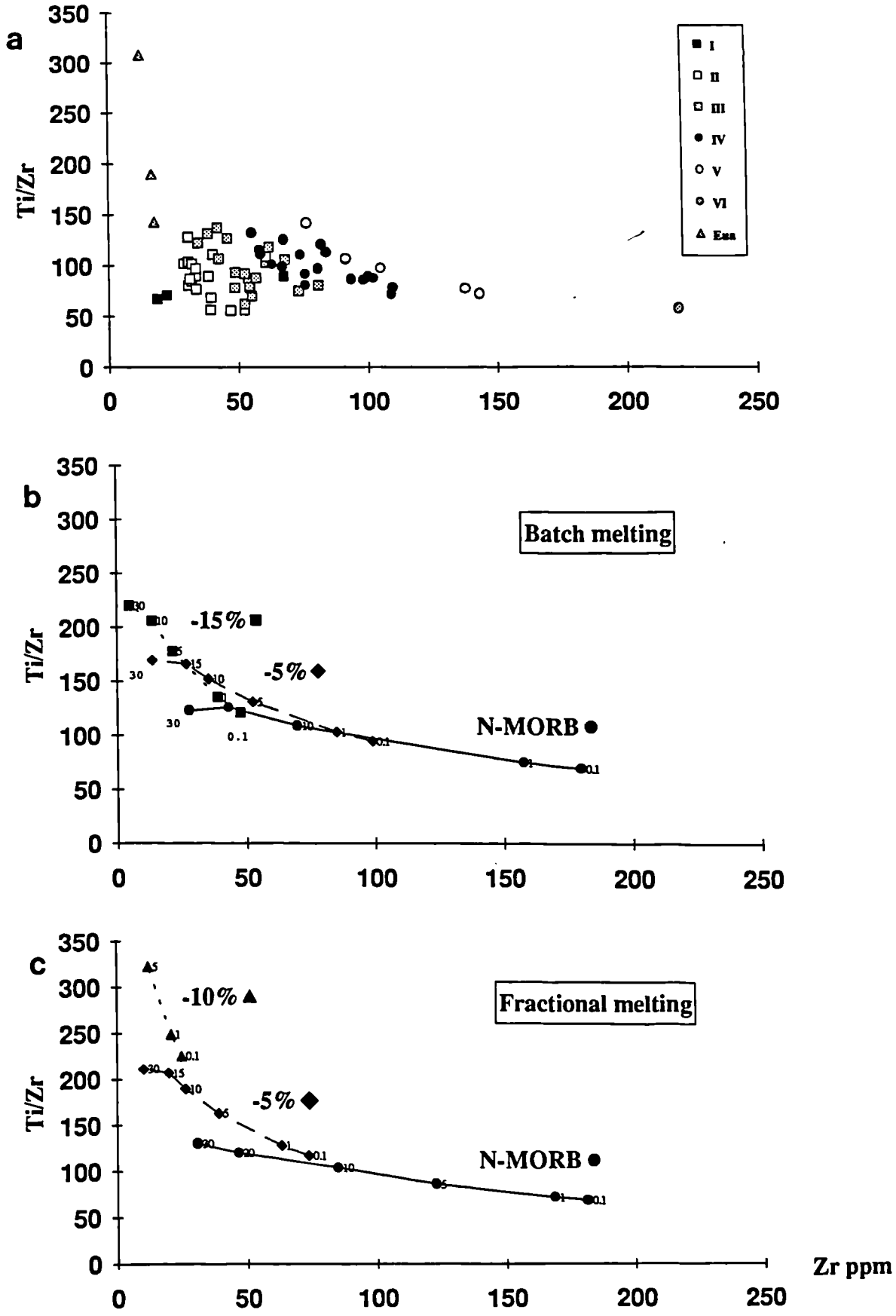

Fig. 6.5 Results of melting models for Ti/Zr ratio using N-MORB and three more depleted sources (-5%, -10% and -15% melt) as summarised in Table 6.1. **b** and **c** illustrate the models for batch and fractional melting respectively. Small figures indicate degree of partial melting and large figures indicate the degree of source depletion.

to reasonably satisfy the low Ti/Zr ratios of YG III and IV. For YG II, only very small degree melts of highly-depleted sources can be considered, while for YG I, none of the modelled melt compositions can adequately account for the low Ti/Zr and low absolute Zr of the data. Even for those samples which can be satisfied by the low-degree melts of the model, the results are difficult to reconcile with the melting constraints imposed by the Sc/Y model (Fig. 6.3) which is only slightly affected by the modified source assemblage ($K_D\ Y^l_{hbl}$ = 0.6-1.0 compared to $K_D\ Y^l_{cpx}$ = 0.5 and $K_D\ Sc^l_{hbl}$ = 1.0-2.0 compared to $K_D\ Sc^l_{cpx}$ = 2.0).

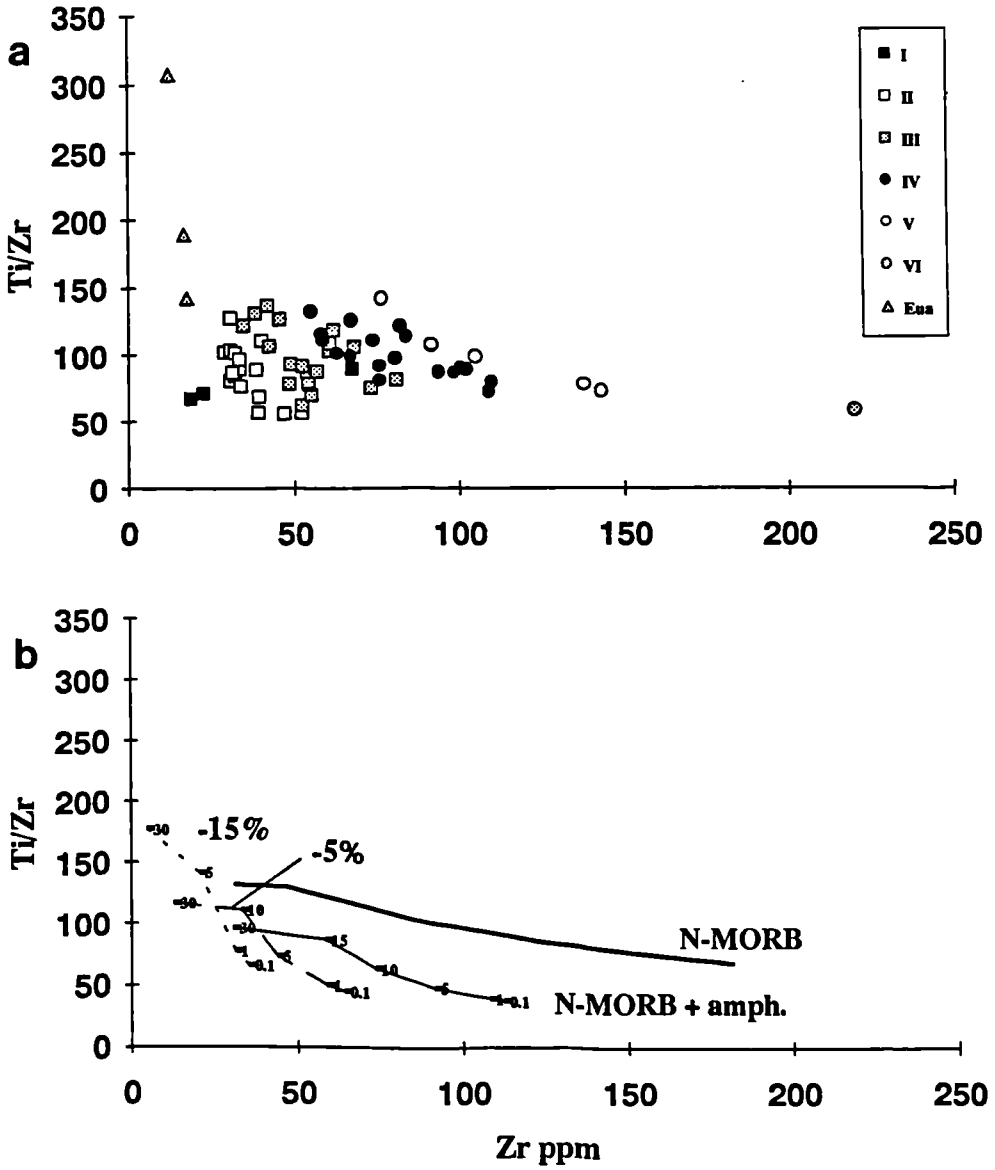

Fig. 6.6 Results of melting model of Ti/Zr ratio using N-MORB, N-MORB+amphibole and two more depleted amphibole-bearing sources (-5%, -15% melt). Small figures indicate degree of partial melting and large figures indicate the degree of source depletion.

6.2.3.2 Addition of a Zr-rich component to the source

Addition of a Zr-rich component to the mantle requires a process whereby Zr can be fractionated from Ti and also other elements such as Y (Fig. 6.2c) and Sm (Fig. 6.2h). Addition of an asthenospheric small-degree melt component (commonly referred to as the OIB-component e.g. Stern et al. 1991; Kostopoulos & Murton 1991) cannot produce such pronounced fractionation between elements which are considered to show very similar petrogenetic behaviour. Only if the enriched component is itself fractionated prior to infiltrating the source, could such a mechanism be considered. Pearce et al. (1992b) consider that a component with these characteristics could be generated by partial melting of hydrated oceanic crust under amphibolite-facies metamorphic conditions. Thermal constraints upon this model require that temperatures are high enough to initiate melting of the slab assemblage under water-deficient conditions but not sufficiently high that hornblende itself melts out. These authors suggest that temperatures between 800°C and 1000°C are likely. In addition, the absence of fractionation in the heavy-rare-earth elements (HREE) constrains the depth of the melting event to sources without residual garnet i.e. depth <60km (Brophy & Marsh 1986). The validity of this model is tested by plotting published ODP Leg 125 data together with the DMM source and proposed Zr-rich component of Pearce et al. (1992b). Fig. 6.7 demonstrates that the Yavuna Group data lies upon potential mixing lines between the modelled DMM and more depleted compositions represented by ellipse A, and the hypothesised low-Ti/Zr, low-εNd enriched component represented by ellipse B. The low εNd of end-member B requires that the melting assemblage includes volcanogenic sediments or transitional oceanic crust, rather than normal, high εNd, Pacific plate crust. The data provides a reasonable fit in the plot involving the Sm/Zr ratio, although in both plots, slightly lower εNd values than those proposed by Pearce et al. (1992b) are required to satisfy mixing criteria for the mantle source end-member. It is noted that the addition of the enriched component is most clearly recognised in the boninitic YG I sample LP143. This is a predictable consequence of the ability of its more depleted source being able to 'sense' the enriched component with a greater resolution than the YG III and IV melts (see later discussion in section 6.2.5).

Although the precise details of this slab-fusion model are difficult to constrain without further isotope data, Pearce et al. (1992b) further note that melts with similar high Zr/Sm and Zr/Y ratios occur in some trondhjemites that were generated through amphibolite facies partial melting and that the inferred thermal conditions necessary for slab-melting could exist for a short time after the onset of subduction (see, for example,

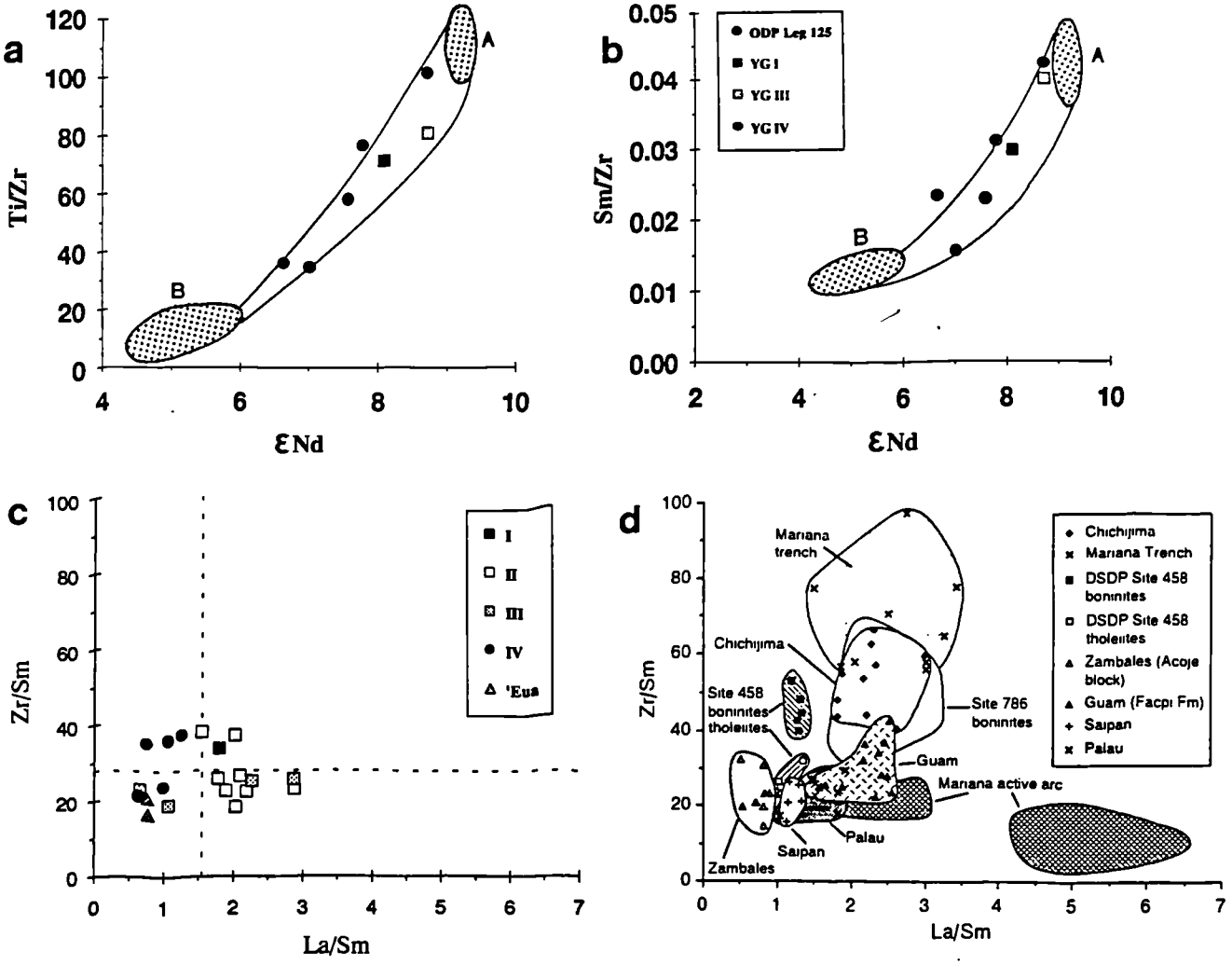

Fig. 6.7 Plots showing potential mixing lines in **a** Ti/Zr-εNd space **b** Sm/Zr-εNd space between the range of calculated depleted sources (ellipse A) and hypothesised enriched component produced by slab-melting (ellipse B). ODP Leg 125 data and field for enriched component from Pearce et al (1992b). **c** Zr/Sm-La/Sm plot for representative Yavuna Group and 'Eua lavas. **d** Comparative Zr/Sm-La/Sm data from other parts of the western Pacific arc province.

the thermal modelling experiments of Peacock 1990). If the unique thermal conditions for slab-melting do recede as the arc system matures, this may explain the absence of boninitic and depleted arc tholeiitic melts with the selective high-Zr signature in upper parts of the Yavuna Group. The Zr/Sm-La/Sm systematics of boninites and arc tholeiites from other parts of the western Pacific arc province are illustrated for comparison with the Yavuna Group and 'Eua data (Fig. 6.7c and 6.7d). It is clear that a wide range of enrichment signatures exist both within and between suites in the province. These include conventional high-La/Sm subduction zone components and possible high Zr/Sm slab-melt components.

6.2.4 Fractionation between HFSE and other groups of elements

Many subduction-related magmas possess high concentrations of large-ion-lithophile elements (LILE) e.g. Rb, K, Ba, Th and light rare earth elements (LREE) e.g. La, Ce,

Nd relative to the high-field-strength-elements (HFSE) and it has been suggested using both trace element and isotopic arguments that much of this additional element flux is derived through transport of these elements in fluids from the subducted oceanic crust (e.g. Gill 1981; Pearce 1983; Hawkesworth 1982). The degree of highly-incompatible element enrichment relative to the moderately-incompatible elements modelled in 6.3 is conveniently assessed using multi-element plots of data normalised to a reference normal mid-ocean ridge basalt (N-MORB) in which element concentrations reflect magma genesis in a non-subduction setting. Fig. 6.8 shows representative data from 'Eua and the Yavuna Group plotted in this form for the least-mobile elements.

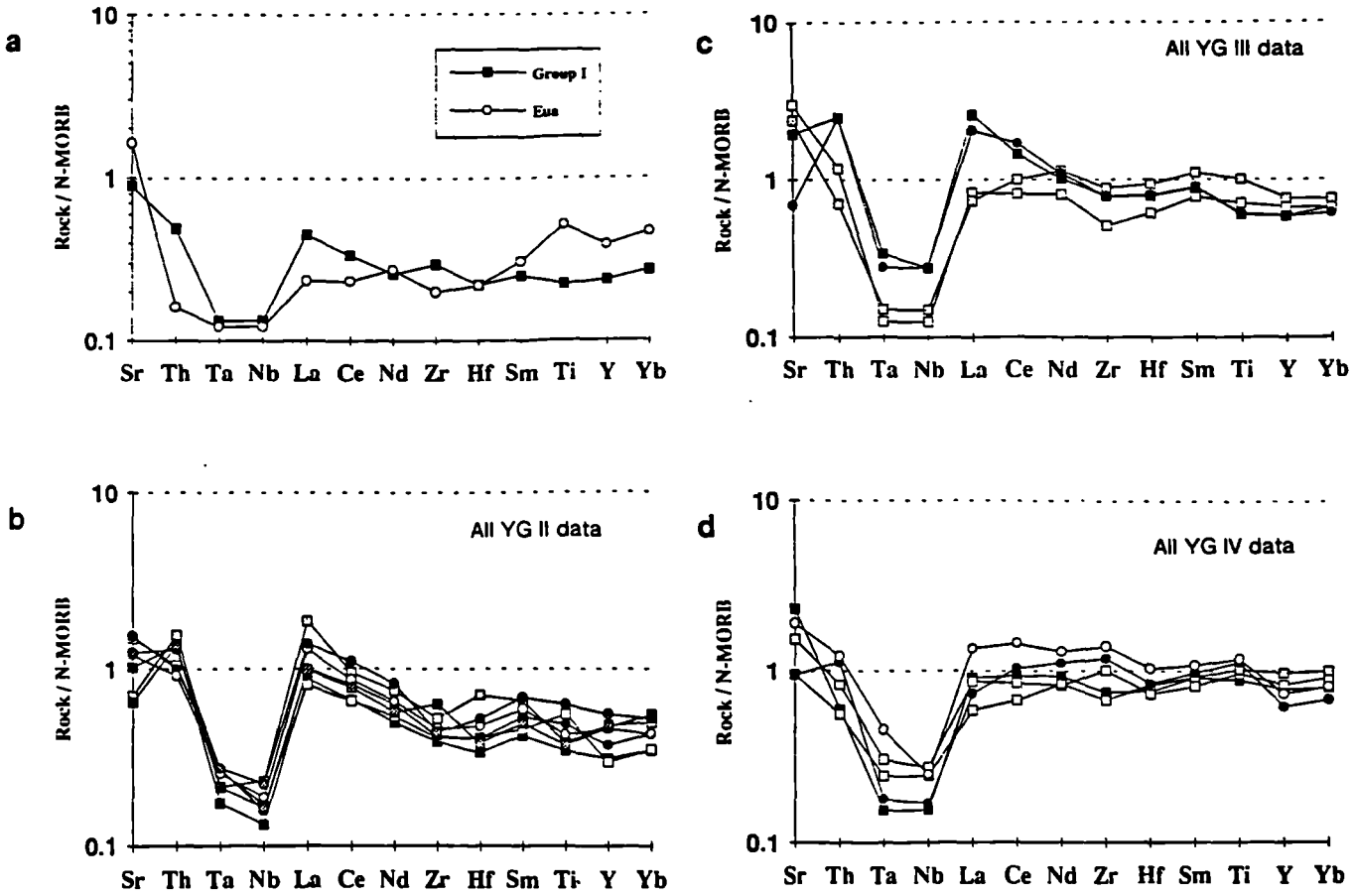

Fig. 6.8. N-MORB normalised multi-element profiles for representative Yavuna Group and 'Eua data. Normalising values are taken from Sun & McDonough (1989).

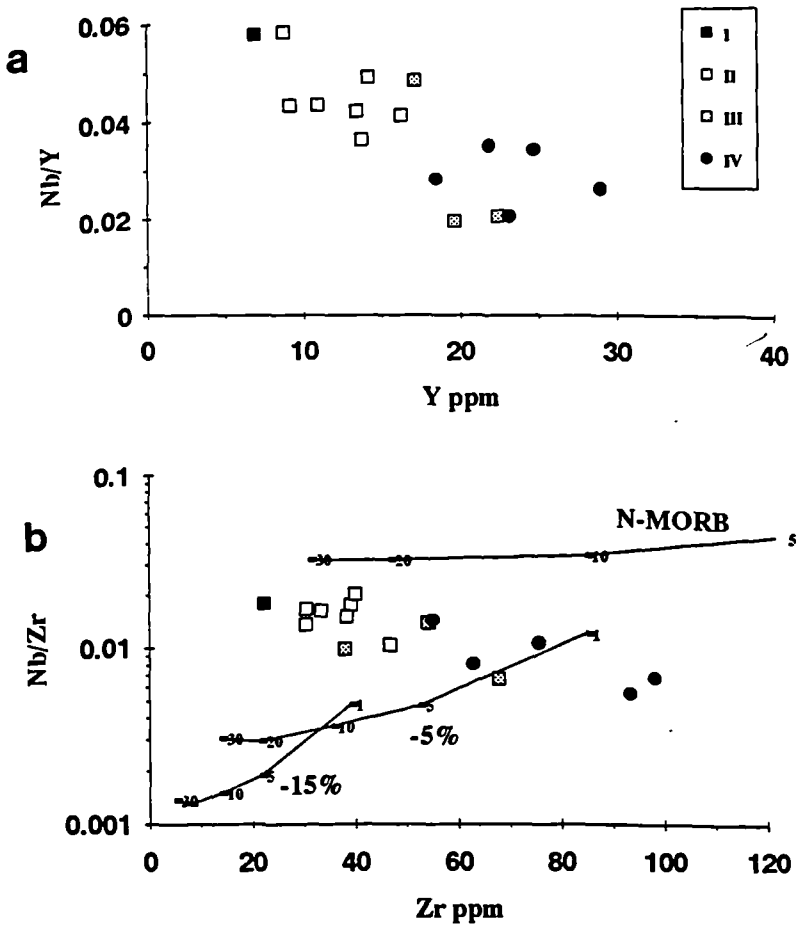

Fig. 6.9a Nb/Y-Y data for representative Yavuna Group lavas. **b** Nb/Zr-Zr data for representative Yavuna Group lavas together with modelled melt compositions for N-MORB and more depleted sources (-5% melt and -15% melt). Small figures indicate degree of partial melting and large figures indicate the degree of source depletion.

Concentrations of moderately-incompatible elements in 'Eua, YG I and II samples are significantly lower than MORB which was interpreted in section 6.2.3 to reflect depletion of the source during previous melting events. Nb and Ta are HFSE which show anomalous behaviour in this respect. Although the elements are depleted relative to MORB (the characteristic 'Nb-Ta trough' of arc basalts generally), their concentrations relative to the moderately-incompatible HFSE actually increase as the moderately-incompatible HFSE decrease across the range from YG IV to YG I. This trend is illustrated for the element pairs, Nb-Y and Nb-Zr, in Fig. 6.9. The modelled melt trends of section 6.2.3 are added to the Zr/Nb versus Zr plot in Fig. 6.9b and indicate that, if source depletion or high degrees of melting are responsible for low Y and Zr concentrations in the lavas, then Nb concentrations should theoretically be reduced to background levels in any subsequent melts (i.e. melts would have extremely low Nb/Zr). The data, however, indicate a trend of increasing Nb/Zr with decreasing Zr. Only by invoking addition of Nb and Ta to the source prior to melting can this apparent paradox be resolved.

A similar conclusion is derived from the data for the light-rare-earth elements (LREE), (represented hereafter by La or Ce) and the large-ion-lithophile elements (LILE), (represented hereafter by Sr and Th) as illustrated in Fig 6.10. All of these elements must be added to the source prior to melting in order to account for their elevated concentrations in samples derived from the most (moderately-incompatible-HFSE) depleted sources. The critical point to be addressed in this part of the petrogenesis is the relative proportions of these elements that are present in the enriched component(s).

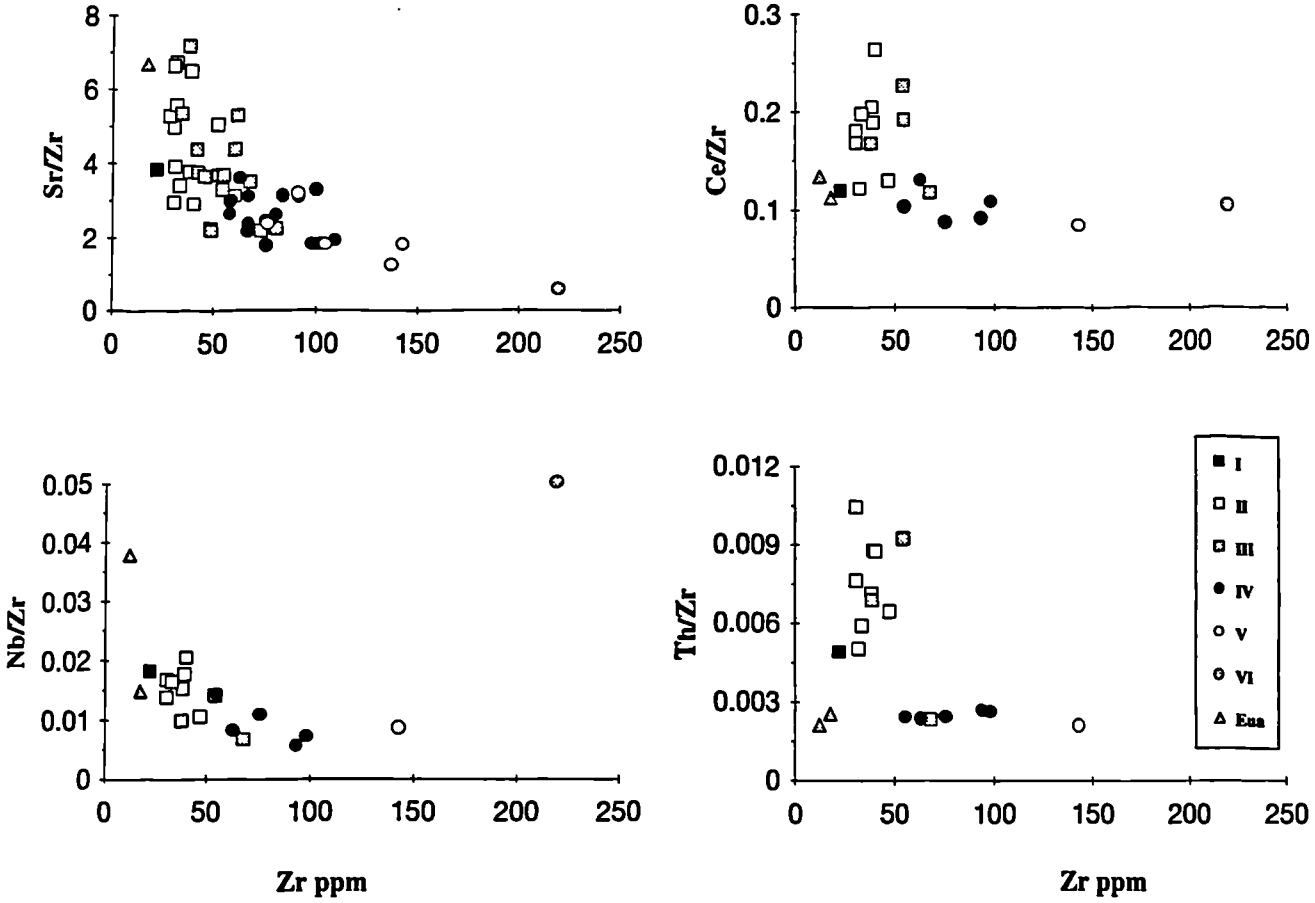

Fig. 6.10 Sr/Zr-Zr, Ce/Zr-Zr, Nb/Zr-Zr and Th/Zr-Zr plots for representative, alteration-screened, Yavuna Group data.

When discussing the nature of enriched components in boninitic and depleted arc tholeiitic rocks in intra-oceanic arc settings, previous authors have reached a consensus that, in general, at least two enriched components are required to satisfy geochemical models for any particular lava suite. The best documented component is widely regarded to be an aqueous fluid phase derived from the subducted oceanic crust which carries elements that are regarded as soluble in such fluids, in particular the LILE, and possibly the LREE. The second component is less well constrained and is usually held to be a silicate melt phase, capable of carrying a wider spectrum of elements including LREE

and some HFSE. However, the ultimate origin of the melt phase, its element budget and the timing of its addition to the source are not well constrained. The proportions in which various enriched components are present in the source now remains a critical question to be addressed.

Fig. 6.11 investigates the relationship between depleted sources as calculated in section 6.2.3, and a number of possible enriched components which could be added to the sources prior to melting. Figs. 6.11a and 6.11b show plots of Nb/Zr-Th/Zr and Nb/Zr-Ce/Zr respectively. These are particularly useful diagrams for assessing the element budget of the melt phase in the Yavuna Group lavas. The addition of a simple 'OIB-component' i.e. an unfractionated small-degree asthenospheric melt is effectively precluded as the sole agent of

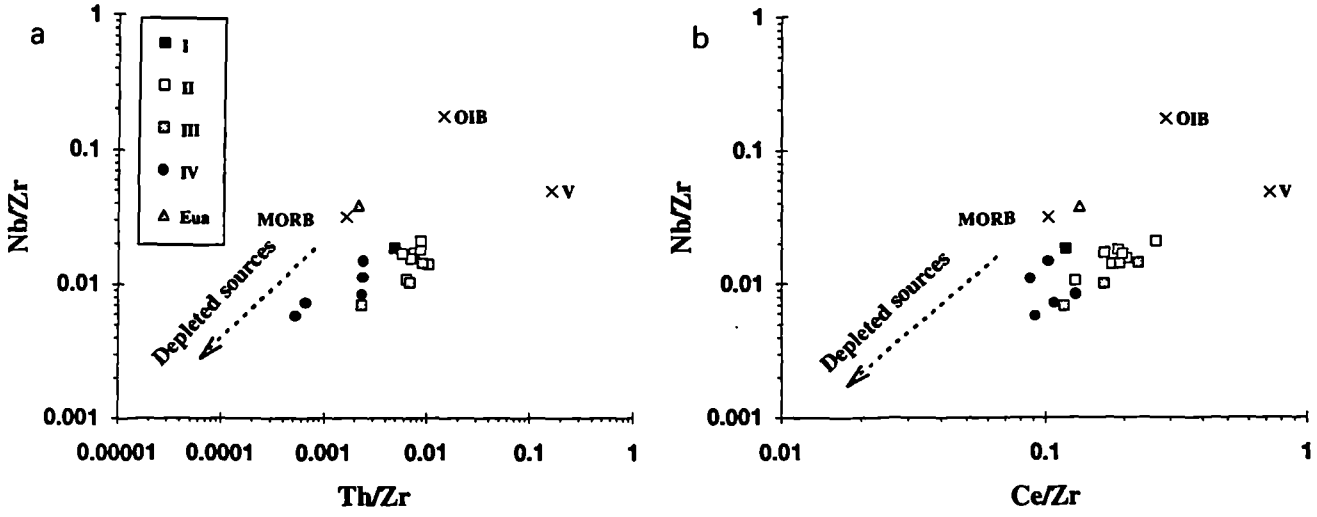

Fig. 6.11 Nb/Zr-Th/Zr and Nb/Zr-Ce/Zr plots for representative Yavuna Group and 'Eua lavas. Dotted arrow shows trend to calculated depleted mantle sources. Typical MORB (mid-ocean ridge basalt) and OIB (ocean island basalt) compositions are taken from Sun & McDonough (1989). Composition of hypothetical enriched component V is an average of three leucite basanites taken from Rogers (1992).

enrichment by the low Nb/Zr and high Th/Zr ratios of the YG data. Mixing lines to calculated depleted sources would require that if a single enriched component is to carry the budget of these elements then it must be fractionated in terms of its Nb/Zr ratio so that the resulting melt will then possess high Th/Nb and high Ce/Nb. One type of melt which does satisfy this trace-element criteria is the high-potassium, low-Ti group of magmas which show strong fractionation between the LILE and HFSE (group III in the classification of ultra-potassic rocks of Foley et al. 1987). On both figures, the

composition of a component with the required Nb/Zr fractionation has been added (component V). This melt is an average of three leucite basanites analysed from the recently active Vulsini centre in the Italian subduction province (Rogers 1992). This enriched component could provide addition of elements in proportions which are commensurate with the fractionation observed in the subsequent melts, with scatter around the mixing trends resulting from a combination of experimental error, alteration affecting Th and Ce concentrations and heterogeneity in both the degree of source depletion, and the composition of the enriched component. In contrast, the composition of the 'Eua sample could be explained by addition of a simple, non-fractionated, OIB-type enriched component.

An alternative interpretation of the Yavuna Group data involves dividing the source enrichment into two individual components. One would be an OIB-type component which would satisfy the Nb/Zr trend and also provide small quantities of other incompatible elements and the other would be an aqueous fluid capable of carrying the LILE and the LREE but not the HFSE. A similar model has been proposed to explain the enrichment patterns of boninites and arc tholeiites on the basis of isotopic evidence (Hickey-Vargas 1992). This option would remove the need for Nb-Ta fractionation to occur in the system, but would rely on the aqueous fluid phase to carry varying proportions of Sr, Th and LREE in different arc settings if it were to be applied to arc rocks generally. The experimental work of Tatsumi et al. (1986) described dehydration experiments run on synthetic serpentine spiked with trace elements including Sr, La and Nb at 12kbar and 850°C and showed that elements with large ionic radii are preferentially transported in aqueous fluids at high P, T conditions. In theory, therefore, LILE and LREE should be mobilised to a greater extent than Nb and other HFSE. Th was not studied in this experiment and, although it is regarded as an element of high ionic potential, it has recently been suggested that its enrichment in many arc suites reflects its mobility in fluid-halide complexes at high temperature (Woodhead 1989). There is thus considerable scope for input of a fluid which could carry LILE and LREE elements into the source and detailed studies of high-LILE arc lavas provide strong support for this hypothesis (e.g. Marianas arc, Stern et al. 1991).

6.2.5 Quantifying the enriched components

The amount of enriched melt component added to the various groups is now investigated. One complexity when addressing this issue is the masking effect that a fertile source, as opposed to a depleted source, will have on any added enriched component. This concept of 'sensing' by variably fertile and depleted sources which have

'seen' the same amount of enriched component is demonstrated in Fig. 6.12. Incorporation of an enriched component is first modelled by assuming bulk addition of an average basanite melt (summarised in Table 6.2) to melts produced from the unmodified DMM and more depleted sources of Table 6.1.

Element	Zr	Nb	Th	Ce	Sr
Concentration (ppm)	124	6.0	20.0	88.7	736

Table 6.2 Element abundances in an average basanite used in modelling of enriched component; taken from Rogers (1992).

The model assumes that the enriched component is preferentially extracted into the earliest melt fraction and in this respect follows the methodology of Kostopoulos & Murton (1992). Melts are produced from the DMM and depleted sources contaminated by bulk addition of 0.1%, 0.05% and 0.01% of the enriched alkali basalt component. The results in Fig. 6.12 show contaminated melts produced by 1-20% accumulated fractional melting plotted in terms of Nb/Zr ratio against absolute (and also contaminated) Zr. If an enriched component is added to the normal DMM source its effects are difficult to detect in all but the very smallest degrees of subsequent accumulated fractional melting (Fig. 6.12b). At reasonable degrees of melting i.e. at least >5%, the compositions of the contaminated melts become indistinguishable from the normal DMM melts (Fig 6.12a). When superimposed upon the more depleted sources, however, the enriched component can lead to the production of melts which can display successively higher Nb/Zr ratios (Fig. 6.12b). The rate of increase in Nb/Zr ratios varys considerably depending upon the amount of enriched component added. For example, if only 0.01% of this enriched component is added, the Nb/Zr signature of the melt is dominated by the depleted source signature (Fig 6.12a). If 0.5% of enriched component is added, however, increasing Nb/Zr ratios result across the range of successively more depleted sources. Similar variations will occur if the initial concentration of Nb in the enriched component is varied. The same arguments apply to Th/Zr-Zr variations as illustrated in Fig. 6.13. In this case, the high Th/Zr ratio of the enriched component means that even the smallest amounts of added enriched component cause increasing Th/Zr ratios in melts derived from successively depleted sources.

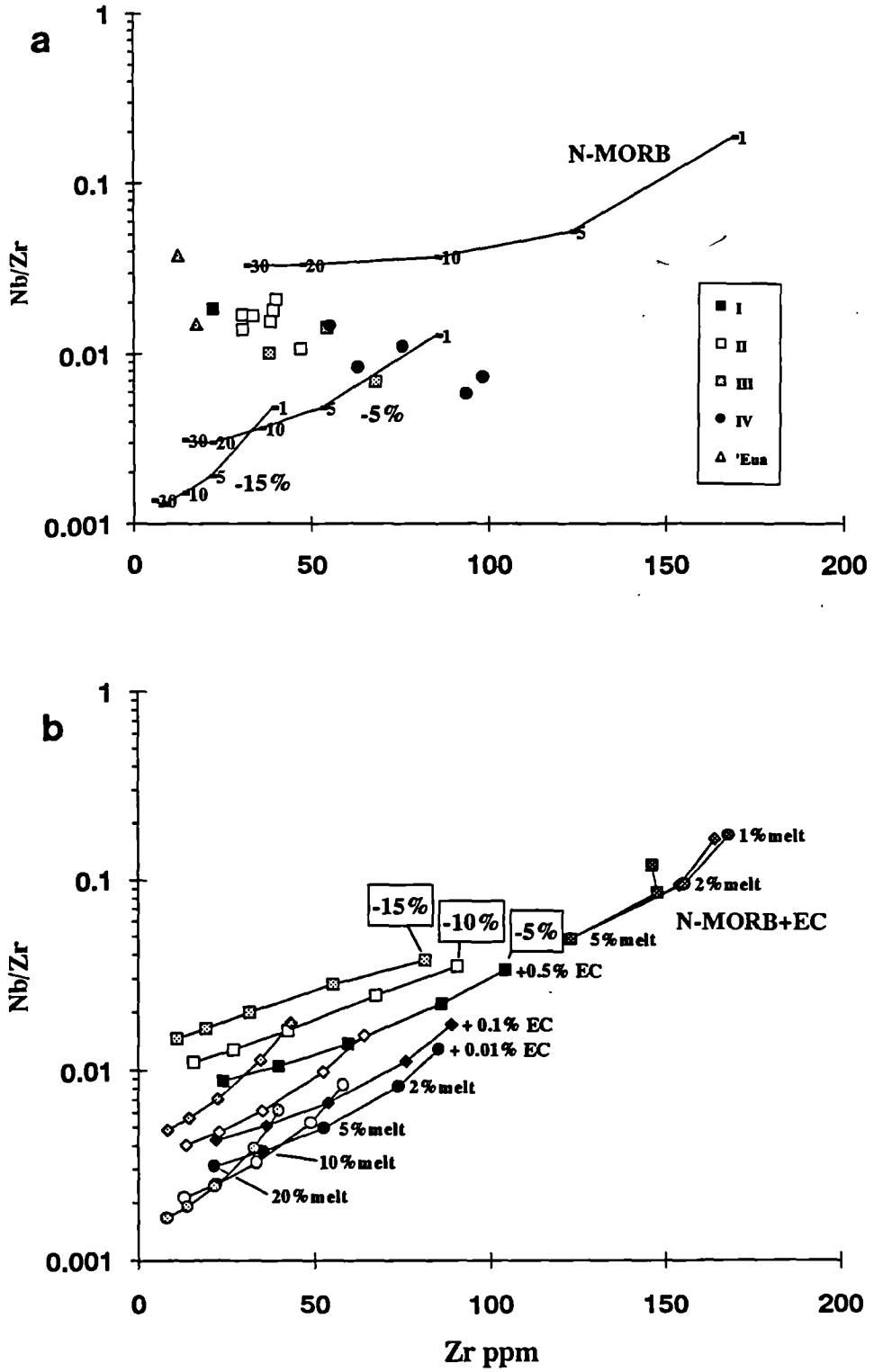

Fig. 6.12 Results of modelling of Nb/Zr ratios using methodology outlined in text. Composition of enriched-melt component is summarised in Table 6.2. **a** Illustrates representative data and modelled melt compositions derived from uncontaminated N-MORB and two more depleted sources (-5% and -15% melt). **b** Modelled melt compositions for contaminated N-MORB (dark shaded symbols) and three more depleted sources: -5% melt (black symbols), -10% melt (open symbols) and -15% melt (light shaded symbols). Three separate quantities of enriched component are added to each source: +0.5% (squares), +0.1% (diamonds), and +0.01% (circles). Small percentage figures indicate amount of melting.

The models indicates that an enriched component may be preferentially 'sensed' by a depleted source even though the same uniform component has been 'seen' by a spectrum of depleted to fertile sources. It is important to note that the addition of a single, uniform, element flux can permit the contaminated trace-element ratios to increase across the range of melts produced from successively more depleted sources. This preferential 'sensing' of the enriched component by the most refractory sources is probably of fundamental importance in producing the trace element enrichment patterns in arc volcanic rocks derived from depleted and ultra-depleted sources. Stern et al. (1991) emphasised this point when describing the geochemistry of Western Pacific boninites, while Ewart & Hawkesworth (1987) use the most depleted Tongan arc volcanic rocks to provide their most accurate estimate of the slab-derived trace-element flux.

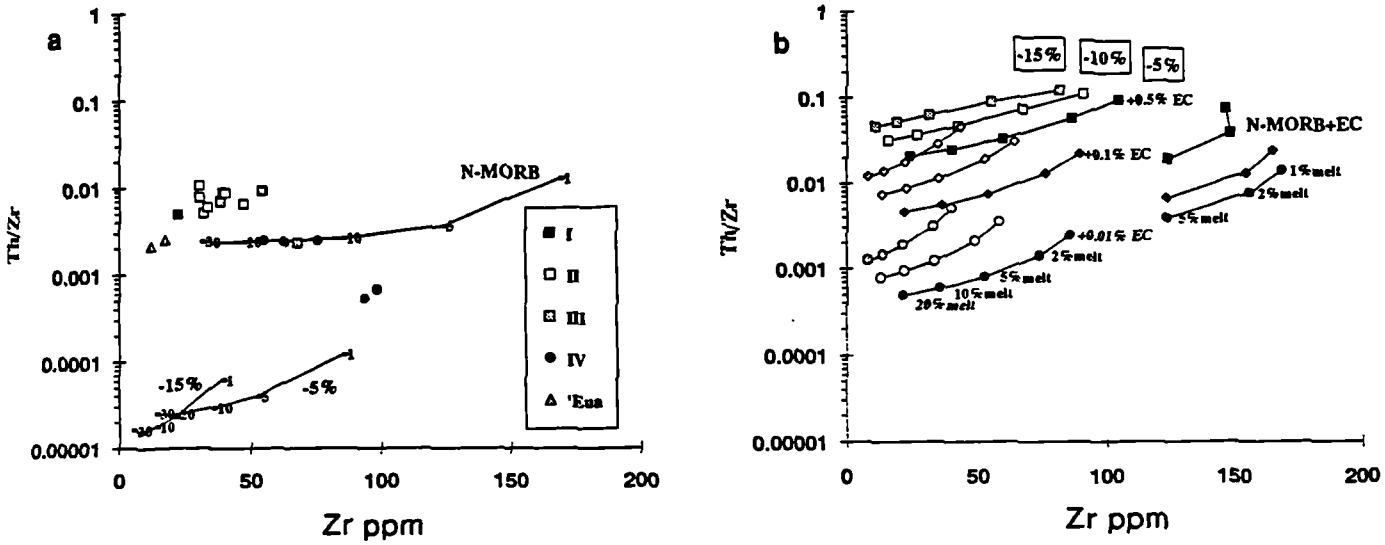

Fig. 6.13 Results of modelling of Th/Zr ratios using methodology outlined in text. Composition of enriched-melt component is summarised in Table 6.2. **a** Illustrates representative data and modelled melt compositions derived from uncontaminated N-MORB and two more depleted sources (-5% and -15% melt). **b** Modelled melt compositions for contaminated N-MORB (dark shaded symbols) and three more depleted sources: -5% melt (black symbols), -10% melt (open symbols) and -15% melt (light shaded symbols). Three separate quantities of enriched component are added to each source: +0.5% (squares), +0.1% (diamonds), and +0.01% (circles). Small percentage figures indicate amount of melting.

The low Nb/Zr samples in Fig. 6.12 also require that the range of depleted sources span a full spectrum down to DMM minus 1-2% melt (modelled melt compositions in this region are omitted for clarity). The Th/Zr data shows good general agreement with these

predictions as would be expected from the trends displayed in Fig. 6.10. Overlap in Nb/Zr and Th/Zr ratios between groups can be interpreted to reflect variations in the degree of melting (a similar conclusion to that drawn from Fig. 6.3) superimposed upon variations in the exact composition of the enriched components. Although the data does not constrain either of these two variables accurately, the angle at which the data set cuts the modelled melt lines for a given added enriched component may be significant. The steep trend of the data relative to the trend of the modelled melt lines implies that the degree of melting undergone by YG I-IV decreases from the more fertile towards the more depleted end of the source spectrum. This conclusion supports the concept of the groups being considered transitional in terms of degree of melting and extent of source depletion (Fig. 6.3) and is in good agreement with the results of Pearce et al. (1992b) who described high-, intermediate- and low-Ca boninites as resulting from progressively lower degrees of melting of successively more depleted sources.

Following the arguments presented above, Sr/Zr ratios modelled using the hypothesised enriched melt of Table 6.2 are too low, by up to an order of magnitude, to satisfy the Yavuna Group data (Fig. 6.14b). Fig 6.14c illustrates that modelled melt lines must include an additional Sr-flux, assumed to be derived from the subducted oceanic crust, in order to produce the high Sr/Zr ratios of the data. The additional flux is calculated by assuming Sr/Zr=100. However, as in the case of the Nb/Zr and Th/Zr models, absolute proportions of components are not well constrained. The addition of the aqueous fluid component can account for the spread of the data to high Sr/Zr if it is superimposed upon a variably depleted source.

6.2.6 Possible origins of the enriched melt component

The proposed single enriched-melt component has a trace-element signature similar to that of some ultra-potassic rocks. This may indicate that the distinctive trace-element fractionation signature is derived via a process common to both high-K suites and the boninite-arc tholeiite suite studied in this thesis.

This theme has been addressed in a petrogenetic study of boninites from the northern Tonga ridge by Falloon & Crawford (1991). These authors recognised the presence of a transient, fractionated, enriched-component involved in the petrogenesis of a high-calcium boninite suite. The component was part of a spectrum of enriching agents which included a conventional high-LILE/(LREE, HFSE) hydrous fluid and a small-degree

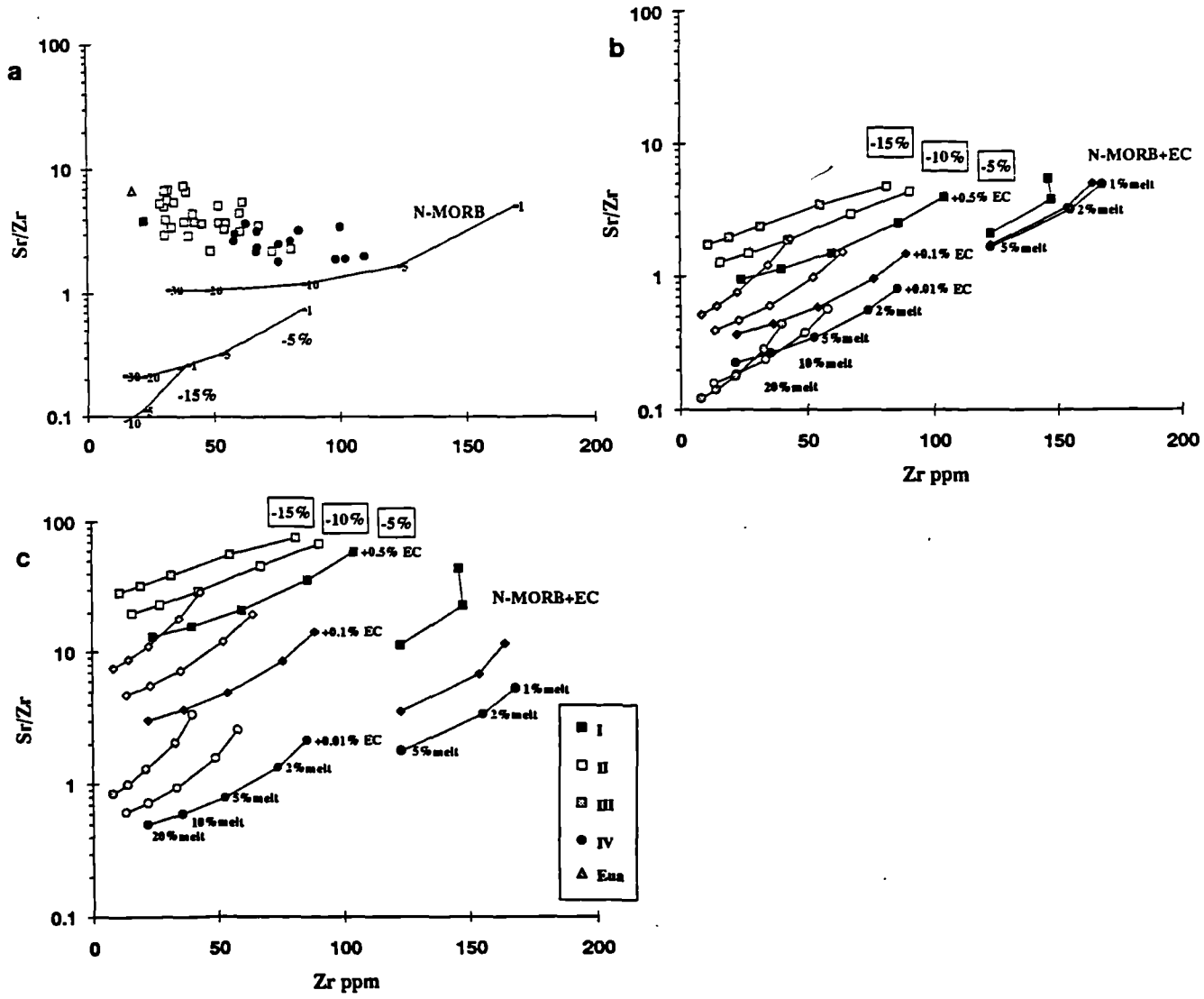

Fig. 6.14 Results of modelling of Sr/Zr ratios using methodology outlined in text. **a** Illustrates representative, alteration screened, data and modelled melt compositions derived from uncontaminated N-MORB and two more depleted sources. **b** Modelled melt compositions for N-MORB (dark shaded symbols) and three more depleted sources: -5% melt (black symbols), -10% melt (open symbols) and -15% melt (light shaded symbols) using enriched-melt component from Table 6.2. Three separate quantities of enriched component are added to each source as described in caption to Fig. 6.12. **c** Modelled melt compositions for N-MORB and more depleted sources contaminated by a hypothesised aqueous fluid with Sr/Zr ratio of 100.

partial melt of OIB-type mantle enriched in LILE, LREE and the HFSE. The distinctive *fractionated* signature of the enriched component was attributed to the presence of a small-degree melt with high abundances of LILE and LREE but low HFSE concentrations due to retention of these elements by a residual TNT phase. The ephemeral nature of the enrichment was interpreted to reflect the differing characteristics

of both melt and residual phases under oxidised and reduced conditions in the presence of C-O-H fluids. Under oxidising conditions, the TNT phases would be stable and the resulting small-degree melt would show a Nb-Ta anomaly. Under reducing conditions, however, the TNT phases would not be stable, Nb-Ta anomalies would not occur, and an unfractionated enriched component would produce melts with an OIB-type trace-element signature.

The pervasive presence of the fractionated signature in the lower Yavuna Group samples suggests that, if similar melts were involved, oxidising conditions were probably prevalent during the earliest stages of subduction. The site of fractionation between the LILE-LREE and HFSE, however, remains an outstanding problem in any model which proposes addition of a fractionated melt. Models which advocate the presence of residual titanates in the mantle wedge during melting (e.g. Morris & Hart 1983, Arculus & Powell 1986) are constrained to only small degrees of melting so that the Nb-Ta phase is not melted out of the source assemblage, thus destroying the Nb-Ta anomaly. Although in the context of recent melting models e.g. McKenzie (1984), Parkinson (1993), the degree of instantaneous melting in a rising column of decompressing mantle may be very small thus allowing an accessory titanate phase to be preserved, the geochemistry of the melts would still require that the phase be present and stabilised prior to the commencement of melting. This is difficult to envisage in a mantle source region which should theoretically have been depleted in all incompatible elements during previous episodes of melt extraction.

6.2.7 The role of fluid-induced melting

Correlations in geochemical data between indices of source enrichment and degree of mantle melting or source depletion have led some authors to propose that melting of the mantle wedge was triggered by the flux of material from the subducted slab into the overlying wedge (e.g. Cameron et al. 1983; Taylor & Nesbitt 1988). This model can be assessed for the Yavuna Group data by referring to Fig. 6.14 and using Zr content as a measure of source depletion or degree of melting, and the Sr/Zr ratio to represent the addition of aqueous fluid added to the source which would then trigger melting according to the hydrous-fluxing model of Davies & Bickle (1991). A broad trend of increasing minimum Sr/Zr is present for each group as Zr decreases. Following the earlier conclusions drawn from Fig. 6.14, however, this trend is interpreted to reflect the preferential 'sensing' abilities of the most depleted sources to a relatively uniform aqueous fluid component rather than having to appeal to an increased proportion of Sr in the aqueous fluid when passing from YG IV to YG I. The trend of maximum Sr/Zr

for each group shows a similar increase from YG IV to YG II, however, for YG I, the Sr/Zr data falls below the trend. If the data is representative of the YG I melts generally, then either a flux containing lower Sr/Zr or a lesser quantity of flux containing similar Sr/Zr to the other groups was added to the YG I source. In either case, the concept of a quantitative fluid-induced melting model, in which more refractory mantle requires an increased proportion of slab-derived fluid to trigger melting, breaks down.

Plank & Langmuir (1988) discussed melting in the mantle wedge from another 'end-member' viewpoint. Their emphasis was based upon the degree of melting being related to the length of the melting column in which the mantle undergoes decompression melting beneath the arc i.e. the vertical distance between the source region and the base of the arc crust (the Moho). They assigned the role of the aqueous fluid to that of a trigger to melting only. The fluid would be released through the pressure-related breakdown of amphibole (Tatsumi 1986) and would lead to gravitational instability and upwelling of mantle which would then melt as it rose adiabatically. The authors discovered a relationship which linked the degree of melting to crustal thickness and, as they had assumed a common depth source for arc volcanics of ~100km, to the length of the melting column. In the case of boninite and transitional boninite lavas such as the YG I melts, however, relatively shallow depths of origin must be invoked in order to satisfy experimental phase equilibrium constraints (maximum of ~60km for high-Ca boninites, Van der Laan et al. 1989). The resulting melting column for the boninites would therefore be shorter than that of the successively more fertile melts represented by YG II, III and IV melts (crustal thickness cannot have been a variable during the synchronous eruptions of the YG I-IV melts).

The total degree of melting thus undergone in the generation of the Yavuna Group melts must therefore be considered to reflect a resultant of two distinct melting regimes. The first melting event which depletes the source to a degree dependent upon its depth can be observed in the moderately-incompatible HFSE systematics e.g. Sc/Y-Zr (Fig. 6.3b). This produces a vertically zoned mantle wedge which becomes increasingly more refractory at shallower levels (Scott & Stevenson 1989; Kostopoulos & Murton 1992). The second melting event is probably triggered by aqueous fluids and continues until the upwelling mantle diapir reaches the Moho. Its effects can be detected when considering the systematics of incompatible elements that have re-enriched the source prior to the second melting event.

6.3 The second arc volcanic event

6.3.1 Moderately-incompatible trace element systematics

As demonstrated in chapter 5, the key HFSE ratios used in evaluating melting processes are lowered by fractional crystallisation. Only samples with relatively high wt.% MgO can therefore be used for comparison with the primitive Yavuna Group suite. Fig. 6.15 illustrates that the HFSE ratios in the most primitive Wainimala Group (WG) samples show a smaller range at the low ratio end of the Yavuna Group ratio spectrum. Depleted boninite and depleted high-Si arc tholeiite compositions corresponding to YG I and YG II are not present. According to the modelling in Fig. 6.3 and Fig 6.5, primitive WG melts can be interpreted to represent moderate degrees of melting of a source similar to the modelled

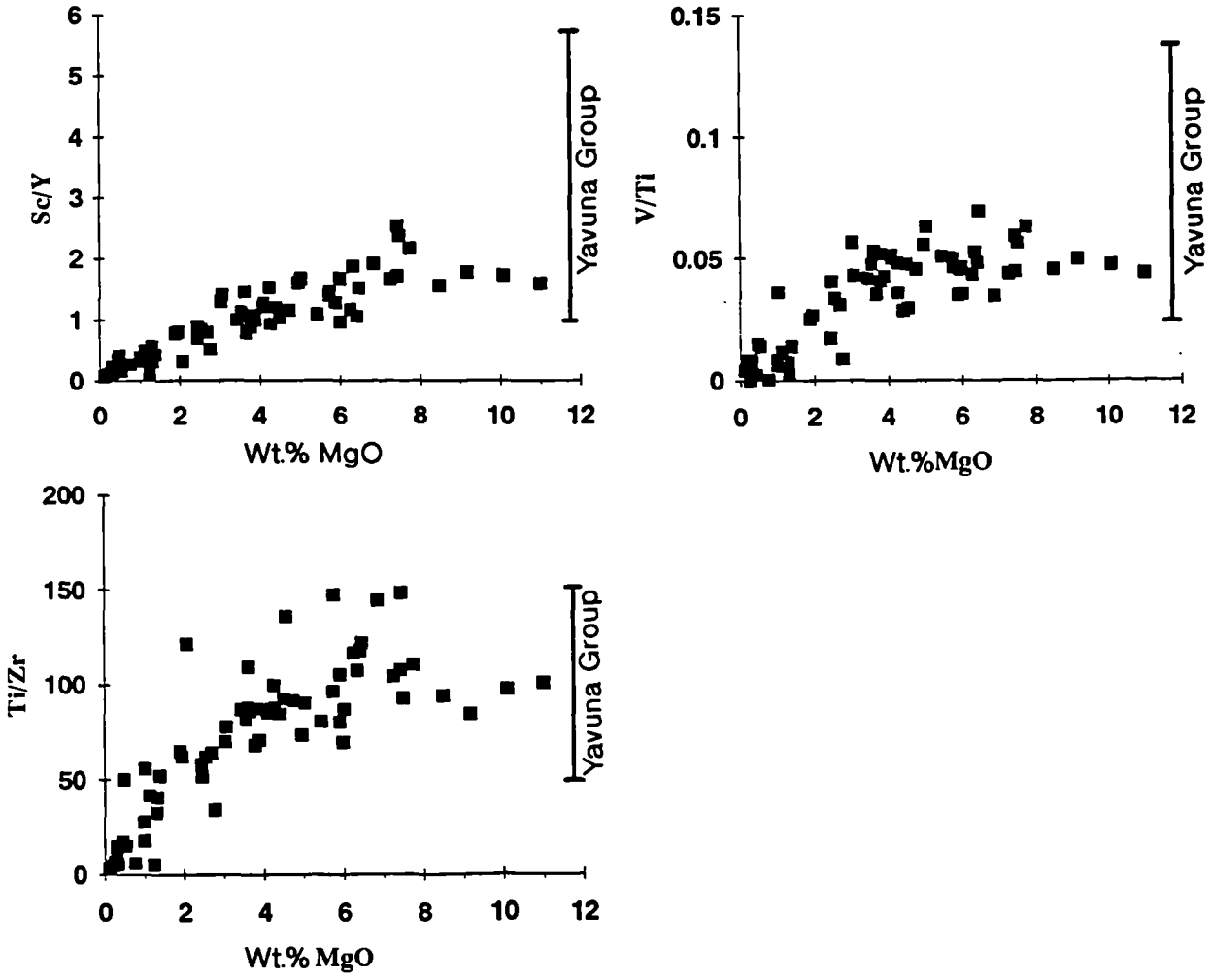

Fig. 6.15 Plots of Sc/Y, V/Ti and Ti/Zr versus wt.% MgO for all Wainimala Group data. Bars on each plot indicate range of the Yavuna Group data.

DMM composition. Other moderately-incompatible trace element ratios, for example, Zr/Y (3.0-3.3) Zr/Hf (35-41), are also similar to those of MORB. Importantly, displacements to low Ti/Zr and high Zr/Sm do not occur in the primitive WG samples (Ti/Zr=85-110, Zr/Sm=21-24 for the four samples with wt.% MgO>8%), supporting the assertion of section 6.2.3.2 that this signature may be unique to the earliest stages of subduction. Sr/Zr ratios for the primitive WG samples range from 4.7-5.5. Inspection of Fig 6.14 reveals that the modelled melt lines for an anhydrous DMM-source are unable to produce Sr/Zr>1 for moderate degrees of melting. The moderately-incompatible HFSE and Sr/Zr ratios of the primitive Wainimala Group lavas therefore document addition of an aqueous fluid component to a DMM-type source to produce melts with similar characteristics to YG III.

6.3.2 Highly-incompatible element systematics

Contrasting highly-incompatible element systematics for the two suites are illustrated in Fig. 6.16. Ta data is utilised in this plot to enable samples from the literature to be plotted.

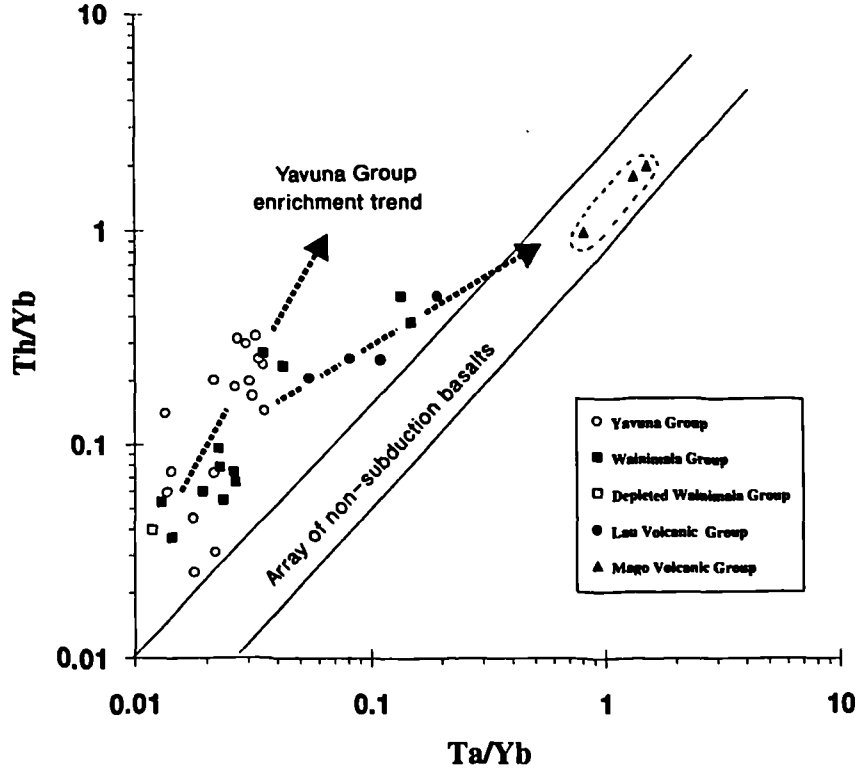

Fig. 6.16 Th/Yb-Ta/Yb plot for representative Yavuna Group and Wainimala Group data. Additional data is taken from Gill (1987) and Cole et al. (1991). Array of non-subduction basalts is taken from Pearce (1982). Nb/Ta ratio of 15 is assumed where data requires conversion.

As discussed in section 6.2.4 the lower Yavuna Group data trend suggests incorporation of a resultant high Th/Nb (high Th/Ta) component into the mantle source during the earliest stages of subduction. While a similar component may be selectively present in the Wainimala Group melts, an important additional component with lower Th/Ta is also identified in some lavas. These two samples have similar trace element signatures to samples from the Lau Volcanic Group of the Lau Ridge (Cole et al 1991) and may indicate selective incorporation of a region-wide enriched component with OIB-type trace element characteristics. Samples from the Mago Volcanic Group of the Lau Ridge have been plotted as an example of this type of melt (data taken from Cole et al. 1991). It is important to note that if an enriched asthenospheric component did provide this input then it is clear that the same component was not present in the early subduction related lavas of the lower Yavuna Group when sources were more depleted and hence more sensitive to the presence of enriched components.

Similar, co-existing, enriched (high-Nb) and depleted (low-Nb) basalts have been recorded from Turriabla volcano in the Central American arc (Reagan & Gill 1989). These authors favour the transient presence of residual titanate phases to explain the 'switch on-off" effect of the Nb-Ta anomalies.

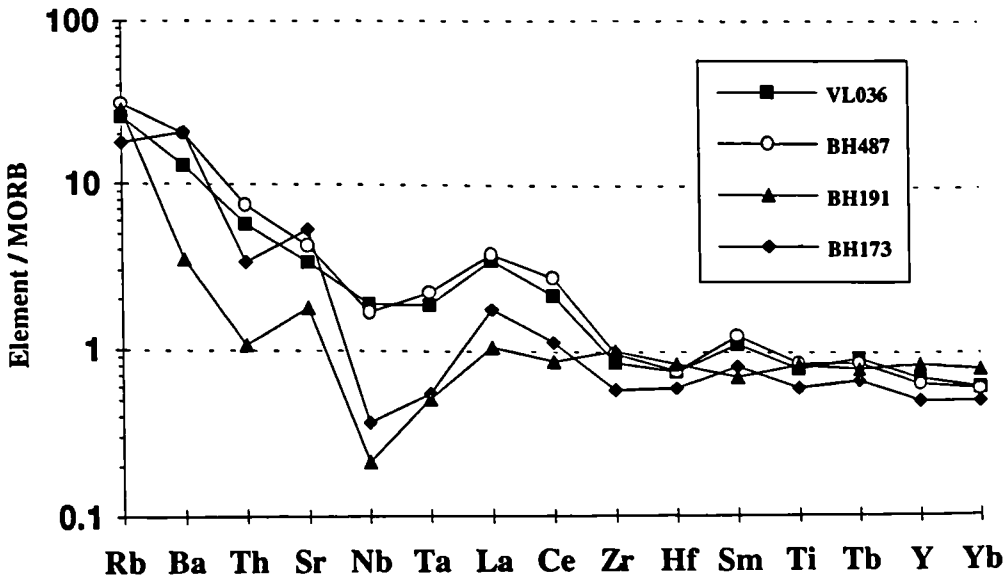

Fig. 6.17 MORB-normalised multi-element profiles for representative enriched and non-enriched Wainimala Group lavas.

However, this scenario alone could not satisfy the lower WG data, because the enrichment pattern is consistent throughout the highly-incompatible LILE and LREE as well as the HFSE. (Fig. 6.17).

An alternative explanation is that the enrichment is related to assimilation of enriched material within the arc crust or lithosphere. The two enriched samples have special significance in this respect in that they are the most primitive melts (Mg#=69-64) and would therefore have the highest liquidus temperatures and be capable of preferentially assimilating any fusible material. The most likely sources of fusible, enriched material would be the Yavuna Stock, however, this option can effectively be discounted because similar primitive samples e.g. BH119 (Mg#=63) crop out as dykes within the stock itself, yet show no enriched signature (Nb/Yb=0.03 c.f. Nb/Yb=0.13-0.15 for enriched samples). Enrichment mechanisms involving small-fraction melt components are well documented in areas underlain by continental lithosphere (e.g. Ellam & Cox 1991, Kerr 1993) and in these areas supporting evidence is also found in mantle xenoliths which show similar trace element enrichments (Menzies et al. 1987). There is no evidence, however, to suggest that young intra-oceanic arcs are underlain by this type of enriched lithosphere and indeed the few xenoliths from the arc lithosphere which have been analysed record only fluid-related enrichment of the source (e.g. Maury et al. 1992).

It is concluded, therefore, that the enriched melts derived their signatures in some way from a fundamentally more enriched asthenospheric source. A similar conclusion was reached for the YG V and VI melts in the upper part of the Yavuna Group (section 6.2.3, Fig. 6.3). Gill (1984) and Gill & Whelan (1989) provide isotopic and trace evidence for the involvement of OIB-source mantle in Fijian volcanics later in the island's history (age<6Ma) and it seems likely that a similar enriched source was selectively tapped for short periods by the late Yavuna arc and early Wainimala arc melting regimes. The inferred melting scenario may be similar to that proposed for some oceanic and backarc basin spreading ridges whereby predominantly depleted upwelling asthenosphere can entrain areas of enriched mantle 'OIB-source' asthenosphere and thus produce a spectrum of depleted and enriched melts (e.g. Williams & Gill 1988; Price et al. 1990; Hochstaedter et al. 1990; Stern et al. 1990). A mixing scheme of this type is illustrated in Fig. 6.18 where the enriched WG and YG VI enriched melts are plotted together with the full dataset of primitive, unenriched samples from the Wainimala Group and Yavuna Group. Mixing lines indicate that incorporation of OIB-type melts could provide the necessary shift to high Nb and in the case of the YG VI

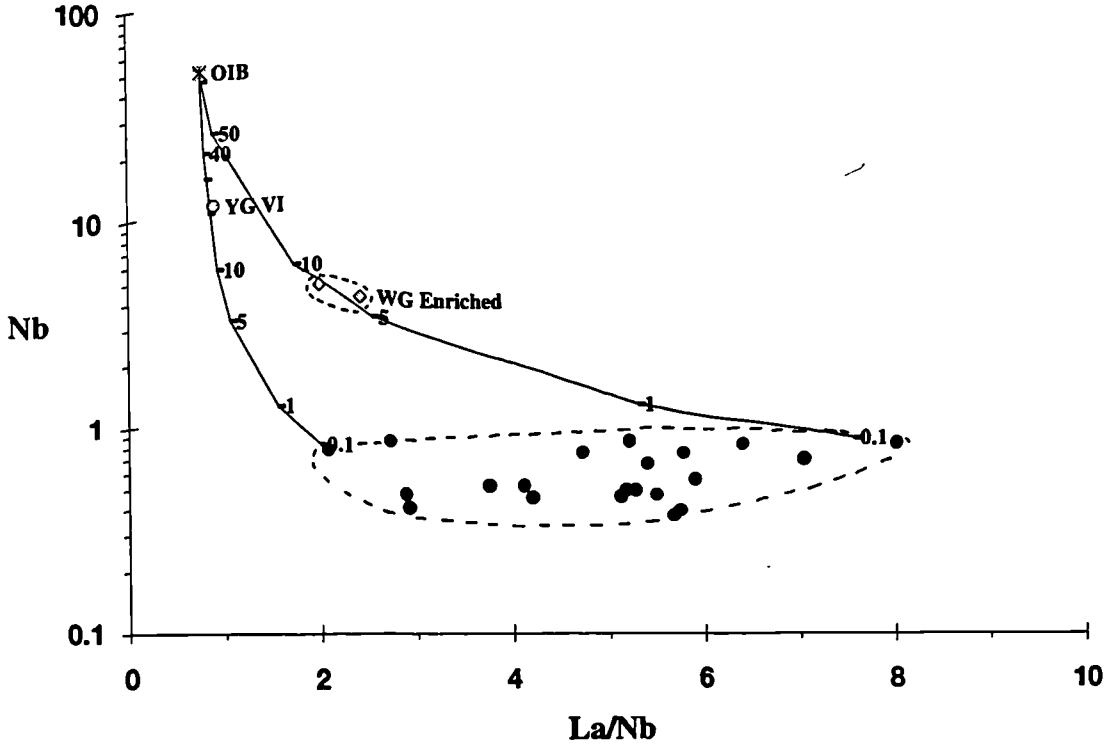

Fig. 6.18 Nb-La/Nb plot for all Yavuna Group and Wainimala Group data. Dotted circle encloses all non-enriched i.e. low-Nb data. Enriched Yavuna Group VI melt is denoted YG VI, enriched Wainimala Group melts are denoted WG enriched. Mixing lines connect ocean island basalt composition of Sun & McDonough (1989) with high-La/Nb and low-La/Nb extremes of main data field.

data, also to lower La/Nb. It is important to notice the possible implications of this model for the aqueous fluid flux to the source. WG samples require that OIB sources are mixed with high La/Nb (high-fluid) melts while YG VI samples require OIB to mix with low La/Nb (low-fluid) melts. Supporting evidence for this aspect of the model is provided by the contrasting Sr/Zr ratios for the two groups (WG Sr/Zr=4.8-5.3 and YG VI Sr/Zr=0.6). This would imply that aqueous fluid contribution into the system was at a minimum during the final stages of protoarc volcanism but then reached its maximum as the second phase of arc volcanism began.

One further line of supporting evidence for the involvement of OIB-type mantle is derived from the εNd isotopic composition of an enriched WG sample. The value of ε Nd=7.47 is significantly lower than the range of unenriched Wainimala Group samples (εNd=8.6-9.4, Gill 1984) and transitional towards the values reported by Gill (1984) for young Fiji OIB (εNd=4.3-5.1). This shift to lower εNd could also be accounted for by the mixing of contrasting enriched and depleted source components as noted for melts from the mid-ocean ridges that have become contaminated by enriched plume material

during asthenospheric upwelling (e.g. Storey et al. 1988). Following this argument, it is predicted that the εNd value of the YG VI melt would be even lower in accord with the greater proportion of OIB-type mantle involved in its petrogenesis (Fig. 6.18).

6.4 Summary

Trace-element modelling suggests that most of the Yavuna Group and Wainimala Group melts can be generated through accumulated fractional melting of a source similar to, or more depleted than, DMM. In contrast, some 'Eua melts require a more extreme mechanism involving pure fractional melting in order to further reduce the levels of incompatible elements in the source.

The resultant melting regime recorded by the arc melts can be divided into two components. The first is documented by HFSE-variations and probably occurred prior to the initiation of subduction leading to a depth-dependant, variably-depleted mantle residue. The second event was triggered by the release of aqueous fluids from the dehydrating subducting slab into the mantle wedge. It is documented by the systematics of a range of incompatible elements which re-enriched the wedge prior to melting. Anomalous thermal conditions during the second event may have led to localised partial melting of the slab assemblage.

Melting of fundamentally enriched, OIB-type, asthenospheric mantle is suggested by the trace-element systematics of some upper Yavuna Group and lower Wainimala Group melts. Incorporation of this previously un-tapped enriched mantle source suggests a mechanism whereby fertile mantle is entrained in the melting column of a upwelling HFSE-depleted arc diapir.

CHAPTER 7

Conclusions and implications

7.1 Introduction and tectonic framework

7.1.1 The protoarc

The degree of tectonic disruption suffered by the island arc ridges in the south of the western Pacific arc province is far greater than that in the north of the province where broadly consecutive episodes of rifting are recorded by the broadly sub-parallel volcanic ridges and spreading axes in the intervening marginal basins (Fig. 1.2). The tectonic history of the northern part of the province is well documented with most authors considering that a subduction zone was created at a transform fault between the Pacific and Western Philippine Sea lithospheric plates in the Middle Eocene (Stern & Bloomer 1991, Pearce et al. 1992b.). A palinspastic reconstruction of this event is shown in Fig. 7.1a. In the south of the province, far fewer fragments of ancestral arc or protoarc crust exist. Some are currently being subducted e.g. the Eocene D'Entrecasteux Ridge beneath the Vanuatu arc (Collot & Fisher 1991) while many other fragments have probably been lost during subduction-erosion processes operating throughout the Tertiary (Hawkins et al. 1984).

Weissel et al. (1982) document Late Paleocene to Late Eocene magnetic anomalies (22-18) in the southern New Hebrides marginal basin, a small fragment of oceanic crust isolated between the younger Loyalty and Vanuatu arc ridges. This crust provides evidence that the configuration of tectonic elements in the south of the province may have been similar to that in the north, prior to the onset of subduction in the Middle Eocene. A possible plate configuration is shown in Fig. 7.2b. In this reconstruction, the effects of later spreading centre activity such as the North and South Fiji basins and the Lau basin are removed. In both the north and south of the province, it is important to note that subduction initiation and transpression at a transform boundary may have involved under-thrusting of young, and thus relatively warm lithosphere beneath a spreading ridge or a ridge beneath young, warm lithosphere. This tectonic situation was probably of fundamental importance in providing the thermal conditions necessary to trigger melting of refractory mantle sources and parts of the subducting slab.

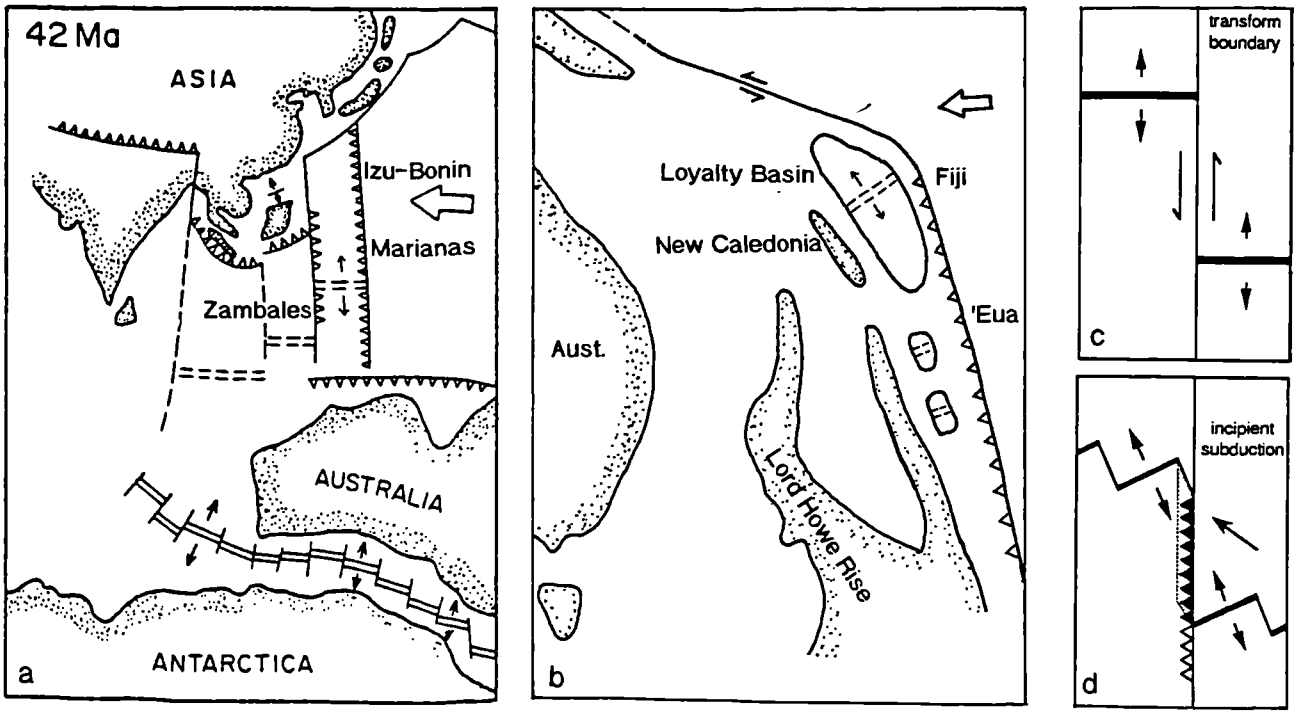

Fig. 7.1a Reconstruction of tectonic elements in the north of the western Pacific arc province at 42Ma (from Stern & Bloomer 1991). **b** Proposed comparative situation in the south of the province adapted from Kroenke (1984). **c** Representation of pre-subduction transform boundary **d** transform placed under transpression following onset of subduction. At **X**, young and therefore warm lithosphere is subducted beneath a spreading ridge. At **Y**, a ridge is subducted beneath young, warm lithosphere.

7.1.2 The protoarc-second arc transition

A major angular unconformity separates the Wainimala Group volcanic rocks from the underlying Yavuna Group. During the intervening hiatus, the magmatic focus of the subduction system was concentrated in the backarc (South Fiji basin) region. However, complex patterns of magnetic anomalies in the basin (Davey 1982) preclude any simple arc-marginal basin geometric relationship as exists in the north (Fig. 1.2) between the protoarc terrane (the Izu-Bonin and Marianas forearc), the backarc basin spreading centre (the Parece-Vela basin) and the remnant arc (the Palau-Kyushu ridge). No remnant arc formed during Yavuna Group rifting has been located with certainty, although possible ridges do exist in the west, in the New Caledonia region, where Late Eocene sediments interbedded with basic volcanic rocks were drilled during ODP Leg 131 (Collot & Fisher 1991). Alternatively, the remnant arc may have been entirely subducted beneath the Vanuatu arc.

The incipient protoarc rifting event may also be marked by the intrusion of the Yavuna Stock at the beginning of the Early Oligocene epoch (chapter 2). The intrusion of large volumes of felsic magma during rifting is a common feature of oceanic island arcs as well as continental margins. Gill (1992) attributes rift-related felsic magmatism to fractional crystallisation and release of confining pressure during extension, rather than to anatexis during crustal thinning. Field and petrographic evidence from the Yavuna Stock provide some support for this assertion in detailing the presence of a basic-cumulate floor and side-wall facies to the intrusion that is complementary to the main tonalite facies.

7.1.3 The second arc

The earliest products of the Wainimala arc erupted onto the rifted margin of the Yavuna protoarc block in the Late Oligocene. Paleomagnetic studies indicate that Viti Levu has rotated in an anti-clockwise direction since the break-up of the continuous Vanuatu-Fiji-Lau Ridge arc in the Late Miocene (Falvey 1978). Recent results have constrained the amount of rotation to approximately 100° (G. K. Taylor personal communication, 1992), enabling a simplified reconstruction of the elements of the arc system to be made for the Late Oligocene (Fig. 7.2a). Wainimala Group volcanism initially occurred, at least in part, on the substrate provided by the Yavuna Group. Within a few million years, the volcanic front retreated away from the trench to become focused nearer to, or at, the frontal arc backarc transition (Fig. 3.14).

7.2 The Yavuna Group

Accretion in the protoarc (the Yavuna arc) was dominated by eruption of basic lavas in shallow water. A lava pile of at least 400m thickness was constructed. Constraints on the duration of protoarc volcanism are provided by interbedded Late Eocene and Early Oligocene limestones. By the Early Oligocene, extrusive volcanism had ceased and sub-aerial reworking within the protoarc led to the deposition of proximal rudites with interbedded limestones on the flanks of basement highs.

The earliest documented protoarc lavas are boninites and depleted arc tholeiites which, during the course of protoarc accretion, were superseded by lavas derived from more fertile and, eventually, fundamentally enriched mantle sources. Trace-element modelling indicates that the lowest Yavuna Group lavas were generated through batch or accumulated fractional melting of a range of sources similar to, and more depleted

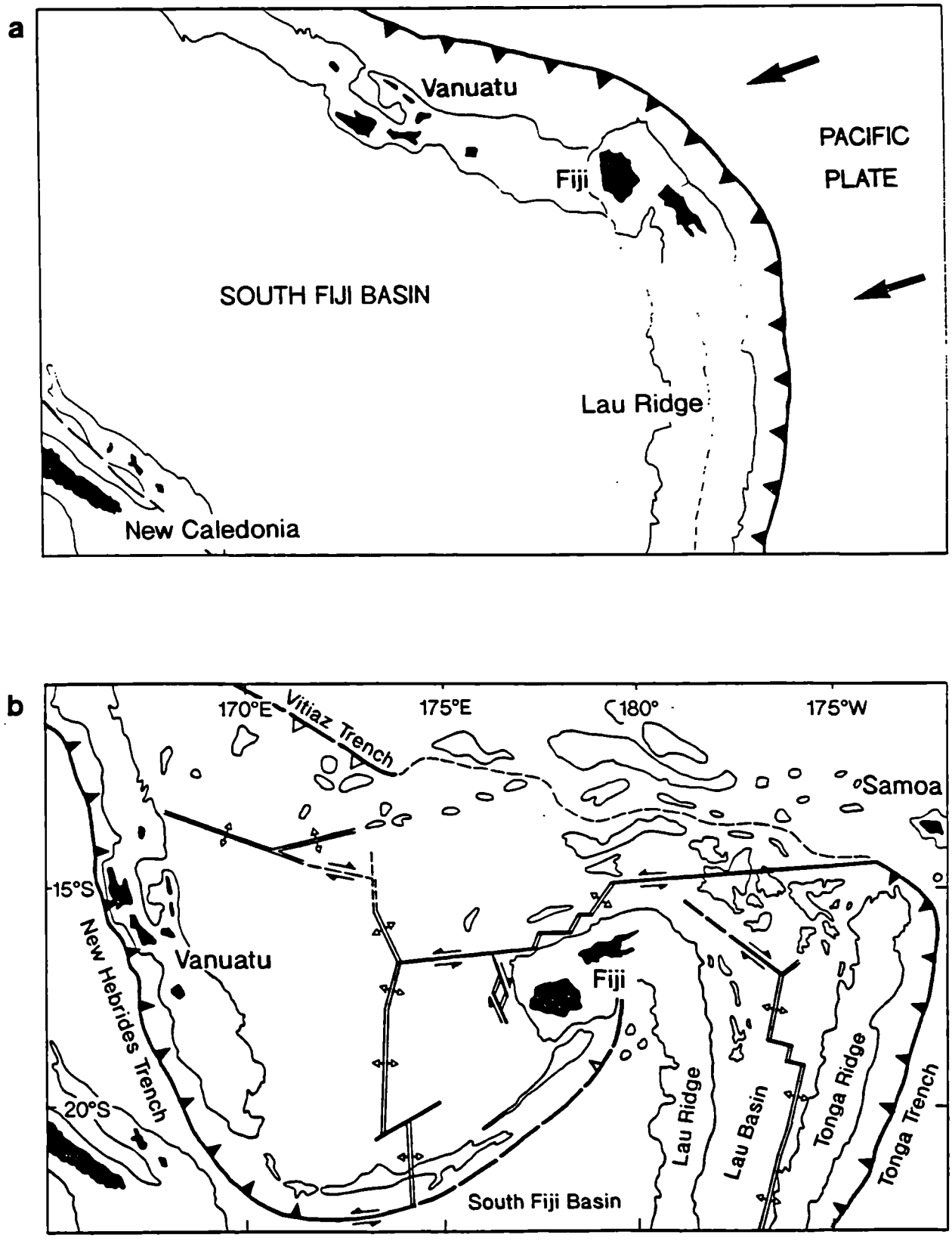

Fig. 7.2a. Regional plate tectonic reconstruction for the Late Oligocene-Early Miocene. Plate convergence vectors inferred from poles of rotation published by Packham & Andrews (1975). **b.** Present-day regional tectonic setting. Modified from Hathway (1993).

than, depleted MORB-mantle (DMM). By implication, following the arguments of Scott & Stevenson (1989) and Kostopoulos & Murton (1991) that depletion of the mantle source is dependant upon depth, it follows that melts from a considerable range of depths in the mantle were simultaneously tapped during protoarc volcanism. This aspect of the early subduction zone is in marked contrast to the widely accepted tenet that the source of arc volcanism is controlled by pressure dependant dehydration reactions (e.g breakdown of amphibole) occurring over a relatively narrow depth interval (Tatsumi 1986, Plank & Langmuir 1988). ODP Leg 125 scientists concluded that a range of sources from relatively shallow levels (low-Ca boninites, 25km depth) to relatively deep levels (high Ca-boninites, 50km depth) were tapped during the initiation of subduction in the north of the western Pacific arc province.

A protoarc melting scenario is illustrated in Fig. 7.3, together with the situation envisaged for normal island arc tholeiite volcanism. It is concluded that the Yavuna Group protoarc lavas document a situation that is transitional between the extreme melting of shallow, highly-refractory harzburgite sources in the Izu-Bonin and Marianas forearc and the more normal melting of deeper, more fertile, DMM-type lherzolite mantle that occurs during island arc tholeiite volcanism. In this respect, the Yavuna Group lavas show similar affinities to lavas preserved in the crustal section of the Zambales ophiolite (Evans et al. 1991).

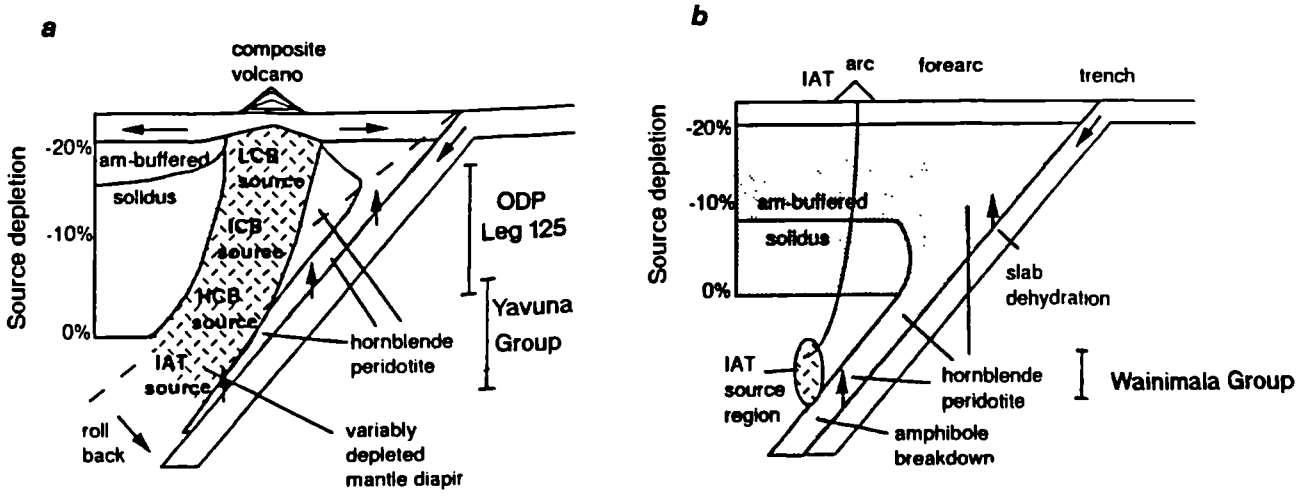

Fig. 7.3a Melting scenario envisaged for boninites and depleted arc tholeiites (modified after Pearce et al. 1992b). **b** Comparative illustration of melting scenario during normal arc tholeiite volcanism. LCB is low-Ca boninite, ICB is intermediate-Ca boninite, HCB is high-Ca boninite. Note that the position of the boninite-depleted arc tholeiite volcanoes is closer to the trench than the normal arc tholeiite case. Higher potential temperatures due to young over-riding plate and strong extension due to early slab rollback enable melting of refractory mantle at relatively shallow levels in the wedge.

The differences in melting regime along the strike of the western Pacific protoarc terrane are viewed as a predictable consequence of the variations in tectonic configuration and mantle potential temperature that accompanied the initiation of subduction beneath marginal basin lithosphere of various age and thus potential temperature.

Melting of DMM and fundamentally more enriched asthenospheric mantle is suggested by the trace-element systematics of melts in the upper Yavuna Group. Following the discussion of data presented in chapter 6, much of the up-sequence transition to enriched lavas is regarded as transitional in nature. No abrupt boundary within the lava pile can, as yet, be delineated that would enable further formalised divisions of the stratigraphy to be made. Incorporation of the previously untapped, enriched asthenospheric source may have been linked to the changes in the tectonic regime which accompanied incipient rifting of the protoarc edifice. The relationship between rifting and tapping of new, and more enriched mantle sources has been clearly demonstrated in the propagating rifts of several marginal basins, for example, the Mariana Trough (Stern et al. 1990); the Sumisu Rift (Hochstaedter et al. 1990); the North Fiji Basin (Price et al 1990); and the Lau Basin (Hergt & Nielson in press). The assertion of Stern & Bloomer (1991) that extensional accretion tectonics in young western Pacific-type plate margins are similar to those observed at slow-spreading ridges, together with the trench-suction effect of subduction zone rollback (Hawkins et al. 1984), may be significant in allowing these areas of enriched mantle to enter the zone of melting.

7.3 The Wainimala Group

7.3.1 Crustal accretion

Accretion in the second arc was characterised by the eruption of a range of basic to felsic lava types. The principal edifice and inter-edifice volcanism seen in the Wainimala Group basinal assemblage resembles that described by Stern et al. (1989) in their discussion of the volcanic sections of supra-subduction zone ophiolites. They suggest that fissure-fed lavas may be important but largely unstudied components of intra-oceanic arcs, making up much of the seafloor between the major volcanic edifices. They predict that the inter-edifice lavas should be slightly less fractionated but otherwise geochemically similar to those erupted from the major edifices. The present study supports the hypothesis of Stern et al. and allows further detail to be added to their model.

Relationships between the Dakadaka Basalt, the Kalaka Dacite and the bimodal dyke swarm cutting the underlying Yavuna Group provide some insight into part of the magmatic feeder system beneath the inter-edifice terrane of the arc. None of the basic dykes intruding the Yavuna Group have compositions appropriate to be considered as feeders for the most geochemically primitive Dakadaka lavas. The basic dykes are therefore considered to represent more evolved equivalents of the Dakadaka Basalt that were emplaced at deeper levels in the arc crust. It is suggested that the Dakadaka Basalt lavas reached the seafloor through deep-seated fractures in the Yavuna Group substrate. These conduits are not exposed but may lie beneath the present outcrop of the Dakadaka Basalt. Such deep-seated fractures would have allowed primitive magmas to ascend from depth with only limited fractionation en-route.

Field relationships indicate that basic and felsic dykes were emplaced in the arc crust broadly contemporaneously. There is little evidence for magma-mixing in the inter-edifice volcanic rocks and dyke swarm and compositional gaps were generated in tholeiitic trends during fractionation of Fe-Ti oxides. These factors suggest that the dykes were emplaced in the arc crust following efficient segregation of basic and felsic magmas in compositionally stratified magma reservoirs. Magmatic overpressure generated through fractionation and melt vesiculation (e.g. Turner & Campbell 1986) may have been the main factor allowing the most evolved, felsic members of the dyke swarm to reach the sea-floor and form the Kalaka Dacite centres. This assertion is supported by fracturing and veining of the country rock seen close to some felsic dykes and by the tendency for felsic sills, as well as dykes, to occur in the arc crust. Magmas with compositions corresponding to the majority of the basic dykes did not erupt in the inter-edifice terrane. These magmas either ponded as small gabbroic intrusions in the crustal substrate or terminated in cm-scale finger-dykes. Further upward progress towards the surface occurred only rarely, in composite dykes, where more differentiated magma was fed into the same conduit.

The feeder system to the principal volcanic edifice terrane is not exposed. However, trace-element profiles indicate that the source for the edifice-forming lavas was similar to that for the inter-edifice lavas. Different fractionation histories in the two terranes and a greater role for dis-equilibrium processes documented for the major edifice lavas thus reflects control operating within the arc crust. A greater crustal filtering effect for the frontal arc substrate beneath the major edifice volcanoes leads to slow magma ascent rates and differentiation at relatively deep levels in the arc crust. In the inter-edifice terrane, less efficient crustal filtering leads to more rapid ascent of magma, relatively shallow levels of crystallisation and a lesser probability of magma-mixing. Contrasting

styles of volcanism in the edifice and inter-edifice terranes may thus reflect the interaction of ascending magmas with pre-existing structural heterogeneities in the frontal-arc substrate.

7.3.2 The rôle of tectonic extension

The pervasive NW-SE dyke swarm has a remarkably consistent orientation across the Yavuna Group outcrop (Fig. 3.12). Both compositional end-members of the swarm occur locally in sheeted forms with internal chilled margins, and veining of the country rock is only rarely observed. Given the large volumes of magma involved in the dyke swarm (up to 60% of the crustal section over an area of 200km^2), tectonic extension must be invoked to explain the passive emplacement of magma into the majority of dykes. A lack of basement exposure trenchwards (ie towards the north of the study area following the reconstruction of Fig. 7.2a), precludes an evaluation of the overall extent of the edifice and inter-edifice terranes. Whether volcanism was occurring in a similar regime in the arc assemblage to the south is also unknown. It is clear, however, that the volcanic front as defined by the trenchward limit of major volcanic edifices retreated southwards within 5-10Ma of the inception of the arc to become concentrated closer to the frontal-arc backarc transition (Fig. 3.14).

7.3.3 Structural controls on extension-related volcanism

If tectonic extension is typical of intra-oceanic arcs throughout their evolution (e.g. Hawkins et al. 1984), then successive phases of arc volcanism should overprint earlier arc crust within similarly oriented stress regimes. In the case of southwestern Viti Levu, this can be demonstrated by the parallel orientations of the Yavuna Stock of the protoarc stage and the dyke swarm of the incipient second arc stage (Fig. 3.12), and by the parallelism of the dyke swarm with the mature arc axis (the Wainimala-Colo plutons in southwestern Viti Levu, Fig. 2.1). The considerable volume of crustal substrate now occupied by intrusions related to later magmatic episodes should be taken into account when estimates of volcanic production rates in older arc terranes are made. Unless direct field observations can be made to substantiate geophysical surveys of submerged volcanic ridges, the widths of volcanic arcs that have been intruded during later extension-related volcanism may be considerably over-estimated. For example, it may be that along-strike equivalents of the Wainimala arc in Vanuatu and the northern Lau Ridge (Fig. 7.2a) are also considerably attenuated and intruded at depth.

7.4 Eua

The oldest volcanic rocks preserved on 'Eua do probably comprise part of the western Pacific protoarc province. The lack of geological control on the exact age of the rocks makes direct correlation with the Yavuna Group impossible. However, many of the source characteristics of the most depleted 'Eua rocks were similar to that beneath the Yavuna protoarc, even though the mechanism involved in creating source depletion may have differed. The nature of mantle source enrichments differed from those of the Yavuna Group lavas. However, these in turn differed widely from the enrichments of other parts of the protoarc province (Fig. 6.7).

The considerable range of geological and geochemical variations which are documented in the Yavuna Group and 'Eua arc basement sequences are a good reflection of the variability which characterises the ancient western Pacific arc province as a whole.

REFERENCES

ALABASTER, T., PEARCE, J. A. & MALPAS, J. 1982. The volcanic stratigraphy and petrogenesis of the Oman ophiolite complex. *Contributions to Mineralogy and Petrology*, **81**, 168-183.

ARCULUS, R. J. & WILLS, K. A. 1980. The petrology of plutonic blocks and inclusions from the Lesser Antilles island arc. *Journal of Petrology*, **21**, 742-799.

ARCULUS, R. J. & POWELL, R. 1986. Source component mixing in the regions of arc magma generation. *Journal of Geophysical Research*, **91**, 5913-5926.

ARCULUS, R. J., PEARCE, J. A., MURTON, B. J. & VAN DER LAAN, S. R. 1992. Igneous stratigraphy and major element geochemistry of holes 786A and 786B. *In*: FRYER, P., PEARCE, J. A., STOCKING, L. B., et al. *Proc. ODP, Sci. Results*, **125**, College Station, TX (Ocean Drilling Program), 143-169.

BALLARD, R. D., HOLCOMB, R. T. & VAN ANDEL, T. H. 1979. The Galapagos Rift at 86°W. Sheet flows, collapse pits, and lava lakes of the rift valley. *Journal of Geophysical Research*, **84**, 5407-5422.

BAYLISS, P., ERD, D. C., MORSE, M. E., SABINA, A. P. & SMITH, D. K. 1986. Mineral powder diffraction file. JCPDS - International centre for diffraction data, Swarthmore, USA.

BECCALUVA, L., MACCIOTTA, G. PICCARDO, G. B. & ZEDA, O. 1989. Clinopyroxene composition of ophiolite basalts as a petrogenetic indicator. *Chemical Geology*, **77**, 165-182.

BOYNTON, W. V. 1984. Cosmochemistry of the rare earth elements: meteorite studies. *In*: HENDERSON, P. (ed) *Rare earth element geochemistry*. Elsevier, Amsterdam, 63-114.

BROPHY, J. G. 1991. Composition gaps, critical crystallinity, and fractional crystallisation in orogenic (calc-alkaline) magmatic systems. *Contributions to Mineralogy and Petrology*, **109**, 173-182.

BROPHY, J. G. & MARSH, B. D. 1986. On the origin of high-alumina basalt and the mechanics of melt extraction. *Journal of Petrology*, **27**, 763-789.

BUTLER, R. F. & CONEY, P. J. 1981. A revised magnetic polarity timescale for the Palaeocene and Early Eocene and implications for Pacific Plate motion. *Geophysical Research Letters*, **8**, 301-304.

CAMERON, W. E. 1985. Petrology and origin of primitive lavas from the Troodos ophiolite, Cyprus. *Contributions to Mineralogy and Petrology*, **89**, 239-255.

CAMERON, W. E., MCCULLOCH, M. T. & WALKER, D. A. 1983. Boninite petrogenesis: Chemical and Nd-Sr isotopic constraints. *Earth and Planetary Science Letters*, **65**, 75-89.

CASEY, J. F. & DEWEY, J. F. 1984. Initiation of subduction zones along transform and accreting plate boundaries, triple junction evolution and forearc spreading centres - implications for ophiolite geology and obduction. *Geological Society of London Special Publication*, **13**, 269-290.

CLAGUE, D. A. & DALRYMPLE, G. B. 1987. The Hawaiian-Emperor volcanic chain. Part I. Geologic Evolution. *In*: Decker R. W., Wright, T. L. & Stauffer, P. H. (eds). *Volcanism in Hawaii (Vol. 1)*, Geol. Surv. Prof. Pap. U.S., **1350**, 5-54.

COLE, J. W., GILL, J. B. & WOODHALL, B. 1985. A petrological history of the Lau Ridge, Fiji. *In*: SCHOLL, D. W. & VALLIER, T. L. (eds) Geology and offshore resources of Pacific island arcs - Tonga region. *Circum-Pacific Council for Energy and Mineral Resources, Earth Science Series*, **2**, 379-414.

COLE, J. W., GRAHAM, I. J. & GIBSON, I.L. 1991 Magmatic evolution of Late Cenozoic volcanic rocks of the Lau Ridge, Fiji. *Contributions to Mineralogy and Petrology*, **104**, 540-554.

COLE, W. S. 1960. Upper Eocene and Oligocene larger foraminifera from Viti Levu, Fiji. US Geological Survey Professional Paper, 374-A.

COLEMAN, P. J. & PACKHAM, G. H. 1976. The Melanesian borderlands and India-Pacific Plates' boundary. *Earth Science Reviews*, **12**, 197-233.

COLLOT, J-Y & FISHER, M. A. 1991. The collision zone between the North D'Entrecasteux Ridge and the New Hebrides island arc 1, sea-beam morphology and shallow structure. *Journal of Geophysical Research*, **96**, 4457-4478.

COLLEY, H. 1984. An ophiolite suite in Fiji? *In*: GASS, I. G., LIPPARD, S. J. & SHELTON, A. W. (eds) *Ophiolites and oceanic lithosphere.* Geological Society, London, Special Publications, **13**, 333-340.

COLLEY, H. & HINDLE, W. H. 1984. The volcano-tectonic evolution of Fiji and adjoining marginal basins. *In*: KOKELAAR, B. P. & HOWELLS, M. F. (eds) *Marginal Basin Geology: Volcanic and associated sedimentary processes in modern and ancient marginal basins.* Geological Society, London, Special Publications, **16**, 151-162.

COLLEY, H., HINDLE, W. H. & HATHWAY, B. 1986. Early arc and basinal activity on Viti Levu, Fiji. *In*: IAVCEI Congress New Zealand, Abs.,p.140.

COLLEY, H. & WALSH, J. N. 1987. Genesis of Fe-Mn deposits of southwest Viti Levu, Fiji. *Transactions of the Institution of Mining and Metallurgy*, **96**, 201-212.

COX, K. G., BELL, J. D. & PANKHURST, R. J. 1979. *The interpretation of igneous rocks.* Allen & Unwin, London.

CRAWFORD, A. J., FALLOON, T. J. & GREEN, D. H. 1989. Classification, petrogenesis and tectonic setting of boninites. *In*: CRAWFORD, A. J. (ed) *Boninites*, 1-49. Unwin Hyman, London.

CROOK, K. A. W. 1963. Burial metamorphic rocks from Fiji. *New Zealand journal of Geology and Geophysics*, **6**, 681-704.

CUNNINGHAM, J. K. & ASCOMBE, K. J. 1985, Geology of 'Eua and other islands, Kingdom of Tonga: *In*: SCHOLL, D. W. & VALLIER, T. L. (eds) Geology and offshore resources of Pacific island arcs - Tonga region. *Circum-Pacific Council for Energy and Mineral Resources, Earth Science Series*, **2**, 221-258.

DAVEY, F. J. 1982. The structure of the South Fiji Basin. *Tectonophysics*, **87**, 185-241.

DAVIES, J. H. & BICKLE, M. J. 1991. A physical model for the volume and composition of melt produced by hydrous fluxing above subduction zones. *Philosophical Transactions of the Royal Society of London*, **A335**, 355-364.

DEER, W. A., HOWIE, R. A. & ZUSSMAN, J. 1983. *An introduction to the rock forming minerals.* Longman, London.

DEPAOLO, D. J. & WASSERBURG, G. J. 1976. Nd isotopic variations and petrogenetic models. *Geophysical Research Letters*, **3**, 249-252.

DICK, H. J. B. & BULLEN, T. 1984. Chromian spinel as a petrogenetic indicator in abyssal and alpine-type peridotites and spatially associated lavas. *Contributions to Mineralogy and Petrology*, **86**, 54-76.

DOBSON, P. F. 1986. *The petrogenesis of boninite: a field, petrologic and geochemical study of the volcanic rocks of Chichi-jima, Bonin Islands, Japan.* PhD thesis, Stanford University (unpublished).

DUNCAN, R. A., VALLIER, T. L. & FALVEY, D. A. 1985. Volcanic episodes at 'Eua, Tonga Islands: *In:* SCHOLL D. W. & VALLIER T. L. (eds) Geology and offshore resources of Pacific island arcs - Tonga region. *Circum-Pacific council for Energy and Mineral Resources, Earth Science Series*, **2**, 281-290.

ELLAM, R. M. & COX, K. G. 1991. An interpretation of Karoo picrite basalts in terms of interaction between asthenospheric magmas and mantle lithosphere. *Earth and Planetary Science Letters*, **105**, 330-342.

ELTHON, D. 1981. Metamorphism in oceanic spreading centres. *In*: EMILIANI, E. (ed) *The Sea, volume 7, the oceanic lithosphere.* Wiley, New York, 285-303.

EVANS, C. E., CASTENEDA, G. & FRANCO, H. 1991. Geochemical complexities preserved in the volcanic rocks of the Zambales ophiolite, Philippines. *Journal of Geophysical Research*, **96**, 16251-16262.

EWART, A. & BRYAN, W. B. 1972. Petrography and geochemistry of the igneous rocks from Eua, Tongan Islands. *Geological Society of America Bulletin*, **83**, 3281-3298.

EWART, A., BROTHERS, R. N. & MATEEN, A. 1977. An outline of the geology and geochemistry, and the possible petrogenetic evolution of the volcanic rocks of the Tonga-Kermadec-New Zealand island arc. *Journal of Volcanology and Geothermal Research*, **2**, 205-250.

EWART, A. & HAWKESWORTH, C. J. 1987. The Pleistocene-Recent Tonga-Kermadec arc lavas: Interpretation of new isotopic and rare earth data in terms of a depleted mantle source model. *Journal of Petrology*, **28** (3), 495-530.

FALLOON, T. J. & CRAWFORD, A. J. 1991. The petrogenesis of high-calcium boninite lavas dredged from the northern Tonga ridge. *Earth and Planetary Science Letters*, **102**, 375-394.

FALVEY, D. A. 1978. Analysis of palaeomagnetic data from the New Hebrides. *Bulletin Australian Society Exploration Geopysicists*, **9**, 117-123.

FANNING, M., 1986, [Results of K-Ar determinations]: AMDEL Report G 6788/87, (unpublished; on file at Mineral Resources Department, Suva, Fiji).

FLOWER, M. F. J. & LEVINE, H. 1987. Petrogenesis of a tholeiite-boninite sequence from Ayios Mamas, Troodos ophiolite: Evidence for splitting of a volcanic arc. *Contributions to Mineralogy and Petrology,* **97**, 509-524.

FOLEY, S. F., VENTURELLI, G., GREEN, D. H. & TOSCANI, L. 1987. The ultrapotassic rocks: characteristics, classification and constraints for petrogenetic models. *Earth and Planetary Science Letters*, **24**, 81-124.

FRYER, P., TAYLOR, B., LANGMUIR, C. H. & HOCHSTAEDER, A. G. 1990. Petrology and geochemistry of lavas from the Sumisu and Torishima backarc rifts. *Earth and Planetary Science Letters*, **100**, 161-178.

GILL, J. B. 1976. Composition and age of Lau Basin and Ridge volcanic rocks: implications for evolution of an interarc basin and remnant arc. *Bulletin of the Geological Society of America*, **87**, 1384-1395.

GILL, J. B. 1981. *Orogenic andesites and plate tectonics.* New York, Springer-Verlag.

GILL, J. B. 1984. Sr-Pb-Nb isotopic evidence that both MORB and OIB sources contribute to oceanic island arc magmas in Fiji. *Earth and Planetary Science Letters*, **68**, 443-458.

GILL, J. B. 1987. Early geochemical evolution of an oceanic island arc and backarc: Fiji and the South Fiji Basin. *Journal of Geology,* **95**, 589-615.

GILL, J. B. 1992. (abs) Effects of rifting on Bonin arc volcanism. *Volcanism associated with extension at consuming plate margins*. Conference abstracts.

GILL, J. B. & STORK, A. L. 1979. Miocene low-K dacites and trondhjemites of Fiji. *In*: BARKER, F. (ed) *Trondhjemites, dacites and related rocks*, Elsevier, Amsterdam.

GILL, J. B. & WHELAN, P. 1989. Post subduction ocean island alkali basalts in Fiji. *Journal of Geophysical Research*, **94**, 4579-4588.

GOVINDARAJU, K. 1989. Compilation of working values and sample description for 272 geostandards. *Geostandards newsletter*, **13**, 1-113.

GREEN, D. H., FALLOON, T. J. & TAYLOR, W. R. 1987. Mantle derived magmas - role of variable source peridotite and variable fluid C-H-O fluid compositions. *In*: MYSON,

B. O. (ed) *Magmatic processes: Physiochemical principles*. Geochemical Society Special Publication, **1**, 139-154.

HARLAND, W. B., ARMSTRONG, R., COX, A., CRAIG, L., SMITH, A. & SMITH, D. 1990. *A geologic time scale 1989*, Cambridge University Press.

HATHWAY, B. 1988. *The Eocene to Miocene Geology of southwest Viti Levu, Fiji.* PhD thesis, Oxford Polytechnic (unpublished).

HATHWAY, B., 1990. New stratigraphic units for southwestern Viti Levu. *In*: RAHIMAN, A. *Mineral Resources Department Report for 1988. Parliament of Fiji, Parliamentary Paper for 1990.*

HATHWAY, B. 1992. Definition of formations in southwestern Viti Levu. *In*: RAHIMAN, A. *Mineral Resources Department: report for the year 1988.* [ISSN 0252-2462] Paper 15 of 1991, 83-89.

HATHWAY, B. 1993. The Nadi Basin: Neogene strike-slip faulting and sedimentation in a fragmented arc, western Viti Levu, Fiji. *Journal of the Geological Society, London*, **150**, 563-581.

HATHWAY, B. in press a. Geology of the Nadi area (1:50 000 map). Fiji Mineral Resources Department.

HATHWAY, B. in press b. Sedimentation and volcanism in an Oligocene-Miocene intraoceanic arc and forearc, southwestern Viti Levu, Fiji. *Journal of the Geological Society, London.*

HATHWAY, B. & COLLEY, H. (in press). Eocene to Miocene geology of southwest Viti Levu. *In:* BALLANCE, P. F., HERZER, R. H. & STEVENSON, A. J. (eds) Geology and offshore resources of Pacific island arcs - Tonga Region II. *Circum Pacific Council Energy Mineral Resources. Earth Science Series.*

HAWKESWORTH, C. J. 1982. Isotopic characteristics of magmas erupted along destructive plate margins. *In*: THORPE, R. S. (ed) *Andesites*, 549-571. Wiley, Chichester.

HAWKINS, J. W. 1976. Petrology and geochemistry of basaltic rocks of the Lau Basin. *Earth and Planetary Science Letters*, **28**, 283-297.

HAWKINS, J. W., BLOOMER, S. H., EVANS, C. A. & MELCHIOR, J. T. 1984. Evolution of intra-oceanic arc-trench systems. *Tectonophysics*, **102**, 175-205.

HERGT, J. M. & NILSSON, K. (in press). Major, trace element and isotope (Pb, Sr and Nd) variations in Site 834 basalts: implications for the initiation of back-arc opening. *Proc. ODP, Sci. Results*, **131**: College Station, TX (Ocean Drilling Program).

HERZER, R. H. & EXON, N. F. 1985. Structure and basin analysis of the southern Tonga forearc. *In*: SCHOLL, D. W. & VALLIER, T. L. (eds) Geology and offshore resources of Pacific island arcs - Tonga region. *Circum-Pacific Council for Energy and Mineral Resources, Earth Science Series*, **2**, 55-74.

HICKEY-VARGAS, R. 1992. A refractory HIMU component in the sources of island-arc magma. *Nature*, **360**, 57-59.

HICKEY, R. L. & FREY, F. A. 1982. Geochemical characteristics of boninite series volcanics: implications for their source. *Geochimica et Cosmochimica Acta*, **46**, 2099-2115.

HOCHSTAEDTER, A. G., GILL, J. B. & MORRIS, J. D. 1990. Volcanism in the Sumisu Rift, II. Subduction and non-subduction related components. *Earth and Planetary Science Letters*, **100**, 195-209.

HOFFMEISTER, J. E., 1932. Geology of Eua, Tonga. Honolulu, *Bernice P. Bishop Museum Bulletin*, **96**, 1-93.

HOUTZ, R. E. 1959. Regional geology of Lomawai-Momi. *Fiji Geological Survey Bulletin*, **3**.

HOUTZ, R. E. 1960. Geology of Sigatoka area. *Fiji Geological Survey Bulletin*, **6**.

HUMPHRIES, S. E., MORRISON, M. A., & THOMPSON, R. N. 1978. Influence of rock crystallisation history upon subsequent lanthanide mobility during hydrothermal alteration of basalts. *Chemical Geology*, **23**, 125-137.

IRVING, T. N. 1976. Chromite crystallisation in the join Mg_2SiO_4-$CaMgSi_2O_6$-$CaAl_2Si_2O_8$-$MgCr_2O_4$-SiO_2. *Carnegie Institute Washington Yearbook*, **76**, 465-472.

JAKES, P. & GILL, J.B. 1970. Rare earth elements and the island arc tholeiite series. *Earth and Planetary Science Letters*, **9**, 17-28.

KARIG, D. E. 1971. Origin and development of marginal basins in the Western Pacific. *Journal of Geophysical Research*, **76**, 2542-2561.

KARIG, D. E. 1974. Evolution of arc systems in the western Pacific. *Annual Review of Earth and Planetary Sciences*, **2**, 51-75.

KAY, S. M. & KAY, R. W. 1982. Tectonic controls on tholeiitic and calc-alkaline magmatism in the Aleutian arc. *Journal of Geophysical Research.* **87**, 4051-4072.

KERR, A. C. 1993. elemental evidence for a small-fraction-melt input into Tertiary Mull basalts, Western Scotland. *Journal of the Geological Society of London*, **150**, 763-769.

KIMBALL, K. L. 1990. Effects of hydrothermal alteration on the compositions of chromian spinels. *Contributions to Mineralogy and Petrology*, **105**, 337-346.

KLEIN, E. M. & LANGMUIR, C. H. 1987. Global correlation of ocean ridge basalt chemistry with axial depth and crustal thickness. *Journal of Geophysical Research.* **92**, 8089-8115.

KOSTOPOULOS, D. K. 1991. Melting of the shallow upper mantle: a new perspective. *Journal of Petrology*, **32**, 671-699.

KOSTOPOULOS, D. K. & JAMES S.D. 1992. Parameterization of the melting regime of the shallow upper mantle and the effects of variable lithospheric stretching on mantle modal stratification and trace-element concentrations in magmas. *Journal of Petrology*, **33**, 665-691.

KOSTOPOULOS, D. K. & MURTON, B. J. 1992. Origin and distribution of components in boninite genesis: significance of the OIB component. *In*: PARSON, L. M., MURTON, B. J. & BROWNING, P. (eds) 1992. *Ophiolites and their modern oceanic analogues.* Geological Society London Special Publication, **60**, 133-154.

KROENKE, L. W. 1984. Cenozoic tectonic development of the southwest Pacific. *UN ESCAP, CCOP/SOPAC*, Technical Bulletin **6**.

KROENKE, L. W. & TONGILAVA, S. L. 1975. A structural interpretation of two reflection profiles across the Tonga Arc. UN ESCAP, *CCOP/SOPAC South Pacific Marine Geological Notes*, **1** (2), 1-15.

KUDO, A. M. & WEILL, D. F. 1970. An igneous plagioclase thermometer. *Contributions to Mineralogy and Petrology*, **25**, 52-65.

KUSHIRO, I. 1969. The system forsterite-diopside-silica with and without water at high pressures. *American Journal of Science*, **267-A**, 269-294.

LAPIERRE, H., TAYLOR, R. N., ROUER, O. & CHAISEMARTIN, H. 1992. Mineral chemistry of forearc volcanic rocks from the Izu-Bonin Arc, holes 792E and 793B. *In*: TAYLOR, B., FUJIOKA, K., et al., *Proc. ODP, Sci. Results*, **126**: College Station, TX (Ocean Drilling Program), 431-447.

LOWE, D. J. & GUNN, J. 1986. Caves and limestones of the islands of Tongatapu and 'Eua, Kingdom of Tonga. *Cave Science*, **13**, 105-130.

MALAHOFF, A., HAMMOND, S. R., NAUGHTON, J. J., KEELING, D. L. & RICHMOND R. N. 1982. Geophysical evidence for post-Miocene rotation of the island of Viti Levu, Fiji, and its relationship to the tectonic development of the North Fiji Basin. *Earth and Planetary Science Letters*, **57**, 398-414.

MANDL, G. 1987. Tectonic deformation by rotating parallel faults: the "bookshelf mechanism". *Tectonophysics*, **141**, 277-316.

MARUYAMA, S. & KURAMOTO, T. 1981. Geology of Oto-jima, Ani-jima and Chichi-jima. *Bulletin of the Volcanological society of Japan Annual Meeting*, **26**, 146. (In Japanese).

MAURY, R. C., DEFANT, M. J. & JORON, J-L. 1992. Metasomatism of the sub-arc mantle inferred from trace elements in Philippine xenoliths. *Nature*, **360**, 661-663.

MCCULLOCH, M. T. & GAMBLE, J. A. 1991. Geochemical and geodynamical constraints on subduction zone magmatism. *Earth and Planetary Science Letters*, **102**, 358-374.

MCDOUGALL, I. 1963. Potassium-argon ages of some rocks from Viti Levu, Fiji. *Nature*, **198**, 677.

MCKENZIE, D.1984. The generation and compaction of partially molten rock. *Journal of Petrology*, **25**, 713-765.

MENZIES, M. A., PALACZ, Z., HUNTER, R. H., UPTON, B. G. J., ASPEN, P. & HAWKESWORTH, C. J. 1987. Evidence from mantle xenoliths for an enriched lithospheric keel under the Outer Hebrides. *Nature*, **325**, 44-47.

MERZBACHER, C. & EGGLER, D. H. 1984. A magmatic geohygrometer: Application to Mount St. Helens and other dacitic magmas. *Geology*, **12**, 587-590.

METAL MINING AGENCY OF JAPAN. Report on the Cooperative Mineral Exploration, Viti Levu area, the Republic of Fiji. Phase II. February 1992.

MITCHELL, J. G. & INESON P. R. 1988. Models of single-stage concomitant potassium-argon exchange: an interpretation of discordant whole rock K-Ar data from hydrothermally altered igneous rocks of the South Pennine Orefield, U.K. *Earth and Planetary Science Letters*, **88**, 69-81.

MITCHELL, J. G., PEATE, D. W., MURTON, B. J., PEARCE, J. A., ARCULUS R. J. & VAN DER LAAN, S.R. 1992. K-Ar dating of samples from sites 782 and 786 (Leg 125): The Izu-Bonin forearc region. *In*: FRYER, P., PEARCE, J. A., STOCKING, L. B., et al. *Proc. ODP, Sci. Results*, **125**, College Station, TX (Ocean Drilling Program), 203-210.

MIYASHIRO, A. 1974. Volcanic rock series in island arcs and active continental margins. *American Journal of Science*, **274**, 321-355.

MORIMOTO, M. 1988. The nomenclature of pyroxenes. *Mineralogical Magazine*, **52**, 535-550.

MORRIS, J. D. & HART, S. R. 1983. Isotopic and incompatible element constraints on the genesis of island arc volcanics from Cold Bay and Amak island, Aleutians, and implications for mantle structure. *Geochimica et Cosmochimica Acta*, **47**, 2015-2030.

MURTON, B. J., PEATE, D. W., ARCULUS, R. J. PEARCE, J. A. & VAN DER LAAN, S. 1992. Trace-element geochemistry of volcanic rocks from Site 786: the Izu-Bonin forearc. *In*: FRYER, P., PEARCE, J. A., STOCKING, L. B., et al. *Proc. ODP, Sci. Results*, **125**, College Station, TX (Ocean Drilling Program), 211-236.

NATLAND, J. 1991. Mineralogy and crystallisation of oceanic basalts. *In*: FLOYD, P. (ed) *Oceanic basalts*. Blackie, London, 63-93.

NEWMAN, S. & VAN DER LAAN, S. R. 1992. Volatile contents of Izu-Bonin forearc volcanic glasses. *In*: FRYER, P., PEARCE, J. A., STOCKING, L. B., et al. *Proc. ODP, Sci. Results*, **125**, College Station, TX (Ocean Drilling Program), 131-139.

NIELSEN, R. L. 1988. A model for the simulation of combined major and trace element liquid lines of descent. *Geochimica et Cosmochimica Acta*, **52**, 27-38.

PACKHAM, G. H. & ANDREWS, J. E. 1975. Results of Leg 30 and the geologic history of South-west Pacific arc and marginal sea complex. *In*: ANDREWS, J. E., PACKHAM, G., et al. *Initial Reports of the Deep Sea Drilling Project*, **30**, Washington (U.S. Government Printing Office), 691-706.

PARKINSON, I. J. 1993. Geochemistry and petrogenesis of forearc peridotites, ODP Leg 125. PhD thesis, University of Durham, UK. Unpublished.

PEACOCK, S. M. 1990. Numerical simulation of metamorphic pressure-temperature-time paths and fluid production in subducting slabs. *Tectonics*, **9**, 1197-1211.

PEARCE, J. A. 1982. Trace element characteristics of lavas from destructive plate boundaries. *In*: Thorpe, R. S. (ed) *Orogenic andesites and related rocks*. Wiley, Chichester, 525-548.

PEARCE, J. A. 1983. Role of the sub-continental lithosphere in magma genesis at active continental margins. *In*: HAWKESWORTH, C. J. & NORRY, M. J. (eds) *Continental basalts and mantle xenoliths*: Nantwich (Shiva), 230-249.

PEARCE, J. A., THIRLWALL, M. F., INGRAM, G., MURTON, B. J., & VAN DER LAAN, S. R. 1992a. Isotopic evidence for the origin of boninites and related rocks drilled in the Izu-Bonin (Ogasawara) forearc, Leg 125. *In*: FRYER, P., PEARCE, J. A., STOCKING, L. B., et al. *Proc. ODP, Sci. Results*, **125**, College Station, TX (Ocean Drilling Program), 237-261.

PEARCE, J. A., VAN DER LAAN, S.R., ARCULUS, R. J., MURTON, B. J., ISHII, T., PEATE, D. W. & PARKINSON, I. J. 1992b. Boninite and harzburgite from Leg 125 (Bonin-Mariana forearc): A case study of magma genesis during the initial stages of subduction. *In*: FRYER, P., PEARCE, J. A., STOCKING, L. B., et al. *Proc. ODP, Sci. Results*, **125**, College Station, TX (Ocean Drilling Program), 623-659.

PEARCE, J. A. & PARKINSON, I. J. in press. Trace element models for mantle melting: Application to volcanic arc petrogenesis. *Ian Gass Memorial Volume.*

PERFIT, M. R., GUST, D. A., BENCE, A. E. ARCULUS, R. J. & TAYLOR, S. R. 1980. Chemical characteristics of island-arc basalts: implications for mantle sources. *Chemical Geology*, **30**, 227-256.

PLANK, T. & LANGMUIR, C. H. 1988. An evaluation of the global variations in the major element chemistry of arc basalts. *Earth and Planetary Science Letters*, **90**, 349-370.

PRICE, R. C., JOHNSON, L. E. & CRAWFORD, A. J. 1990. Basalts of the North Fiji Basin: The generation of backarc basin magmas by mixing of depleted and enriched mantle sources. *Earth and Planetary Science Letters*, **105**, 106-121.

RAO, B. in press. Revised geology of the Lautoka area. *Fiji Mineral Resources Department Bulletin*, **5**.

RAUTENSCHLEIN, M. 1987. The geochemistry of volcanic glasses from the Akaki Canyon, Troodos ophiolite, Cyprus. PhD thesis, University of Mainz, Germany. Unpublished.

REAGAN, M. K. & MEIJER, A. 1984. Geology and geochemistry of early arc-volcanic rocks from Guam. *Geological Society of America Bulletin*, **95**, 701-713.

REAGAN, M. K. & GILL, J. B. 1989. Coexisting calkalkaline and high-niobium basalts from Turriabala volcano, Costa Rica: implications for residual titanates in arc magma sources. *Journal of Geophysical Research*, **94**, 4619-4633.

RODDA, P. 1983. Fiji radiometric dates recalculated. Fiji Mineral Resources Department note. Unpublished, on file at Fiji Mineral Resources Department, Suva, Fiji.

RODDA, P. & BAND, R. B. 1967. Geology of Viti Levu: *Legislative Council, Fiji.* Council Paper 1967 **35**, 8-16.

ROGERS, N. W. 1992. Potassic magmatism as a key to understanding trace-element enrichment processes in the upper mantle. *Journal of Volcanology and Geothermal Research*, **50**, 85-99.

RYERSON, F. J. & WATSON, E. B. 1987. Rutile saturation in magmas: implications for Ti-Nb-Ta depletion in island arc basalts. *Earth and Planetary Science Letters*, **86**, 225-239.

SCOTT, D. R. & STEVENSON, D. J. 1989. A self-consistent model of melting, magma migration and bouyancy driven circulation beneath mid-ocean ridges. *Journal of Geophysical Research*, **94**, 2973-2988.

SHAW, D. M. 1970. Trace element fractionation during anatexis. *Geochimica et Cosmochimica Acta*, **34**, 237-242.

SHAW, D. M. 1977. Trace element melting models. *Physics and Chemistry of the Earth*, **11**, 577-587.

SIGURDSON, H. & SCHILLING, J. G. 1976. Spinels in Mid-Atlantic Ridge basalts: chemistry and occurrence. *Earth and Planetary Science Letters*, **29**, 7-20.

SINTON, J. M. & FRYER, P. 1987. Mariana trough lavas from 18°N: Implications for the origin of backarc basin basalts. *Journal of Geophysical Research*, **94**, 4697-4707.

STAUDIGEL, H., HART, S. R. & RICHARDSON, S. H. 1981. Alteration of the oceanic crust: processes and timing. *Earth and Planetary Science Letters,* **52,** 311-327.

STERN, R. J., BLOOMER, S. H., PING-NAN LIN & SMOOT, N. C. 1989. Submarine arc volcanism in the southern Mariana arc as an ophiolite analogue. *Tectonophysics,* **168,** 151-170.

STERN, R. J., PING-NAN LIN, MORRIS, J. D., JACKSON, M. C., FRYER, P., BLOOMER, S. H. & ITO, E. 1990. Enriched back-arc basin basalts from the northern Mariana trough: implications for the magmatic evolution of back-arc basins. *Earth and Planetary Science Letters,* **100,** 210-225.

STERN, R. J., MORRIS, J. D., BLOOMER, S. H., & HAWKINS, J. W. 1991. The source of the subduction component in convergent margin magmas: Trace element and radiogenic isotope evidence from Eocene boninites, Mariana forearc. *Geochimica et Cosmochimica Acta,* **55,** 1467-1481.

STERN, R. J. & BLOOMER, S. H. 1992. Subduction-zone infancy: Examples from the Eocene Izu-Bonin-Mariana and Jurassic California arcs. *Geological Society of American Bulletin,* **104,** 1621-1636.

STEARNS, H. T. 1971. Geological Setting of an Eocene fossil deposit on 'Eua Island, Tonga. *Geological Society of American Bulletin,* **82,** 2541-2552.

STOREY, M., SAUNDERS, A. D., TARNEY, J., LEAT, P., THIRLWALL, M. F., THOMPSON, R. N., MENZIES, M. A. & MARRINER, G. F. 1988. Geochemical evidence for plume-mantle interactions beneath Kerguelan and Heard islands, Indian Ocean. *Nature,* **336,** 371-374.

SUN, S. S. & MCDONOUGH, W. F. 1989. Chemical and isotopic systematics of ocean basalts: implications for mantle composition and processes. *In*: SAUNDERS, A. D. & NORRY, M. J. (eds) *Magmatism in the Ocean Basins.* Geological Society, London, Special Publications, **42,** 313-345.

SUN, S. S. & NESBITT, R. W. 1978. Geochemical regularities and genetic significance of ophiolitic basalts. *Geology,* **6,** 689-693.

TAPPIN, D. R. (in press). The Tonga forearc basin. *In:* BALLANCE, P. F., HERZER, R. H. & STEVENSON, A. J. (eds) Geology and offshore resources of Pacific island arcs - Tonga Region II. *Circum Pacific Council for Energy and Mineral Resources. Earth Science Series.*

TAPPIN, D. R., & BALLANCE, P. F. (in press). Contributions to the sedimentary geology of 'Eua island, Kingdom of Tonga: reworking in an oceanic forearc. *In:* BALLANCE, P. F., HERZER, R. H. & STEVENSON, A. J. (eds) Geology and offshore resources of Pacific island arcs - Tonga Region II. *Circum Pacific Council for Energy and Mineral Resources. Earth Science Series.*

TATSUMI, Y. 1986. Formation of the volcanic front in subduction zones. *Geophysical Research Letters*, **13**, 717-720.

TATSUMI, Y. 1989. Migration of fluid phases and genesis of basalt magmas in subduction zones. *Journal of Geophysical Research,* **94**, 4697-4707.

TATSUMI, Y., HAMILTON, D. L. & NESBITT, R. W. 1986. Chemical characteristics of fluid phase released from a subducted lithosphere and origin of arc magmas: evidence form high-pressure experiments and natural rocks. *Journal of Volcanology and Geothermal Research*, **29**, 293-309.

TAYLOR, B. 1992. Rifting and tectonic evolution of the Izu-Bonin-Mariana arc. *In*: TAYLOR, B., FUJIOKA, K., et al., *Proc. ODP, Sci. Results*, **126**: College Station, TX (Ocean Drilling Program), 627-652.

TAYLOR, R. N. 1990. Geochemical stratigraphy of the Troodos extrusive sequence: Temporal developments of a spreading centre magma chamber. *In*: MALPAS, J., MOORES, E. M., PANAYIOTOU, A. & XENOPHONTOS, C. (eds) *Ophiolites: Oceanic crustal analogues*. The Geological Survey Department, Ministry of Agriculture and Natural Resources, Nicosia, Cyprus.

TAYLOR, R. N. & NESBITT, R. W. 1988. Light rare-earth enrichment of supra-subduction zone mantle: evidence from the Troodos ophiolite, Cyprus. *Geology*, **16**, 448-451.

TAYLOR, R. N., LAPIERRE, H., VIDAL, P., NESBITT, R.W. & CROUDACE, I. W. 1992. Igneous geochemistry and petrogenesis of the Izu-Bonin forearc basin. *In*: TAYLOR, B., FUJIOKA, K., et al., *Proc. ODP, Sci. Results*, **126**: College Station, TX (Ocean Drilling Program), 405-430.

THOMPSON, G. 1991. Metamorphic and hydrothermal processes: basalt-seawater interaction. *In*: FLOYD, P. (ed) *Oceanic basalts*. Blackie, London, 148-173.

THY, P. & XENOPHONTOS, C. 1991. Crystallisation orders and phase chemistry of glassy lavas from the pillow sequences, Troodos ophiolite, Cyprus. *Journal of Petrology*, **32**, 403-428.

TURNER, J. S. & CAMPBELL, I. H. 1986. Convection and mixing in magma chambers. *Earth Science Reviews*, **23**, 255-332.

UMINO, S. 1985. Volcanic geology of Chichi-jima, the Bonin Islands (Ogasawara Islands). *Journal of the Geological Society of Japan*, **91**, 505-523).

UMINO, S. 1986. Magma mixing in boninite sequence of Chichi-jima, Bonin Islands. *Journal of Volcanology and Geothermal Research*, **29**, 125-157.

VALSAMI, E. & CANN, J. 1992. Mobility of rare-earth elements in zones of intense hydrothermal alteration in the Pindos ophiolite, Greece. *In*: PARSON, L. M., MURTON, B. J. & BROWNING, P. (eds) 1992. *Ophiolites and their modern oceanic analogues*. Geological Society London Special Publication, **60**, 219-232.

VAN DER LAAN, S. R., FLOWER, M. F. J. & KOSTER VAN GROSS, A. F. 1989. Experimental evidence for the origin of boninites: Near liquidus phase relations to 7.5kbar. *In*: Crawford, A. J. (ed) *Boninites*. Unwin-Hyman, London. 112-147.

VAN DER LAAN, S. R., ARCULUS, R. J., PEARCE, J. A. & MURTON, B. J. 1992. Petrography, mineral chemistry, and phase relations of the basement boninite series of Site 786, Izu-Bonin forearc. *In*: FRYER, P., PEARCE, J. A., STOCKING, L. B., et al. *Proc. ODP, Sci. Results*, **125**, College Station, TX (Ocean Drilling Program), 171-201.

WEBB. 1990, [Results of K-Ar determinations]: AMDEL Report (unpublished; on file at Mineral Resources Department, Suva, Fiji).

WEISSEL, J. K. & WATTS, A. B. 1977. Tectonic complexities in the South Fiji Marginal Basin. *Earth and Planetary Science Letters*, **28**, 121-126.

WEISSEL, J. K., WATTS, A. B., & LAPOUILLE A. 1982. Magnetic anomaly evidence for late Paleocene to late Eocene seafloor in the southern New Hebrides Basin. *Tectonophysics*, **87**, 243-251.

WHARTON, M. R., HATHWAY, B. & COLLEY, H. C. in press. Volcanism associated with extension in an Oligocene-Miocene arc, southwestern Viti Levu, Fiji. *Journal of the Geological Society, London.*

WHELAN, P. M., GILL, J. B., KOLLMAN, E., DUNCAN, R. A. & DRAKE R.E. 1985. Radiometric dating of magmatic stages in Fiji. *In*: SCHOLL D. W. & VALLIER T. L. (eds) Geology and offshore resources of Pacific island arcs - Tonga region. *Circum-Pacific Council for Energy and Mineral Resources, Earth Science Series*, **2**, 415-441.

WILLIAMS, R. W. & GILL, J. B. 1988. Effects of partial melting on the U decay-series. *Geochimica et Cosmochimica Acta*, **53**, 1607-1619.

WINKLER, H. 1979. *The petrogenesis of metamorphic rocks*. Springer-Verlag, New York

WOODHEAD, J. D. 1989. Geochemistry of the Mariana arc (western Pacific): Source composition and processes. *Chemical Geology*, **76**, 1-24.

WOODHEAD, J. D., EGGINS, S. & GAMBLE, J. 1993. High field strength and transition element systematics in island arc and back-arc basin basalts: Evidence for multi-phase melt extraction and a depleted mantle wedge. *Earth and Planetary Science Letters*, **114**, 491-504.

APPENDIX 1

Analytical geochemistry

A1.1 Powdered sample preparation

Bulk-rock samples of between 0.5-1kg were first cleaned with water and a bristle brush to remove soil and loose weathered material. Further weathered material was trimmed from the samples using a stainless steel splitting edge linked to a hydraulic press. This process was repeated until the sample was reduced to blocks of rock approximately $3cm^3$ which were again washed and then dried with paper towels. At this stage samples that were extensively cut by secondary veins were further trimmed or diamond-sawn to exclude the vein material. The blocks of rock were then crushed using a Fritsch Pulverisette jaw crusher (type 01-704). Special care was taken in the cleaning of the apparatus prior to crushing in order to avoid contamination from the powders of other users. Crushing reduced the sample to a grit of approximately 5mm grain-size. At this stage, a second screening procedure was performed. Visible highly-altered particles of grit were hand-picked under a binocular microscope to produce a 'cleaner' sample. The resulting grit was washed and dried again and then coned and quartered to produce a representative sub-aliquot of material for grinding. Grinding was performed in an agate grinding-mill which was run for about 30 minutes to produce a fine powder which was bagged, labelled and stored in dry conditions.

A1.2 XRF analysis

Fusion discs for major element oxide analysis were prepared by mixing a 1:5 mixture of sample and dried, lithium tetraborate flux (Spectroflux 100B). The mixture was extensively agitated with a glass rod and heated in a furnace to 1050°C for 20 minutes. The molten glass was then poured into moulds on a hot-plate set at 250°C before being quenched using a stainless steel plunger. The discs were allowed to cool and bagged and stored in a desiccator prior to analysis.

Pressed powder pellets for trace element analysis were prepared by measuring out about 6g of dry, powdered sample and adding between 6 and 12 drops of Mowiol binding

agent. The powder and binder were mixed and then compressed for 20 seconds at 10-15 bars before being dried in an oven at 100°C prior to analysis.

XRF analysis was carried out on a Philips PW 1500 spectrometer with a Rhodium anode tube. A full range of international standards from across the compositional range were run as calibration standards. An internal monitor was run over the full study period to monitor between-run variations and machine drift. Estimates of analytical accuracy and precision were made by repeated analysis of international reference standards (Table A1.1) and also internal standards (Table A1.2) which were run as unknowns outside of the machine calibration. Details of the errors are summarised in 2 sigma form and recommended values for the standards from Govindaraju (1989) are shown for comparison. Fig. A1.1 illustrates comparison plots for the Yavuna Group XRF and ICP-MS data obtained at Durham. Correlation coefficients for these data range from 0.98 to 1.00 indicating the good reproducibility of the two techniques.

Loss-on-ignition values were determined by heating a 2g powder aliquot of the sample in a porcelain crucible at 900°C for two hours.

A1.3 ICP-MS analysis

A sub-set of trace elements was analysed by inductively-coupled-plasma-mass-spectrometry on a VG elemental Plasma quad machine at the University of Durham Industrial Research Laboratories (UDIRL). A powder aliquot of 0.1±0.001g was weighed out and digested with 4ml of 48% hydrofluoric acid and 1ml of nitric acid in a Savillex bomb for 24 hours. The samples were evaporated to dryness to effect quantitative removal of the hydrofluoric acid and form nitrate salts. The samples were then redissolved with 20ml of deionised water and 2.5ml of nitric acid and boiled for one hour. The solutions were allowed to cool and spiked with 1.25ml of a 2ppm Rh, Re and Bi spike solution and made up accurately to 50ml with deionised water. Detection limits for all elements are typically 0.01-0.02ppm (at 3 s of background) except for Zr, Nd, Sm, Gd (0.05ppm) and Ba, La and Pb (0.1-0.2ppm). Precision typically ranges from 15% at less than 10x detection limit, to about 3% at 100x detection limit (Murton et al. 1992). Significant problems involving Ta analysis were encountered during ICP-MS runs. This Ta-contamination was found to be a machine memory effect that resulted from the running of other worker's samples that had been crushed using tungsten carbide equipment. The consequent high detection limit for Ta during these runs means that the Ta data for some samples has no petrogenetic significance. The affected samples are denoted *n.d.* in the dataset.

International standards run as unknowns outside the calibration

	BOB-1			DNC-1			G-2		
	rec	n=7 av	2.s.d.	rec	n=8 av	2.s.d	rec	n=7 av	2.s.d.
SiO2	50.84	51.00	0.22	47.07	47.33	0.12	69.08	69.45	0.05
Al2O3	16.75	15.58	0.13	18.30	18.44	0.18	15.38	15.34	0.06
TiO2	1.29	1.32	0.00	0.48	0.47	0.01	0.48	0.47	0.01
FeO*	8.72	8.74	0.16	9.15	9.85	0.17	2.53	2.62	0.02
MgO	7.66	7.74	0.08	10.05	10.35	0.29	0.75	0.81	0.01
CaO	11.35	11.10	0.06	11.27	11.29	0.05	1.96	1.92	0.02
K2O	0.36	0.36	0.00	0.23	0.23	0.00	4.48	4.42	0.02
Na2O	3.12	3.05	0.07	1.87	1.82	0.03	4.08	4.24	0.06
MnO	0.14	0.15	0.00	0.15	0.14	0.00	0.03	0.03	0.00
P2O5	0.17	0.16	0.00	0.09	0.09	0.01	0.14	0.14	0.01
Rb	5	7	1.42	5	5	0.68	170	161	1.18
Sr	194	194	1.54	145	140	2.68	478	480	7.18
Y	25	25	1.36	18	16	1.53	11	13	1.39
Zr	101	104	1.36	41	40	1.47	309	294	2.63
Nb	4	8	1.07	3	5	1.54	12	11	1.09
Cr	280	297	3.46	285	277	4.97	9	9	4.58
Ni	113	110	6.96	247	237	9.29	5	14	8.93
V	240	233	6.35	148	146	4.45	36	36	6.27
Zn	n.a.	64	6.01	66	64	5.66	86	86	4.18
Cu	n.a.	61	6.79	96	85	10.12	11	8	9.38
Ga	17	15	4.19	15	11	4.89	23	21	3.05
Sc	32	37	4.22	31	29	4.78	4	3	2.39
Co	n.a.	47	1.33	55	53	2.67	5	2	0.65

	T-1		
	rec	n=6 av	2.s.d.
SiO2	62.70	63.49	0.07
Al2O3	16.69	15.74	0.09
TiO2	0.58	0.55	0.00
FeO*	5.69	5.72	0.07
MgO	1.89	2.13	0.03
CaO	5.08	4.99	0.01
K2O	1.24	1.24	0.00
Na2O	4.39	4.50	0.02
MnO	0.10	0.10	0.00
P2O5	0.14	0.16	0.00
Rb	32	29	1.73
Sr	390	377	3.63
Y	n.a.	19	0.76
Zr	150	148	2.53
Nb	n.a.	15	0.94
Cr	20	26	2.01
Ni	10	21	5.84
V	96	81	8.56
Zn	180	184	9.51
Cu	48	45	4.86
Ga	20	18	3.71
Sc	n.a.	13	2.93
Co	13	18	1.44

Table A1.1 International standards run as unknowns outside of the XRF machine calibration. Recommended values (rec) are taken from Govindaraju (1989) and the compilation of J. A. Pearce (BOB-1, personal communication, 1990).

Internal standards run as unknowns outside the calibration

	BH092		BOB-1		QUBS5		G-1	
	n=6 av	2.s.d.	n=3 av	2.s.d.	n=3 av	2.s.d.	n=3 av	2.s.d.
SiO2	47.64	0.47	50.92	0.08	58.41	0.23	72.89	0.33
TiO2	1.16	0.01	1.28	0.00	1.00	0.01	0.26	0.00
Al2O3	14.61	0.29	16.67	0.09	15.94	0.06	14.30	0.05
FeO*	15.11	0.11	8.68	0.03	6.39	0.12	1.99	0.11
MnO	0.18	0.00	0.15	0.01	0.11	0.00	0.03	0.01
CaO	10.63	0.07	11.19	0.02	5.44	0.02	1.35	0.02
MgO	5.82	0.07	7.61	0.08	4.77	0.06	0.40	0.01
Na2O	4.00	0.09	3.19	0.00	4.26	0.29	3.42	0.08
K2O	0.12	0.01	0.39	0.01	3.37	0.01	5.52	0.02
P2O5	0.13	0.01	0.16	0.01	0.47	0.02	0.08	0.01
Total	99.42		100.27		100.39		100.37	

	E-4		VL015	
	n=16 av	2 s.d.	n=11 av	2 s.d.
Rb	2	1.43	15	3.51
Sr	108	1.70	224	5.26
Y	23	1.56	20	2.67
Zr	46	1.38	68	4.23
Nb	4	1.17	4	1.14
Cr	83	4.49	141	15.71
Ni	33	8.41	183	25.18
V	331	9.65	190	15.63
Zn	98	4.19	54	8.24
Cu	5	7.77	150	15.00
Ga	16	3.72	15	9.08
Sc	38	2.98	25	6.63
Co	49	1.50	43	3.27

Table A1.2 Internal standards run as unknowns outside of the XRF machine calibration.

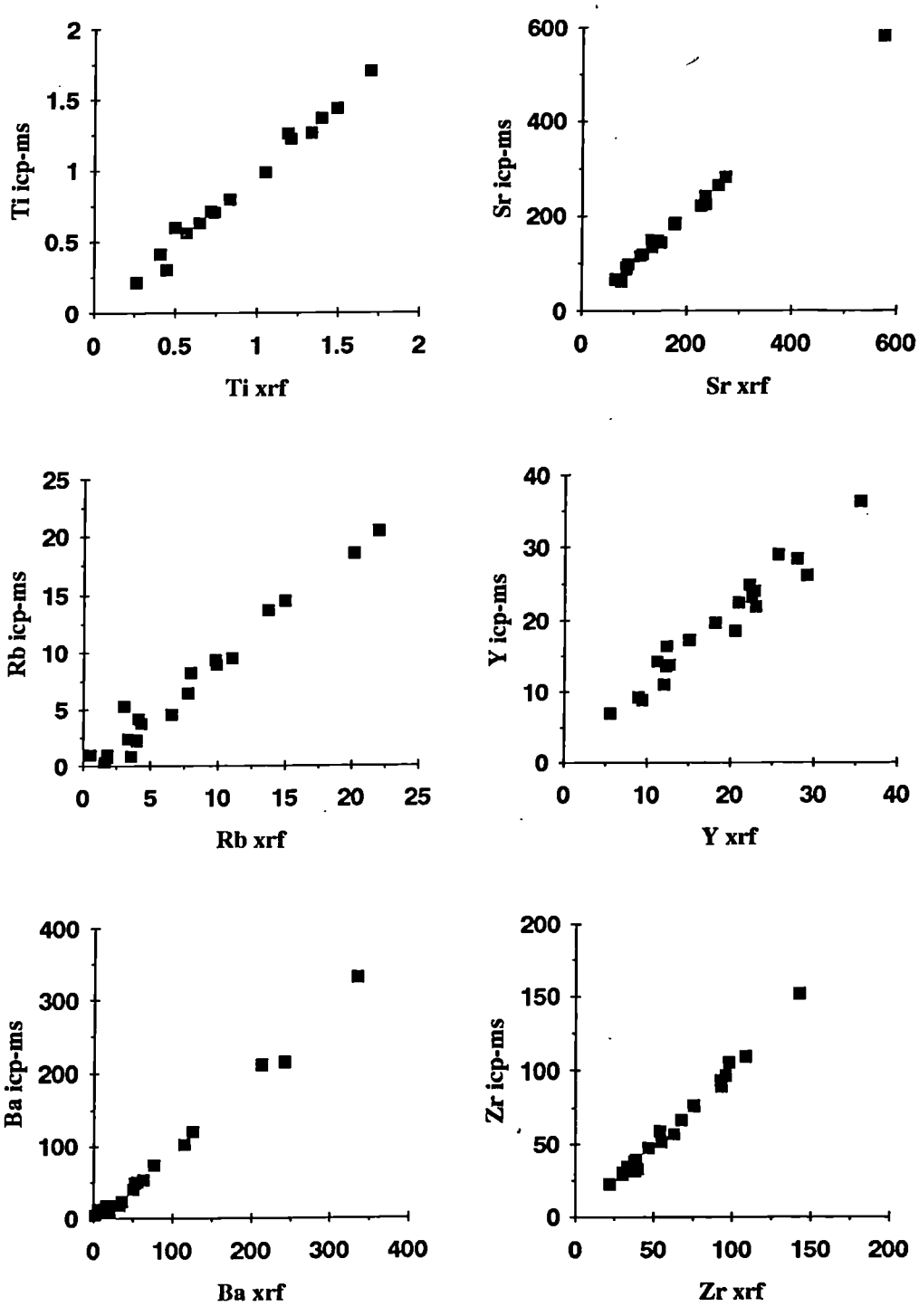

Fig. A1.1 Plots to illustrate comparison between data obtained using the XRF and ICP-MS analytical techniques at Durham.

A1.4 Electron microprobe analysis

Polished thin-sections prepared by G. Randall at the University of Durham were carbon-coated at Durham and stored in a desiccator. Analyses were performed at the University of Manchester on a modified Cambridge Instruments Geoscan Microprobe fitted with Energy Dispersive Spectrometers (EDS) and Wavelength Dispersive Spectrometers (WDS). The most important difference in the techniques with regard to this study is poor peak resolution obtained using EDS when analysing for the trace elements Ti and Na. However, EDS provides a much more rapid facility for multi-element oxide analysis and consequently most of the data was collected using EDS. The accurate low-level Ti and Na data collected by WDS and used in chapter 4 is indicated with italic script in the dataset. The machine was operated at a beam current of 5nA with an accelerating voltage of 15kV. A 'live-time' of 100 seconds was used for each analysis and processing was carried out using a Link-290 electronic facility. Standards spectra are held on hard disc on the on-line computer. These are compared with the unknown spectra using a cobalt metal standard for the calibration of unknown element concentrations. The cobalt analysis thus corrects any long-term drift, acting as a 'monitor' sample.

A similar instrument set-up at the Royal School of Mines, Imperial College, London, was used in reconnaissance work when investigating the nature of mineral alteration. An additional combined scanning-electron-microscope (SEM) facility was available on this machine. The back-scattered electron images produced by the SEM proved useful in the selection of minerals to be analysed.

A1.5 Radiogenic isotope analysis

Isotope work was carried out in collaboration with Dr. M. Thirlwall at RHBNC, London using a VG354 five-collector mass spectrometer. Full details of analytical procedures and errors are presented by Pearce et al (1992a). Conventional ion-exchange methods were used to effect element separations. Extensive secondary alteration within the suite required that all samples were subjected to heavy leaching using 6N HCl for several hours at 180°C, followed by careful rinsing with water. Unfortunately, due to the allocation of lab-time, comparative analyses of unleached samples were not performed, and consequently the effects of alteration on Sr and Pb isotope analyses were not assessed. Nd isotope analyses are assumed to be unaffected by alteration following the discussion of element mobility in chapter 5. Pearce et al. (1992a) make an alteration-related correction for Sr and Pb isotopic ratios of ODP Leg 125 samples, based upon the assumption that alteration did not post-date significantly the eruption age. However,

in the case of southwest Viti Levu and 'Eua, the results of radiometric dating presented in chapter 2 indicate that several episodes of post-eruptive alteration have affected the samples. As each episode may in some way have affected the isotope systematics of the samples, Sr and Pb isotope results are presented in parentheses pending further investigation and are not used in the petrogenetic arguments presented in this thesis.

A1.6 XRD analysis

Clay mineral fractions were separated using conventional floatation techniques and run on a Phillips PW1130 3kW X-Ray diffractometer at Durham. Samples were pipetted into separate aliquots to check reproducibility which was found to be excellent.

APPENDIX 2

Geochemical dataset

This appendix lists the geochemical data collected during the course of study. Rare-earth element normalising values used in the thesis are taken from Boynton (1984) and MORB-normalising values are from Sun & McDonough (1989).

A2.1 XRF and ICP-MS data

All grid references describing sample localitites in the following tables refer to the Viti Levu series X754, edition 6-GSGS map sheets. Abreviations are as follows:

n.a. element not analysed using this technique
n.d. element below detection limit using this technique

In the Yavuna Group data tables,

Mass	Massive lava
Pill	Pillow lava
Micgabb	Microgabbro
Gabb	Gabbro
Clast	Pillow breccia clast

In the Wainimala Group data tables,

Dakadaka	Dakadaka Basalt
DD dyke	Dyke intruding the Dakadaka Basalt
Basic dyke	Basic dyke cutting the Yavuna Group
Nadele	Nadele Breccia
Kawa	Kawa Formation
Felsic dyke	Felsic dyke cutting the Yavuna Group
Kalaka	Kalaka Dacite

Group	I	I	II	II	II	II	II	II
Sample no.	90-25	LP143	90-51	BH096	90-79	90-65	VL90-69	VL028
Lithology	MASS	FLOAT	DYKE	DYKE	PILL	MASS	MASS	MASS
Location	Masi	Namosi	Namosi	L. Kawa	Namosi	L. Kawa	L. Kawa	Namosi
Grid reference	462256	522299	523298	679250	547289	673244	676240	527299
SiO2	44.41	50.52	52.59	52.51	54.51	61.90	56.94	57.98
TiO2	0.21	0.26	0.41	0.65	0.49	0.37	0.43	0.45
Al2O3	15.67	12.62	14.83	17.51	15.63	13.51	15.20	14.92
FeO*	10.71	8.22	7.60	8.91	8.15	5.91	7.65	6.85
MnO	0.21	0.15	0.13	0.14	0.19	0.09	0.14	0.14
CaO	23.42	12.10	9.02	4.17	8.56	6.56	5.88	8.69
MgO	5.14	15.25	9.26	10.61	5.72	6.26	7.51	3.88
Na2O	0.26	0.69	4.80	5.56	5.68	3.75	5.52	6.25
K2O	0.15	0.13	0.08	0.28	0.14	0.36	0.03	0.01
P2O5	0.04	0.03	0.06	0.07	0.03	0.09	0.06	0.06
LOI	2.95	2.42	3.89	6.76	2.08	4.84	6.74	1.85
TOTAL	100.26	99.98	98.2	100.41	99.14	98.83	99.37	99.24
Nb XRF	1	3	4	4	2	3	3	5
Zr	19	22	31	31	29	39	34	39
Y	8	6	9	9	10	10	10	11
Sr	329	86	89	152	152	254	59	66
Ga	19	14	12	12	15	17	12	13
Zn	49	60	63	71	52	43	45	27
Cu	20	16	108	92	2	647	3	28
Ni	207	283	104	101	79	124	80	46
Co	31	42	37	42	37	29	35	26
Cr	123	1034	352	462	253	230	289	169
V	167	173	214	294	285	170	190	328
Rb	3	4	2	3	2	5	3	2
Ba	19	51	33	53	26	44	26	n.a.
Sc	33	33	37	34	33	18	31	30
Ti ICP-MS		0.21	0.41	0.63				0.30
V		154.00	217.01	264.64				266.00
Cr		905.00	409.27	411.09				147.00
Ni		211.23	89.12	88.29				25.40
Rb		2.29	0.95	2.33				0.72
Sr		85.31	96.99	141.85				66.62
Y		6.95	9.19	8.78				14.19
Zr		22.00	28.77	30.31				39.13
Nb		0.40	0.40	0.51				0.69
Cs		0.12	0.01	0.02				0.00
Ba		39.39	17.20	47.67				3.87
La		1.17	2.28	2.10				4.89
Ce		2.62	5.18	5.10				7.39
Pr		0.42	0.76	0.78				1.13
Nd		1.88	3.61	3.92				5.45
Sm		0.65	1.09	1.18				1.70
Eu		0.25	0.43	0.50				0.55
Gd		0.84	1.28	1.44				1.93
Tb		0.15	0.23	0.25				0.34
Dy		1.11	1.51	1.55				2.14
Ho		0.22	0.32	0.34				0.48
Er		0.71	0.99	0.98				1.38
Tm		0.12	0.15	0.15				0.20
Yb		0.76	0.97	0.98				1.39
Lu		0.11	0.15	0.16				0.21
Hf		0.44	0.68	0.82				1.42
Ta		n.d.	0.03	0.05				0.04
Pb		0.50	0.40	0.81				1.57
Th		0.11	0.30	0.23				0.34
U		0.05	0.08	0.09				0.08

Group	II	II	II	II	II	II	II	II
Sample no.	LP121	90-21	90-66	90-23	BH097	VL021	90-62	BH093
Lithology	PILL	MASS	MASS	MASS	CLAST	MASS	MASS	CLAST
Location	Namosi	Masi	L. Kawa	Masi	Kawa	Namosi	L. Kawa	L. Kawa
Grid reference	533289	463252	673243	463258	679250	525303	680246	679245
SiO2	54.61	50.92	55.49	48.19	64.69	48.42	55.02	57.68
TiO2	0.53	0.57	0.49	0.54	0.50	0.74	0.54	0.44
Al2O3	15.90	15.76	15.78	15.00	11.99	12.51	15.14	15.96
FeO*	9.08	9.59	6.87	11.31	7.00	11.03	8.31	7.80
MnO	0.14	0.19	0.13	0.22	0.09	0.17	0.19	0.13
CaO	6.03	8.92	9.01	11.10	3.06	9.22	8.99	5.77
MgO	7.66	10.03	4.68	8.35	8.78	16.79	5.47	6.34
Na2O	5.00	3.37	5.35	2.87	2.94	0.95	5.26	5.99
K2O	0.87	0.46	0.30	0.39	0.24	0.08	0.07	0.05
P2O5	0.08	0.06	0.12	0.07	0.07	0.07	0.08	0.06
LOI	3.60	4.06	4.50	2.11	6.07	5.20	8.75	6.75
TOTAL	99.90	99.87	98.25	98.07	99.44	99.98	99.09	100.13
Nb XRF	3	4	2	1	4	5	1	4
Zr	31	38	52	32	34	40	34	47
Y	12	12	12	12	12	12	13	13
Sr	203	144	263	178	113	116	114	76
Ga	15	14	16	15	15	14	14	12
Zn	73	108	59	120	74	59	52	31
Cu	59	12	75	35	65	77	2	32
Ni	80	127	130	137	160	287	60	49
Co	43	46	34	48	34	56	37	33
Cr	201	400	301	363	486	613	193	177
V	274	255	235	249	186	259	281	219
Rb	15	8	4	3	4	8	2	3
Ba	107	64	58	62	18	36	16	6
Sc	31	36	23	44	25	34	30	30
Ti ICP-MS		0.56			0.60	0.70		n.a.
V		234.05			158.00	213.00		183.00
Cr		380.52			384.00	568.00		154.00
Ni		106.60			108.14	96.95		n.a.
Rb		6.42			3.70	8.16		5.26
Sr		146.56			114.41	117.46		61.18
Y		10.97			13.47	16.31		13.74
Zr		31.01			34.15	32.51		47.00
Nb		0.47			0.56	0.67		0.50
Cs		0.06			0.01	0.04		0.01
Ba		52.01			17.45	22.12		12.79
La		2.61			3.33	3.61		2.57
Ce		6.35			6.73	8.55		6.09
Pr		0.89			0.99	1.23		0.85
Nd		4.55			4.76	6.01		4.13
Sm		1.38			1.52	1.77		1.27
Eu		0.60			0.48	0.58		0.44
Gd		1.64			1.96	2.32		1.74
Tb		0.29			0.34	0.42		0.32
Dy		1.86			2.12	2.60		2.23
Ho		0.43			0.42	0.49		0.51
Er		1.14			1.21	1.59		1.52
Tm		0.17			0.19	0.23		0.24
Yb		1.20			1.20	1.46		1.53
Lu		0.18			0.19	0.25		0.25
Hf		0.80			0.94	1.04		0.76
Ta		0.05			0.05	0.05		0.04
Pb		0.60			0.95	0.86		0.97
Th		0.22			0.20	0.28		0.30
U		0.10			0.16	0.06		0.08

Group	II	III	III	III	III	III	III	III
Sample no.	BH439	BH402	90-52	VL019	90-64	VL031	LP132	VL022
Lithology	MASS	MASS	CLAST	PILL	DYKE	MASS	PILL	MASS
Location	Nawaka	Vunalolo	Namosi	Vatubasaga	L. Kawa	Namosi	Namosi	Namosi
Grid reference	543210	482281	543300	538265	674249	533294	538291	525303
SiO2	48.56	54.57	53.28	52.29	50.68	52.84	53.03	50.13
TiO2	0.45	0.54	0.63	0.64	0.70	0.70	0.72	0.75
Al2O3	14.25	14.64	16.77	15.30	17.84	14.67	14.75	12.68
FeO*	13.22	8.62	8.79	7.29	10.30	7.86	8.06	10.39
MnO	0.44	0.13	0.14	0.13	0.14	0.13	0.14	0.15
CaO	7.68	8.31	8.79	9.98	4.54	8.59	8.18	9.21
MgO	11.24	7.36	7.69	8.18	8.82	9.85	10.01	15.31
Na2O	2.65	3.96	4.75	3.03	4.99	3.93	4.22	1.06
K2O	0.30	0.48	0.03	2.47	0.58	0.94	0.51	0.21
P2O5	0.18	0.11	0.11	0.09	0.09	0.10	0.09	0.08
LOI	3.82	1.82	5.10	4.11	6.64	5.59	4.55	5.09
TOTAL	99.54	99.36	100.5	99.45	98.7	99.60	99.71	99.98
Nb XRF	1	4	5	3	1	5	5	4
Zr	31	52	49	55	35	54	54	42
Y	15	16	15	14	16	15	15	15
Sr	122	193	108	203	184	178	65	159
Ga	15	13	16	16	18	10	13	15
Zn	151	76	70	55	77	60	64	61
Cu	4	72	22	58	9	35	59	118
Ni	194	102	146	123	36	213	178	279
Co	59	40	42	32	47	38	40	53
Cr	670	520	483	418	132	532	457	627
V	211	202	283	283	355	209	207	251
Rb	4	8	2	18	7	10	7	5
Ba	49	121	30	220	52	116	56	103
Sc	48	33	37	24	37	29	28	31
Ti ICP-MS						n.a.	0.71	
V						187.00	201.00	
Cr						480.00	409.00	
Ni						n.a.	131.00	
Rb						9.31	4.52	
Sr						183.78	64.83	
Y						17.18	17.19	
Zr						58.86	58.47	
Nb						0.83	0.83	
Cs						0.01	0.06	
Ba						102.03	49.38	
La						6.61	5.29	
Ce						11.31	13.25	
Pr						1.75	1.83	
Nd						7.35	7.92	
Sm						2.30	2.33	
Eu						0.68	0.82	
Gd						2.64	2.79	
Tb						0.46	0.50	
Dy						2.99	2.86	
Ho						0.68	0.62	
Er						1.88	1.70	
Tm						0.29	0.28	
Yb						1.86	1.69	
Lu						0.28	0.27	
Hf						1.56	1.59	
Ta						0.06	n.d.	
Pb						0.77	0.68	
Th						0.54	0.54	
U						0.11	0.11	

Group	III	III	III	III	III	III	III	III
Sample no.	90-1	BH133	BH136	BH278	LP124	90-63	90-57	90-96
Lithology	PILL	PILL	PILL	PILL	PILL	DYKE	MASS	PILL
Location	Kawa	Kawa	Kawa	Nawaka	Namosi	L. Kawa	Namosi	Malakua
Grid reference	664214	672221	671217	688219	530294	678246	560287	423243
SiO2	54.07	52.64	53.11	52.48	46.86	53.59	51.81	49.26
TiO2	0.76	0.78	0.80	0.83	0.83	0.91	0.95	0.96
Al2O3	15.35	16.27	14.58	17.86	14.50	16.69	15.28	18.07
FeO*	8.27	8.88	8.65	8.85	8.70	9.71	10.06	8.83
MnO	0.15	0.14	0.17	0.16	0.13	0.16	0.18	0.14
CaO	8.27	7.59	9.06	7.51	12.46	9.21	9.25	10.73
MgO	7.43	8.15	7.83	6.91	11.36	6.62	7.74	8.28
Na2O	5.27	5.13	5.07	4.87	2.24	2.21	4.05	2.44
K2O	0.10	0.03	0.03	0.02	1.60	0.39	0.66	0.22
P2O5	0.10	0.09	0.08	0.15	0.08	0.11	0.07	0.06
LOI	4.36	5.80	6.73	5.57	10.16	3.67	1.48	9.70
TOTAL	99.76	99.69	99.37	99.64	98.77	99.62	100.10	98.99
Nb XRF	4	4	4	5	4	3	2	5
Zr	49	54	52	57	38	73	42	46
Y	15	16	18	17	18	21	19	19
Sr	107	61	71	101	273	157	182	165
Ga	14	16	14	20	15	19	15	13
Zn	64	72	70	59	66	77	97	61
Cu	11	3	6	4	54	86	43	87
Ni	133	91	140	76	294	48	69	232
Co	39	41	43	40	45	36	43	45
Cr	395	270	393	245	701	126	265	565
V	283	255	307	216	185	320	287	200
Rb	4	2	2	2	20	3	8	4
Ba	29	21	22	23	126	74	203	58
Sc	33	35	34	33	38	34	37	35
Ti ICP-MS					0.79			
V					186.00			
Cr					649.00			
Ni					211.19			
Rb					18.51			
Sr					279.66			
Y					19.64			
Zr					37.90			
Nb					0.38			
Cs					0.21			
Ba					120.36			
La					2.14			
Ce					6.34			
Pr					0.92			
Nd					5.84			
Sm					2.00			
Eu					0.73			
Gd					2.54			
Tb					0.50			
Dy					3.18			
Ho					0.69			
Er					2.08			
Tm					0.31			
Yb					1.86			
Lu					0.35			
Hf					1.21			
Ta					n.d.			
Pb					0.55			
Th					0.26			
U					0.06			

Group	III	III	III	III	III	III	IV	IV
Sample no.	90-80	90-95	BH428	VL029	VL025	VL015	VL018	90-38
Lithology	NAD CL	PILL	PILL	MASS	DYKE	GABB	PILL	MASS
Location	Namosi	Malakua	Civocake	Namosi	Namosi	Vatubasaga	Vatubasaga	Masi
Grid reference	526305	423244	511197	524296	524303	534268	538265	462259
SiO2	47.98	47.20	50.13	47.52	53.27	45.26	50.25	54.54
TiO2	1.21	1.03	1.09	1.08	1.00	1.19	1.00	1.02
Al2O3	16.58	15.13	17.33	17.38	14.76	17.19	16.44	16.03
FeO*	10.91	8.01	9.17	9.36	8.28	8.67	10.62	8.62
MnO	0.18	0.16	0.20	0.15	0.14	0.14	0.21	0.20
CaO	11.05	16.50	9.74	11.00	9.16	9.64	10.11	10.62
MgO	8.35	5.44	8.31	11.23	7.85	9.18	6.13	6.83
Na2O	2.16	5.52	3.43	1.44	4.33	1.98	4.71	3.66
K2O	0.25	0.06	0.36	0.59	0.10	0.78	0.07	0.16
P2O5	0.23	0.28	0.08	0.09	0.11	0.14	0.13	0.12
LOI	n.a.	12.72	3.65	3.91	3.58	3.86	n.a.	0.99
TOTAL	98.9	99.35	99.84	99.84	99.00	98.28	99.70	99.74
Nb XRF	4	7	3	4	3	3	3	3
Zr	62	61	61	81	67	68	67	76
Y	17	18	19	18	19	21	21	22
Sr	326	187	265	180	99	236	208	183
Ga	17	13	17	13	14	16	17	15
Zn	71	64	127	63	66	55	113	89
Cu	57	15	23	81	49	145	20	4
Ni	52	83	141	234	64	179	140	68
Co	38	30	43	45	35	39	41	38
Cr	188	293	359	457	187	144	483	236
V	364	259	254	172	276	221	357	287
Rb	5	2	5	11	4	14	2	2
Ba	71	15	114	227	18	213	17	34
Sc	39	31	33	33	31	23	38	36
Ti ICP-MS						1.26		
V						200.00		
Cr						132.00		
Ni						187.12		
Rb						13.68		
Sr						223.71		
Y						22.44		
Zr						66.27		
Nb						0.45		
Cs						0.13		
Ba						210.42		
La						1.90		
Ce						7.80		
Pr						1.36		
Nd						8.28		
Sm						2.87		
Eu						1.11		
Gd						3.54		
Tb						0.65		
Dy						3.79		
Ho						0.83		
Er						2.31		
Tm						0.35		
Yb						2.11		
Lu						0.35		
Hf						1.86		
Ta						n.d.		
Pb						0.64		
Th						0.15		
U						0.02		

Group	IV	IV	IV	IV	IV	IV	IV	IV
Sample no.	LP145	90-20	VL030	90-49	BH092	LP130	90-30	BH160
Lithology	PILL	PILL BR	PILL	PILL	MASS	PILL	PILL	PILL
Location	Namosi	Lidilidi	Namosi	Namosi	L. Kawa	Namosi	Koromba	Wailulu
Grid reference	532296	608376	534292	533293	679245	527295	637216	683276
SiO2	45.76	48.78	46.71	46.94	47.66	54.04	46.46	48.89
TiO2	1.05	1.08	1.10	1.11	1.15	1.21	1.29	1.30
Al2O3	14.36	17.27	15.29	14.91	14.59	17.72	15.65	17.99
FeO*	9.46	10.17	8.92	9.90	14.82	8.82	9.81	8.83
MnO	0.12	0.21	0.14	0.15	0.18	0.09	0.15	0.13
CaO	12.63	9.79	13.25	10.20	10.48	10.99	14.59	8.84
MgO	9.85	6.22	8.73	12.31	5.67	3.37	6.29	7.53
Na2O	2.66	4.71	2.97	3.53	4.24	4.48	4.37	5.62
K2O	2.23	0.97	1.62	0.28	0.11	0.09	0.59	0.24
P2O5	0.11	0.12	0.10	0.11	0.12	0.11	0.11	0.16
LOI	11.61	7.37	10.54	9.09	1.68	2.68	9.14	8.52
TOTAL	98.24	99.70	98.83	99.45	99.03	100.48	99.35	99.78
Nb XRF	4	3	4	2	5	4	2	5
Zr	63	59	67	58	76	55	81	109
Y	23	20	23	21	22	26	21	26
Sr	227	173	143	152	133	85	208	65
Ga	14	15	14	15	20	16	13	19
Zn	71	62	62	72	76	70	64	65
Cu	55	20	32	58	11	82	73	52
Ni	255	117	255	286	74	141	284	93
Co	47	47	43	53	67	46	55	41
Cr	704	428	711	728	233	377	566	210
V	213	301	214	248	323	311	212	259
Rb	22	10	22	4	1	4	5	7
Ba	335	153	156	101	16	n.a.	151	n.a.
Sc	31	41	33	31	37	41	33	32
Ti ICP-MS	0.98				n.a.	1.23		
V	217.00				287.00	274.00		
Cr	672.00				216.00	333.00		
Ni	208.98				n.a.	111.10		
Rb	20.47				0.91	2.16		
Sr	220.01				146.55	91.07		
Y	23.19				24.76	29.01		
Zr	56.55				76.00	51.06		
Nb	0.46				0.83	0.74		
Cs	0.08				0.03	0.09		
Ba	330.33				16.65	3.15		
La	2.38				2.26	1.54		
Ce	7.36				6.63	5.26		
Pr	1.16				1.06	0.91		
Nd	6.80				6.04	6.13		
Sm	2.38				2.12	2.39		
Eu	0.82				0.82	1.06		
Gd	3.24				2.93	3.72		
Tb	0.59				0.57	0.77		
Dy	3.74				4.04	4.40		
Ho	0.79				0.95	0.90		
Er	2.45				2.51	2.87		
Tm	0.33				0.41	0.41		
Yb	2.26				2.56	2.81		
Lu	0.32				0.36	0.48		
Hf	1.53				1.47	1.66		
Ta	n.d.				0.06	n.d.		
Pb	0.33				0.98	0.19		
Th	0.13				0.18	0.12		
U	0.11				0.05	0.04		

Group	IV	IV	IV	IV	IV	IV	IV	IV
Sample no.	90-50	BH408	90-33A	VL024	BH446	90-10	90-02	90-3
Lithology	MASS	PILL	PILL	PILL	CONTACT	PILL	DYKE	PILL
Location	Namosi	Sokia	Votuma	Namosi	Namosi	Tubenarara	U. Kawa	Kawa
Grid reference	531296	473202	494234	523306	563289	512263	663213	662212
SiO2	44.63	49.83	49.91	47.05	49.02	47.29	48.61	47.31
TiO2	1.34	1.35	1.40	1.48	1.49	1.57	1.64	1.43
Al2O3	17.38	16.31	16.25	18.46	17.37	17.91	14.72	17.07
FeO*	10.65	10.68	11.01	10.30	9.35	10.54	10.05	9.47
MnO	0.20	0.18	0.16	0.19	0.19	0.17	0.20	0.26
CaO	12.96	6.24	5.90	10.88	10.99	6.75	10.29	13.55
MgO	11.40	8.32	8.69	7.38	8.77	10.30	7.45	6.91
Na2O	0.86	5.20	4.52	3.44	2.80	3.91	4.63	3.11
K2O	0.30	0.79	1.34	0.06	0.34	0.80	1.28	0.12
P2O5	0.10	0.18	0.21	0.10	0.11	0.10	0.19	0.12
LOI	3.88	6.28	5.41	6.65	3.24	6.67		6.81
TOTAL	99.82	99.58	99.42	99.33	100.46	99.39	99.06	99.35
Nb XRF	3	4	3	4	4	2	3	4
Zr	94	74	67	100	102	84	82	110
Y	21	24	26	23	27	26	28	27
Sr	86	99	157	328	187	261	69	210
Ga	13	12	17	14	14	18	17	15
Zn	101	105	73	84	84	94	90	74
Cu	102	13	22	38	67	59	56	77
Ni	346	103	77	171	129	181	63	352
Co	58	51	48	54	37	52	45	48
Cr	664	235	204	359	351	356	243	695
V	195	304	365	260	241	312	267	233
Rb	15	8	13	8	7	5	17	5
Ba	242	n.a.	117	60	45	70	69	23
Sc	33	35	30	41	37	37	34	39

Ti ICP-MS	1.26
V	191.70
Cr	677.71
Ni	339.73
Rb	14.49
Sr	90.22
Y	18.48
Zr	89.25
Nb	0.51
Cs	0.15
Ba	214.82
La	1.92
Ce	8.14
Pr	1.39
Nd	8.17
Sm	2.54
Eu	0.84
Gd	3.07
Tb	0.54
Dy	3.51
Ho	0.68
Er	1.99
Tm	0.33
Yb	1.91
Lu	0.28
Hf	1.69
Ta	0.03
Pb	0.57
Th	0.05
U	0.01

Group	IV	V	V	V	V	V	V
Sample no.	90-5	90-08	90-08R	90-34	90-72	BH145	90-73
Lithology	PILL	PILL	PILL	PILL	MASS	PILL	PILL
Location	Kawa	Tubenarara	Tubenarara	Votuma	Masi	Wailulu	Masi
Grid reference	662208	512265	512265	494234	482204	674278	482202
SiO2	48.10	49.61	50.40	49.03	52.30	50.07	48.40
TiO2	1.40	1.61	1.62	1.79	1.76	1.70	1.70
Al2O3	16.49	17.51	17.75	15.97	15.76	16.78	18.64
FeO*	10.05	10.41	10.68	12.07	10.18	10.20	7.99
MnO	0.33	0.13	0.14	0.21	0.13	0.17	0.12
CaO	10.09	7.35	7.41	5.89	7.68	8.38	9.05
MgO	10.58	5.66	5.74	8.43	7.56	6.18	10.16
Na2O	2.01	5.50	5.58	3.92	3.89	5.21	3.17
K2O	0.03	1.16	1.19	1.75	0.73	0.80	0.22
P2O5	0.10	0.14	0.15	0.19	0.19	0.16	0.08
LOI	6.14	6.42	6.26	4.27	5.73	8.70	8.01
TOTAL	99.17	99.12	100.69	99.29	100.20	99.73	98.65
Nb XRF	4	3	3	3	3	4	5
Zr	98	92	92	76	138	105	143
Y	23	31	31	32	31	31	29
Sr	177	282	289	180	171	189	260
Ga	14	16	18	19	16	16	13
Zn	62	80	79	86	92	82	69
Cu	72	33	35	0	4	36	27
Ni	412	101	100	85	166	114	230
Co	53	54	51	50	43	42	48
Cr	785	275	270	194	397	323	517
V	202	324	319	399	258	289	254
Rb	4	13	14	16	7	14	10
Ba	21	126	125	281	73	62	77
Sc	26	36	38	32	30	29	42
Ti ICP-MS	1.36						1.70
V	200.59						220.09
Cr	692.72						494.03
Ni	348.31						207.65
Rb	0.85						8.91
Sr	181.51						263.01
Y	21.90						26.15
Zr	105.06						151.54
Nb	0.75						1.22
Cs	0.04						0.10
Ba	7.35						72.60
La	3.55						3.51
Ce	11.38						12.66
Pr	1.73						2.08
Nd	9.52						11.35
Sm	2.81						3.58
Eu	1.09						1.27
Gd	3.27						4.10
Tb	0.59						0.72
Dy	3.95						4.65
Ho	0.85						1.00
Er	2.29						2.72
Tm	0.36						0.44
Yb	2.28						2.63
Lu	0.35						0.42
Hf	2.07						2.81
Ta	0.09						0.11
Pb	0.57						1.20
Th	0.07						0.10
U	0.03						0.22

Group	VI	IIE	IIE	IIE	IIE	IIE	IIE
Sample no.	BH543	BH397	90-07	90-61	VL032	90-75	BH326
Lithology	PILL	CLAST	DACITE	CLAST	MASS	MASS	PILL
Location	Talia	Votuma	U. Kawa	Kawa	Namosi	Masi	Momasau
Grid reference	683286	500224	661207	683250	532294	479209	604243
SiO2	48.99	74.59	82.95	54.73	54.26	53.44	51.94
TiO2	2.09	0.33	0.15	0.86	1.12	1.39	1.83
Al2O3	15.97	11.91	9.39	18.00	16.29	15.11	15.07
FeO*	9.99	2.45	0.98	9.16	10.65	11.79	12.99
MnO	0.14	0.05	0.01	0.19	0.19	0.21	0.19
CaO	6.70	1.86	0.06	9.18	3.82	3.22	5.96
MgO	7.99	0.92	0.03	3.99	5.18	4.28	4.02
Na2O	4.97	3.79	5.14	2.85	4.68	4.20	5.99
K2O	0.94	2.29	0.41	0.18	1.79	3.63	0.07
P2O5	0.39	0.07	0.03	0.07	0.14	0.15	0.18
LOI	8.03	2.49	1.00	2.75	4.00	2.94	3.94
TOTAL	99.14	100.79	99.12	99.21	99.07	98.48	98.25
Nb XRF	11	5	6	4	4	2	3
Zr	220	114	109	51	93	94	105
Y	36	13	18	20	28	30	39
Sr	131	201	47	237	134	63	64
Ga	17	13	10	11	15	17	21
Zn	80	27	16	42	120	86	61
Cu	41	3	1	26	69	63	30
Ni	119	2	2	6	23	12	8
Co	46	3	0	36	56	32	35
Cr	210	16	10	6	4	3	3
V	243	53	16	271	430	409	393
Rb	9	22	5	4	11	31	1
Ba	46	583	58	44	n.a.	475	7
Sc	26	6	1	31	33	34	37
Ti ICP-MS	(By XRF)				n.a.		
V					378.00		
Cr					15.00		
Ni					n.a.		
Rb					9.47		
Sr					132.28		
Y					28.45		
Zr					93.00		
Nb					0.48		
Cs					0.06		
Ba					206.35		
La	9.93				4.14		
Ce	22.91				10.31		
Pr					1.65		
Nd	13.74				8.52		
Sm					2.88		
Eu					0.96		
Gd					4.21		
Tb					0.75		
Dy					4.53		
Ho					0.95		
Er					2.76		
Tm					0.43		
Yb					2.55		
Lu					0.38		
Hf					1.78		
Ta					0.02		
Pb					1.83		
Th					0.12		
U					0.11		

Group	IIE	IIE	IIE	IIE	IIIE	IIIE	IIIE	IIIE
Sample no.	90-44	90-6	90-97	BH389	90-41	LP135	BH403	90-67
Lithology	DYKE	DYKE	CLAST	MASS	PILL	PILL	MASS	DYKE
Location	Namosi	Kawa	Malakua	Roroniki	Masi	Namosi	Vugavuga	L. Kawa
Grid reference	526304	662208	424239	482235	464252	540292	458211	676241
SiO2	48.57	58.09	67.99	57.03	50.38	52.43	51.46	51.91
TiO2	2.00	1.03	0.36	1.13	1.40	0.61	1.11	0.56
Al2O3	14.80	13.95	14.92	15.89	16.43	16.75	15.40	18.45
FeO*	15.78	11.28	2.82	10.13	10.99	9.73	11.98	9.97
MnO	0.22	0.13	0.04	0.17	0.16	0.19	0.17	0.20
CaO	6.92	1.79	2.32	5.28	5.91	8.48	9.22	6.87
MgO	5.16	3.16	1.66	3.77	8.71	5.91	6.04	7.01
Na2O	5.18	0.02	6.50	5.32	4.57	4.97	3.50	4.79
K2O	0.30	5.96	1.85	0.46	1.34	0.02	0.42	0.23
P2O5	0.27	0.14	0.09	0.17	0.21	0.12	0.11	0.06
LOI	2.79	4.70	2.84	1.93	2.47	6.09	1.34	2.26
TOTAL	99.21	100.31	98.59	99.69	100.12	99.64	99.73	100.09
Nb XRF	2	5	4	5	2	4	4	2
Zr	48	123	126	84	46	49	69	37
Y	24	38	18	30	17	19	21	16
Sr	70	56	149	192	209	25	167	229
Ga	16	19	13	16	16	18	17	19
Zn	91	93	26	82	115	137	43	67
Cu	21	45	3	27	31	55	167	28
Ni	9	6	3	16	84	35	42	28
Co	52	46	7	40	55	46	52	43
Cr	3	2	2	1	103	64	46	38
V	442	114	63	189	231	282	373	321
Rb	2	0	20	10	4	2	5	4
Ba	40	5	225	n.a.	65	n.a.	n.a.	27
Sc	37	31	6	34	48	38	43	39
Ti ICP-MS								
V								
Cr								
Ni								
Rb								
Sr								
Y								
Zr								
Nb								
Cs								
Ba								
La								
Ce								
Pr								
Nd								
Sm								
Eu								
Gd								
Tb								
Dy								
Ho								
Er								
Tm								
Yb								
Lu								
Hf								
Ta								
Pb								
Th								
U								

Group	IIIE	IIIE	IIIE	IIIE	IIIE	IVE	IVE	IVE
Sample no.	VL020	VL017	90-101	VL016	BH385	BH566	90-32	BH597
Lithology	MICGABB	DYKE	PILL	DYKE	MASS	DYKE	PILL	MASS
Location	Vatubasaga	Vatubasaga	Nawaka	Vatubasaga	Vulavula	Namaka	Votuma	Log road
Grid reference	538265	538265	522252	538265	446244	493215	491240	574266
SiO2	51.00	55.45	53.11	57.02	62.53	54.25	58.58	53.08
TiO2	0.95	1.28	1.37	1.49	1.11	1.22	1.50	1.24
Al2O3	17.41	11.81	14.06	15.52	13.98	14.85	14.84	15.69
FeO*	11.19	10.61	13.10	12.80	4.72	12.21	10.67	13.24
MnO	0.22	0.18	0.21	0.21	0.07	0.18	0.13	0.24
CaO	7.93	17.18	5.85	7.15	5.41	8.22	4.34	7.06
MgO	5.06	3.05	4.26	3.52	2.25	4.95	3.08	4.65
Na2O	3.19	0.30	4.71	2.44	5.74	3.19	6.54	4.10
K2O	1.95	0.01	0.91	0.02	0.05	0.33	0.14	0.61
P2O5	0.08	0.14	0.16	0.19	0.28	0.15	0.16	0.12
LOI	2.78	2.65	5.30	3.18	1.16	2.86	5.16	5.25
TOTAL	99.06	98.46	98.91	99.41	98.06	99.80	100.01	100.30
Nb XRF	2	4	5	3	7	3	5	5
Zr	50	96	109	109	222	85	91	68
Y	18	23	29	36	60	25	30	23
Sr	230	573	137	235	101	216	100	178
Ga	19	18	16	19	15	15	10	14
Zn	162	52	91	128	24	64	56	107
Cu	58	15	55	65	2	79	139	115
Ni	18	15	24	7	13	24	29	21
Co	35	21	45	45	13	51	46	60
Cr	32	15	8	7	5	20	12	18
V	388	343	275	331	89	383	385	383
Rb	25	4	21	2	1	2	3	10
Ba	457	16	272	3	n.a.	72	14	n.a.
Sc	38	36	24	34	17	32	31	39
Ti ICP-MS		n.a.		1.43				
V		367.00		289.00				
Cr		14.00		15.00				
Ni		n.a.		21.05				
Rb		4.10		0.32				
Sr		579.13		239.77				
Y		24.00		36.31				
Zr		96.00		109.00				
Nb		0.20		1.29				
Cs		0.01		0.01				
Ba		7.80		3.92				
La		5.05		4.67				
Ce		13.80		13.92				
Pr		2.32		2.13				
Nd		12.64		11.07				
Sm		2.80		3.56				
Eu		1.05		1.28				
Gd		4.36		4.87				
Tb		0.91		0.93				
Dy		5.56		5.84				
Ho		1.23		1.17				
Er		3.37		3.60				
Tm		0.54		0.49				
Yb		2.93		3.11				
Lu		0.50		0.46				
Hf		3.04		1.98				
Ta		0.02		0.13				
Pb		12.70		6.31				
Th		0.26		0.27				
U		0.08		0.13				

Group	IVE	IVE	IVE	IVE	VE	VIE
Sample no.	BH414	BH407	BH413	BH416	90-55	90-93
Lithology	MASS	GABB	MICGABB	GABB	CLAST	PILL
Location	Tubenarara	Iasi Tributary	Tubenarara	Tubenarara	Namosi	Malakua
Grid reference	515224	479216	515225	554221	543299	224247
SiO2	53.30	49.91	52.25	51.77	56.99	50.89
TiO2	1.32	1.88	1.21	2.12	0.88	2.40
Al2O3	13.85	14.64	17.07	13.41	16.33	15.24
FeO*	13.24	11.88	11.65	13.22	10.66	14.33
MnO	0.20	0.17	0.18	0.22	0.05	0.21
CaO	7.90	7.18	8.88	4.52	5.49	6.38
MgO	6.87	6.90	4.07	3.98	1.67	5.86
Na2O	0.22	0.38	3.59	0.18	8.55	6.19
K2O	2.93	3.52	0.43	6.02	0.14	0.38
P2O5	0.11	0.26	0.12	0.35	0.35	0.27
LOI	1.28	2.75	4.24	2.44	5.99	6.60
TOTAL	101.33	99.59	99.73	98.31	100.55	101.05
Nb XRF	5	6	3	7	5	6
Zr	76	145	73	222	60	117
Y	23	33	24	63	32	36
Sr	175	184	214	87	140	92
Ga	17	21	19	20	9	18
Zn	90	81	47	105	67	95
Cu	45	29	61	16	22	38
Ni	18	23	12	11	34	38
Co	57	54	31	57	41	67
Cr	17	16	15	6	39	54
V	450	428	416	206	166	526
Rb	5	7	7	4	3	4
Ba	n.a.	91	55	n.a.	27	43
Sc	39	35	41	16	33	38
Ti ICP-MS						
V						
Cr						
Ni						
Rb						
Sr						
Y						
Zr						
Nb						
Cs						
Ba						
La						
Ce						
Pr						
Nd						
Sm						
Eu						
Gd						
Tb						
Dy						
Ho						
Er						
Tm						
Yb						
Lu						
Hf						
Ta						
Pb						
Th						
U						

Group	Dakadaka	Dakadaka	Dakadaka	Dakadaka	Dakadaka	Dakadaka	Dakadaka	Dakadaka
Sample	VLO36	VLO35	BH487	90-88	BH527	VLO37	BH173	BH191
Location	Qaraqara	Qaraqara	Togitogi	Naivalasau	Vunamakedre	Qaraqara	Rewesali	Savulevu
G.R.	663097	663097	554166	416178	408196	664096	676185	652178
SiO2	45.01	47.07	47.79	48.02	48.19	48.61	48.78	49.40
TiO2	1.00	0.72	1.09	1.12	1.10	0.90	0.77	1.06
Al2O3	18.41	19.92	17.61	17.22	18.01	16.94	20.37	17.62
FeO*	10.48	9.48	10.15	10.53	10.26	9.69	9.48	11.85
MnO	0.18	0.17	0.17	0.17	0.17	0.16	0.16	0.23
MgO	11.01	7.45	8.50	7.45	7.27	10.10	5.04	4.98
CaO	11.22	11.53	9.90	11.81	11.85	10.53	10.06	9.52
Na2O	2.71	2.03	2.41	2.20	2.59	2.35	3.86	3.63
K2O	1.02	0.82	1.34	0.39	0.39	0.72	0.56	0.62
P2O5	0.26	0.13	0.27	0.19	0.21	0.22	0.15	0.27
LOI	5.17	7.62	5.36	3.50	3.01	6.62	5.57	6.10
Total	101.29	99.37	99.30	101.34	101.56	100.33	99.28	99.17
Nb XRF	8	3	6	4	4	7	4	4
Zr	60	29	70	63	63	55	51	87
Y	18	10	19	18	19	17	15	26
Sr	283	393	383	324	286	284	509	203
Ga	14	13	15	15	16	17	19	18
Zn	59	60	55	54	56	63	66	106
Cu	13	90	59	63	70	51	18	61
Ni	135	52	74	63	63	128	24	11
Co	46	43	45	37	41	45	38	45
Cr	509	97	149	162	152	408	36	35
V	263	256	299	301	288	255	290	354
Rb	14	24	19	12	5	13	8	14
Ba	97	378	152	90	80	90	168	32
Sc	28	26	29	30	31	29	25	41
Rb ICP-MS	14.29	24.42	17.07				9.94	15.74
Sr	305.53	399.50	384.89				483.33	161.95
Y	19.34	10.71	17.86				14.16	23.53
Zr	63.41	26.82	72.19				43.00	74.71
Nb	4.42	0.76	3.94				0.86	0.50
Cs	0.04	0.06	0.07				0.06	0.48
Ba	81.11	312.38	126.47				130.03	22.27
La	8.81	4.38	9.53				4.47	2.63
Ce	16.19	8.38	20.66				8.50	6.50
Pr	2.50	1.42	2.65				1.51	1.19
Nd	12.08	7.35	13.51				7.86	6.61
Sm	2.92	2.16	3.28				2.14	1.85
Eu	0.95	0.67	1.14				0.72	0.65
Gd	3.61	1.75	3.62				2.71	2.70
Tb	0.61	0.30	0.57				0.45	0.53
Dy	3.35	1.95	3.27				2.51	3.74
Ho	0.64	0.43	0.68				0.54	0.83
Er	1.92	1.17	1.79				1.57	2.43
Tm	0.27	0.17	0.29				0.26	0.35
Yb	1.86	1.12	1.83				1.54	2.40
Lu	0.30	0.17	0.29				0.25	0.38
Hf	1.55	0.74	1.55				1.23	1.73
Ta	0.25	0.05	0.30				0.07	0.07
Pb	0.72	1.08	0.70				1.03	0.80
Th	0.69	0.26	0.90				0.41	0.13
U	0.28	0.12	0.39				0.18	0.14

Group	Dakadaka	Dakadaka	Dakadaka	Dakadaka	DD Dyke	DD Dyke	DD Dyke
Sample	BH492	BH067	BH515	BH045	90-87	BH181	VLO38
Location	Vunamoli	Veitubanaki	Ailio	Vunabululu	Naivalasau	Rewasali	Qaraqara
G.R.	546184	632174	483181	599173	416178	675178	664096
SiO2	51.10	51.14	52.62	56.83	48.36	48.47	49.05
TiO2	1.23	0.95	1.56	1.20	1.23	0.93	0.91
Al2O3	14.84	19.63	14.72	14.16	18.38	18.54	16.13
FeO*	10.42	9.96	14.18	9.77	10.07	9.86	9.32
MnO	0.21	0.22	0.21	0.10	0.14	0.16	0.17
MgO	6.87	3.05	5.75	2.09	3.08	6.48	9.18
CaO	7.43	7.09	7.73	8.68	11.05	8.51	11.47
Na2O	4.59	6.85	2.90	2.87	2.36	4.83	2.23
K2O	1.38	1.10	0.10	0.71	0.19	0.53	0.84
P2O5	0.20	0.32	0.15	1.80	0.33	0.14	0.24
LOI	4.74	7.59	5.40	8.00	6.05	6.47	4.99
Total	98.27	100.35	99.97	98.20	100.66	98.49	99.65
Nb XRF	4	5	5	5	6	3	6
Zr	51	82	98	60	96	46	65
Y	15	29	30	100	24	19	18
Sr	254	207	172	219	373	826	337
Ga	12	12	11	16	18	17	15
Zn	71	80	113	87	80	57	62
Cu	32	46	127	20	29	68	46
Ni	51	34	21	8	11	35	117
Co	47	42	62	28	28	34	44
Cr	85	89	70	9	21	59	524
V	256	322	467	760	318	387	273
Rb	19	17	2	8	4	9	16
Ba	76	41	29	32	68	262	93
Sc	29	37	41	31	33	28	31
Rb ICP-MS				7.94			
Sr				208.68			
Y				103.76			
Zr				44.16			
Nb				0.42			
Cs				0.02			
Ba				35.09			
La				8.81			
Ce				7.95			
Pr				2.86			
Nd				14.97			
Sm				4.25			
Eu				1.62			
Gd				6.58			
Tb				1.17			
Dy				7.59			
Ho				1.85			
Er				5.78			
Tm				0.92			
Yb				5.50			
Lu				1.06			
Hf				1.07			
Ta				0.03			
Pb				0.73			
Th				0.04			
U				0.44			

Group	Basic dyke	Basic dyke	Basic dyke	Basic dyke	Basic dyke	Basic dyke	Basic dyke	Basic dyke
Sample	BH119	90-26	BH383	90-39A	LP159	90-15	90-78	90-106
Location	Nasolo	Masi	Vulavula	Masi	Vitilevu	Tubenarara	Namosi	Namosi
G.R.	634242	464259	444242	462257	498217	515260	525303	580284
SiO2	47.73	49.28	49.76	50.23	51.92	52.15	52.32	53.59
TiO2	0.64	1.32	1.75	1.67	1.06	1.52	1.43	1.40
Al2O3	19.20	15.62	14.88	15.60	15.75	15.31	14.33	14.83
FeO*	9.64	11.66	15.01	14.54	11.46	13.33	14.07	11.85
MnO	0.18	0.15	0.23	0.28	0.18	0.24	0.22	0.23
MgO	7.75	5.92	4.91	5.79	6.35	5.77	4.51	3.63
CaO	9.11	7.05	6.35	6.83	7.01	3.64	5.69	8.01
Na2O	2.92	4.48	5.10	4.72	4.93	6.37	5.57	4.84
K2O	1.30	2.55	1.00	0.59	1.53	0.61	0.69	0.11
P2O5	0.05	0.23	0.15	0.15	0.09	0.13	0.12	0.14
LOI	4.00	4.57	2.93	3.27	4.06	4.36	3.00	6.74
Total	98.52	98.34	99.24	100.45	100.28	99.07	98.96	98.66
Nb XRF	3	2	4	2	4	2	4	2
Zr	35	75	57	51	59	62	93	77
Y	14	25	23	23	18	25	28	26
Sr	200	187	61	149	288	96	74	158
Ga	15	18	16	20	15	21	18	19
Zn	70	85	83	95	68	81	87	164
Cu	60	52	38	37	107	25	69	101
Ni	47	27	10	16	25	18	11	11
Co	38	39	51	53	45	41	56	34
Cr	129	55	17	20	50	6	0	2
V	242	360	469	463	334	423	407	442
Rb	27	29	6	5	14	4	7	1
Ba	98	514	126	197	184	102	142	25
Sc	31	31	44	40	34	36	29	38

Rb ICP-MS	27.62
Sr	202.17
Y	11.20
Zr	27.41
Nb	0.46
Cs	0.35
Ba	72.97
La	1.33
Ce	3.31
Pr	0.57
Nd	3.33
Sm	1.12
Eu	0.47
Gd	1.49
Tb	0.29
Dy	1.88
Ho	0.45
Er	1.15
Tm	0.19
Yb	1.10
Lu	0.19
Hf	0.77
Ta	0.08
Pb	1.57
Th	0.08
U	0.01

Group	Basic dyke	Basic dyke	Basic dyke	Basic dyke	Basic dyke	Basic dyke	Basic dyke	Basic dyke
Sample	LP158	BH126	90-98	90-33	90-36	90-14	LP140	LP120
Location	Vitilevu	Qalilevu	Malakua	Vatuma	Vatuma	Tubenarara	Namosi	S Namosi
G.R.	498217	597283	425245	493237	496223	515260	525301	536287
SiO2	53.63	53.65	53.71	53.89	53.91	54.03	54.16	54.30
TiO2	1.65	1.59	1.33	1.32	1.37	1.25	1.21	1.25
Al2O3	15.45	14.56	15.79	14.34	15.30	15.74	15.38	15.08
FeO*	13.72	13.97	12.30	12.85	12.45	12.21	11.30	12.31
MnO	0.21	0.23	0.18	0.21	0.20	0.19	0.22	0.19
MgO	4.76	4.28	5.47	4.11	3.81	6.28	6.43	4.09
CaO	4.07	5.83	3.99	6.77	5.82	2.27	5.25	5.11
Na2O	6.35	4.91	5.12	5.79	5.58	4.92	4.01	7.25
K2O	0.04	0.03	0.47	0.35	0.90	1.79	0.38	0.01
P2O5	0.17	0.17	0.14	0.14	0.15	0.12	0.13	0.14
LOI	5.45	2.50	6.57	7.53	6.17	5.25	3.07	3.50
Total	100.06	99.20	98.52	99.81	99.50	98.85	98.57	99.73
Nb XRF	5	5	5	4	2	6	5	4
Zr	108	109	99	94	94	64	62	86
Y	33	32	31	29	32	25	30	25
Sr	73	52	87	35	47	114	147	52
Ga	20	16	14	18	17	16	17	17
Zn	118	256	98	91	73	89	152	68
Cu	97	155	91	113	56	30	63	70
Ni	6	13	8	6	7	4	17	8
Co	47	41	40	43	44	40	37	44
Cr	2	3	28	7	3	24	21	6
V	450	344	403	406	425	326	349	374
Rb	2	3	7	5	6	16	5	14
Ba	9	8	70	44	88	116	63	4
Sc	38	29	34	37	34	28	31	29

Rb ICP-MS	2.91
Sr	53.58
Y	32.21
Zr	81.18
Nb	1.21
Cs	0.14
Ba	8.96
La	4.81
Ce	10.98
Pr	1.95
Nd	9.69
Sm	2.75
Eu	1.12
Gd	4.48
Tb	0.83
Dy	5.21
Ho	1.09
Er	3.27
Tm	0.51
Yb	3.35
Lu	0.50
Hf	2.19
Ta	0.12
Pb	1.50
Th	0.32
U	0.12

Group	Basic dyke	Basic dyke	Basic dyke	Basic dyke	Basic dyke	Basic dyke	Basic dyke	Basic dyke
Sample	90-28	VLO27	90-94	LP139	LP160	90-59	LP136	90-12
Location	Namendre	Namosi	Malakua	Namosi	W Navasakai	Namosi	Namosi	Tubenarara
G.R.	638218	523300	424244	525295		565291	545285	514263
SiO2	54.44	54.49	54.78	54.90	54.90	55.22	55.23	55.84
TiO2	1.22	1.42	1.35	1.38	1.47	1.33	1.30	1.43
Al2O3	15.58	14.81	16.08	14.84	14.70	15.41	14.62	14.94
FeO*	11.36	13.76	11.74	11.79	12.84	11.74	12.14	11.67
MnO	0.19	0.22	0.17	0.18	0.22	0.21	0.19	0.21
MgO	3.69	4.26	3.45	3.80	3.91	3.57	3.62	4.56
CaO	3.52	6.17	3.74	5.29	5.57	6.90	5.51	2.66
Na2O	7.08	5.92	6.03	4.12	5.09	4.79	6.12	6.60
K2O	0.80	0.04	1.14	2.55	0.82	0.08	0.02	0.16
P2O5	0.19	0.12	0.20	0.18	0.15	0.16	0.13	0.17
LOI	2.94	3.52	4.20	3.44	2.58	3.56	4.32	4.88
Total	98.08	101.28	98.70	99.03	99.67	99.32	99.18	98.25
Nb XRF	3	5	3	5	6	3	4	2
Zr	86	86	94	122	125	98	89	63
Y	34	24	36	31	33	30	26	28
Sr	102	36	83	90	173	178	59	33
Ga	20	17	23	21	16	20	16	17
Zn	66	98	93	87	85	92	87	80
Cu	63	105	123	126	70	43	44	4
Ni	7	10	3	7	9	7	12	1
Co	40	49	35	35	42	40	41	34
Cr	1	3	5	2	11	3	2	2
V	260	409	340	336	376	380	412	256
Rb	14	1	12	23	10	2	1	2
Ba	51	3	107	530	109	14	11	21
Sc	26	36	36	27	32	34	28	32

Rb ICP-MS	2.13
Sr	37.80
Y	26.88
Zr	85.63
Nb	0.71
Cs	0.01
Ba	7.03
La	3.09
Ce	7.85
Pr	1.54
Nd	8.31
Sm	2.27
Eu	0.89
Gd	3.57
Tb	0.74
Dy	4.65
Ho	0.99
Er	2.84
Tm	0.48
Yb	3.07
Lu	0.45
Hf	2.16
Ta	0.06
Pb	1.09
Th	0.11
U	0.05

Group	Basic dyke	Basic dyke	Nadele	Nadele	Nadele	Nadele	Nadele
Sample	BH058	BH117	VL013	VL012	VL011	VL007	VL010
Location	Buseta	Nasolo	Sabeto	Sabeto	Sabeto	Nasasa	Nasasa
G.R.	585182	634246	589399	589399	592400	598388	596390
SiO2	56.04	58.69	50.40	51.20	51.52	52.24	61.30
TiO2	1.11	1.32	1.08	1.28	1.36	1.60	1.30
Al2O3	18.32	14.88	17.07	16.04	16.21	15.58	16.08
FeO*	10.05	10.54	9.94	10.86	10.86	11.42	5.91
MnO	0.16	0.20	0.16	0.16	0.14	0.18	0.29
MgO	6.01	2.70	7.51	5.91	6.02	4.43	1.03
CaO	1.50	4.88	9.20	9.71	5.75	8.42	8.35
Na2O	4.25	5.65	2.46	2.70	4.32	3.45	3.87
K2O	1.65	0.10	1.01	0.79	1.15	0.81	0.93
P2O5	0.15	0.20	0.19	0.17	0.30	0.27	0.94
LOI	13.46	2.89	5.20	5.09	8.28	5.66	1.34
Total	99.26	99.15	99.02	98.82	97.63	98.40	100.00
Nb XRF	5	5	4	3	3	5	6
Zr	96	125	70	96	94	114	141
Y	17	36	21	30	33	35	83
Sr	122	102	195	208	171	236	236
Ga	20	18	18	20	20	19	19
Zn	80	109	80	95	95	106	133
Cu	145	56	44	64	60	43	35
Ni	9	5	24	33	23	24	9
Co	30	32	43	44	45	49	18
Cr	12	3	57	88	93	47	7
V	310	246	365	268	288	276	280
Rb	12	3	10	13	20	17	15
Ba	115	16	54	35	47	51	78
Sc	29	28	50	38	31	42	29

Rb ICP-MS	15.88
Sr	100.39
Y	16.57
Zr	90.99
Nb	0.68
Cs	0.15
Ba	91.33
La	3.49
Ce	8.71
Pr	1.37
Nd	6.67
Sm	2.02
Eu	0.63
Gd	2.43
Tb	0.49
Dy	3.06
Ho	0.72
Er	1.94
Tm	0.34
Yb	2.16
Lu	0.37
Hf	2.48
Ta	0.04
Pb	7.17
Th	0.47
U	0.14

Group	Nadele	Nadele	Nadele	Kawa	Kawa	Kawa	Kawa
Sample	VL009	VL005	VL008	W2	BH222	BH197	VLO34
Location	Nasasa	Nasasa	Nasasa	Wailulu	Damu	Wailulu	Wailulu
G.R.	596390	600385	598389	736258	705222	724253	696284
SiO2	64.95	68.23	72.30	58.32	59.70	60.59	58.27
TiO2	0.73	0.77	0.72	0.94	0.76	0.85	0.91
Al2O3	12.76	13.06	13.36	17.59	16.18	16.16	18.02
FeO*	7.11	4.75	3.36	7.26	9.91	8.33	5.31
MnO	0.16	0.18	0.15	0.20	0.13	0.10	0.14
MgO	1.33	0.47	0.33	2.47	2.46	2.56	1.97
CaO	3.96	3.17	2.92	6.61	4.01	5.24	8.30
Na2O	5.07	5.26	4.46	4.25	5.88	3.99	3.90
K2O	0.85	1.41	1.33	1.23	0.30	0.69	0.53
P2O5	0.40	0.27	0.13	0.20	0.14	0.11	0.16
LOI	4.00	1.00	1.83	3.95	5.00	2.62	2.89
Total	101.40	98.65	99.06	99.11	99.51	98.65	100.48
Nb XRF	6	9	7	4	5	5	5
Zr	109	270	292	109	79	83	89
Y	66	76	64	29	23	30	34
Sr	160	145	124	217	224	191	256
Ga	20	25	18	19	16	16	16
Zn	88	85	77	94	45	43	49
Cu	6	3	34	20	17	40	19
Ni	10	4	5	4	24	10	16
Co	21	11	4	15	30	31	15
Cr	7	23	4	3	3	97	14
V	9	10	37	228	79	172	145
Rb	8	14	13	18	3	6	10
Ba	NA	NA	114	145	84	96	74
Sc	20	25	14	26	16	25	27
Rb ICP-MS							7.58
Sr							290.91
Y							32.74
Zr							86.19
Nb							1.14
Cs							0.40
Ba							72.15
La							3.66
Ce							12.71
Pr							1.83
Nd							10.35
Sm							3.67
Eu							1.20
Gd							4.79
Tb							0.84
Dy							4.93
Ho							0.94
Er							2.84
Tm							0.45
Yb							3.03
Lu							0.46
Hf							2.00
Ta							0.09
Pb							1.69
Th							0.16
U							0.10

Group	Kawa	Kawa	Kawa	Kawa	Felsic dyke	Felsic dyke	Felsic dyke
Sample	VL033	BH279	W3	BH295	90-86	BH125	90-71
Location	Wailulu	Nawaga	Wailulu	Damu	Naivalasau	Qalilevu	Nawaka
G.R.	696284	689215	736258	722222	416178	596282	480204
SiO2	59.16	64.21	64.77	67.71	61.92	71.83	74.67
TiO2	1.01	0.85	1.04	0.80	1.00	0.32	0.20
Al2O3	16.97	16.36	17.15	15.05	15.52	13.36	12.80
FeO*	5.72	5.97	3.52	3.47	7.42	4.23	2.89
MnO	0.25	0.07	0.32	0.13	0.16	0.15	0.06
MgO	1.91	1.40	0.50	1.15	2.78	0.34	1.26
CaO	6.79	8.07	4.40	4.14	3.93	2.19	0.20
Na2O	4.61	4.60	6.05	4.67	4.31	5.96	6.40
K2O	0.56	0.87	1.03	0.69	0.72	0.85	0.13
P2O5	0.23	0.42	0.29	0.18	0.37	0.06	0.04
LOI	3.07	7.05	0.76	0.83	3.65	2.56	1.37
Total	100.34	101.35	99.10	98.88	98.18	99.28	98.64
Nb XRF	5	5	6	5	8	8	7
Zr	94	98	125	115	177	170	247
Y	37	52	42	40	38	52	49
Sr	241	189	234	205	210	107	36
Ga	18	16	18	17	22	17	18
Zn	73	60	113	64	82	100	48
Cu	31	2	6	4	0	1	16
Ni	12	8	1	11	0	1	2
Co	16	17	5	5	16	9	3
Cr	3	3	6	3	3	2	4
V	152	71	94	57	52	14	9
Rb	8	14	9	11	8	7	1
Ba	90	NA	153	109	188	134	29
Sc	28	22	17	19	19	12	5
Rb ICP-MS	6.66					5.47	
Sr	252.58					107.32	
Y	37.38					49.20	
Zr	94.76					120.15	
Nb	1.23					2.30	
Cs	0.13					0.01	
Ba	85.24					104.02	
La	4.01					6.83	
Ce	9.55					15.00	
Pr	2.11					2.79	
Nd	12.57					14.42	
Sm	3.30					4.31	
Eu	1.20					1.33	
Gd	5.09					6.39	
Tb	0.92					1.19	
Dy	6.17					7.82	
Ho	1.38					1.67	
Er	3.99					4.87	
Tm	0.60					0.76	
Yb	3.97					5.40	
Lu	0.59					0.81	
Hf	2.82					3.21	
Ta	n.d.					n.d.	
Pb	1.99					1.26	
Th	0.23					0.35	
U	0.10					0.15	

Group	Felsic dyke	Felsic dyke	Felsic dyke	Kalaka	Kalaka	Kalaka	Kalaka
Sample	BH382	BH373	90-11	BH524	90-82	BH049	90-42
Location	Vulavula	Lawataya	Tubenarara	Korovudi	Nadogaga	Vunabulubulu	Nanunu
G.R.	444241	450259	514263	416196		599173	
SiO2	75.31	75.69	78.61	62.49	66.42	70.66	73.94
TiO2	0.19	0.17	0.29	0.94	0.59	0.80	0.46
Al2O3	12.99	12.50	11.45	16.90	15.66	12.90	13.06
FeO*	3.06	2.90	2.95	6.16	4.91	4.20	4.32
MnO	0.06	0.08	0.03	0.16	0.13	0.06	0.08
MgO	0.22	0.31	0.78	1.32	1.02	1.02	0.56
CaO	0.11	1.43	0.67	5.15	4.20	3.61	0.70
Na2O	7.12	5.99	5.16	4.89	4.37	4.38	4.85
K2O	0.12	0.16	0.92	0.74	1.48	0.78	1.24
P2O5	0.04	0.03	0.07	0.32	0.18	0.30	0.06
LOI	0.91	1.07	1.27	3.00	5.18	1.99	2.09
Total	99.22	99.26	100.92	99.07	99.02	98.71	99.28
Nb XRF	9	8	9	9	11	6	5
Zr	244	210	292	174	202	175	186
Y	64	58	40	38	31	46	47
Sr	24	67	12	278	265	171	137
Ga	20	18	20	18	18	17	19
Zn	102	36	72	102	64	138	41
Cu	3	4	5	7	3	1	8
Ni	1	2	0	2	1	1	1
Co	4	3	2	10	9	14	8
Cr	0	1	1	2	2	1	4
V	9	2	1	40	29	29	38
Rb	2	4	8	10	53	9	38
Ba	25	40	29	140	412	116	183
Sc	7	8	10	21	10	17	7
Rb ICP-MS							
Sr							
Y							
Zr							
Nb							
Cs							
Ba							
La							
Ce							
Pr							
Nd							
Sm							
Eu							
Gd							
Tb							
Dy							
Ho							
Er							
Tm							
Yb							
Lu							
Hf							
Ta							
Pb							
Th							
U							

Group	Kalaka	Kalaka	Kalaka
Sample	90-43	VLO14	BH507
Location	Nanunu	Legalega	Vevelutu
G.R.		516366	506172
SiO2	78.98	79.32	80.20
TiO2	0.22	0.17	0.16
Al2O3	10.90	10.61	9.99
FeO*	2.62	2.36	2.29
MnO	0.04	0.02	0.05
MgO	0.28	0.14	0.35
CaO	0.40	0.84	0.96
Na2O	4.52	4.69	3.77
K2O	1.09	1.09	1.15
P2O5	0.03	0.03	0.02
LOI	1.56	2.62	1.63
Total	99.08	99.27	98.94
Nb XRF	6	9	7
Zr	185	347	184
Y	49	99	46
Sr	90	51	72
Ga	16	20	12
Zn	49	77	59
Cu	11	12	4
Ni	1	1	1
Co	7	1	4
Cr	7	2	1
V	0	4	5
Rb	11	12	11
Ba	129	103	216
Sc	5	7	6
Rb ICP-MS		7.08	
Sr		48.73	
Y		116.18	
Zr		309.58	
Nb		4.01	
Cs		0.14	
Ba		81.48	
La		23.15	
Ce		35.22	
Pr		11.28	
Nd		56.81	
Sm		16.14	
Eu		2.40	
Gd		20.15	
Tb		3.54	
Dy		19.41	
Ho		3.79	
Er		11.66	
Tm		1.81	
Yb		10.94	
Lu		1.63	
Hf		7.74	
Ta		0.33	
Pb		2.42	
Th		0.84	
U		0.45	

Sample	E1	E2	E3	E4	E5	E6	E7	E8
Litholgy	Lava float	Dyke	Lava float	Lava float	Lava float	Lava float	Lava float	Lava float
Location	Liku	Liku	Liku	Liku	Liku	Liku	Liku	Liku
SiO2	71.97	55.58	66.98	50.68	50.39	50.17	50.53	70.02
Al2O3	14.02	15.35	14.29	18.79	15.86	15.86	15.57	13.99
TiO2	0.43	0.66	0.68	0.92	1.24	1.06	1.07	0.45
FeO*	3.86	10.89	6.43	10.61	10.14	11.70	11.65	4.96
MgO	1.85	4.16	1.90	4.82	3.05	3.15	3.09	0.76
CaO	2.26	9.23	3.04	6.21	10.90	10.75	10.74	3.52
K2O	0.10	0.56	0.10	0.09	0.15	0.04	0.04	0.12
Na2O	4.39	2.27	5.19	6.99	6.99	6.05	6.06	4.35
MnO	0.32	0.18	0.29	0.22	0.15	0.15	0.15	0.45
P2O5	0.10	0.11	0.14	0.09	0.56	0.10	0.11	0.12
LOI	4.00	0.50	3.24	7.00	11.50	8.60	2.40	4.40
TOTAL	99.30	99.14	99.04	99.42	99.43	99.04	99.01	98.72
Nb XRF	6	4	5	5	6	5	6	5
Zr	77	37	95	45	128	57	78	78
Y	48	16	46	22	43	30	47	45
Sr	120	214	117	106	106	89	145	148
Ga	18	16	18	15	15	22	20	16
Zn	111	89	177	98	151	95	353	271
Cu	883	128	18	5	68	85	46	27
Ni	8	30	10	32	20	28	13	12
Co	8	50	22	49	42	49	14	13
Cr	8	37	8	81	3	8	9	10
V	30	340	75	338	183	380	9	10
Rb	4	7	3	3	11	3	3	3
Ba	55	140	38	n.a.	46	27	52	75
Sc	16	40	22	39	37	37	18	14
Rb ICP-MS				1.36				
Sr				105.59				
Y				25.31				
Zr				44.11				
Nb				0.89				
Cs				0.21				
Ba				30.80				
La				1.50				
Ce				4.84				
Pr				0.90				
Nd				5.48				
Sm				2.03				
Eu				0.71				
Gd				3.33				
Tb				0.62				
Dy				4.03				
Ho				0.87				
Er				2.63				
Tm				0.41				
Yb				2.73				
Lu				0.42				
Hf				1.42				
Ta				0.28				
W				0.60				
Tl				0.05				
Pb				2.21				
Th				0.06				
U				0.17				

Sample	E9	E10	E11	E12	E13	E14	E15	E16
Litholgy	Lava float	Dyke	Lava float	Lava float	Lava float	Lava float	Lava float	Lava float
Location	Liku	Liku	Liku	Liku	Liku	Liku	Liku	Liku
SiO2	66.93	69.57	52.23	56.65	55.12	50.76	57.32	55.63
Al2O3	14.61	14.94	18.53	14.11	17.00	19.31	14.43	14.39
TiO2	0.64	0.46	0.68	1.21	1.13	0.81	1.20	1.11
FeO*	6.59	4.62	9.02	13.00	10.14	9.94	12.80	12.84
MgO	1.49	1.58	5.29	3.58	4.02	5.27	3.07	3.75
CaO	1.16	2.85	10.68	6.94	7.39	9.17	6.33	4.09
K2O	0.18	0.14	0.22	0.11	0.58	0.57	0.20	0.36
Na2O	7.25	4.96	2.40	3.31	4.28	3.10	4.25	6.17
MnO	0.11	0.32	0.15	0.21	0.16	0.21	0.17	0.12
P2O5	0.16	0.12	0.06	0.09	0.11	0.07	0.12	0.11
LOI	2.43	2.38	2.38	2.68	3.40	2.96	1.65	2.28
TOTAL	99.12	99.20	99.27	99.21	99.92	99.21	99.90	98.58
Nb XRF	6	6	5	5	4	4	5	5
Zr	101	85	36	63	59	51	68	60
Y	46	45	14	35	27	19	37	29
Sr	117	128	116	101	139	123	102	39
Ga	19	22	15	14	20	21	13	16
Zn	124	150	80	114	89	84	63	42
Cu	33	229	193	150	272	7	160	84
Ni	21	9	44	22	24	20	13	18
Co	20	11	41	58	42	42	51	50
Cr	8	6	135	10	33	28	9	16
V	35	11	263	479	353	296	365	420
Rb	12	2	3	2	5	5	3	12
Ba	66	n.a.	59	51	127	140	60	51
Sc	13	18	39	44	33	37	38	38
Rb ICP-MS								
Sr								
Y								
Zr								
Nb								
Cs								
Ba								
La								
Ce								
Pr								
Nd								
Sm								
Eu								
Gd								
Tb								
Dy								
Ho								
Er								
Tm								
Yb								
Lu								
Hf								
Ta								
W								
Tl								
Pb								
Th								
U								

Sample	E17	E18	E28	E29	E30	E31	E32	E33
Litholgy	Lava float	Lava float	Lava float	Basalt clast	Lava float	Lava float	Gabbro float	Lava float
Location	Liku	Liku	Liku	Vaingana	Liku	Liku	Liku	Liku
SiO2	47.29	54.30	61.52	50.95	53.51	51.65	48.86	60.26
Al2O3	20.56	17.58	16.00	18.24	17.40	16.97	19.23	14.54
TiO2	0.71	1.17	0.83	0.53	0.72	0.72	0.76	0.94
FeO*	11.01	10.74	7.87	11.14	7.96	8.03	10.69	12.14
MgO	6.25	4.22	2.70	3.98	5.67	7.51	5.99	2.90
CaO	9.33	5.63	2.67	9.20	9.36	9.35	11.91	4.39
K2O	0.51	0.44	0.86	0.46	0.19	0.17	0.05	0.27
Na2O	3.29	4.16	6.62	4.11	3.81	3.69	1.49	3.83
MnO	0.27	0.21	0.15	0.19	0.15	0.14	0.18	0.14
P2O5	0.07	0.12	0.12	0.08	0.07	0.07	0.03	0.08
LOI	6.18	3.86	3.40	4.68	2.14	1.84	3.00	2.90
TOTAL	99.31	98.58	99.34	99.07	98.83	98.30	99.20	99.44
Nb XRF	5	4	5	3	4	4	3	5
Zr	39	83	100	17	54	55	22	62
Y	18	23	34	9	23	22	10	25
Sr	118	35	108	125	113	115	112	86
Ga	16	18	16	14	17	16	18	16
Zn	125	93	69	77	48	41	60	40
Cu	9	94	27	127	14	12	38	22
Ni	46	24	12	18	55	50	28	19
Co	50	60	30	49	30	30	47	46
Cr	72	9	19	20	169	157	65	23
V	264	404	147	384	240	240	444	270
Rb	6	2	8	6	3	3	2	3
Ba	148	11	n.a.	n.a.	n.a.	n.a.	n.a.	n.a.
Sc	42	33	21	49	36	37	48	34
Rb ICP-MS	5.20							
Sr	119.29							
Y	20.81							
Zr	41.36							
Nb	0.54							
Cs	0.16							
Ba	135.41							
La	0.97							
Ce	3.71							
Pr	0.66							
Nd	4.17							
Sm	1.56							
Eu	0.59							
Gd	2.42							
Tb	0.47							
Dy	2.97							
Ho	0.73							
Er	2.05							
Tm	0.31							
Yb	2.02							
Lu	0.34							
Hf	1.13							
Ta	0.09							
W	0.30							
Tl	0.21							
Pb	1.95							
Th	0.05							
U	0.08							

Sample	E34	E35	E36	E37	E38	E40	E41	E42
Litholgy	Lava float	Gabbro float	Gabbro float	Gabbro float	Gabbro float	Lava float	Gabbro float	Lava float
Location	Liku	Liku	Liku	Liku	Liku	Liku	Liku	Liku
SiO2	57.45	49.25	47.87	49.59	49.11	54.13	50.14	60.99
Al2O3	16.41	21.20	20.17	19.32	20.52	17.64	17.21	16.93
TiO2	1.21	0.48	0.78	0.55	0.34	0.83	0.56	0.53
FeO*	10.39	8.42	10.77	9.57	8.31	9.73	10.27	7.07
MgO	3.21	5.79	5.56	6.28	7.61	4.38	7.93	3.24
CaO	5.61	12.24	12.27	11.67	12.71	8.48	11.08	6.36
K2O	0.46	0.15	0.07	0.03	0.02	0.25	0.06	0.29
Na2O	3.94	1.67	1.35	1.77	1.21	2.78	1.64	3.45
MnO	0.26	0.18	0.17	0.18	0.15	0.19	0.22	0.14
P2O5	0.13	0.03	0.03	0.03	0.02	0.09	0.03	0.07
LOI	2.50	2.35	2.00	2.10	1.46	2.00	2.64	2.63
TOTAL	99.07	99.42	99.04	99.00	99.99	98.56	99.15	99.09
Nb XRF	5	3	4	3	5	4	4	5
Zr	85	19	19	19	83	64	24	60
Y	36	8	6	10	37	21	12	21
Sr	144	117	117	115	141	125	98	132
Ga	15	17	14	13	19	15	13	15
Zn	430	58	65	54	63	114	55	85
Cu	132	52	81	24	22	37	54	27
Ni	13	39	27	48	7	21	63	2
Co	42	34	45	44	9	40	48	17
Cr	12	69	57	93	9	24	125	2
V	234	282	362	278	36	217	270	129
Rb	5	2	3	2	2	5	2	3
Ba	n.a.	n.a.	n.a.	n.a.	n.a.	n.a.	n.a.	n.a.
Sc	32	44	47	47	14	36	40	23
Rb ICP-MS								
Sr								
Y								
Zr								
Nb								
Cs								
Ba								
La								
Ce								
Pr								
Nd								
Sm								
Eu								
Gd								
Tb								
Dy								
Ho								
Er								
Tm								
Yb								
Lu								
Hf								
Ta								
W								
Tl								
Pb								
Th								
U								

549- samples, XRF data from Ewart & Bryan (1972)

Sample	549-12	549-15	549-20	549-7
Litholgy	Dyke	Dyke	Basalt clast	Basalt float
Location	Liku	Liku	Vaingana	Liku
SiO2	55.21	51.40	49.18	49.19
Al2O3	13.97	16.76	19.75	20.61
TiO2	1.17	0.96	0.63	0.42
FeO*	12.86	10.65	9.64	8.56
MgO	4.28	5.46	4.30	5.93
CaO	7.13	9.32	6.48	11.78
K2O	0.13	0.21	0.55	0.24
Na2O	3.23	2.61	4.96	1.21
MnO	0.22	0.34	0.17	0.18
P2O5	0.11	0.11	0.07	0.04
LOI	0.59	1.12	3.43	1.63
TOTAL	100.25	99.73	99.71	100.22
Nb XRF	n.a.	n.a.	n.a.	n.a.
Zr	59	59	13	20
Y	39	39	14	12
Sr	100	100	200	115
Ga	18	18	18	13
Zn	n.a.	n.a.	n.a.	n.a.
Cu	200	200	100	51
Ni	19	19	9	25
Co	34	34	29	30
Cr	15	15	10	75
V	370	370	330	230
Rb	1	1	6	1
Ba	n.a.	61	100	14
Sc	42	42	40	43
Rb ICP-MS	0.73	2.31	5.00	2.44
Sr	104.71	125.97	190.02	118.18
Y	33.74	26.97	9.92	12.83
Zr	59.00	39.29	12.31	17.64
Nb	0.91	0.96	0.47	0.26
Cs	0.05	0.03	0.16	0.11
Ba	48.00	46.33	72.00	26.08
La	2.34	1.55	0.58	0.65
Ce	6.69	4.97	1.65	1.98
Pr	1.19	0.96	0.33	0.37
Nd	7.36	5.89	1.91	2.09
Sm	2.78	2.22	0.75	0.85
Eu	1.02	0.83	0.31	0.40
Gd	4.22	3.15	1.16	1.39
Tb	0.84	0.65	0.23	0.28
Dy	5.26	3.90	1.58	1.91
Ho	1.14	0.90	0.35	0.41
Er	3.55	2.73	1.06	1.33
Tm	0.56	0.37	0.19	0.21
Yb	3.54	2.81	1.20	1.41
Lu	0.59	0.45	0.19	0.21
Hf	1.31	1.50	0.40	0.48
Ta	0.14	0.09	0.09	0.21
W	0.17	0.17	0.20	0.15
Tl	0.02	0.00	0.05	0.02
Pb	1.95	1.61	0.68	0.47
Th	0.17	0.12	0.03	0.04
U	0.24	0.18	0.20	0.02

A2.2 Microprobe data **Clinopyroxene data**

Sample	LP143	VL031	VL030	BH278	90-50	BH096	VL021	VL031	VL029	BH119	BH492
Lithology	Float	Massive	Pillow	Pillow	Massive	Dyke	Massive	Massive	Gabbro	Dyke	Massive
SiO2	53.35	50.50	47.06	52.05	50.04	51.09	52.73	51.28	49.09	51.60	49.14
TiO2	0.06	0.52	1.95	*0.31*	*1.59*	*0.33*	0.40	0.78	1.82	*0.61*	1.05
Al2O3	3.37	4.46	4.75	2.32	3.71	2.90	2.89	5.04	4.29	2.21	4.89
FeO	5.50	5.25	9.54	4.31	7.81	5.70	5.57	6.49	8.79	8.37	7.97
MgO	18.54	15.89	12.07	17.09	13.46	16.17	16.92	15.95	13.30	16.00	14.29
CaO	16.51	21.50	20.86	21.30	21.19	20.98	21.23	19.89	20.93	20.35	21.15
Na2O	0.50	*0.22*	*0.35*	*0.20*	*0.49*	*0.16*	0.40	0.63	0.56	*0.23*	*0.35*
Cr2O3	0.77	0.78	0.22	0.86	0.14	0.61	0.57	0.19	0.14	0.18	0.21
Total	98.82	99.22	96.93	98.65	98.67	98.17	100.96	100.51	99.28	99.78	99.21
Si	1.98	1.87	1.83	1.93	1.89	1.91	1.92	1.87	1.85	1.92	1.84
Ti	0.002	0.015	0.057	0.009	0.045	0.009	0.011	0.021	0.052	0.017	0.030
Al	0.07	0.19	0.22	0.10	0.16	0.13	0.12	0.22	0.19	0.10	0.22
Fe	0.17	0.16	0.31	0.13	0.25	0.18	0.17	0.20	0.28	0.26	0.25
Mg	1.03	0.88	0.70	0.94	0.76	0.90	0.92	0.87	0.75	0.89	0.80
Ca	0.66	0.85	0.87	0.85	0.86	0.84	0.83	0.78	0.85	0.81	0.85
Na	0.018	0.016	0.027	0.014	0.036	0.011	0.028	0.044	0.041	0.017	0.026
Cr	0.01	0.02	0.01	0.03	0.01	0.02	0.02	0.01	0.00	0.01	0.01
Total	3.94	4.01	4.02	4.01	4.00	4.01	4.02	4.02	4.02	4.02	4.03
Mg#	86	84	69	88	75	83	84	81	73	77	76

Sample	VL009	VL033
Lithology	Clast	Clast
SiO2	51.34	52.12
TiO2	0.39	0.55
Al2O3	1.32	2.10
FeO	15.51	10.49
MgO	12.17	14.70
CaO	18.00	19.68
Na2O	0.56	0.46
Cr2O3	0.04	0.05
Total	100.29	100.64
Si	1.96	1.94
Ti	0.012	0.015
Al	0.06	0.09
Fe	0.49	0.33
Mg	0.69	0.81
Ca	0.74	0.78
Na	0.041	0.033
Cr	0.00	0.00
Total	4.02	4.02
Mg#	58	71

The accurate low-level TiO2 and Na2O data collected by WDS and used in chapter 4 is denoted by italic script

Spinel data

Sample	BH402	BH097	LP143	LP132	90-1	VL031	BH136	BH278	BH160	BH133	LP124
Lithology	Massive	Clast	Float	Pillow	Pillow	Massive	Pillow	Pillow	Pillow	Pillow	Pillow
MgO	10.41	11.40	2.02	12.79	11.78	12.58	12.64	5.70	13.71	13.77	16.47
Al2O3	14.63	15.43	16.57	16.99	18.19	19.66	19.51	18.90	24.05	23.71	29.58
TiO2	0.23	0.36	0.15	0.37	0.77	0.64	0.86	0.80	0.88	0.82	0.45
Cr2O3	51.71	50.22	43.68	42.90	42.70	42.79	40.54	34.67	39.63	38.42	35.95
MnO	0.53	0.35	0.24	0.29	0.32	0.25	0.00	1.35	0.32	0.00	0.21
FeO	22.10	22.15	35.03	17.44	24.28	25.35	26.11	30.75	21.58	23.92	17.36
Total	100.41	99.91	97.69	90.79	98.60	101.27	99.66	92.95	100.69	100.63	100.01
Mg	4.02	4.41	0.84	5.29	4.57	4.73	4.84	2.39	5.01	5.08	5.82
Al	4.48	4.72	5.44	5.55	5.57	5.85	5.91	6.33	6.95	6.91	8.27
Ti	0.05	0.07	0.03	0.08	0.15	0.12	0.17	0.17	0.16	0.15	0.08
Cr	10.61	10.32	9.62	9.41	8.78	8.54	8.23	7.80	7.68	7.52	6.74
Mn	0.12	0.08	0.06	0.07	0.07	0.06	0.00	0.33	0.07	0.00	0.04
Fe	4.81	4.81	8.17	4.04	5.28	5.35	5.61	7.34	4.42	4.95	3.44
Total	24.35	24.41	24.16	24.44	24.58	24.64	24.76	24.61	24.44	24.62	24.40
Mg#	46	48	9	57	46	47	46	25	53	51	63
Cr#	70	69	64	63	61	59	58	55	53	52	45

Sample	VL030	LP145	90-96	VL029	LP130	BH428	90-5	90-3	90-73	90-16
Lithology	Pillow	Pillow	Pillow	Gabbro	Pillow	Pillow	Pillow	Pillow	Pillow	Clast
MgO	17.03	16.43	15.96	17.21	16.86	15.73	16.16	17.39	17.05	19.02
Al2O3	30.86	30.63	31.50	32.88	33.50	33.30	34.30	36.93	39.71	44.64
TiO2	0.51	0.65	0.68	0.52	0.66	0.57	0.65	0.52	0.59	0.36
Cr2O3	35.16	34.48	32.45	32.90	31.64	31.18	29.08	29.75	25.05	21.91
MnO	0.00	0.00	0.17	0.00	0.00	0.11	0.12	0.22	0.21	0.17
FeO	16.11	19.33	17.92	17.06	18.47	18.18	16.56	15.99	17.41	12.90
Total	99.67	101.52	98.67	100.57	101.12	99.55	96.87	101.18	100.69	99.45
Mg	5.98	5.73	5.67	5.94	5.82	5.50	5.75	5.85	5.73	6.23
Al	8.57	8.45	8.85	8.98	9.14	9.21	9.64	9.83	10.55	11.56
Ti	0.09	0.11	0.12	0.09	0.11	0.10	0.12	0.09	0.1	0.06
Cr	6.54	6.38	6.12	6.03	5.78	5.79	5.49	5.31	4.46	3.81
Mn	0.00	0.00	0.03	0.00	0.00	0.02	0.02	0.04	0.04	0.03
Fe	3.18	3.78	3.58	3.30	3.58	3.57	3.31	3.02	3.28	2.37
Total	24.35	24.45	24.39	24.35	24.42	24.32	24.32	24.26	24.36	24.18
Mg#	65	60	61	64	62	61	63	66	64	72
Cr#	43	43	41	40	39	39	36	35	30	25

A2.3 Radiogenic isotope data

	$^{204/206}Pb$	$^{207/204}Pb$	$^{208/204}Pb$	$^{87/86}Sr$	$^{143/144}Nd$	εNd^1
Viti Levu						
LP145	(18.708)	(15.512)	(38.122)	(0.70480)	0.51309	8.72
LP132	(18.716)	(15.536)	(38.279)	(0.70391)	0.51306	8.10
LP143	(18.023)	(15.542)	(37.877)	(0.70374)	0.51309	8.72
BH487	(18.813)	(15.568)	(38.409)	(0.70393)	0.51302	7.47
'Eua						
549-7	(18.615)	(15.566)	(38.286)	(0.70397)	0.51310	8.93
549-20	(18.756)	(15.573)	(38.371)	(0.70440)	0.51307	8.29

Figures in parenthesis are not used in the petrogenetic arguments presented in this thesis. See analytical geochemistry in appendix 1 for discussion.

[1]εNd is calculated using the equation:

$$\varepsilon Nd = \left[\frac{\left(^{143}Nd/^{144}Nd\right)}{I^{t}_{CHUR}} \text{initial} - 1 \right] \times 10^{4}$$

where CHUR refers to the chondritic uniform reservoir as defined by Depaolo & Wasserburg (1976).

APPENDIX 3

Radiometric dating

A3.1 Experimental Methods

Conventional whole-rock K-Ar ages were determined at the Department of Geophysics at the University of Newcastle using a Kratos MS 10 mass spectrometer coupled to a ultra-high vacuum gas extraction line. Isotope dilution analyses were performed by means of a ^{38}Ar "spike" calibrated against standard micas P-207 and B2303. Typical sample weights for Ar analysis were 300-mg aliquots. K was determined using a Corning EEL 450 flame photometer with lithium internal standard. Results, including error limits are shown in Table A3.1. The quoted values are the mean of two Ar analyses, and the reported errors take into account both random effects (discrepancies between duplicates) and systematic effects (from spike calibration).

Sample	Lithology	K_2O	^{40}Ar ($10^{-4}mmg^{-1}$)	Atmospheric content (%)	Age ($\pm1\sigma$)
BH097	Yavuna Group clast	0.223±0.001	2.06±0.07	79.5	28.4±1.0
BH096	Yavuna Group dyke, cuts BH097	0.251±0.004	4.73±0.13	60.6	57.5±1.8
BH007	Gabbro, Nadi Basin inlier	0.189±0.002	1.49±0.09	92.1	24.3±1.5
VL031	Yavuna Group lava	0.930±0.014	7.67±0.19	60.2	25.4±0.7
VL033	Kawa Formation porphyritic andesite	0.589±0.001	5.38±0.12	80.4	28.1± 0.6
BH197	Kawa Formation porphyritic andesite	0.709±0.004	5.43±0.12	81.5	23.6± 0.5
BH119	Wainimala Group-related dyke	1.290±0.010	9.61±0.13	61.0	22.9±0.4
BH058	Wainimala Group-related dyke	1.600±0.020	5.51±0.09	68.2	10.6±0.2
BH045	Dakadaka Basalt	0.674±0.010	1.80±0.06	79.7	8.26±0.3
VL036	Dakadaka Basalt	0.836±0.008	3.67±0.09	68.3	13.6±0.4
VL035	Dakadaka Basalt	0.802±0.004	1.55±0.08	88.6	5.98±0.31

Table A3.1 Results of radiometric dating

APPENDIX 4

Petrographic data

This appendix provides summary petrographic information for Yavuna Goup, Wainimala Group and 'Eua samples including phenocryst and vesicle contents, alteration index as defined in chapter 4, and groundmass texture.

Yavuna Group

Gp.	n	Sample	Lith.	Ol	Opx	Cpx	Pl	Mt	Sp	Gmass	Ves%	Order	AI	Notes
I	1	90-25	M	?5						? glassy			5	Cataclased
I	2	LP143	FL	20	?	30				glassy			4	
II	1	90-51	DY			2				mph agg	5		3	
II	2	BH096	DY	5		1			1C	felsitic	3		4	
II	3	90-79	P	5		3	1			felsitic	6	Ol-Cpx-Pl	3	
II	4	90-65	P	5		10				glassy	30	Ol-Cpx	3	
II	5	90-69	M	1		1			1C	felsitic			5	Partly recrystallised
II	6	VL028	M						2C	felsitic	10		3	
II	7	LP121	P	3		5	25			glassy	15	Ol-Cpx Pl	4	
II	8	90-21	M	5					1C	mph agg	15		5	
II	9	90-66				5	15			felsitic	4	Cpx-Pl	4	
II	10	90-23	M	5		3	1			felsitic	10		5	
II	11	BH097	CL	10		10				chl-qtz-sph	10		3	Partly recrystallised
II	12	VL021	M	?15		25	20	5		mph agg		Unclear	3	
II	13	90-62								felsitic	10		3	
II	14	BH093	CL			1				mph agg	2		5	Partly recrystallised
II	15	BH439	M			4				mph agg	?15		5	
III	1	BH402	M	1		2	1		1,2C	felsitic			5	
III	2	90-52	CL							felsitic	5		3	
III	3	VL019	P				1			mph agg			3	
III	4	90-64	DY							mph agg			5	Partly recrystallised
III	5	VL031	M							mph agg	2		4	
III	6	LP132	P						2B	mph agg	5		4	
III	7	VL022	M							mph agg			4	
III	8	90-1	P							glassy	?5		3	
III	9	BH133	P			5				felsitic	5		3	
III	10	BH136	P	2						mph agg	?5		3	
III	11	BH278	P	1		2	5		1B	felsitic	10	Pl-Cpx	4	
III	12	LP124	P	5		?2	?2		2B	mph agg	10		3	
III	13	90-63	DY			20	60	5		mph agg		Pl-Cpx-Mt	3	
III	14	90-57	M			?10	?2			unclear		Pl-Cpx	5	Cataclased
III	15	90-96	P	1			1		1B	mph agg	1		3	
III	16	90-80	CL	3		2	1		1C	mph agg		Cpx-Pl	3	
III	17	90-95	P	3					1C	mph agg	2		3	
III	18	BH428	P				10			glassy			3	
III	19	VL029	M			30	40	5		mgabb		Pl-Cpx-Mt	3	
III	20	VL025	DY				5			mph agg			3	
III	21	VL015	G			25	50	5		gabb		Pl-Cpx-Mt	3	
IV	1	VL018	P	?5						glassy			3	Intensely veined & altered
IV	2	90-38	M	1			4			mph agg		Pl-Cpx	5	
IV	3	LP145	P	5			3		2B	felsitic	15		3	
IV	4	90-20	CL			1	3	1		felsitic			3	
IV	5	VL030	P							mph agg	3		3	
IV	6	90-49	P	1		?3	?4		1B	glassy	10		3	
IV	7	BH092	M			?2				felsitic	?10		5	Partly recrystallised
IV	8	LP130	P	1			1		1C	felsitic	1		3	
IV	9	90-30	P	5					1B	glassy	1		3	
IV	10	BH160	P							felsitic			3	
IV	11	90-50	M			15				unclear			4	Cataclased
IV	12	BH408	P	2			1		1C	felsitic			3	
IV	13	90-33A	P				1			mph agg			3	
IV	14	VL024	P	3			8			felsitic		Ol-Pl	3	
IV	15	BH446	M							hornfels			6	
IV	16	90-10	P	1			1		1B	felsitic		Ol-Pl	3	
IV	17	90-2	DY			1	4			felsitic		Pl-Cpx	3	
IV	18	90-3	P						1B	felsitic			3	
IV	19	90-5	P	2					2A	felsitic			3	
V	1	90-08	P	1			1			felsitic	1	Ol-Pl	3	

Yavuna Group

Gp.	n	Sample	Lith.	Ol	Opx	Cpx	Pl	Mt	Sp	Gmass	Ves%	Order	AI	Notes
V	2	90-08R	P	1			1			felsitic	2	Ol-Pl	3	
V	3	90-34	P	1			8			glsssy		Ol-Pl	3	
V	4	90-72	M	2						felsitic	2		3	
V	5	BH145	P	1		1	1		1A		5	Ol-Pl	2	
V	6	90-73	P	?5			1		1C	mph agg		Ol-Pl	3	
VI	1	BH543	P							mph agg			3	
IIE	1	BH397	CL			?	20	1		glsssy			3	20% Qtz, some altered mafics
IIE	2	90-07	CL											No section
IIE	3	90-61	CL			3	40	1		mph agg	5		2	Resorbed, zoned phenocrysts
IIE	4	VL032	M							mph agg	15		4	
IIE	5	90-75	M							recrystallised			3	Partly recrystallised
IIE	6	BH326	P							glassy	10		4	
IIE	7	90-44	DY											No section
IIE	8	90-6	DY			1				trachytic			4	
IIE	9	90-97	CL			30	20	2		glassy			3	10% Qtz, 5% exotics fragments, ?3% hbl
IIE	10	BH389	M			25	65	4		mgabb			5	
IIIE	1	90-41	P			3				mph agg			5	
IIIE	2	LP135	P							felsitic	4		5	
IIIE	3	BH403	M			1	1			mph agg		Pl-Cpx	5	
IIIE	4	90-67	DY										3	Partly recrystallised
IIIE	5	VL020	MG							mph agg			4	
IIIE	6	VL017	DY							mgabb			4	
IIIE	8	90-101	P				10			mgabb			3	
IIIE	9	VL016	DY			20	30	5		mgabb			4	
IIIE	10	BH385	M							schistose			3	Recrystallised
IVE	1	BH566	DY			20	40	5		gabb	40	Pl-Cpx-Qtz	3	Late quartz
IVE	2	90-32	P				3			felsitic	5		5	
IVE	3	BH597	M			15	60	5					4	10% Qtz
IVE	4	BH414	M							mgabb			4	Late Qtz
IVE	5	BH407	G											No section
IVE	6	BH413	MG			30	40	10		mph agg			5	15% Qtz
IVE	7	BH416	G			20	70	5		mph agg			4	
VE	1	90-55	CL				10			glassy	15		4	Includes small exotic lava fragments
VIE	1	90-93	P							felsitic			3	

Key to abbrieviations:

P	Pillow lava	**Ol**	% Olivine phenocrysts	**Gmass**	Groundmass texture
M	Massive lava	**Opx**	% Orthopyroxene phenocrysts	**Ves%**	Percentage of vesicles
DY	Feeder dyke	**Cpx**	% Clinopyroxene phenocrysts	**Order**	Phenocryst crystallisation order
CL	Pillow breccia clast	**Pl**	% Plagioclase phenocrysts	**AI**	Alteration index (groups listed in chapter 4)
G	Gabbro	**Mt**	% Magnetite phenocryts	**Notes**	Details of tectonic deformation,
MG	Microgabbro	**Sp**	Cr-spinel (classification from chapter 4)		other minerals etc.

	Sample	Ol	Opx	Cpx	Pl	Mt	Hbl	Gmass	Ves%	Order	AI	Notes
	VLO36	5		5	10a	3		felsitic			1	
	VLO35			2	30			mph agg	5		1	
	BH487	?3				2		mph agg			1	
	90-88											no section
	BH527											no section
Dakadaka	VLO37			3	1			mph agg	10		1	
Basalt	BH173	?		4	30	1		mph agg	20		1	
	BH191				3			felsitic			1	
	BH492			3	1	-		felsitic	40		1	
	BH067			1	4	-		glassy	50		1	
	BH515											no section
	BH045							glassy	60		1	
Dakadaka	90-87											no section
dykes	BH181	?3		2	15	1		glassy	10		1	
	VLO38	15		10	5	1		mph agg			1	
	BH119	2		3	10			mph agg			3	
	90-26				1			felsitic	2		3	
	BH383							mph agg			4	
	90-39A				1			mph agg	2		4	
	LP159				2			mph agg			4	
	90-15							felsitic	1		4	
	90-78							felsitic			5	
	90-106							glassy			3	
	LP158							felsitic			4	
	BH126							mph agg			3	
Basic dykes	90-98							felsitic			3	
cutting	90-33							felsitic			3	
Yavuna Group	90-36							felsitic	3		3	
	90-14							mph agg			4	
	LP140							mph agg			4	
	LP120			1				felsitic			3	
	90-28			2				mph agg			4	
	VLO27							mph agg			4	
	90-94					1		mph agg			4	
	LP139					1		felsitic			4	
	LP160							mph agg			4	
	90-59				1			mph agg			3	
	LP136							mph agg			3	
	90-12							felsitic			3	
	BH058			4	20			mph agg			3	
	BH117							mph agg			3	
	VL013			2	40	3		felsitic			1	zoned, corroded plag
	VL012			3	35			glassy	30		1	zoned, corroded plag
	VL011				15			glassy	35		1	zoned plag
Nadele	VL007			1	4			felsitic			1	corroded plag
Breccia	VL010				30		2	felsitic			1	zoned plag
	VL009				3			felsitic			1	zoned plag
	VL005				3	1		felsitic			1	zoned, corroded plag
	VL008				3	1	1	glassy	2		1	
	W2			2	3		1		2		3	corroded plag
	BH222				50	5	8	mph agg	5		3	zoned, corroded plag
	BH197				60	3					3	zoned, corroded plag
Kawa	VLO34			3	25	1					2	zoned, corroded plag
Formation	VL033											no section

Wainimala Group

	Sample	Ol	Opx	Cpx	Pl	Mt	Hbl	Gmass	Ves%	Order	AI	Notes
	BH279											no section
	W3			1	2	1	3	felsitic			3	
	BH295			1	20	1	?2	felsitic			2	corroded plag
	90-86											no section
	BH125				10			mph agg			5	
Felsic dykes	**90-71**				12			felsitic			4	
cutting	**BH382**				4			mph agg			3	
Yavuna Group	**BH373**				15			mph agg			3	
	90-11				2			glassy			3	
	BH524		?2		4		?1	glassy			1	
	90-82										1	no section
Kalaka	**BH049**				3				?10		1	
Dacite	**90-42**				4		1	mph agg			1	
	90-43				1		?1	mph agg	4		1	
	VLO14				2						1	
	BH507				5			glassy	7		1	

Eua

Sample	Ol	Opx	Cpx	Pl	Mt	Hbl	Gmass	Ves%	Order	AI	Notes
E1			1	2	1		mph agg		cpx-pl	3	
E2			1	4			glassy			1	Resorbed phenocrysts
E3			5	3	1		mph agg			4	
E4				15			felsitic	10		3	
E5				1	1		felsitic			3	
E6							felsitic	30		1	
E7				2			mph agg			3	
E8				2			mph agg			3	
E9				3			felsitic	3		1	
E10				2	2		mph agg			3	
E11			1	25						1	
E12				1			glassy			1	? siltstone
E13				25			felsitic	15		1	
E14			5	25			mph agg			1	Zoned plagioclase
E15										1	? siltstone
E16				1			felsitic	3		1	
E17		?5		20			mph agg			3	
E18				20			glassy	10		1	
E28			1		2		glassy			3	
E29				30			glassy	5		3	
E30			2	30	1		mph agg			3	
E31		?5	5	80						3	much chlorite
E32		?15	20	65	5					3	much chlorite
E33			?5				glassy			3	
E34				5	3		felsitic			3	
E35		?	5	70	2					3	much chlorite
E36			20	60	2					3	
E37			20	60	2					3	
E38			10	80	1					3	much chlorite
E40		?10	5	10	3		mph agg			1	
E41			10	55	1					4	
E42			6	20	2		mph agg			4	